# Mechanisms of lumen formation during sprouting angiogenesis *in vivo*

**Véronique Marie Gebala**

University College London

and

Cancer Research UK London Research Institute

PhD Supervisor: Holger Gerhardt

A thesis submitted for the degree of

Doctor of Philosophy

University College London

March 2016

## Declaration

I, Véronique Marie Gebala, confirm that the work presented in this thesis is my own. Where information has been derived from other sources, I confirm that this has been indicated in the thesis.

# Abstract

During development, vascular networks expand following a process known as sprouting angiogenesis. New vascular branches arise from pre-existing vessels through the coordinated migration and proliferation of endothelial cells, and eventually connect to form new vascular loops. The functionality of these new vessel segments is dependent on the opening of a central lumen to allow perfusion. While mechanisms of lumen formation during the establishment of the primary vasculature by vasculogenesis have been well characterised, the mechanisms underlying lumen formation during sprouting angiogenesis *in vivo* are still poorly understood and subject to debate.

In this work, I established high spatial and temporal imaging of apical membrane dynamics during sprouting angiogenesis *in vivo*, both in the zebrafish trunk vasculature and the mouse retina primary inner plexus. By doing so, I identified a novel mechanism of lumen formation, where blood flow expands luminal compartments by driving spherical deformations reminiscent of membrane blebs at the apical membrane of sprouting endothelial cells. Additionally, I show that this process, that I chose to term inverse membrane blebbing, is tightly controlled through local and transient recruitment and contraction of actomyosin at the surface of growing blebs. This mechanism eventually leads to the selective retraction of inverse blebs along the apical membrane, allowing unidirectional lumen expansion. When endothelial cells ability to retract is inhibited through expression of a dominant-negative form of myosin II, cells fail to lumenise or show dilated lumens with multiple unresolved side blebs and branches.

Together, this work provides a mechanism for lumen expansion within sprouting endothelial cells *in vivo*, and identifies for the first time inverse blebbing as a reaction of membranes to high external pressure. In the context of sprouting endothelial cells, I show that a tight equilibrium between the forces exerted by the blood and the contractile responses from the cells is required for lumen expansion within angiogenic sprouts.

## Acknowledgements

To my thesis supervisor, Holger Gerhardt. Thank you for the freedom you gave me to follow my scientific curiosity and explore my own ideas, I could not have dreamt of better circumstances to grow as a scientist. Your enthusiasm, kindness and support made working with you the most enjoyable experience. Thank you for always challenging me and trusting me.

To Li-Kun Phng. I learnt so much by working with you. Thank you for always providing great input and support, and for welcoming me in Leuven when I was desperate to play with more microscopes!

To my PhD sister, Filipa Neto. I was so lucky to share this journey with you. Thank you for having taken such good care of me, and for all the amazing memories I keep from our time in London.

To all the VBL/iVBL/VPL extended family:
To the past members of the London Vascular Biology Lab. To my British English and Physics tutor, running coach, and digestives supplier, Martin Jones; to Benedetta "Cookie Monster" Ubezio; to Claudio Franco, Raquel Blanco, Irene Aspalter, Anan Ragab, Andrea Taddei, Katie Bentley, Eleonora Lapi, Jane Babbage, Giovanni Mariggi, and Dominique Sauvaget.
To our new team in Berlin: Anne-Clémence Vion, Russell Collins, André Rosa, Irene Hollfinger, Baptiste Coxam, Anna Szymborska, Santiago Andrade, Elena Cano-Rincon, Marta Bastos de Oliveira, Eireen Bartels-Klein, Ines Uhlenhut, Iris Unterweger, and Alexandra Klaus.
To past and present members of the Vascular Patterning Lab in Leuven: Fabio Stanchi, Ilse Geudens, Thomas Mathivet, Claire Bouleti, Marly Balcer, Pavel Nedvetsky, Petya Georgieva, Ken Matsumoto, Xiaocheng Zhao, and Andrin Wacker.
To our short-term but fondly remembered visitors: Helena Serra, Julia Schopp and Tuyu Zheng.

Working with you all was such a rewarding experience. Thank you for the daily support, helpful discussions, and most of all for the unique entertainment you provided every single day of my PhD!

To my classmates of the London Research Institute PhD programme: Martina, Marianne, Sakshi, Nil, Ichha, Yaiza, Mauro, Steffi, Aldona, Molly, Pavel, Kristyna. Thank you for your friendship, the parties, and the invaluable support!

To friends from the 6th floor and beyond: Solène, Florent, Lars, Delphine, Justin, Eyal.

To everyone at the LRI and Cancer Research UK. Your dedication to the fight against cancer is inspirational and made the LRI a very special place to be.

To Cancer Research UK and all its generous donators for funding my PhD, and allowing us scientists to work towards a better understanding of the disease, even in its most fundamental aspects.

To everyone at the LRI PhD programme and to my thesis committee members, Barry Thompson and Thomas Surrey, for making sure the journey was as smooth as possible.

To all the staff at the Animal and Fish Facilities of the LRI, Max Delbrück Center and Vesalius Research Center. A special thank you to Sue Watling, Caroline Zverev and Claire Darnbrough at Clare Hall, and to our fish whisperers, Chris Sergeant and Darren Martin at Lincoln's Inn Fields, and Robby Fechner at the MDC.

To Thomas Surrey and Nicholas Cade at the LRI for granting me access to their 3i spinning disk microscope, and Peter Vanden Berghe for letting me use the Andor spinning disk confocal of the Cell Imaging Core Facility at KU Leuven.

To my friends and family back home, for their incredible support:

To Virginie, ma Ninou, for being the most supportive and inspirational friend. You kept me sane and hopeful throughout this whole journey. I look forward to our reunion and the many adventures awaiting for us on this planet.

To my friends from Ginette: the one-and-only Caroline Bailleux, Guigui, and my “co”s Cha and Pierrick. Thank you for visiting me everywhere I ended up and for staying the same crazy bunch over the years! To Buchette, and my friend-without-borders Maï, I am so lucky to have you by my side.

Finally:

To the Feest family, for having welcomed us, “the kids”, in Berlin with the greatest kindness.

To Jianni, for having made Berlin feel like home.

And last but not least:

To my brother and best friend, Nicolas. For having been there every step of the way, every single day. For having come to my rescue when I needed it the most, and for being up for anything, always. You are the best.

À Maman et Papa, pour votre soutien et votre amour inconditionnels.

# Table of Contents

# Table of figures

# List of tables

# Abbreviations

| | |
|---|---|
| ADAM | A disintegrin and metalloprotease |
| ADP | Adenosine diphosphate |
| aISV | Arterial intersegmental vessel |
| ALPS | Amphipathic lipid-packing sensor |
| AMIS | Apical membrane initiation site |
| AmotL2 | Angiomotin-like protein 2 |
| Ang-1 | Angiopoietin 1 |
| Ang-2 | Angiopoietin 2 |
| Anx2 | Annexin 2 |
| AQP-8 | Aquaporin 8 |
| ATPase | Adenosine triphosphatase |
| aPKC | Atypical protein kinase C |
| BAR | Bin-Amphiphysin-Rvs |
| Bcl-2 | B-cell lymphoma 2 |
| BSA | Bovine serum albumin |
| bFGF | Basic fibroblast growth factor |
| CA | Caudal artery |
| CAAX | Cystein, aliphatic amino acid, aliphatic amino acid, any amino acid |
| cAMP | Cyclic adenosine monophosphate |
| CBP | Creb-binding protein |
| CCM1 | Cerebral cavernous malformation protein 1 |
| CDS | Coding DNA sequence |
| CFTR | Cystic fibrosis transmembrane conductance receptor |
| CoR | Co-repressor complex |
| COUP-TFII | Chicken ovalbumin upstream promoter-transcription factor II |
| CRISPR | Clustered regularly-interspaced short palindromic repeats |
| CV | Caudal vein |
| DA | Dorsal aorta |
| DAPI | 4’,6-diamidino-2-phenylindole |

| | |
|---|---|
| DE-Cadherin | Drosophila epithelial cadherin |
| DIAPH3 | Diaphanous related formin 3 |
| DLAV | Dorsal longitudinal anastomotic vessel |
| Dll4 | Delta-like ligand 4 |
| DNA | Deoxyribonucleic acid |
| Dpf | Days post-fertilisation |
| E(x) | Embryonic day (x) |
| EBP-50 | Ezrin radixin moesin-binding phosphoprotein 50 |
| ECM | Extracellular matrix |
| EGFP | Enhanced green fluorescent protein |
| EGFP-F | Farnesylated enhanced green fluorescent protein |
| EGFR | Epidermal growth factor receptor |
| ELC | Essential light chain |
| ERM | Ezrin radixin moesin |
| F-actin | Filamentous actin |
| FAK | Focal adhesion kinase |
| FCS | Fetal calf serum |
| FGF-2 | Fibroblast growth factor 2 |
| FHOD1 | Formin homology 2 domain-containing protein 1 |
| FIP5 | Rab11 family interacting protein 5 |
| FMNL2/3 | Formin-like protein 2/3 |
| FRET | Fluorescence resonance energy transfer |
| GEF | Guanine nucleotide exchange factor |
| GSK-3β | Glycogen synthase kinase 3β |
| GTP | Guanosine triphosphate |
| HDAc | Histone deacetylase |
| HGF | Hepatocyte growth factor |
| Hes | Hairy/enhancer of split |
| HIF | Hypoxia-inducible factor |
| Hpf | Hours post-fertilisation |
| hPR-LBD | Human progesterone receptor ligand binding domain |
| HRE | Hypoxia-response element |

| | |
|---|---|
| HUVEC | Human umbilical vein endothelial cell |
| IAP | Inhibitor of apoptosis |
| ICAM-2 | Intercellular adhesion molecule 2 |
| IFB-1 | Intermediate filament protein 1 |
| IL-3 | Interleukin 3 |
| INF2 | Inverted formin 2 |
| INL | Inner nuclear layer |
| ISV | Intersegmental vessel |
| LDA | Lateral dorsal aorta |
| LexA-DBD | LexA DNA binding domain |
| LexOP | LexA operon promoter |
| LexPR | LexA progesterone receptor |
| LFA-1 | Lymphocyte function-associated protein 1 |
| LPM | Lateral plate mesoderm |
| MAML | Mastermind-like |
| MDCK | Madin-Darby canine kidney |
| mDia1/2 | Mammalian Diaphanous 1/2 |
| MMP | Matrix metalloprotease |
| MT-MMP | Membrane-type matrix metalloprotease |
| MLCK | Myosin light chain kinase |
| mRFP-F | Farnesylated monomeric red fluorescent protein |
| mRNA | Messenger ribonucleic acid |
| NA | Numerical aperture |
| Nck1/2 | Tyrosine kinase adaptor proteins 1/2 |
| NF-κB | Nuclear factor kappa-light-chain-enhancer of activated B cells |
| NHERF-1 | $Na^+/H^+$-exchange regulatory factor 1 |
| nmMyosin IIA | Non-muscle myosin IIA |
| NICD | Notch intracellular domain |
| OIR | Oxygen-induced retinopathy |
| p65-AD | p65 activation domain |
| P(x) | Post-natal day (x) |
| PAP | Pre-apical patch |

| | |
|---|---|
| PCP | Planar cell polarity |
| PCV | Posterior cardinal vein |
| PDGF | Platelet-derived growth factor |
| PDGFR | Platelet-derived growth factor receptor |
| PH | Pleckstrin homology |
| PHD | Prolyl-hydroxylase domain-containing enzyme |
| Pi | Inorganic phosphate |
| PKC | Protein kinase C |
| pMLC2 | Phospho-myosin light chain 2 |
| $PIP_2$ | Phosphatidylinositol (4,5)-biphosphate |
| $PIP_3$ | Phosphatidylinositol (3,4,5)-trisphosphate |
| PLC$\partial$ | Phospholipase C, $\partial$ isoform |
| PKC | Protein kinase C |
| PTEN | Phosphatase and tensin homolog |
| pVHL | Von Hippel-Lindau tumor suppressor protein |
| RBP-Jκ | Recombination signal-binding protein for immunoglobulin-kappa J region |
| RFP | Red fluorescent protein |
| RhoGAP | Rho GTPase activating protein |
| RIP | Receptor interacting protein |
| RLC | Regulatory light chain |
| ROCK | Rho-associated protein kinase |
| (x)S | Somite (x) |
| S1P | Sphingosine-1-phosphate |
| S1PR | Sphingosine-1-phosphate receptor |
| SCF | Stem cell factor |
| SDF-1α | Stroma-derived factor 1α |
| SH2 | Src homology 2 |
| SHH | Sonic hedgehog |
| siRNA | Silencing ribonucleic acid |
| SIRT2 | Sirtuin 2 |
| SIV | Sub-intestinal vein |

| | |
|---|---|
| Slp2a/4a | Synaptotagmin-like protein 2a/4a |
| SNX18 | Sorting nexin 18 |
| SPIM | Single plan illumination microscopy |
| TALEN | Transcription activator-like effector nuclease |
| TGF-β | Transforming growth factor β |
| TIAM1 | T-cell lymphoma invasion and metastasis 1 |
| Tnnt2a | Troponin 2a |
| TPA | 12-O-tetradecanoyl-phorbol-13-acetate |
| VE-Cadherin | Vascular endothelial cadherin |
| VEGF | Vascular endothelial growth factor |
| VEGFR | Vascular endothelial growth factor receptor |
| vISV | Venous intersegmental vessel |
| vSMC | Vascular smooth muscle cell |
| WT | Wild-type |
| ZO-1 | Zona occludens 1 |

# Chapter 1. Introduction

## 1.1 The cardiovascular system: structure, development and associated diseases

### 1.1.1 Organisation and function of the cardiovascular system

The growth, survival and reproduction of living organisms rely on the delivery and recycling of metabolites to and from all cells in the body. Throughout evolution, as organisms grew in size and complexity, the simple diffusion of metabolites through cell membranes and multiple cell layers had to be complemented with the development of specialised transport and exchange structures. To this end, vertebrates expanded highly complex and hierarchised blood vascular systems (Monahan-Earley et al., 2013). Additionally to ensuring the delivery and recycling of respiratory gases and nutrients to all tissues in the body, these circuits developed as guardians of the organism's global homeostasis by allowing, notably, temperature regulation, hormonal communication, and the circulation of immune factors and cells.

From ancient Greece up until the 17$^{th}$ century, the cardiovascular system was thought to be comprised of two distinct networks of arteries and veins. It is in 1628, in his book *Exercitatio Anatomica de Motu Cordis et Sanguinis in Animalibus*, that William Harvey presented for the first time evidence to support the model of the circulatory system as we know it today (Figure 1.1). However, it was not until 1661, and the development of light microscopy, that capillaries, and thus the link between arteries and veins, was discovered by Marcello Malpighi. In further centuries, the development of animal models and advances in microscopy techniques allowed scientists to considerably increase their understanding of the formation and functioning of the cardiovascular system.

The blood vascular system of vertebrates is organised in a closed network of collecting (veins and venules) and distributing (arteries and arterioles) vessels connected to a

central peristaltic pump known as the heart (Figure 1.1). In tissues, exchange of gases and metabolites takes place through networks of fine capillaries, whose organisation in parallel throughout the body guarantees adequate distribution of resources to all organs (Figure 1.1), in contrast to the perfusion of tissues in series in open circulatory systems such as those found in many invertebrate species (Monahan-Earley et al., 2013).

The efficiency and adaptability of the vertebrates cardiovascular system lies in the structural specialisation and hierarchical organisation of the vessels within its network. Capillaries are made of a single layer of endothelial cells and are surrounded by a basement membrane and mesenchymal cells (pericytes) (Figure 1.2). By regulating their permeability at various levels through fenestration, opening of cell junctions, partial digestion of the basement membrane, and/or detachment from pericytes, they can locally adapt to the metabolic needs of the surrounding tissue. On the other hand, larger vessels such as arteries and veins, surrounded by multiple layers of connective tissue and vascular smooth muscle cells (vSMCs) (Figure 1.2), can cope with higher blood volumes and pressure levels and adapt their diameter to modulate flow between tissues.

### 1.1.2 Blood vessel formation during embryonic development

Because of its critical role in nutrient and oxygen delivery, the cardiovascular system is the first organ system to reach a functional state during embryonic development. In mouse embryos, a simple circulatory loop made of a heart, dorsal aorta, sinus venosus and yolk sac plexus is complete as early as embryonic day E8.0-E9.0 (Drake and Fleming, 2000, Walls et al., 2008). In humans, cardiac morphogenesis takes place from the third to the ninth week of gestation (Dhanantwari et al., 2009). Heartbeat can be recorded from four to five weeks of gestation.

This primitive network of blood vessels, which ramifies into a plexus made of arteries, veins and a dense mesh of capillaries, forms through the migration and aggregation of mesoderm-derived progenitors called angioblasts. This process of *de novo* blood vessel formation is known as vasculogenesis (Figure 1.3).

Once established, this primitive plexus remodels and expands through a second mechanism of blood vessel formation known as angiogenesis. Angiogenesis refers to the formation of new blood vessels from pre-existing ones, and happens either through the sprouting, and later fusion, of vessel branches from a parent vessel (sprouting angiogenesis), or through the splitting of existing vessels (intussusceptive angiogenesis) (Figure 1.3). This second wave of blood vessel formation by angiogenesis leads to the formation of dense plexi of capillaries from which arteries and veins later segregate and mature to map a fully functional body vasculature.

After birth, angiogenesis still contributes to organ growth, but reaching adulthood most endothelial cells become and remain quiescent. The average lifetime of quiescent endothelial cells varies between organs, ranging from a few months (in the liver and lungs) to several years (in the brain and muscle) (Alberts et al., 2002). However, endothelial cells keep their ability to respond to pro-angiogenic stimuli through proliferation and sprouting, allowing the formation of new blood vessels in case of, for example, physiological adaptations (e.g. physical training, obesity, menstrual cycle), or during wound healing following injury.

### 1.1.3 Associated diseases and therapeutic perspectives

Endothelial cell quiescence relies as much on intrinsic mechanisms as on a tight balance between pro- and anti-angiogenic signals present in the tissue microenvironment. Many diseases have been associated with defects in one or both of these parameters. A wide range of pathologies - the most prominent being cancer, but also included are ocular and inflammatory diseases, diabetes and multiple sclerosis - are associated with enhanced and abnormal angiogenesis. In the well-studied case of tumour angiogenesis, blood vessels organise themselves into a chaotic network with juxtaposition of highly and poorly vascularised regions. The architecture and functionality of the vessels are altered. Their diameter is uneven, their lumen often small or collapsed. Perfusion is poor and leakage into the microenvironment is common (Potente et al., 2011). On the other hand, pathologies such as ischemic heart disease, preeclampsia or neurodegeneration are

characterised by low angiogenic response to physiological pro-angiogenic stimuli, impairing re-vascularisation and healing (Carmeliet, 2005, Potente et al., 2011).

While the past years have seen tremendous progress in the development and optimisation of pro- and anti-angiogenic drugs for use in clinics, the efficacy of these therapies is still limited and their effects not fully understood. In particular, it has become apparent that the control of vessel density alone is insufficient to normalise vasculatures in these pathologies, and that greater focus should be placed on the functionality of the affected vessels (Carmeliet, 2005, Potente et al., 2011). In light of these results, it appears crucial to develop our understanding of the basic cellular and molecular mechanisms regulating sprouting angiogenesis, with the aim of designing better therapies with greater impact for patients suffering from these diseases.

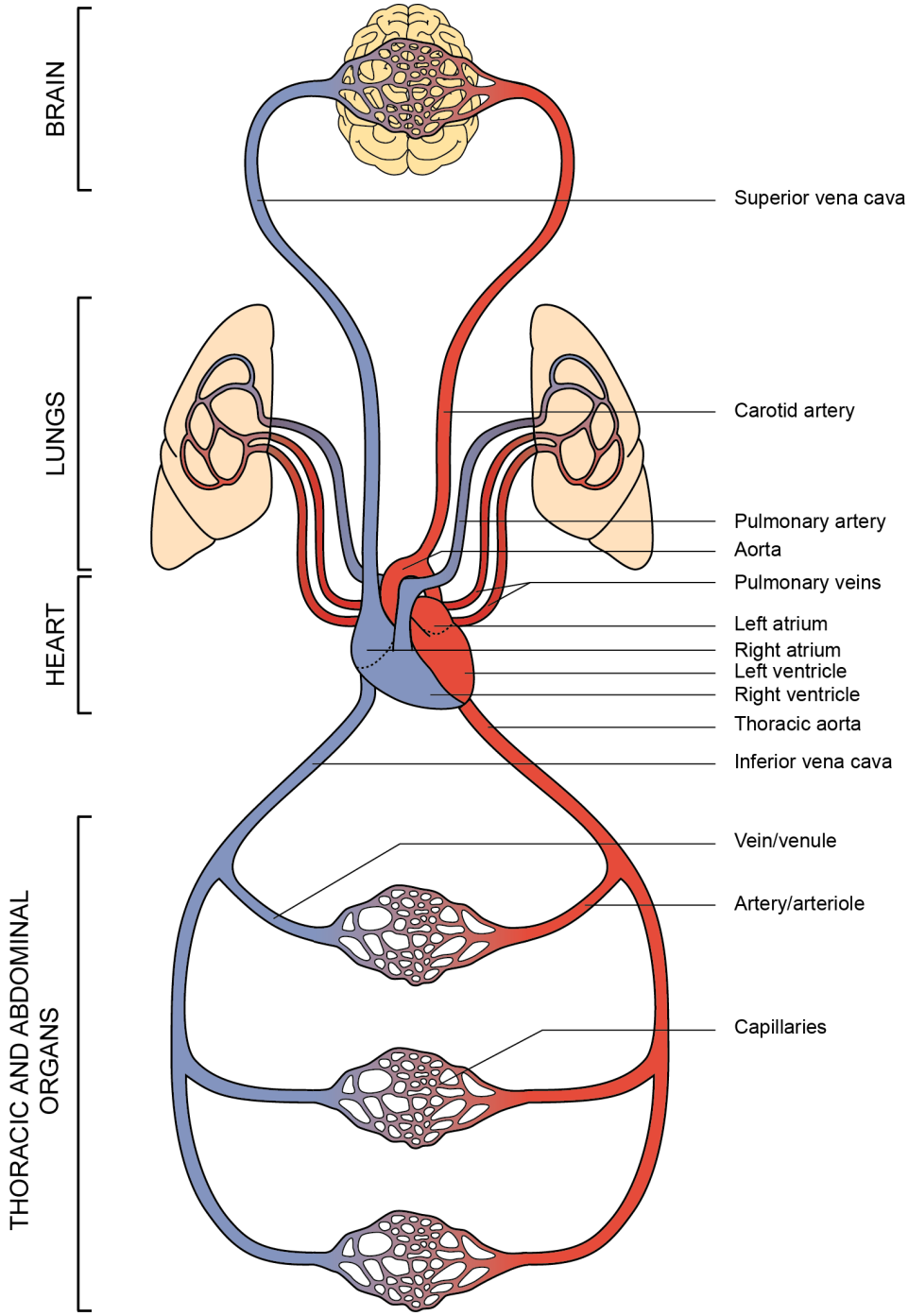


**Figure 1.1. The vertebrates cardiovascular system**
The cardiovascular system of vertebrates is organised as a closed network of blood vessels with distributing vessels (arteries and arterioles) and collecting vessels (veins and venules) connected to a peristaltic pump, the heart. The separation of the heart allows the separation of deoxygenated and oxygenated blood. Deoxygenated blood is sent to the lungs, where gas exchange within a network of fine capillaries allows the capture of oxygen and release of carbon dioxide. Oxygenated blood comes back to the heart where it is propelled through arteries to all organs in the body. Gas exchange in tissues takes place in complex networks of fine capillaries.

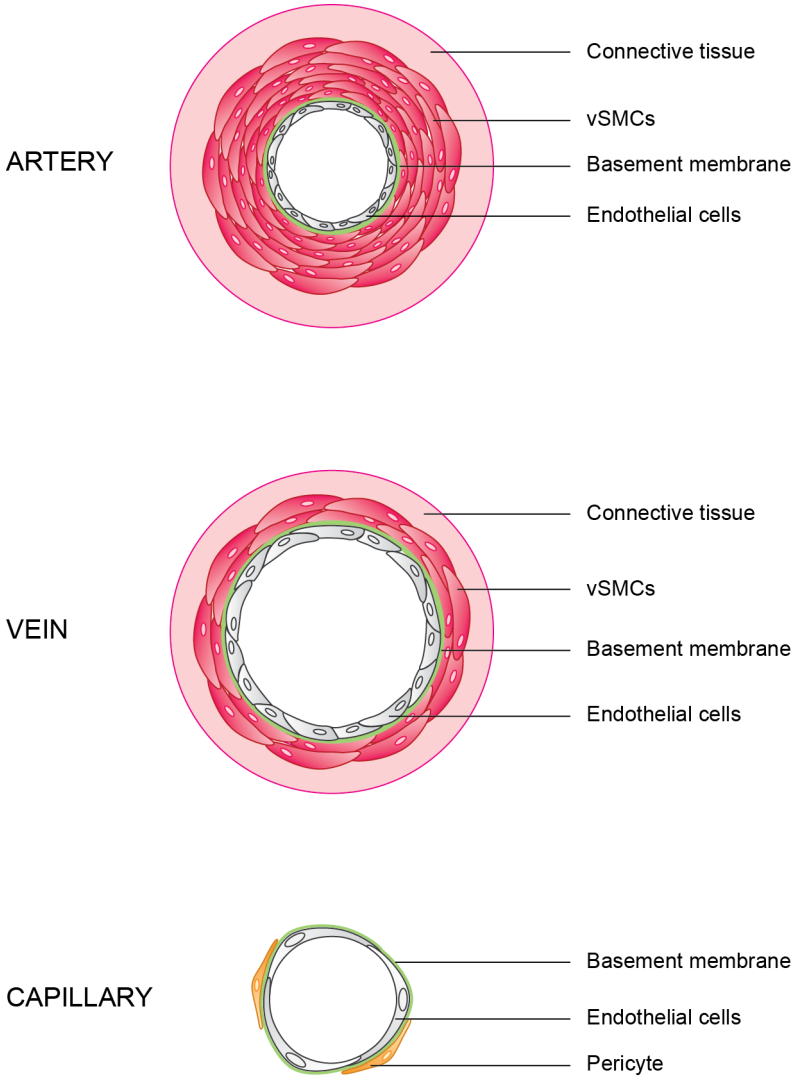


**Figure 1.2. Cross-sections of arteries, veins, and capillaries**
Arteries, veins and capillaries differ in function and structure. Arteries are surrounded by multiple layers of vascular smooth muscle cells (vSMCs) and connective tissue, while veins are only surrounded by a few layers of vSMCs and a thinner layer of connective tissue. Capillaries are only supported by a basement membrane and isolated pericytes.

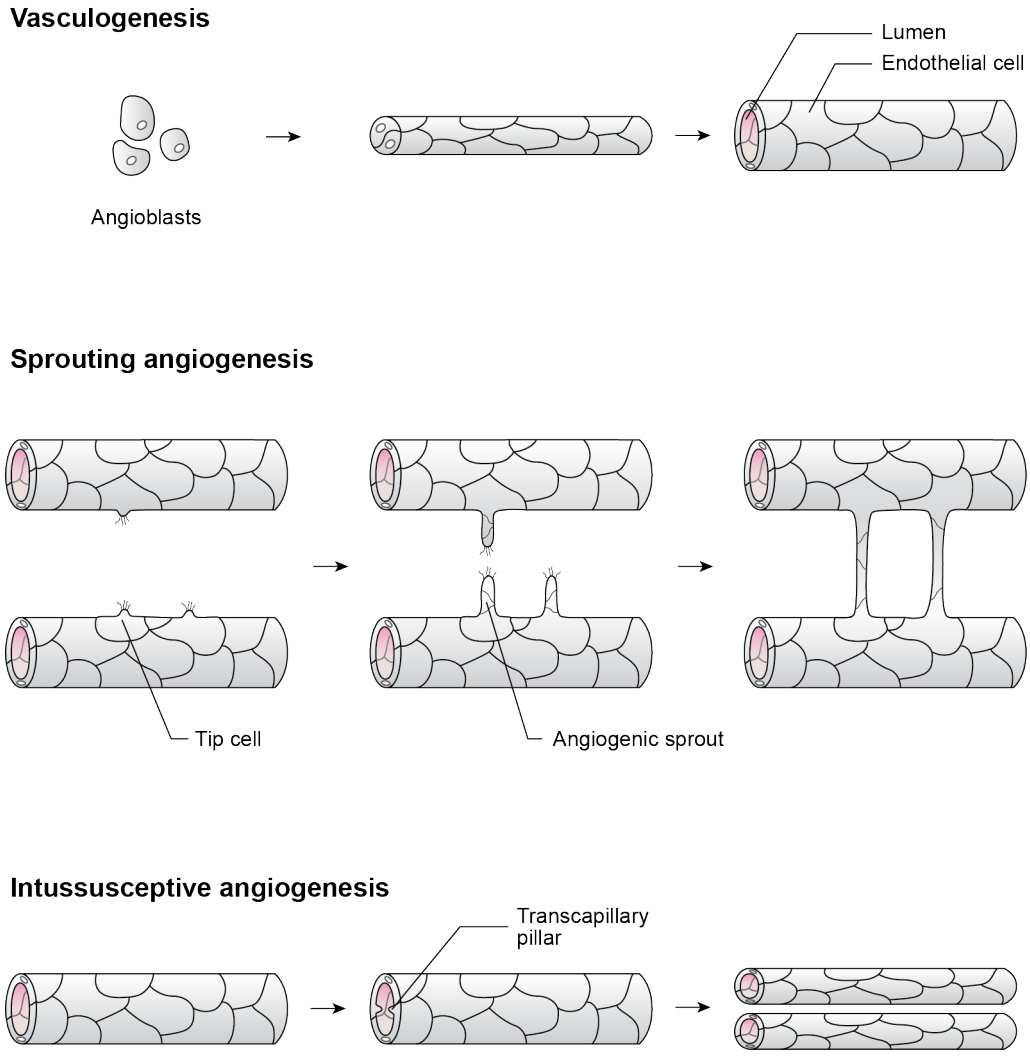


**Figure 1.3. Modes of blood vessel formation**
During embryonic development, a primary network of blood vessels forms through the aggregation of endothelial progenitors called angioblasts in a process known as vasculogenesis. New blood vessels then arise either through the sprouting of vascular branches from pre-existing vessels (sprouting angiogenesis), or through the splitting of blood vessels (intussusceptive angiogenesis).

## 1.2 Cellular and molecular mechanisms of sprouting angiogenesis

Sprouting angiogenesis is a multi-step process resulting from the secretion of pro-angiogenic factors by poorly oxygenated tissues. The binding of such factors to the surface of quiescent endothelial cells initiates a cascade of signalling events that lead to their reactivation and to the sprouting of new vascular branches. Through coordinated cell migration and proliferation, angiogenic sprouts elongate and eventually fuse to form new vascular loops, which later lumenise to allow perfusion (Figure 1.4). The maturation and specification of these new vessel connections lead to the expansion of functional vascular networks to allow the efficient delivery and recycling of metabolites to the tissues in need (Potente et al., 2011).

The following paragraphs will present in detail the cellular and molecular mechanisms driving and regulating the different steps of the angiogenic process, from the secretion of pro-angiogenic factors to the maturation and remodelling of the newly formed network.

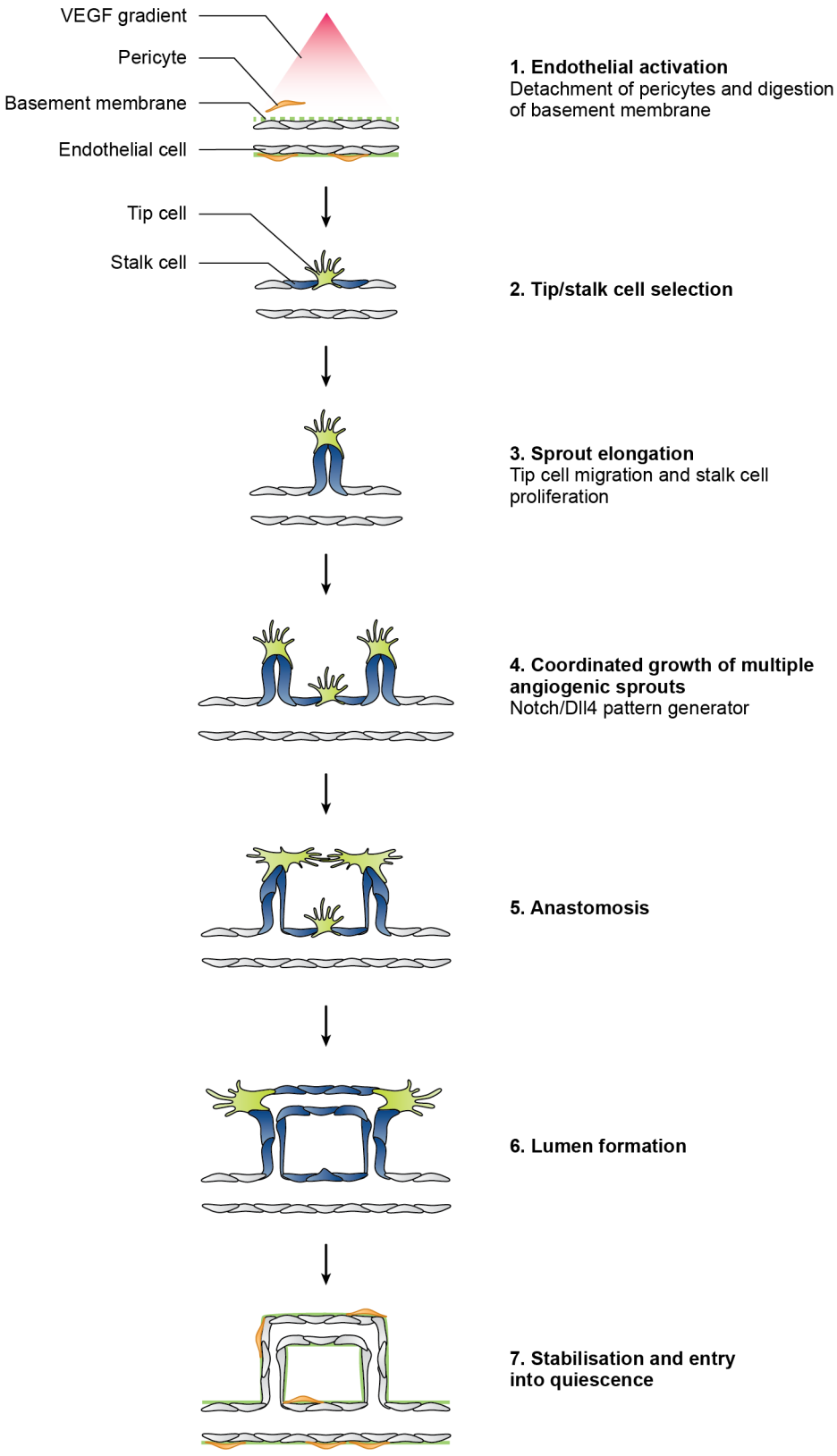


**Figure 1.4. Sprouting angiogenesis: overview of a multistep process**
Adapted from (Potente et al., 2011).

### 1.2.1 Hypoxia and secretion of pro-angiogenic factors

Physiologically, sprouting angiogenesis is a response of the endothelium in tissues experiencing poor oxygenation (hypoxia), whether because of higher demands or lower supplies in oxygen. At the cellular level, responses to low levels of oxygen are mediated by hypoxia-inducible factors (HIFs), highly conserved transcription factors that control the expression of numerous cell cycle, differentiation, metabolic and pro-angiogenic genes (Krock et al., 2011, Greer et al., 2012). HIFs are comprised of two subunits, an oxygen-labile α subunit and an ubiquitously-expressed β subunit (Figure 1.5). At normal levels of oxygen (normoxia), HIFα is hydroxylated on two proline residues by prolyl-hydroxylase domain-containing enzymes (PHDs) (Epstein et al., 2001, Ivan et al., 2001, Jaakkola et al., 2001, Masson et al., 2001). When hydroxylated, HIFα is recognised by the von Hippel-Lindau tumour suppressor protein (pVHL), ubiquitylated by the pVHL E3 ubiquitin ligase complex, and targeted for degradation by the 26S proteasome (Maxwell et al., 1999, Ohh et al., 2000). PHDs require oxygen for their catalytic activity. In the case of sub-optimal levels of oxygen (hypoxia), hydroxylation, and therefore degradation, of HIFα is abrogated. HIFα can therefore translocate to the nucleus, where it dimerises and binds to the HIFβ subunit. Together, HIFα/β bind to hypoxia-response elements (HREs) in the promoters of HIF-responsive genes, where they interact with the transcriptional co-activator p300/Creb-binding protein (CBP) to drive the transcription of a specific subset of genes (Arany et al., 1996, Wenger et al., 2005) (Figure 1.5). Among these are a host of pro-angiogenic genes, including but not limited to, vascular endothelial growth factor (VEGF), angiopoietin 1 (Ang-1), angiopoietin 2 (Ang-2), Tie2, platelet-derived growth factor (PDGF) and basic fibroblast growth factor (bFGF) (Krock et al., 2011), making HIF a central regulator of angiogenesis in developing as well as diseased tissues. Following their secretion, pro-angiogenic factors diffuse through and bind to the extracellular matrix, generating a gradient of growth signals directly available for binding to their specific receptors at the surface of endothelial cells.

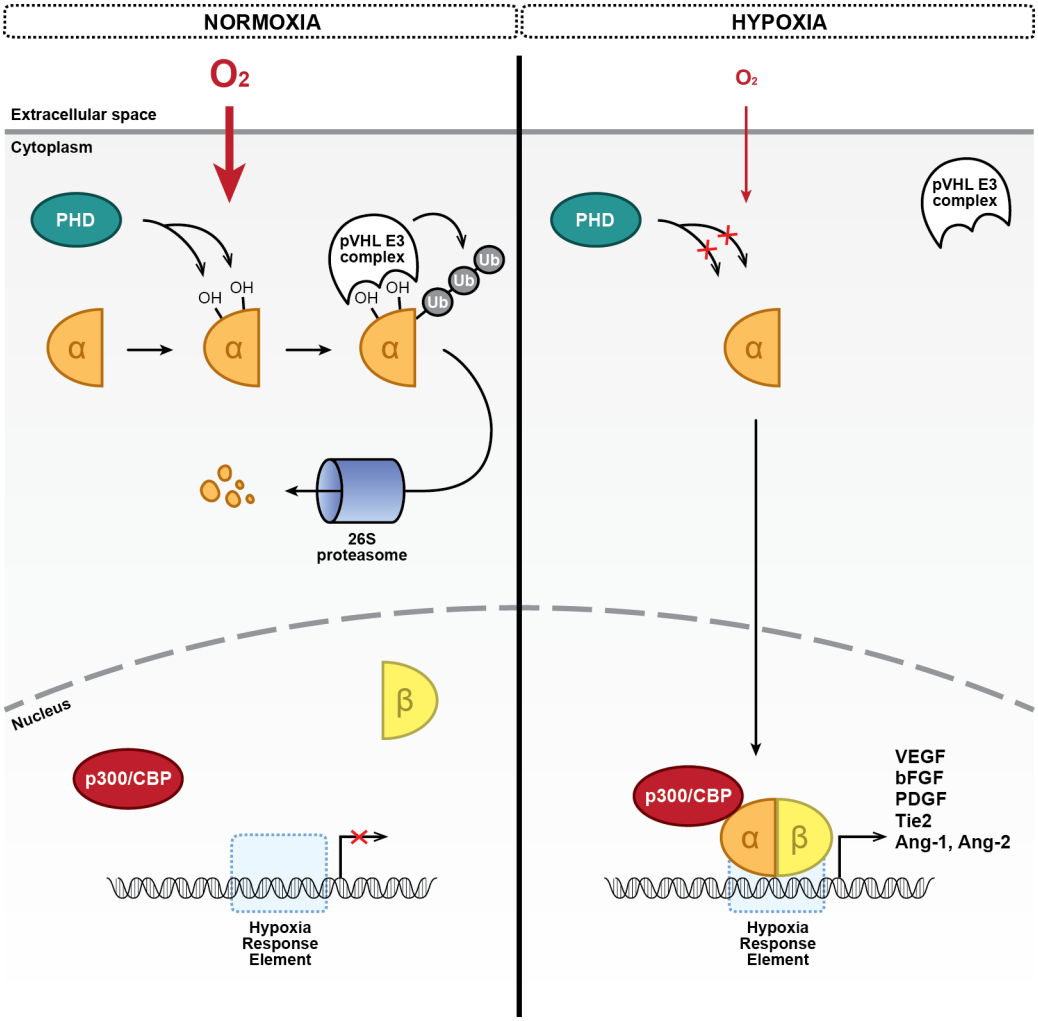


**Figure 1.5. Molecular regulation of pro-angiogenic factors secretion under hypoxia** Under normoxia, the alpha subunit of HIF (α) is hydroxylated by PHDs, polyubiquitylated by the pVHL E3 ligase complex, and degraded through the 26S proteasome. Under hypoxia, α translocates to the nucleus where it associates to the beta subunit of HIF (β) and binds to hypoxia-response elements (HREs) to drive the expression of pro-angiogenic factors.

### 1.2.2 Exit from quiescence

The first step towards the exit from quiescence and subsequent sprouting of endothelial cells is the breakdown of the physical barriers present at their basal side, that is the layer of supporting pericytes and their secreted basal membrane (Figure 1.4). Detachment of pericytes is mediated through concomitant activation of VEGF signalling and binding of Ang-2 to the Tie-2 receptor at the surface of endothelial cells (Augustin et al., 2009). The degradation of the endothelial cell basement membrane, made of an array of collagen IV fibres, laminin, heparin-sulfated proteoglycans and entactin (Kalluri, 2003), is mediated by a subset of proteolytic enzymes called matrix metalloproteases (MMPs). Both VEGF and bFGF, but also other pro-angiogenic factors at various levels, greatly increase the expression, activation and secretion of MMP-2, MMP-9 and membrane type (MT)-MMP-1 in endothelial cells (Ghajar et al., 2008). Released in the extracellular matrix, these enzymes cleave the components of the endothelial basement membrane, removing the physical barrier to sprouting but also exposing cryptic binding sites that further regulate sprouting, and promoting the release of additional growth factors sequestered in the matrix (Arroyo and Iruela-Arispe, 2010).

### 1.2.3 Tip and stalk cell selection

#### *1.2.3.1 Cellular behaviours within angiogenic sprouts*

Following the binding of pro-angiogenic factors to their respective receptors, single endothelial cells sprout from the parent vessel and lead the growth of multicellular vascular branches into the hypoxic tissue (Figure 1.4). Endothelial cells show different phenotypes and behaviours depending on their position along the sprouts. Cells at the tip, referred to as ‘tip cells’, extend long and numerous filopodia indicative of a migratory behaviour. In contrast, trailing cells, defined as ‘stalk cells’, show shorter and fewer membrane protrusions and higher proliferation rates. This dichotomy led to suggest a model where tip cells guide the sprout by sensing and migrating towards pro-angiogenic cues, while stalk cells support the growth of the sprout through cell proliferation (Gerhardt et al., 2003). Recent work using live imaging of endothelial cell behaviour in three-dimensional *in vitro* angiogenic assays and in zebrafish embryos

showed that endothelial cells regularly switch between tip and stalk cell phenotypes, leading to constant swapping of cells within the sprout and competition for the tip position (Jakobsson et al., 2010, Pelton et al., 2014).

#### *1.2.3.2 Molecular regulation of endothelial cell specification*

The acquisition of a 'tip' or 'stalk' phenotype by endothelial cells is dependent on the levels of VEGF and Notch signalling within individual cells as well as within their immediate neighbours.

Upon binding of VEGF-A, VEGFR-2 receptors expressed at the surface of endothelial cells form homo- as well as heterodimers with other VEGFRs, leading to the activation of their tyrosine kinase domains and their autophosphorylation. Phosphorylated VEGFRs then recruit Src homology 2 (SH2) domain-containing adaptors and kinases, inducing the activation of multiple downstream signalling pathways and transcription programmes regulating cell proliferation, migration and specification towards a tip cell phenotype (Olsson et al., 2006).

Among the genes whose expression is activated upon VEGF-A stimulation, Delta-like ligand 4 (Dll4) has been identified as a master regulator of the acquisition of the tip cell phenotype by endothelial cells (Hellstrom et al., 2007, Phng and Gerhardt, 2009). Dll4 is a transmembrane protein and the main ligand for the Notch1 receptor in endothelial cells (Hofmann and Iruela-Arispe, 2007). The binding of Dll4 to the extracellular domain of Notch1 at the surface of apposing cells triggers a series of proteolytic cleavages of the receptor by multiple enzymes, including ADAM metalloproteases and γ-secretase complexes, leading to the release in the cytoplasm of the Notch intracellular domain (NICD) and its translocation to the nucleus (Figure 1.6). In the absence of NICD, the recombination signal-binding protein for immunoglobulin-kappa J region (RBP-Jκ) represses the expression of Notch target genes through the recruitment of co-repressor complexes (CoR) and histone deacetylases (HDAc) to their promoter regions. Upon its translocation to the nucleus, NICD displaces these co-repressors from RBP-Jκ, and recruits co-activators such as Mastermind-like (MAML) proteins and histone

acetyltransferases (p300/CBP) to form a transcriptional activator complex (Borggrefe and Oswald, 2009) (Figure 1.6). Notch direct and indirect target genes in endothelial cells are numerous; Notch direct targets include genes coding for Hairy/enhancer of split (Hes) and Hes-related proteins (Hey/HRT/HERP), themselves transcriptional repressors of further downstream genes. Importantly, the transcriptional programme thus activated leads to a suppression of the tip cell phenotype and the activation of signalling pathways specific to stalk cells (Phng and Gerhardt, 2009).

A 'salt-and-pepper' distribution of tip and stalk cells arises along activated blood vessels following small stochastic differences in the levels of VEGF signalling, and therefore of Dll4 expression, between individual cells. Endothelial cells expressing higher levels of the Dll4 ligand will become tip cells, and repress this same phenotype in their neighbouring cells, which will adopt stalk cell characteristics. This phenomenon is known as lateral inhibition (Phng and Gerhardt, 2009). Multiple layers of regulation add complexity to the model presented here, and form the basis for the dynamic regulation of tip and stalk phenotypes during sprouting. Notably, VEGF and Notch signalling have been shown to regulate the expression of their own as well as respective components, reinforcing the differences established between neighbouring cells in a positive feedback loop mechanism (Figure 1.7). Briefly, the activation of Notch signalling, additionally to inducing the expression of stalk cell-related genes, down-regulates the expression of VEGFR-2, therefore inhibiting the acquisition of a tip cell phenotype in the same cell. Notch also induces the expression of the decoy receptor VEGFR-1, which possesses high affinity for VEGF-A but lacks kinase activity, therefore titrating VEGF-A away from VEGFR-2 (Figure 1.7). These mechanisms, together with additional regulatory pathways acting at various levels of the VEGF/Notch signalling cascades (Phng and Gerhardt, 2009), ensure the control of tip and stalk cell distribution and the coordinated elongation of multiple sprouts along the activated vessels (Figure 1.4).

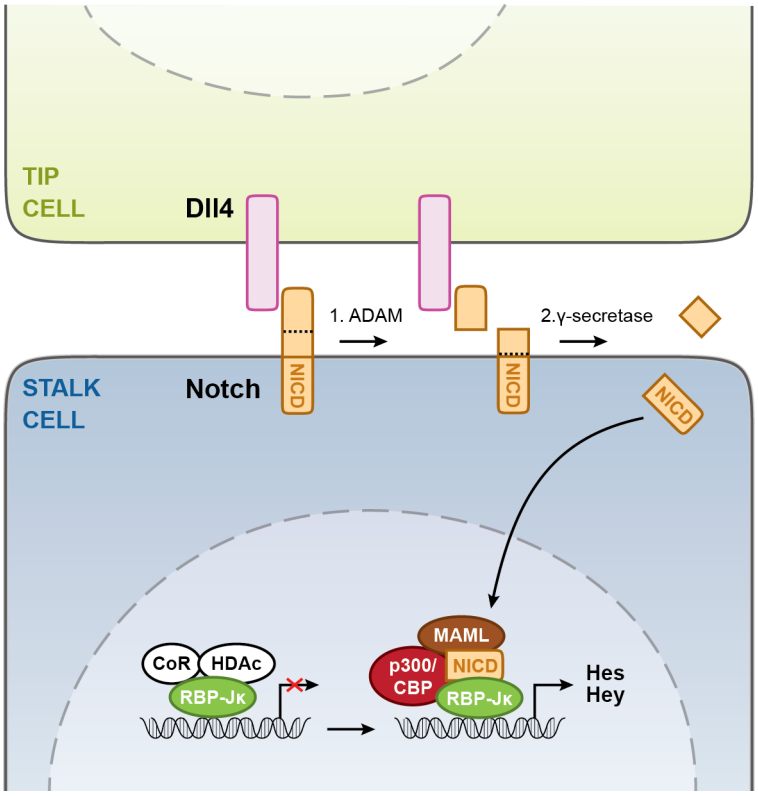


**Figure 1.6. Notch signalling pathway**
Binding of Dll4 to its Notch receptor on a neighbouring cell triggers a series of proteolytic cleavages leading to the release of the Notch intracellular domain (NICD) in the cytoplasm of the signal-receiving cell. NICD translocates to the nucleus where it binds to RBP-Jκ, displacing co-repressors (CoR) and histone deacetylases (HDAc) and recruiting transcriptional co-activators (MAML, p300/CBP), ultimately inducing the expression of the transcription factors Hes and Hey. These factors then regulate the expression of genes associated with the stalk cell phenotype.

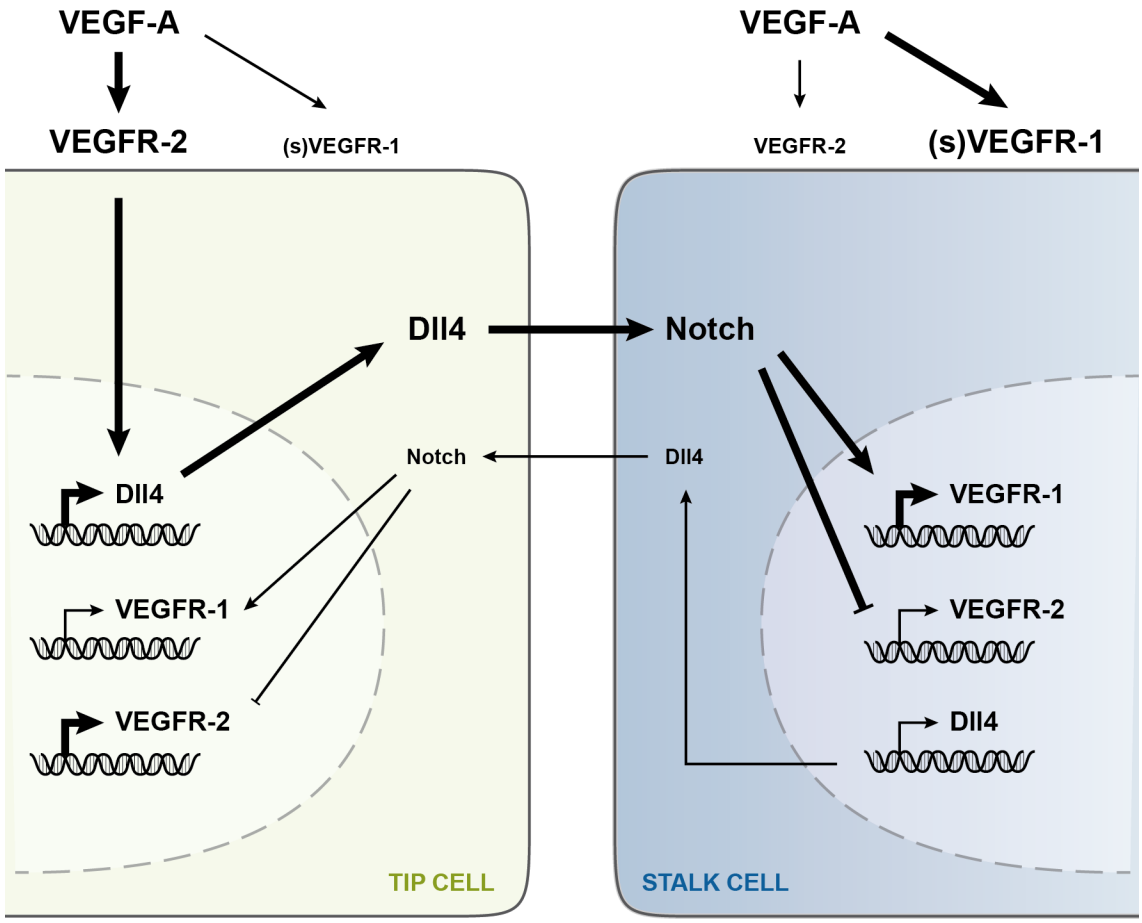


**Figure 1.7. VEGF/Notch signalling positive feedback loop**
Upon VEGF signalling, Dll4 expression is up-regulated. Dll4 binds to Notch on neighbouring cells, stimulating in the signal-receiving cell the expression of the decoy receptor VEGFR-1, and down-regulating the expression of VEGFR-2, therefore limiting VEGF signalling and expression of Dll4 in the signal-receiving/stalk cell.
Adapted from (Phng and Gerhardt, 2009).

### 1.2.4 Anastomosis and lumen formation

Following the specification of multiple tip cells along their length, several sprouts emerge from activated vessels and grow towards the same source of pro-angiogenic molecules by means of cell migration and proliferation. Eventually, tip cells from neighbouring sprouts meet and establish cell-cell contacts, to finally undergo a process of vessel fusion defined as anastomosis (Figures 1.4 and 1.8).

Studies using live imaging of blood vessel fusion in zebrafish embryos (Blum et al., 2008, Herwig et al., 2011, Lenard et al., 2013) showed that anastomosis relies both on the formation and elongation of cell contacts between anastomosing cells, and on the expansion of apical membrane (i.e. lining the lumen) domains to obtain a fully lumenised connection. Briefly, upon the formation of small contacts identifiable as discrete spots of junctional complexes between their respective filopodia (Figure 1.8), tip cells from neighbouring sprouts establish stable cell junctions, which then elongate while cells migrate over each other. Concomitantly, lumen forms *de novo* at the new junction, while lumens invaginate from the stalk of both sprouts into the tip cells. Eventually, all luminal compartments connect to form a vascular tube connected to the main circulation. Further cell rearrangements within the newly formed connection finally participate in its stabilisation as a multicellular tubular structure (Figure 1.8).

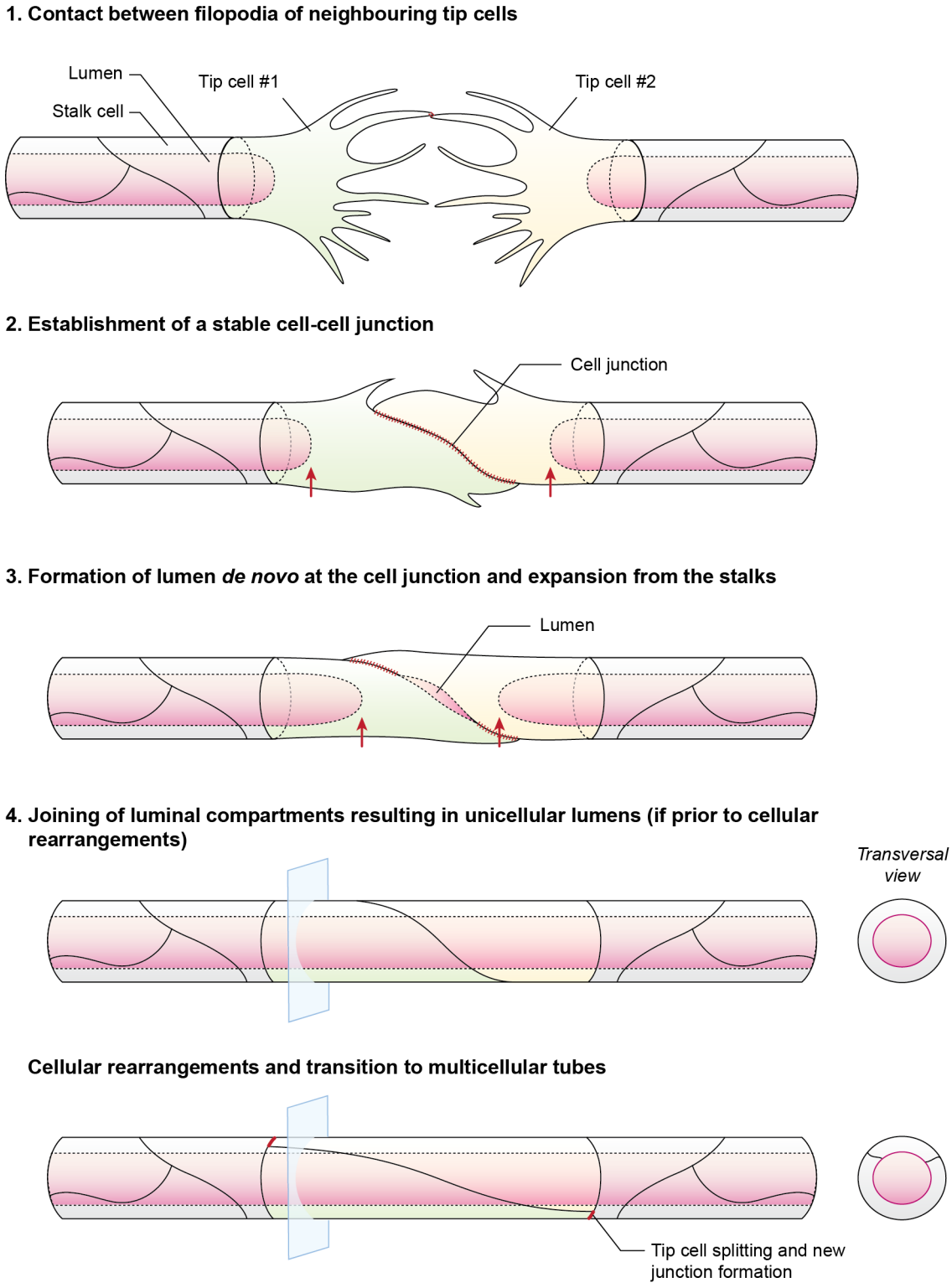


**Figure 1.8. Sequence of cellular events leading to anastomosis**
Adapted from (Herwig et al., 2011) and (Lenard et al., 2013).

### 1.2.5 Vessel maturation

Following anastomosis and lumen formation, newly formed vessels rapidly mature into perfused functional segments. Mirroring the mechanisms of endothelial cell activation at the onset of the angiogenic process, maturation of new vascular connections involves the deposition of extracellular matrix and recruitment of perivascular cells (Figure 1.4).
The deposition of extracellular matrix is crucial to provide the attachment and stiffness required for endothelial cells to cope with the establishment of blood circulation and the resulting mechanical stresses involved. On the other hand, the matrix also provides a plethora of signalling cues essential to maintain endothelial cell homeostasis, regulating, for example, proliferation and entry into or exit from quiescence (Jain, 2003, Potente et al., 2011).
Perivascular cells surround endothelial cells and, similarly to the extracellular matrix, fulfil both structural and signalling functions. Pericytes coat the surface of capillaries and immature vessels, while vSMCs support arteries and veins (Figure 1.2). The differentiation and recruitment of mural cells rely on multiple signals originating from endothelial cells. The proliferation, differentiation and recruitment of pericytes require signalling through the PDGFB-PDGF receptor (PDGFR)-β pathway. Secretion of transforming growth factor (TGF)-β by endothelial cells has, on the other hand, been shown to promote vSMC differentiation and function and, as a consequence, their attachment to endothelial cells (Pardali et al., 2010). Finally, sphingosine-1-phosphate (S1P) and Ang-1 have been reported as two ligands whose secretion by endothelial cells and signalling to their respective receptors, S1P receptors (S1PRs) and Tie2, promote mural cell adhesion (Gaengel et al., 2009, Potente et al., 2011).

### 1.2.6 Arterial-venous specification

A critical step in making or expanding functional vascular networks is the specification and remodelling of the newly formed vessels into arteries and veins. While arteries transport oxygenated blood under high pressure, supported by multiple layers of contractile vSMCs, veins, on the other hand, carry blood under low pressure with the help of specialised valve structures. Although the specification of immature vessels into

arteries and veins was first thought to be determined by the differences in haemodynamics experienced by vessels depending on their position in the network, many studies since showed that arterial and venous identities can be found even prior to blood perfusion, and identified many regulatory pathways controlling this process (Swift and Weinstein, 2009, Potente et al., 2011).

The first genes discovered to be differentially expressed in arteries and veins were the genes coding for the transmembrane protein ephrinB2 and its receptor EphB4, respectively (Wang et al., 1998). The complementary expression of ephrinB2 and EphB4 in arterial and venous endothelium is required for the proper remodelling of vascular networks but also for the maintenance of arterial and venous identities later during development (Swift and Weinstein, 2009).

Additionally to its role in tip and stalk cell selection at the onset of sprouting, Notch was also identified as a major regulator of arterial-venous specification, functioning cell-autonomously to repress the venous fate, downstream of VEGF, itself downstream of sonic hedgehog (SHH) signalling (Swift and Weinstein, 2009).

While these pathways repress venous fate and promote arterial fate acquisition, chicken ovalbumin upstream promoter-transcription factor II (COUP-TFII) was identified as an inducer of venous specification (You et al., 2005).

Interestingly, graft experiments performed in chick embryos revealed that the identity of single vessels within the network remains plastic, and that arterial and venous identities can even be reversed (Moyon et al., 2001, Othman-Hassan et al., 2001). This also proved true in cases of experimental modification of blood flow patterns, additionally suggesting that blood flow itself is a regulator of arterial-venous specification (le Noble et al., 2004).

### 1.2.7 Vascular remodelling

Once established, vascular networks constantly remodel to adapt to local changes in metabolic needs and/or haemodynamics. Indeed, both low concentrations of VEGF (Hlushchuk et al., 2011) and local loss of perfusion (Chen et al., 2012) have been shown to trigger regression (also referred to as pruning) of vascular segments.

Two major mechanisms of vessel regression have been described to date. In the cases of the pupillary membrane and the hyaloid vessels, two transient vascular networks of the eye, vessel segments regress via apoptosis of the endothelial cells making the regressing segment (Meeson et al., 1999, Lobov et al., 2005). By contrast, endothelial cells in regressing vessels of the developing rat and mouse retinas do not undergo apoptosis (Hughes and Chang-Ling, 2000, Franco et al., 2015). Live imaging of regressing vessels in the brain, trunk and sub-intestinal vein (SIV) plexus of zebrafish embryos showed that vessels regress instead through the coordinated migration of endothelial cells away from the pruning vessel into the neighbouring branches they are connected to (Chen et al., 2012, Franco et al., 2015, Lenard et al., 2015). Interestingly, vascular pruning through endothelial cell migration follows the same steps than anastomosis (Figure 1.8) but in reverse order: junctions rearrange and cells slide away from each other, giving rise to unicellular vessel segments; lumen collapses, generating isolated lumen fragments; and finally, cells lose connections and the vessel segment breaks, while endothelial cells migrate into the neighbouring vessels (Franco et al., 2015, Lenard et al., 2015). The signalling pathways regulating this process are only starting to be uncovered. In an oxygen-induced retinopathy (OIR) model of pathological angiogenesis, Notch/Dll4 signalling was found to promote vessel regression through the up-regulation of the expression of the vasoconstrictor angiotensinogen and down-regulation of the expression of the vasodilator adrenomedullin (Lobov et al., 2011). Interestingly, this study and others (Kochhan et al., 2013, Franco et al., 2015) establish a correlation between low perfusion and sites of regression in different vascular beds and organisms, suggesting the existence of robust feedback mechanisms between blood flow dynamics and endothelial cell behaviour at the level of single capillaries.

### 1.2.8 Concluding remarks

The past decades have seen tremendous advances in our understanding of the cellular and molecular mechanisms driving sprouting angiogenesis. The most recent investigations, taking advantage of time-lapse imaging of sprouting endothelial cells, and local and inducible genetic, chemical and mechanical manipulations, have revealed an extreme plasticity and adaptability of endothelial cells to varying microenvironments.

Basic questions however remain unanswered. The nature of the mechanisms driving lumen formation during sprouting angiogenesis *in vivo* is, for example, still subject to debate, and will be the focus of the present work.

## 1.3 Working models for the study of vascular lumen formation

Multiple models have been developed and tested over the years to allow the study of the cellular and molecular mechanisms that regulate blood vessel formation during both development and disease. The following paragraphs will focus on some of the *in vitro* and *in vivo* models of vasculogenesis and angiogenesis currently used in the field and particularly relevant for the study of lumen formation.

### 1.3.1 In vitro models

The complexity of the cellular behaviours observed during blood vessel formation *in vivo* called for the development of simplified yet truthful *in vitro* models of endothelial cell self-assembly and sprouting. Although many endothelial cell behaviours can be recapitulated and studied in 2D culture assays, the arrangement of endothelial cells into complex three-dimensional structures proved crucial to allow the study of morphogenetic events such as lumen formation, and therefore led to the development of 3D culture assays where endothelial cells are allowed to form capillary networks within 3D matrices.

The laboratory of George Davis at the University of Missouri (USA) pioneered the use of such assays and developed over the years standardised protocols for generating lumenised capillary networks *in vitro* (Davis and Camarillo, 1996, Koh et al., 2008b, Davis et al., 2013). Briefly, endothelial cells self-assembly into vascular networks is obtained by including human umbilical vein endothelial cells (HUVECs) at a density of $2.10^6$ cells/mL in 3D matrices made exclusively of type I collagen at a final concentration of 3.75 mg/mL. After polymerisation of the matrix, cells are treated with standard culture medium supplemented with VEGF-165, FGF-2, ascorbic acid and 12-O-tetradecanoyl-phorbol-13-acetate (TPA) (Table 1.1). Under these conditions,

endothelial cells self-assemble into cords and lumenise within 72 hours (Figure 1.9). While this assay recapitulates the morphogenetic events observed during vasculogenesis, a similar assay was developed to follow angiogenic sprouting, by seeding HUVECs on top of the polymerised collagen gel instead of including them into the gel prior to polymerisation. Using the same medium composition as previously described and the same matrix supplemented with sphingosine-1-phosphate (S1P) and stromal-derived factor-1α (SDF-1α) (Table 1.1), cells can be seen invading the underlying matrix, organising themselves into sprouts resembling closely the angiogenic sprouts observed *in vivo* (Koh et al., 2008b, Davis et al., 2013).

In an effort to guarantee reproducible and truthful results, these assays have recently been modified to allow formation of capillary networks in serum-free and TPA-free conditions. Collagen gels are instead supplemented with FGF-2 and the hematopoietic stem cell cytokines SDF-1α, stem cell factor (SCF) and interleukin-3 (IL-3) (Stratman et al., 2011, Davis et al., 2013).

While these assays have been used for most of the *in vitro* studies that will be mentioned later in this introduction, many laboratories developed similar protocols using endothelial cells from different species or vascular beds, and matrices of varying composition (Morin and Tranquillo, 2013). More complex systems also include co-culture with pericytes (Stratman et al., 2009, Waters et al., 2013, Bowers et al., 2015, Kim et al., 2015), and recent development of microfluidic devices now allows perfusion of lumenised vessels *in vitro* (Zheng et al., 2012, Moya et al., 2013, Bichsel et al., 2015, Wang et al., 2016).

| | **Collagen** | **Medium** |
|---|---|---|
| Medium | M199 | M199 |
| Collagen type I | 3.75 mg/mL | - |
| Fetal calf serum (FCS) | - | 20 % |
| Bovine brain extract | - | 400 µg/mL |
| Bovine serum albumin (BSA) | - | 0.5 mg/mL |
| Sodium selenite | - | 5 ng/mL |
| Human insulin | - | 5 ng/mL |
| Human holo-transferrin | - | 5 ng/mL |
| Oleic acid | - | 4.28 µg/mL |
| VEGF-165 | - | 40 ng/mL |
| FGF-2 | - | 40 ng/mL |
| TPA | - | 50 ng/mL |
| *- Added for sprouting assay* | | |
| SDF-1α | 200 ng/mL | - |
| S1P | 1 µM | - |
| *- Added for serum-free/TPA-free assays* | | |
| SDF-1α | 200 ng/mL | - |
| SCF | 200 ng/mL | - |
| IL-3 | 200 ng/mL | - |
| FGF-2 | 200 ng/mL | - |

**Table 1.1. Composition of collagen gels and media used for *in vitro* models of vasculogenesis and sprouting angiogenesis**
According to (Koh et al., 2008b) and (Davis et al., 2013).

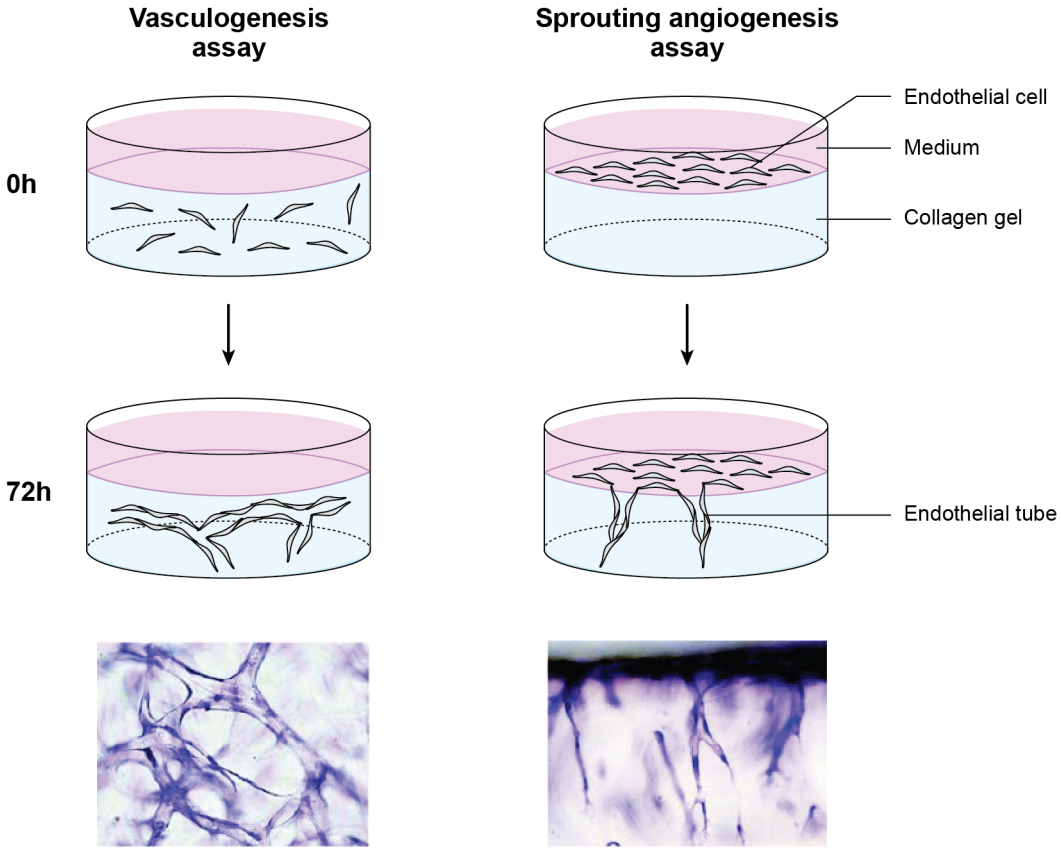


**Figure 1.9. *In vitro* models of vasculogenesis and sprouting angiogenesis, as developed by Davis and colleagues**
In both assays, endothelial cells are plated into (vasculogenesis) or on top (angiogenesis) of type I collagen gels. After 72h of culture, endothelial cells self-assemble into vascular cords, sprout, and lumenise.
Adapted from (Koh et al., 2008b).

### 1.3.2 In vivo models

#### *1.3.2.1 Mouse retina*

One of the most widely used model of sprouting angiogenesis *in vivo* is the development of the primary inner plexus of the mouse retina (Fruttiger, 2007). This vascular network, which starts developing around mid-gestation in humans and around birth in mice, supplies oxygen and nutrients to the inner portion of the retina. Initially, the inner part of the eye is supported by the hyaloid vasculature, a network of arteries running from the optic nerve through the vitreous, and exiting through an annular collection vessel at the front of the eye (Figure 1.10). Around birth, the hyaloid vasculature regresses to be replaced by a vascular plexus growing from the optic nerve below the surface of the retinal tissue. This primary plexus grows radially, from the optic nerve to the periphery of the retina (Figures 1.10 and 1.11), during the first eight days of life in mice, and do so by sprouting angiogenesis following gradients of VEGF secreted by immature retinal astrocytes. While new sprouts arise and connect at the periphery of the plexus, the more central regions mature and organise themselves into networks of arteries, veins and capillaries (Figure 1.11). About one week after birth, a second wave of sprouting from veins, venules and capillaries in venous regions leads to the formation of the deeper plexus of the retina, starting from the centre of the retina and expanding towards its periphery. Vascular sprouts grow towards the inner nuclear layer (INL) of the retina, and change direction sideways at both its upper and lower limits to lead to the formation of two additional networks, parallel to the primary network present at the surface of the retina (Figure 1.10).

The formation and maturation of the primary plexus of the mouse retina established itself as a robust model for the study of sprouting angiogenesis. This model first offers many technical advantages: it benefits from the powerful genetic tools available in mice; it is one of the few vasculatures developing after birth; and its development within one single plane at the surface of the tissue allows easy access and bears potential for high resolution imaging because of the limited working distance (Figure 1.11). Most of all, from a biological point of view, the primary plexus offers the possibility to observe endothelial cells at different stages of the angiogenic process. At

post-natal day 6 (P6), endothelial cells present along the periphery of the growing plexus can be found undergoing, in an asynchronous manner, tip/stalk selection, anastomosis, or lumen formation. Concomitantly, vessels in the most central part of the retina undergo regression and remodel into veins and arteries (Figure 1.11).

Finally, the mouse retina vasculature also offers the possibility to study pathological vessel growth, or neovascularisation, a common feature of blinding eye diseases such as diabetic retinopathy and age-related macular degeneration. A model for oxygen-induced retinopathy (OIR) has been developed, where mouse pups are maintained in hyperoxia chambers then returned to room air, leading to the formation of tuft-like structures made of highly tortuous and leaky vessels that resemble the structures found in human pathologies (Scott and Fruttiger, 2010).

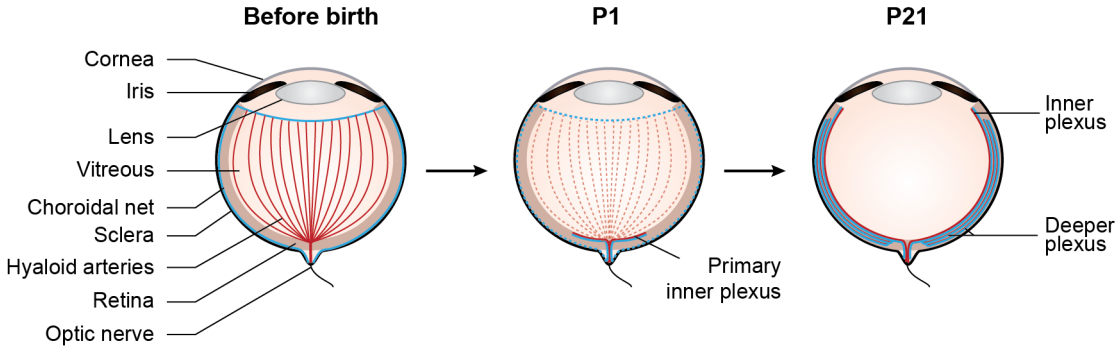


**Figure 1.10. Post-natal development of the mouse retina vasculature**
Before birth, blood is supplied to the eye through hyaloid arteries originating from the optic nerve and drained into collecting veins (choroidal net). At birth, hyaloid vessels regress to be replaced by a primary inner plexus, which expands into the deeper layers of the retina to form the deeper plexus about a week after a birth.

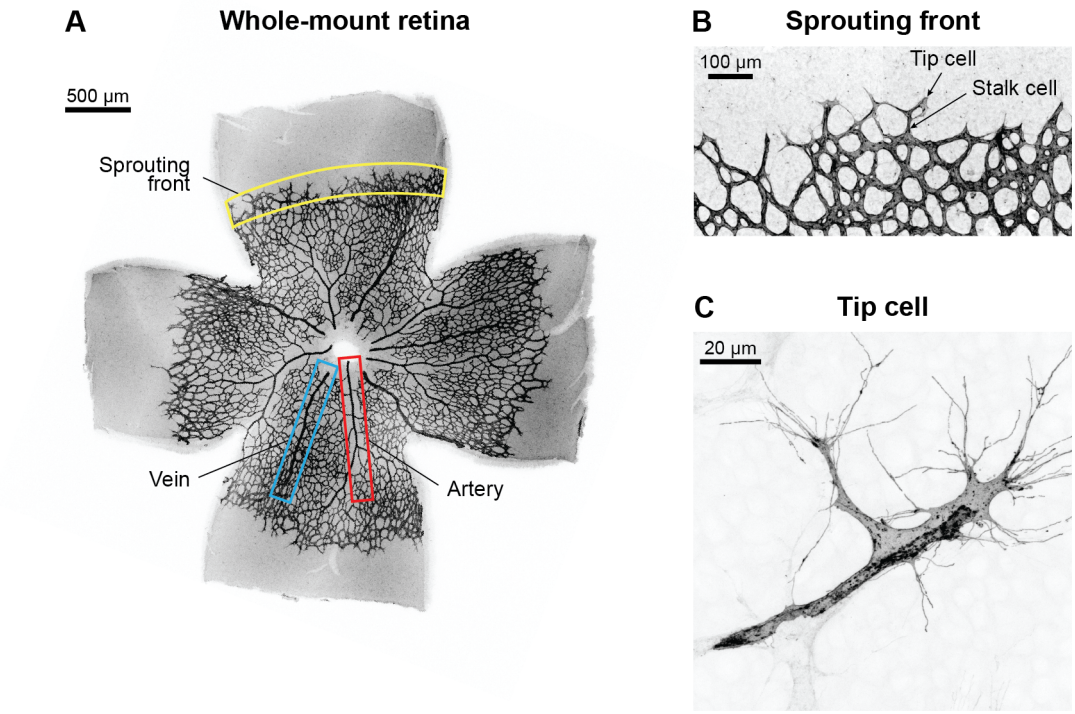


**Figure 1.11. The development of the mouse retina primary inner plexus: a model for high resolution imaging of sprouting angiogenesis**
Harvested at P6, mouse retinas allow the imaging of endothelial cells at all stages of the angiogenic process. The growth of the plexus at the surface of the tissue allows high resolution imaging of single endothelial cells (C). Blood vessels in A and B are immunostained with isolectin GS-$IB_4$. A single endothelial cell expressing membrane-bound GFP is shown in C.

#### *1.3.2.2 Zebrafish*

Although the mouse retina model allowed the identification and in-depth characterisation of the key morphogenetic events and some of the major signalling pathways regulating sprouting angiogenesis, the plasticity and dynamics of endothelial cells called for the development of new models allowing live imaging of their behaviour *in vivo*. In particular, as blood flow quickly appeared as a major regulator of endothelial cell biology, the study of live organisms where blood flow is maintained and can be monitored became necessary.

The zebrafish (*Danio rerio*), a small tropical freshwater fish, established itself as a model of choice for such studies. Zebrafish is a popular model organism in the field of developmental biology due to its small size, short life cycle, and large clutch size. Many genetic tools are now available to generate transgenic reporter and mutant lines. Most importantly, zebrafish embryos bear the advantage of remaining transparent until 2 days post-fertilisation (dpf), allowing non-invasive intra-vital imaging of early vertebrate development.
While the injection of tracers into the circulation of zebrafish embryos allowed the detailed description of its vasculature at different stages of development (Isogai et al., 2001), a major advance in the use of zebrafish as a model for blood vessel development was the engineering of transgenic lines expressing fluorescent proteins exclusively in endothelial cells. Generated through random integration into the genome of the coding DNA sequence (CDS) of standard fluorophores under the control of the promoter regions of endothelial-specific genes, such as *fli1* or *flk1/vegfr2*, these lines allowed the tracking of endothelial cells and the time-lapse imaging of blood vessel formation in developing embryos (Lawson and Weinstein, 2002, Jin et al., 2005).

Vascular development in zebrafish starts around 12-14 hours post-fertlisation (hpf) (Lawson and Weinstein, 2002, Jin et al., 2005, Herbert et al., 2009, Ellertsdottir et al., 2010). Angioblasts start migrating from the lateral plate mesoderm (LPM) on both sides of the embryo towards the trunk midline where they coalesce to form one single vascular cord by 19.5 hpf. Establishment of cell junctions between angioblasts and subsequent lumenisation leads to the formation of the first primordial vessel, the dorsal

aorta (DA), by 22 hpf. Between 21 and 23 hpf, a subset of venous-fated cells sprout ventrally from the dorsal aorta to form the posterior cardinal vein (PCV) by 24 hpf (Herbert et al., 2009). These events lead to the formation of a simple circulatory loop, where blood starts flowing as early as 24-26 hpf. From the heart, blood leaves through the bulbus arteriosus and the ventral aorta to the right and left mandibular aortic arches, which empty into the lateral dorsal aortas (LDAs). LDAs then merge in the cranial trunk to form the DA. In the tail region, the DA and PCV connect as caudal artery (CA) and vein (CV). At this stage, the CV is an intricate mesh of vessels that merge in the trunk into the PCV. In the cranial trunk, the PCV splits into a pair of vessels that each empties across the yolk in the duct of Cuvier, which then connects to the sinus venosus of the heart (Figure 1.12).

From this first circulatory loop, multiple vascular plexi develop through sprouting angiogenesis and have been used to study various stages of the angiogenic process *in vivo*. The most studied network is the trunk vasculature (Figure 1.12), which starts developing around 20-23 hpf (Childs et al., 2002, Isogai et al., 2003). While venous-fated cells in the dorsal aorta migrate ventrally to participate in the formation of the PCV, arterial-fated cells later sprout dorsally to form the intersegmental vessels (ISVs). ISVs sprout from the DA on both sides of the embryo, growing as paired vessels at regular intervals between somites. Passing the notochord and neural tube, ISVs connect to their anterior and posterior counterparts on the same side of the embryo through anastomosis to form the dorsal longitudinal anastomotic vessels (DLAVs) (Figure 1.13). By 40 hpf, this primary network of ISVs and DLAVs is fully lumenised and perfused (Figure 1.12). Concomitantly to DLAV formation, a secondary set of angiogenic sprouts arises at 32 hpf from the dorsal side of the PCV and migrates towards the horizontal myoseptum, where sprouts either connect to ISVs or specify as parachordal lymphangioblasts that will later take part in the lymphatic vasculature. As connections between ISVs and secondary sprouts stabilise and lumenise, the connections of these ISVs with the dorsal aorta regress, leading to a remodelling of the ISV network into arterial ISVs (aISVs) and venous ISVs (vISVs) (Isogai et al., 2003) (Figure 1.13). Although DLAVs remain as two paired vessels in the cranial regions, many anastomotic

vessels form between the right and left vessels in the most posterior region of the embryo (Isogai et al., 2001).

The formation of the primary network of ISVs quickly became a model of choice for the study of sprouting angiogenesis *in vivo*. In particular, reproducibility from embryo to embryo, as well as the fact that multiple sprouts undergo the same morphogenetic events along the trunk of one same embryo, made it suitable for reverse genetic studies aimed at identifying regulators of sprouting angiogenesis *in vivo*. The growth of the ISVs close to the surface of the embryo, and within a relatively thin volume (about 50 μm in depth), also offered advantageous conditions for imaging. Tracing of single endothelial cells during ISV and DLAV formation allowed fine analysis of processes such as cell migration, cell proliferation, cell rearrangements and lumen formation during sprouting angiogenesis *in vivo* (Childs et al., 2002, Kamei et al., 2006, Blum et al., 2008, Wang et al., 2010, Herwig et al., 2011, Phng et al., 2013, Sauteur et al., 2014, Aydogan et al., 2015, Phng et al., 2015, Yu et al., 2015).

Although the trunk vasculature has become the model of reference for the study of endothelial cell sprouting, other vascular plexi developing in early zebrafish embryos have allowed to follow various steps of the angiogenic process *in vivo*. The brain vasculature is, for example, another plexus that develops through a highly stereotypical sequence of morphogenetic events, with multiple vessel connections forming and pruning while the vasculature settles into its final pattern (Figure 1.12). Imaging of the brain vasculature has proved particularly suitable for the study of anastomosis (Lenard et al., 2013) and vessel remodelling (Chen et al., 2012, Kochhan et al., 2013). More recently, detailed description of the remodelling of the sub-intestinal vein plexus (SIV) identified it as a model for the study of vascular pruning (Lenard et al., 2015).

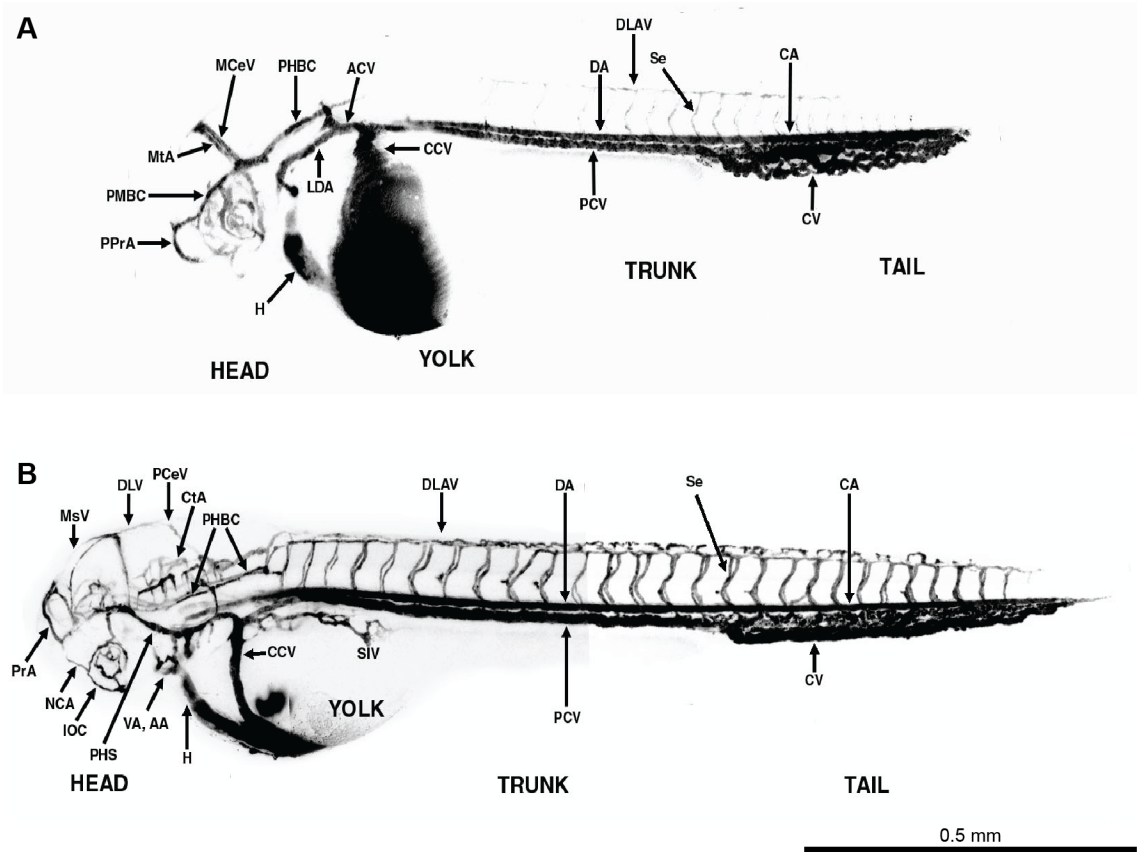


**Figure 1.12. Anatomy of the zebrafish vasculature at 1.5 and 2.5 dpf**
The vasculature of 1.5 (A) and 2.5 (B) dpf zebrafish embryos was imaged by confocal microangiography. Pictures are from The Interactive Atlas of Zebrafish Vascular Anatomy (Isogai et al., 2001). AA, aortic arch; ACV, anterior cardinal vein; CA, caudal artery; CCV, common cardinal vein; CtA, central artery; CV, caudal vein; DA, dorsal aorta; DLAV, dorsal longitudinal anastomotic vessel; DLV, dorsal longitudinal vein; H, heart; IOC, inner optic vesicle; MCeV, middle cerebral vein; MsV, mesencephalic vein; NCA, nasal ciliary artery; LDA, lateral dorsal aorta; MtA, metencephalic artery; PCeV, posterior cerebral vein; PCV, posterior cardinal vein; PHBC, primordial hindbrain channel; PHS, primary head sinus; PMBC, primordial midbrain channel; PPrA, primitive prosencephalic artery; PrA, prosencephalic artery; Se, intersegmental vessel; SIV, subintestinal vein; VA, ventral aorta.

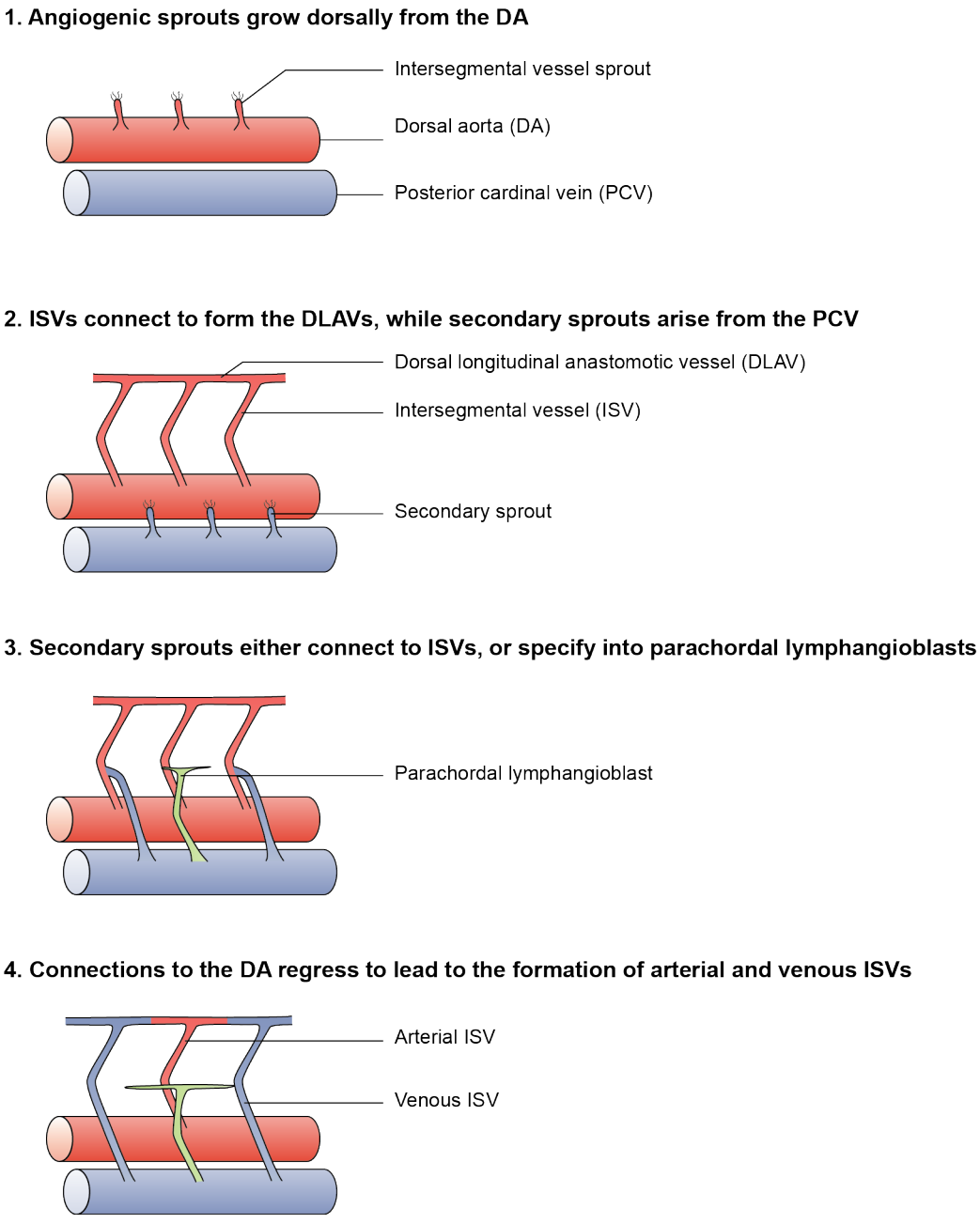


**Figure 1.13. Formation of the trunk vasculature in the zebrafish embryo**
The sprouting of endothelial cells from the dorsal aorta (DA) leads to the formation of a primary network of intersegmental vessels (ISVs). Secondary sprouts growing from the posterior cardinal vein (PCV) either connect to ISVs to form venous ISVs after regression of the connection to the DA, or specify into parachordal lymphangioblasts to later take part into the lymphatic vasculature.

## 1.4 Lumen formation during vascular development

The opening of a lumen is an essential step in the formation of epithelial tubes, and has been the focus of many studies both *in vitro* and *in vivo*. In the following paragraphs, I will present the general principles and main mechanisms of lumen formation identified to date in epithelial tissues, illustrated by key examples in both invertebrate and vertebrate species, to finally give a detailed review of the literature on lumen formation in blood vessels.

### 1.4.1 General principles of apical-basal polarity establishment and lumen formation in epithelial tissues

Biological tubes are found in organs with exchange and/or transport functions, and are made of one or several layers of highly polarised epithelial cells lining a central lumen. Epithelial cells have two distinct membrane domains: an apical domain facing the lumen, and a basal domain in contact with the extracellular matrix (ECM) and underlying cell layers. Both domains are separated by cellular junctions − tight and adherens junctions in vertebrates, septate junctions in invertebrates – which prevent the mixing of the lipid and protein components specific to each domain, and control the overall permeability of the epithelial barrier. Apical-basal polarity is essential for the function of the epithelium. The segregation of specific lipids and proteins between the two domains allows directed and controlled transport of molecules between the apical and basal sides of the cells.

The coordinated acquisition of apical-basal polarity within groups of cells is necessary for the opening of a lumen during the formation of epithelial tissues. Mechanisms driving apical-basal polarity establishment and lumen formation are diverse. Careful analysis and review of these mechanisms in various models of epithelial morphogenesis led to their classification in the following categories: wrapping and budding, where epithelial sheets deform to give rise to epithelial tubes; cavitation, where cells present at the center of a cord die by apoptosis to leave an empty space behind; cord hollowing, driven by the separation of apposing membranes at cell junctions; cell hollowing, with the generation and fusion of large vacuoles within single cells; and finally, membrane

invagination, where lumen expands through the invagination of plasma membrane within single cells (Lubarsky and Krasnow, 2003, Sigurbjornsdottir et al., 2014) (Figure 1.14). It is interesting to note that in the case of wrapping and budding, lumens form from already polarised epithelia, while all other mechanisms require establishment of apical-basal polarity *de novo*. The cellular and molecular basis of these mechanisms is detailed below.

### 1.4.2 Mechanisms of apical-basal polarity establishment and lumen formation in epithelial tissues

#### *1.4.2.1 Lumen formation from already polarised tissues*

##### 1.4.2.1.1 Wrapping

The most common example of lumen formation by wrapping is the formation of the neural tube, or primary neurulation, in vertebrates (Andrew and Ewald, 2010). During embryonic development, a population of cells within the ectoderm germ layer differentiate into neuronal precursors, thus forming the neural plate. At this stage, neuronal precursors are already polarised, with their apical membrane facing the extraembryonic space, and their basal membrane in contact with the underlying mesoderm. Neurulation is the result of active cell shape changes driven by the remodelling of the microtubule and actin cytoskeletons in neuronal precursors. It starts with the coordinated elongation of the cells in their apical-basal axis, a process dependent on the microtubule cytoskeleton (Schoenwolf and Powers, 1987). Subsequently, apical domains constrict through actomyosin contraction and cell divisions maintain nuclei towards the basal side of the cells (Smith and Schoenwolf, 1988), giving rise to wedge-shaped cells and thus allowing the folding of the neural plate. Eventually, the edges of the neural plate come together and fuse to lead to the separation of the neural tube, running parallel to the ectoderm germ layer it originated from (Andrew and Ewald, 2010) (Figure 1.14).

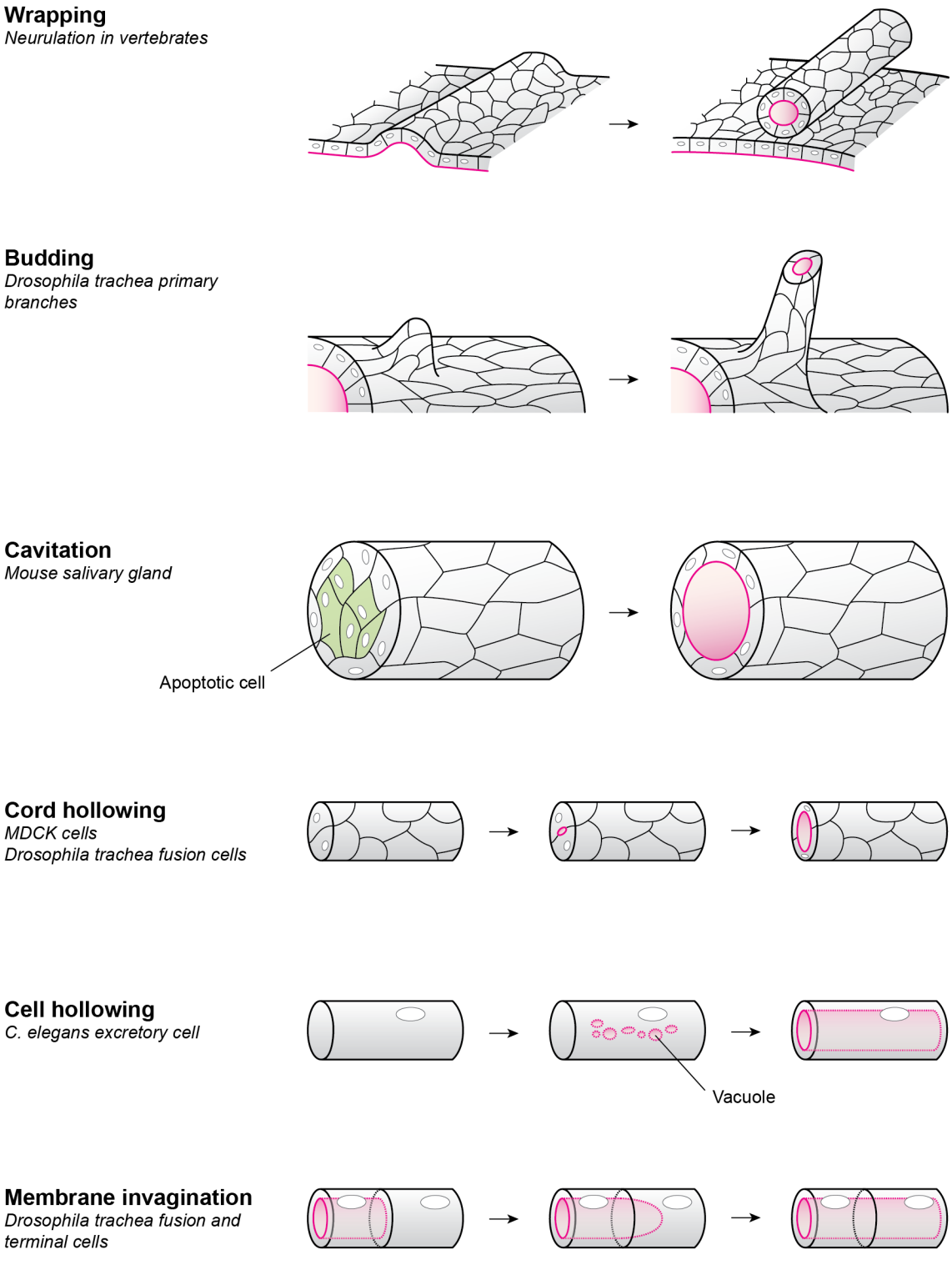


**Figure 1.14. Mechanisms of lumen formation**
Magenta, apical membrane. Black, basolateral membrane. Adapted from (Lubarsky and Krasnow, 2003).

#### 1.4.2.1.2 Budding

Another mechanism of lumen formation involving the reshaping of an already polarised epithelium is the formation of lumens by budding. One example of such a mechanism is the growth of the primary branches of the trachea in *Drosophila melanogaster*. The tracheal system of Drosophila forms from twenty epidermal placodes, ten on each side of the embryo, from which primary tracheal branches emerge through bending of the tissue, generating epithelial invaginations or "buds". Similarly to wrapping, budding is marked by the elongation of groups of about six cells per placode in their apical-basal axis, followed by actomyosin-driven constriction of their apical membrane while nuclei are maintained close to the basal domain, driving the change in cell shape necessary to bend the tissue (Brodu and Casanova, 2006, Sawyer et al., 2010) (Figure 1.14).

#### 1.4.2.1.3 Mechanisms of apical constriction

In both wrapping and budding, lumen formation relies on the constriction of the apical domains of groups of polarised cells to induce the cell shape changes required for local bending of the tissue. Apical constriction is a common mechanism underlying tissue shaping during embryogenesis (Sawyer et al., 2010, Martin and Goldstein, 2014). Although the modalities of apical constriction show some levels of variability between cell types, all rely on the contraction of filamentous actin (F-actin) networks by the molecular motor non-muscle myosin II. In polarised cells, actomyosin networks can be found at the apical membrane in two locations: at junctions, forming an actomyosin belt made of linear actomyosin fibres; and under the apical membrane, as an actomyosin cortex spanning the entire surface of the apical domain. Roles in apical constriction have been described for both networks. Junctional actomyosin belts can drive contraction in a purse-string-like fashion. Dynamic contraction of actomyosin within the cortex can, on the other hand, generate cortical flows and drive constriction of apical domains. In both cases, coupling to cell junctions is critical to reduce apical surfaces and coordinate behaviours between cells in the tissue (Sawyer et al., 2010, Martin and Goldstein, 2014).

Additionally to the spatial control of actomyosin assembly, apical constriction relies on a tight temporal regulation of the contractility of apical actomyosin networks. First reported in Drosophila embryos during mesoderm invagination, actomyosin networks were found to contract in a pulsatile manner during apical constriction, with alternating phases of contraction and stabilisation allowing incremental reduction of the apical surface in a ratchet-like manner (Martin et al., 2009). The role of pulsatile contractions versus continuous deformation remains to be addressed, but is very likely to allow the generation of higher forces and greater exploration of cellular shapes through the stabilisation of intermediate spatial configurations (Levayer and Lecuit, 2012, Martin and Goldstein, 2014).

In the previously described case of neural tube formation, neuroepithelial cells have been found to accumulate F-actin and non-muscle myosin II in an apical belt at their cell junctions, and major efforts have been placed on understanding how the assembly and contraction of this actomyosin network are spatially and temporally controlled during development. Shroom3, an actin-binding protein, has been identified as a major regulator of apical constriction during neurulation (Hildebrand and Soriano, 1999, Hildebrand, 2005). Apically enriched in neuronal progenitors, Shroom3 recruits Rho-associated protein kinase (ROCK) to cell junctions, promoting the formation of actomyosin cables and their contraction through the phosphorylation of the regulatory light chain of non-muscle myosin II (Hildebrand, 2005, Kinoshita et al., 2008, Nishimura and Takeichi, 2008). Recently, an additional level of regulation of ROCK by a set of planar cell polarity (PCP) proteins, possibly through RhoA, was found to restrict its activation to a subset of adherens junctions, therefore allowing the anisotropic shortening of apical domains required for tube formation (Nishimura et al., 2012, Martin and Goldstein, 2014).

Similarly, both F-actin and non-muscle myosin II are found enriched at the apical membrane of tracheal cells during invagination (Brodu and Casanova, 2006). In this system, the enrichment and contraction of actomyosin at the apical membrane is dependent on the expression by invaginating cells of the transcription factor Trachealess, a positive regulator of epidermal growth factor receptor (EGFR) signalling. In turn, EGFR signalling upregulates the expression of the Rho GAP Crossveinless, promoting

apical actin enrichment in part by enabling specific activation of Rho1 at the apical membrane of invaginating cells (Brodu and Casanova, 2006, Affolter and Caussinus, 2008, Sawyer et al., 2010).

Together, these models are great examples of how the specialisation of apical and basal domains in polarised cells allows compartmentalisation of signalling events − here tight regulation of actomyosin assembly and contraction − to drive the cell shape changes required for lumen formation in developing tissues.

#### *1.4.2.2 Lumen formation from non-polarised tissues*

##### 1.4.2.2.1 Cavitation

During cavitation, apoptosis within cords of cells drives the formation of a central luminal space (Lubarsky and Krasnow, 2003) (Figure 1.14). One example of lumen formation by cavitation *in vivo* is the development of the mouse submandibular salivary gland (Wells and Patel, 2010). In this system, epithelial buds first expand as compact clusters of cells, and later undergo lumenisation through the clearing of the cells at the centre of the mass. The initiation of cavitation was found to rely on the relaying of polarisation signals from the extracellular matrix (ECM) to the outermost layer of cells within the bud. Upon attachment to the ECM, these cells establish strong intercellular junctions, and in turn up-regulate cell survival signals. Among those, survivin, a member of the inhibitor of apoptosis (IAP) family of proteins, translocates into the nucleus of polarising cells in the mouse salivary gland, where it prevents caspase activity and apoptosis. Additional anti-apoptotic effectors, such as Bcl-2, NF-κB and receptor interacting protein (RIP), an upstream regulator of NF-κB signalling, were also found to be specifically expressed in the outermost cell layer (Melnick et al., 2001). In contrast, cells in the centre, missing attachment to the matrix and to neighbouring cells, express pro-apoptotic genes and undergo caspase-dependent apoptosis (Melnick and Jaskoll, 2000). In this sense, cavitation is therefore a good example of how the sensing of extracellular polarisation cues is crucial in organising cells within a developing tissue to drive lumen formation.

#### 1.4.2.2.2 Cord hollowing

##### *1.4.2.2.2.1 Madin-Darby canine kidney (MDCK) cyst model*

Cord hollowing refers to the formation of a lumen at the contact between adjacent cells (Figure 1.14), and has been extensively studied *in vitro* in the MDCK cyst model, allowing fine and detailed analysis of the cellular and molecular mechanisms at play during this process (Martin-Belmonte and Mostov, 2008, Datta et al., 2011, Overeem et al., 2015). MDCK cells, when grown in 3D Matrigel matrices, organise themselves into spherical cysts made of a monolayer of epithelial cells surrounding a central lumen and encircled by a basement membrane (Hall et al., 1982). When treated with hepatocyte growth factor (HGF), cysts develop multicellular extensions that later lumenise to form tubular ramifications (Montesano et al., 1991b, Montesano et al., 1991a, Pollack et al., 1998). Both initial lumen formation within the cyst, and subsequent formation of lumens within tubules, happen through cord hollowing.

Upon embedding in 3D matrices, MDCK cells randomly distribute apical and basal markers around their plasma membrane (Figure 1.15). Segregation of apical and basal components happens only upon the entry of the cells into their first division. Basolateral markers such as E-cadherin segregate at the nascent junction between the two daughter cells, while apical markers, such as podocalyxin and Crumbs3a, are internalised in Rab11-positive endosomes and relocalise to the membrane facing the ECM (Schluter et al., 2009, Bryant et al., 2010) (Figure 1.15). There, podocalyxin associates into a complex with $Na^+/H^+$-exchanger regulatory factor-1 (NHERF1)/ezrin radixin moesin (ERM)-binding phosphoprotein 50 (EBP50) and ezrin, whose phosphorylation through polarised activation of RhoA and ROCK1 at the ECM-facing membrane stabilises the complex through coupling to the actin cytoskeleton (Bryant et al., 2014) (Figure 1.15).

Upon completion of cell division, apical-basal polarity is established following a stereotyped sequence of cellular and signalling events. The first step in this process is the internalisation of apical determinants following binding to the ECM. Binding to the ECM through integrin receptors, mainly $\alpha_2\beta_1$ and $\alpha_6\beta_4$ dimers, activates Rac1 at the plasma membrane (Yu et al., 2005, Myllymaki et al., 2011). Rac1, through mechanisms that remain unclear, in turn promotes the secretion and assembly of laminin and thus the formation of a basement membrane at the surface of contact with the ECM (O'Brien et

al., 2001). An other major regulator of laminin assembly is Par1b, which also recruits laminin-binding receptors specifically to the ECM-facing membrane (Masuda-Hirata et al., 2009). Following laminin deposition and binding of specific receptors, downstream signalling, partly via focal adhesion kinase (FAK), recruits p190A-RhoGAP at the plasma membrane, thus limiting RhoA/ROCK signalling, inhibiting the phosphorylation of ezrin and destabilising the podocalyxin/NHERF1/ezrin complex. Subsequent phosphorylation of the complex by protein kinase C (PKC) then drives the internalisation of podocalyxin, and potentially other apical markers such as Crumbs3a, into recycling endosomes that associate to Rab11a to form apical carriers (Bryant et al., 2014) (Figure 1.15).

In a second step, apical carriers are targeted to a region referred to as the apical membrane initiation site (AMIS) at the site of cytokinesis (Bryant et al., 2010) (Figure 1.15). Both microtubule-based and actin-based transport of Rab11a-positive apical carriers have been reported. During telophase, Rab11a interacts with Rab11a family-interacting protein 5 (FIP5) and, through FIP5, to the microtubule-associated molecular motor Kinesin 2, allowing transport to the midbody at cytokinesis (Li et al., 2014a). This directional transport of Rab11-positive vesicles is controlled by the phosphorylation of FIP5 by glycogen synthase kinase 3β (GSK-3β). In metaphase and anaphase, GSK-3β phosphorylates FIP5, preventing its association to the sorting nexin 18 (SNX18), which is necessary for the maturation of recycling endosomes into apical carriers. Dephosphorylation of FIP5 in late telophase allows the generation and transport of Rab11-positive carriers along microtubules to the AMIS (Willenborg et al., 2011, Li et al., 2014b). Rab11a-positive vesicles also undergo actin-based trafficking. Association of Rab11a with the guanine nucleotide exchange factor (GEF) Rabin8 drives the activation and binding of Rab8a to Rab11a at the surface of the vesicles. Rab8a/Rab11a then bind to the actin-based motor protein myosin Vb, driving their delivery to the AMIS. At the AMIS, Rab8a/Rab11a-positive vesicles tether to the membrane through interaction between components of the exocyst complex − Sec15A at the surface of the vesicles, and Sec8 and Sec10 within the AMIS (Bryant et al., 2010). At the AMIS, Rab8a/Rab11a-positive vesicles interact with Rab27a/b and Rab3b, allowing their binding to synaptotagmin-like protein 2a (Slp2a) and 4a (Slp4a), whose

interaction with syntaxin-3 drives membrane fusion and integration of the apical determinants into the membrane (Galvez-Santisteban et al., 2012) (Figure 1.15).

How the AMIS is defined in the first place is still not fully understood. The earliest determinants of the AMIS identified to date are the phosphoinositide phosphatidylinositol (4,5)-biphosphate ($PIP_2$), the phosphatase and tensin homolog PTEN, and the Par polarity complex protein Par3 (Datta et al., 2011). Segregation of phosphoinositides is one of the earliest symmetry-breaking events occuring during apical-basal polarity establishment. While $PIP_2$ gets enriched at the apical membrane, phosphatidylinositol (3,4,5)-trisphosphate ($PIP_3$) is found exclusively at the basal membrane. Both have scaffolding roles and respectively recruit apical and basal determinants through specific phosphoinositide-binding motifs (Martin-Belmonte and Mostov, 2007). Elegant manipulations show that ectopic insertion of $PIP_2$ into the basal membrane leads to the recruitment of apical markers, while the ectopic insertion of $PIP_3$ on the apical side of the cell recruits basal markers, thus showing the central role of $PIP_2$ and $PIP_3$ in identifying and organising the apical and basal domains (Gassama-Diagne et al., 2006, Martin-Belmonte et al., 2007). The segregation of $PIP_2$ and $PIP_3$ between the two domains relies on the presence of PTEN at the apical membrane, where it drives the conversion of $PIP_3$ into $PIP_2$, therefore excluding $PIP_3$ from the apical membrane (Martin-Belmonte et al., 2007). What recruits PTEN to the AMIS is still not fully understood. Interaction between PTEN and Par3 has been reported, and presence of either of these two proteins at the AMIS is required for the proper localisation of the other (von Stein et al., 2005, Feng et al., 2008). Par3 also binds to $PIP_2$, which could explain its early recruitment to the AMIS (Wu et al., 2007, Krahn et al., 2010). Since $PIP_2$ is also involved in cytokinesis, it could be that its concentration at the nascent junction between the two daughter cells is the first signal directing recruitment of Par3, and therefore PTEN, to the AMIS, but this remains to be investigated.

An important role for $PIP_2$ in orchestrating the targeting of apical carriers to the AMIS is to recruit Annexin 2 (Anx2), which in turn targets the small GTPase Cdc42 to the AMIS (Martin-Belmonte et al., 2007). At the AMIS, Cdc42 associates with Par6 and recruits atypical PKC (aPKC) to form the Par complex together with Par3. There, Cdc42 plays an essential role in allowing the exocytosis of apical carriers through interactions with Rab11a/Rab8a (Martin-Belmonte et al., 2007, Bryant et al., 2010)

(Figure 1.15). It is also believed to be involved in the remodelling of the actin cytoskeleton, in part through the recruitment of the inverted formin INF2 (Madrid et al., 2010).

Upon delivery of apical determinants, the AMIS matures into a pre-apical patch (PAP), where apical membranes are defined but no luminal space is present between them (Figure 1.15). The transition from the AMIS to the PAP is marked by the exclusion of Par3/aPKC complexes from the apical membrane, and their relocation to tight junctions, along with junctional proteins and the exocyst complex proteins Sec8 and Sec10 (Bryant et al., 2010). Although it has not been confirmed in this model, extensive work in Drosophila suggests that exclusion of Par3/aPKC could be the result of an antagonism with Crumbs3a, delivered by apical carriers to the AMIS (Datta et al., 2011). Eventually, lumen expands between PAPs, a step for which podocalyxin has been identified as a major regulator. Podocalyxin is a member of the CD34 family of transmembrane sialomucins (Nielsen and McNagny, 2008). Through extensive O-glycosylation and syalylation of their extracellular domain, podocalyxin molecules accumulate negative charges at their surface, conferring anti-adhesive properties responsible for the repulsion of apposing membranes and inhibition of cell-cell contacts (Takeda et al., 2000). Because of the presence in their intracellular domains of binding sites for ERM proteins, podocalyxin and Crumbs3a are also thought to act as bridges to the actin cytoskeleton and allow the separation of luminal membranes through its remodelling (Nielsen and McNagny, 2008, Bulgakova and Knust, 2009, Datta et al., 2011). Detailed analysis of actin organisation during the different steps of lumen formation is however still missing. Finally, fluids are secreted into the lumen through the action of ion pumps and channels. Among those, the $Na^+/K^+$-ATPase and the cyclic AMP (cAMP)-dependent chloride channel cystic fibrosis transmembrane conductance regulator (CFTR) have been found to promote fluid secretion into the lumen (Datta et al., 2011). A role for claudin-15 has also been demonstrated in generating paracellular pores further regulating these fluxes (Bagnat et al., 2007).

The findings mentioned here established a robust model for the establishment of apical-basal polarity at cell junctions *in vitro*. Current and future work will have to address whether these mechanisms are conserved *in vivo* and how they adapt to specific cellular and tissue contexts during development.

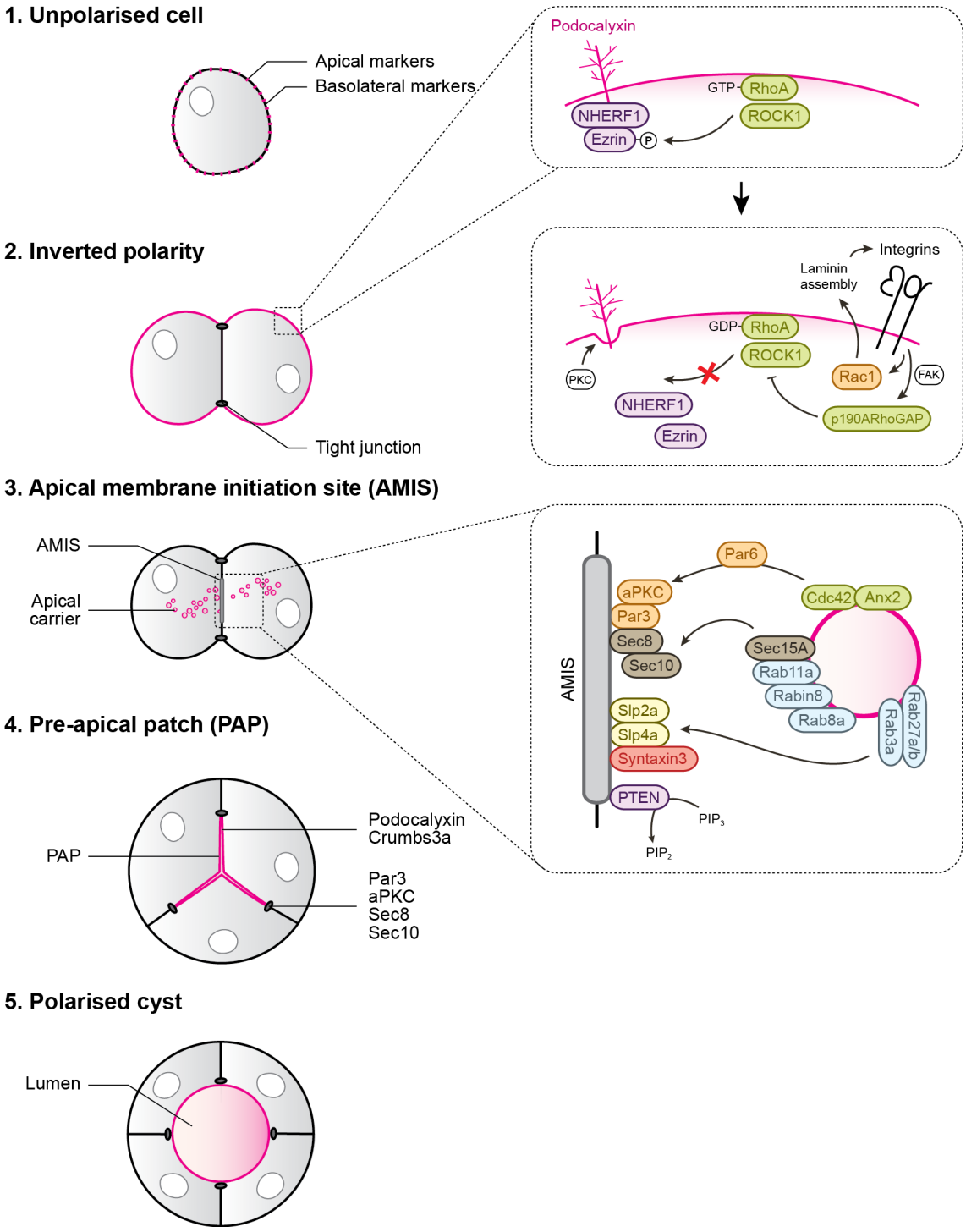


**Figure 1.15. Mechanism of lumen formation by cord hollowing in MDCK cysts**
Adapted from (Bryant et al., 2010, Galvez-Santisteban et al., 2012, Bryant et al., 2014).

*1.4.2.2.2.2 Drosophila fusion cells*

One example of cord hollowing *in vivo* is the formation of lumens between fusion cells during trachea development in Drosophila. Following the formation of primary branches by budding (see 1.4.2.1.2), tracheal branches elongate and connect in stereotyped positions to form a continuous tubular network. Fusion of tracheal branches involves specialised cells at the tip of branches called fusion cells. Similarly to tip cells during blood vessel formation (Figure 1.8), tracheal fusion cells anastomose after establishing a stable cell-cell contact. During anastomosis, fusion cells expand lumens *de novo* at their nascent junction. Concomitantly, lumens expand from their respective stalk cell neighbours, and fusion of all three luminal compartments eventually leads to the full lumenisation of the new connection (Figure 1.16).

Similarly to what has been described for MDCK cells, the site of contact between fusion cells accumulates apical markers as it expands. While aPKC and Crumbs accumulate along the entire contact, forming a structure comparable to the PAP found in MDCK cysts, Par3 localises with Drosophila epithelial cadherin (DE-Cadherin) in a junctional ring around the PAP periphery (Gervais et al., 2012). Subsequently, fusion cells extensively remodel their actin and microtubule cytoskeletons to form a track spanning the entire length of the cells and bridging their two apical domains (Lee and Kolodziej, 2002, Gervais et al., 2012). Additionally to its potential role in adapting the shape of fusion cells to allow the expansion of luminal compartments, the cytoskeletal track is thought to serve as a scaffold for the directed transport of vesicles to apical membranes. Although vesicular trafficking remains challenging to follow *in vivo*, Sec5, a component of the exocyst complex, and the small GTPase Arl-like 3 were found enriched in apical membranes of fusion cells, and co-localised with Rab11-positive vesicles along the cytoskeletal track and at close proximity to the apical membranes (Jiang et al., 2007, Kakihara et al., 2008). Importantly, both Sec5 and Arl-like 3 are required to form lumens in fusion cells (Jiang et al., 2007, Kakihara et al., 2008), suggesting that vesicle fusion might also take part in the formation of lumens in tracheal fusion cells, similarly to what was described in MDCK cysts. Finer analysis would however be needed to fully differentiate mechanisms responsible for *de novo* lumen formation at the site of fusion from the mechanisms regulating expansion of the lumens coming from the stalks.

#### 1.4.2.2.3 Cell hollowing

Certain cells possess the ability of generating lumens *de novo* through the generation and fusion of vacuolar compartments within their cytoplasm, generating an intracellular luminal space (Figure 1.14). One such example is the excretory cell of *Caenorhabditis elegans*. The excretory organ of *C.elegans*, responsible for maintaining the osmotic homeostasis of the organism, is formed by four distinct cell types: one pore cell, one duct cell, one excretory cell, and a pair of fused gland cells. The excretory cell, shaped as an H, extends four lumenised canals that span the entire length of the worm, and drain liquids towards the duct and pore cells. The formation of the lumen within the excretory cell happens through the generation of intracellular vesicles/vacuoles, whose alignment and fusion in the center of the cell and canals lead to the formation, and later expansion, of a central luminal space *de novo*. Genetic screens have identified multiple genes involved in tube formation, extension and maintenance, and their characterisation is still under way (Buechner et al., 1999, Buechner, 2002). Among those, $\beta_H$-spectrin, the intermediate filament IFB-1, and the ezrin homolog ERM-1, were all found to line the apical membrane of the canals and to be required for lumen formation and/or maintenance, highlighting a key role for the cytoskeleton in this process. $\beta_H$-spectrin is thought to link the apical membrane to the actin cytoskeleton. Its loss leads to swollen lumens in larvae and short and dilated cysts in adults, suggesting it is required to maintain lumen diameter throughout the canals (Buechner, 2002). Similarly, loss of IFB-1 leads to the formation of dilated cysts or, even, to the total collapse of the lumen, highlighting a similar function for IFB-1 in maintaining lumen integrity (Kolotuev et al., 2013). Finally, another study identified a crucial role for ERM-1 in regulating vacuole alignment and fusion in the middle of the cell body, possibly by linking the actin cytoskeleton lining the apical and vacuole membranes together during these processes (Khan et al., 2013). Interestingly, this same study identified an interaction between ERM-1 and a water channel, aquaporin 8 (AQP-8), during phases of lumen expansion, and found that water transport through AQP-8 is required for intracellular lumen expansion, thus suggesting a tight cooperation between pressure-building mechanisms and actin-based support in expanding apical membranes in these cells (Khan et al., 2013).

#### 1.4.2.2.4 Membrane invagination

A fourth and last mechanism of *de novo* lumen formation, membrane invagination, was recently defined in light of studies both during trachea development in Drosophila and, as will be detailed later, during blood vessel formation in vertebrates. In this case, lumen expands through the invagination of the lumen from an already lumenised cell into its neighbour (Figure 1.14). Although the definition of membrane invagination as an additional mechanism of *de novo* lumen formation distinct from cell hollowing could appear debatable at first, the present work and detailed analysis of lumen formation in terminal and fusion cells in the Drosophila trachea called for such a distinction (Sigurbjornsdottir et al., 2014).

As presented earlier, following the budding of a set of primary branches, the tracheal system of Drosophila develops from the elongation and fusion of these branches into an interconnected network of respiratory tubes. The formation of a lumen *de novo* at the junction between fusion cells during branch fusion was previously described (1.4.2.2.2.2). This process is tightly coupled to the invagination of lumens from stalk cells on both sides of the fusion site (Caviglia and Luschnig, 2014) (Figure 1.16). Single-cell labelling revealed that most of the lumen in fusion cells is contributed by the stalk cells, pushing into the fusion cells as “fingers poking into a balloon”. This configuration is generated by extensive cell shape changes, as stalk cells elongate and deform fusion cells which undergo extreme compaction. Staining for cell junctions revealed that, similar to what is observed between the two fusion cells, a junctional ring connects stalk cells to their fusion cell neighbour, beyond which a small lumen invagination contributed by fusion cells can be resolved (Figure 1.16). There, vesicular trafficking along the cytoskeletal track (previously described in 1.4.2.2.2.2) contributes to lumen expansion and, later, to the fusion of all three luminal compartments (Gervais et al., 2012, Caviglia and Luschnig, 2014).

Another example of membrane invagination is the formation of the lumen in tracheal terminal cells. Terminal cells form a subset of specialised cells within the tracheal system of Drosophila, and are easily identifiable by the long cellular protrusions they extend to establish large gas exchange surfaces within the surrounding tissues. During development, terminal cells concomitantly undergo extensive elongation and lumen formation (Gervais and Casanova, 2010). Lumens growing in terminal cells are detected

as membrane invaginations originating from the connection of the terminal cells with their parent tracheal branch (Figure 1.16). Single-cell labelling shows that membrane invaginations are entirely generated by terminal cells, and accumulate apical markers (Par3 and DPatj, respectively part of the Par and Crumbs complexes). The presence of a track of F-actin, moesin and microtubules along and ahead of the lumen, and colocalisation of Rab11-positive recycling endosomes and vesicles carrying luminal components, strongly suggests that the formation of the invaginating membrane relies on membrane recycling and trafficking of apical determinants along a cytoskeletal track (Gervais and Casanova, 2010). Eventually, these invaginations grow in diameter, with secretion of chitin forming a transient apical matrix with shaping and stabilising functions (Tonning et al., 2005, Gervais and Casanova, 2010).

#### *1.4.2.3 Concluding remarks*

Together, these studies show how a same morphogenetic event, lumen formation, can be driven by a plethora of different mechanisms depending on the tissue and cellular contexts. A common feature of all these mechanisms is, however, the central role played by the actin cytoskeleton during lumen formation, through its regulation of both cell shape and membrane trafficking between membrane domains. In wrapping and budding, apical constriction is entirely dependent on the assembly and contraction of actomyosin at the apical side of the cells; during cord hollowing, the actin cytoskeleton is essential in driving apposing membranes apart and shaping the nascent lumen; finally, membrane invaginations arise from extensive cell shape changes. On the other hand, the actin cytoskeleton also plays a major role in organising apical and basal domains, by allowing the targeted trafficking of apical and basal determinants and membrane material. How these findings relate to the formation of lumens in the blood vascular system is the focus of the present study.

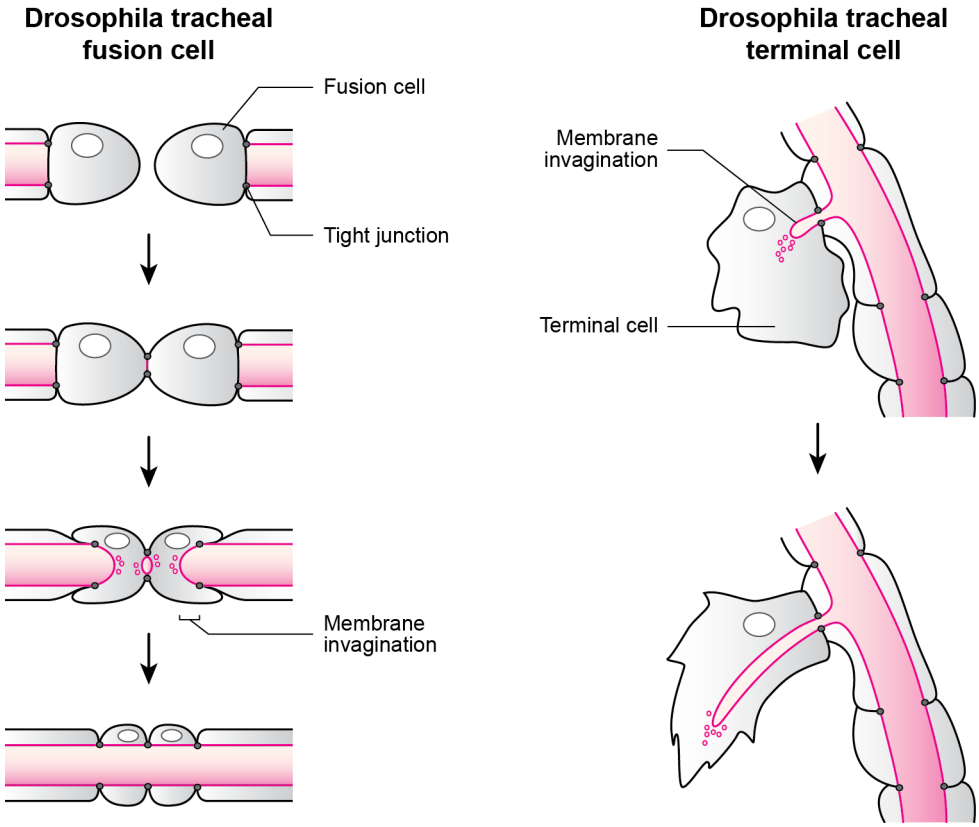


**Figure 1.16. Lumen formation by membrane invagination during trachea formation in Drosophila**
Adapted from (Sigurbjornsdottir et al., 2014).

### 1.4.3 Vascular lumen formation

#### *1.4.3.1 Lumen formation during blood vessel formation in vitro*

##### 1.4.3.1.1 Cellular mechanisms

Vascular lumen formation was first observed *in vitro* by angiogenesis pioneer Judah Folkman. In a 1980 study, he found that both bovine and human capillary cells extracted from various healthy and tumor tissues grow complex vascular networks and undergo lumen formation when cultured on gelatin-coated plates. Imaging of these cells by electron microscopy revealed the presence of large vacuoles in the cytoplasm of endothelial cells as they lumenise, suggesting for the first time that endothelial cells may form lumens through a mechanism of cell hollowing *in vitro* (Folkman and Haudenschild, 1980).

This model was confirmed more than fifteen years later with studies using models of endothelial cell assembly and tubulogenesis in 3D collagen and fibrin matrices (as described in 1.3.1). In this system, endothelial cells were found to lumenise through the generation and fusion of large vacuoles in their cytoplasm. The addition of fluorescent tracers in the culture medium, or labelling of the plasma membrane, showed that these vacuoles arise from the engulfing of culture medium at the ECM-facing membrane, in a process resembling macropinocytosis (Davis and Camarillo, 1996). When cultured at low density, cells are thus able to form unicellular (also referred to as seamless) tubes. On the other hand, cells in contact or in close proximity to each other form multicellular lumens through the generation and fusion of vacuoles at their shared junction (Figure 1.17). Although vacuole formation is systemically associated with lumen formation, it is possible that a mechanism similar to cord hollowing also participates in the opening of a luminal space at cell junctions prior/concomitantly to vacuole fusion, but this remains to be investigated.

##### 1.4.3.1.2 Molecular mechanisms

The development of robust and reproducible assays of *in vitro* vascular lumen formation enabled researchers to investigate the molecular mechanisms at play during this process

(Davis et al., 2011, Sacharidou et al., 2012) (Figure 1.18). Similarly to what was described for epithelial cells, signalling from both cell-ECM and cell-cell interfaces was found to regulate lumen formation in endothelial cells *in vitro*. Binding and signalling through $\alpha_2\beta_1$ integrin is required for lumen formation in collagen matrices (Davis and Camarillo, 1996), while $\alpha_5\beta_1$ and $\alpha_V\beta_3$ integrins mediate lumen formation in fibrin matrices (Bayless et al., 2000). Pericytes also influence lumen maintenance by promoting basement membrane deposition, thus stabilising endothelial tubes through their attachment to components of the basement membrane via $\alpha_5\beta_1$, $\alpha_3\beta_1$, $\alpha_6\beta_1$ and $\alpha_1\beta_1$ integrins (Stratman et al., 2009). On the other hand, expression of both adherens and tight junction proteins – vascular endothelial cadherin (VE-Cadherin) and cerebral cavernous malformation protein 1 (CCM1), and JamB and JamC respectively − was found to be required for lumen formation. VE-Cadherin and CCM1 associate at cell junctions in a complex that is required for the proper localisation of Par3, PKCζ, and the Rho GTPase regulator Tiam1. VE-Cadherin additionally regulates phosphorylation of PKCζ (Lampugnani et al., 2010). JamB and JamC also bind to Par3 (Ebnet et al., 2003), and are required for its recruitment at cell junctions and subsequent lumen formation (Sacharidou et al., 2010).

Rho GTPases play a central role in relaying signalling from the ECM and cell junctions to establish apical-basal polarity in endothelial cells *in vitro*. Both Cdc42 and Rac1 are found at the surface of vacuoles, and have been identified as master regulators of lumen formation (Bayless and Davis, 2002, Koh et al., 2008a). In contrast, RhoA is dispensable for lumen formation, and instead promotes lumen collapse, an effect mediated by ROCK (Bayless and Davis, 2002). During lumen formation, Cdc42 and Rac1 antagonise RhoA activity through the activation of Src and Erk1/2 (Mavria et al., 2006, Im and Kazlauskas, 2007).

Extensive biochemical interaction studies identified the association of Cdc42 and Rac1 with $\alpha_2\beta_1$ integrin, JamB, JamC, Par3, Par6a, Par6b, and the matrix metalloproteinase MT1-MMP in a master regulatory complex (Sacharidou et al., 2010). All individual components of this complex are required for lumen formation *in vitro*, and their recruitment within the complex is dependent on the presence of its other constituents, as loss of any of these proteins leads to its disruption. A number of target kinases were

found downstream of this complex and mediate its effects on lumen formation *in vitro*. These include Pak2, Pak4, Mek1, Erk1/2, Src, Yes, C-Raf, B-Raf, PKCε and aPKC (Sacharidou et al., 2010).
Recently, additional small GTPases (kRas, Rac2, Rap1b), as well as upstream regulators of Rho GTPases (Arhgap31 (inhibitor of Cdc42 and Rac), Arhgap29 (inhibitor of RhoA), Rasa1 (inhibitor of kRas)) and multiple downstream effectors (IQGAP1 and MRCKβ (Cdc42 effectors), beta-Pix and GIT1 (Pak2 binding partners), Rasip1 (Ras and Rap effector)) were further identified and complement the signalling network characterised to date (Norden et al., 2016) (Figure 1.18).

Although the siRNA screens and biochemical interaction assays performed in these studies allowed the identification of key regulators of lumen formation *in vitro*, how these signals orchestrate membrane trafficking events and vacuole formation within endothelial cells is still poorly understood. Unlike in the MDCK cyst model, no role for small Rab GTPases and/or the exocyst complex have been reported, and their possible involvement in membrane remodelling during lumen formation in endothelial cells *in vitro* remains to be investigated. A role for the microtubule and actin cytoskeletons has however been demonstrated, although the distinction between their trafficking and structural/scaffolding functions remains to be addressed. *In vitro*, treatment with microtubule depolymerisation agents prevents lumen formation and induces the collapse of already formed lumens (Bayless and Davis, 2004). A number of microtubule modifying and capping proteins were found to regulate lumen formation *in vitro*. Tubulin acetylation and detyrosination, two marks of microtubule maturation and stability, accumulate during lumen formation, and the deacetylase sirtuin 2 (SIRT2) and histone deacetylase 6 (HDAC6) both negatively regulate lumen formation (Kim et al., 2013). On the other hand, microtubule plus-end-binding proteins EB1, $p150^{Glued}$ and Clasp1 are required for lumen formation upstream of the Pak/Raf/Erk kinase cascade (Kim et al., 2013). Immunofluorescence stainings suggest that acetylated microtubules organise themselves as a subapical network where Cdc42, Rac, kRas and Rap1b GTPases concentrate during lumen formation (Kim et al., 2013, Norden et al., 2016), although further localisation studies will need to confirm these findings. Staining for phalloidin, on the other hand, shows the presence of a dense network of F-actin at the

basal membrane *in vitro*, while significantly lower amounts of F-actin are detected at the apical membrane (Chaki et al., 2015, Norden et al., 2016). Treatment with cytochalasin B, an actin polymerisation inhibitor, prevents lumen formation *in vitro* (Bayless and Davis, 2004). Recently, a role for non-catalytic regions of tyrosine kinase adaptor proteins 1 and 2 (Nck1/2) has been reported during lumen formation *in vitro*. Nck1/2 are adaptor proteins involved in the coupling of tyrosine kinase signalling with the remodelling of the actin cytoskeleton. In 3D collagen matrices, silencing of Nck1/2 disrupts F-actin organisation and VE-Cadherin localisation at cell junctions, preventing the segregation of apical determinants and the fusion of vacuoles (Chaki et al., 2015). These results suggest a role for F-actin in polarity establishment and vacuole fusion. Finer analysis of actin structures and dynamics will however be required to fully understand the role of actin in vascular tube morphogenesis *in vitro*.

#### 1.4.3.1.3 Concluding remarks

Together, these studies identified key molecular regulators of vascular lumen formation *in vitro* (Figure 1.18), some of which were also identified as such during epithelial morphogenesis, both *in vitro* and *in vivo*. In the future, higher resolution live imaging studies will hopefully allow a deeper understanding of how these proteins control morphogenetic events at the cellular level during lumen formation, and how vacuole formation and fusion is regulated during this process.

It has to be noted that all these studies were performed in models mimicking vasculogenesis. *In vitro* models of angiogenesis, on the other hand, have only been used anecdotally for the study of lumen formation, presumably because of the difficulty of setting up and studying such systems in comparison to the ease of use of *in vivo* models such as the zebrafish.

Finally, it is important to point out that *in vitro* systems differ from *in vivo* situations where endothelial tubes are exposed to high flow and blood pressure and rapidly recruit mural cells. Both generate strong apical and basal polarisation cues that are likely to affect the polarisation and lumen formation mechanisms involved in vascular tubulogenesis *in vivo*. Therefore, conservation of the signalling events identified as drivers of lumen formation *in vitro* needs to be carefully addressed.

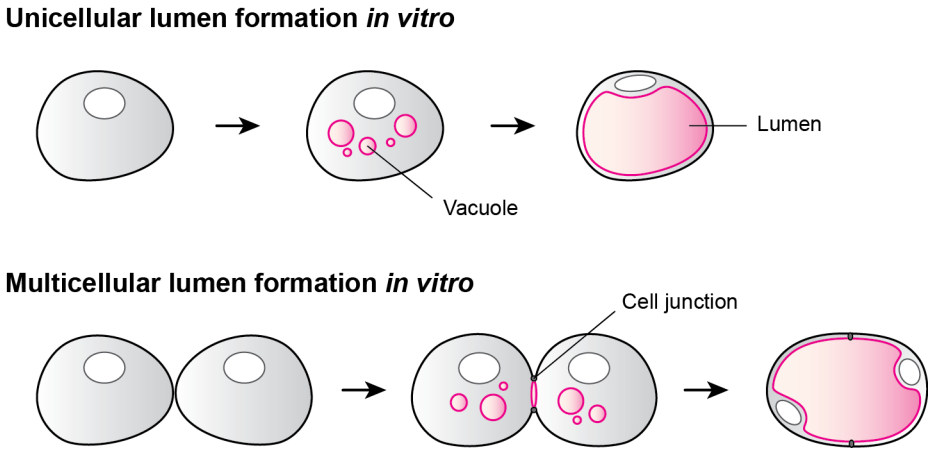


**Figure 1.17. Cellular mechanisms of vascular lumen formation *in vitro***

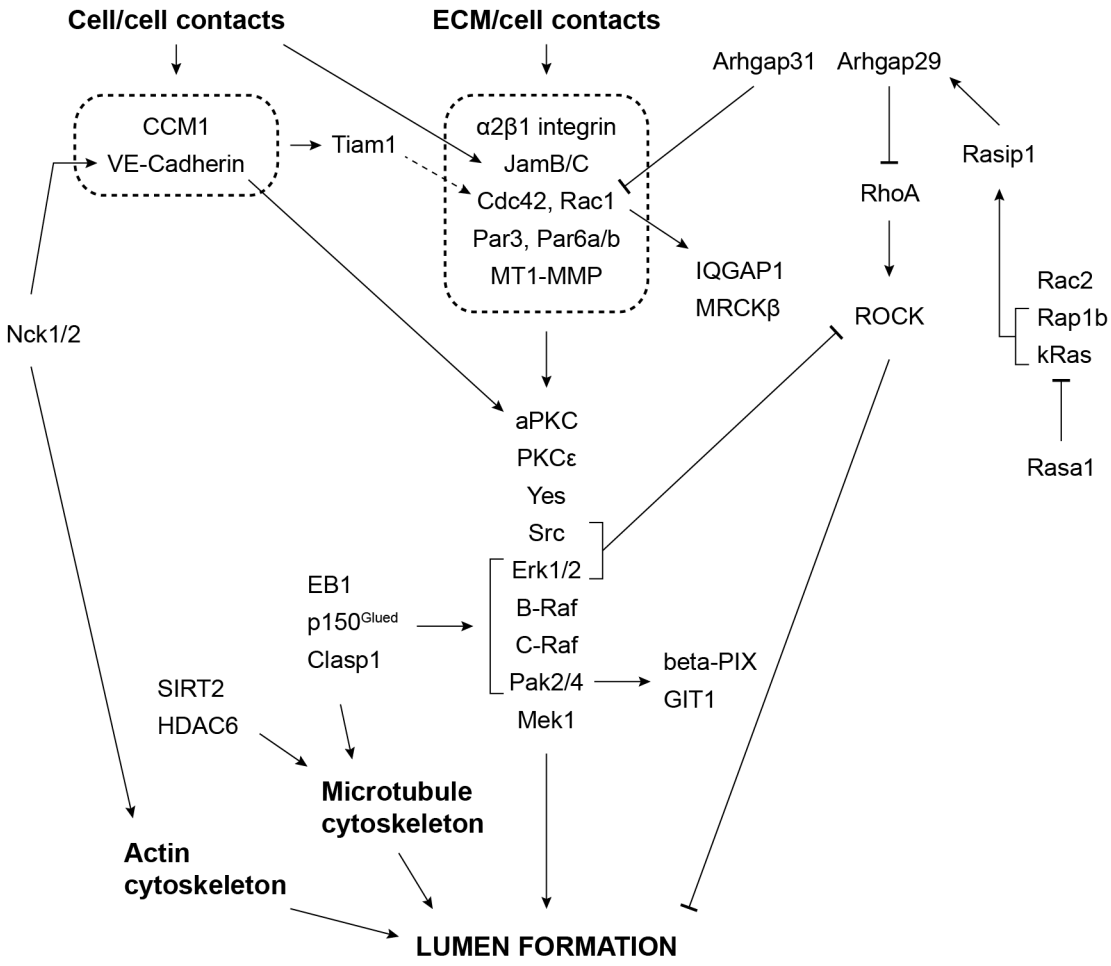


**Figure 1.18. Molecular mechanisms of vascular lumen formation *in vitro***

#### *1.4.3.2 Lumen formation during vasculogenesis in vivo*

Most of our understanding of the mechanisms of lumen formation during vasculogenesis *in vivo* comes from the combination of studies in zebrafish and mouse embryos. While live imaging of transgenic reporter zebrafish lines allowed dynamic analysis of endothelial cell behaviour, the powerful genetic tools available in mice made possible the investigation of the genetic basis of lumen formation *in vivo*. In zebrafish embryos, the dorsal aorta forms directly through the migration and aggregation of angioblasts into one single vascular cord (Lawson and Weinstein, 2002, Jin et al., 2005). In contrast, in mouse embryos, vasculogenesis leads to the formation of a pair of primary dorsal aortae underneath the lateral plate mesoderm, which then migrate towards the midline to fuse and form a single large vessel (Drake and Fleming, 2000, Strilic et al., 2009). Lumen formation in the single zebrafish dorsal aorta and mouse aortae is however driven by similar morphogenetic events.

In zebrafish embryos, angioblasts are detected within the lateral plate mesoderm around 12 hpf, and then migrate to the midline in two consecutive waves at 14 and 16 hpf to aggregate as a cord dorsal to the endoderm and ventral to the hypochord. At 17 hpf, cells establish cell-cell-junctions and by 18 hpf a lumen starts forming by cord hollowing, giving rise to a vascular tube made of 4 to 6 cells in circumference (Jin et al., 2005). This process is accompanied by drastic cell shape changes. Prior to lumen formation, endothelial cells show a cuboidal shape with long lateral junctions. Upon lumen formation, cells elongate in their anteroposterior axis and only maintain thin lateral junctions (Jin et al., 2005, Hultin et al., 2014). Interestingly, this process is independent of blood flow, as lumen formation occurs normally in the dorsal aorta of *silent heart* embryos mutant for the cardiac troponin 2a (tnnt2a) and thus lacking heart beat and blood circulation (Sehnert et al., 2002, Isogai et al., 2003, Hultin et al., 2014). In this context, endothelial cells still elongate and open a patent lumen (Hultin et al., 2014). A similar result was recently obtained in Xenopus embryos, where the ablation of the cardiac region did not prevent normal formation and lumenisation of the dorsal aorta (Charpentier et al., 2015). Together, these studies therefore suggest that the formation of the aortic lumen by cord hollowing, and the observed changes in cell shape, are solely driven by intrinsic mechanisms within the endothelial cells.

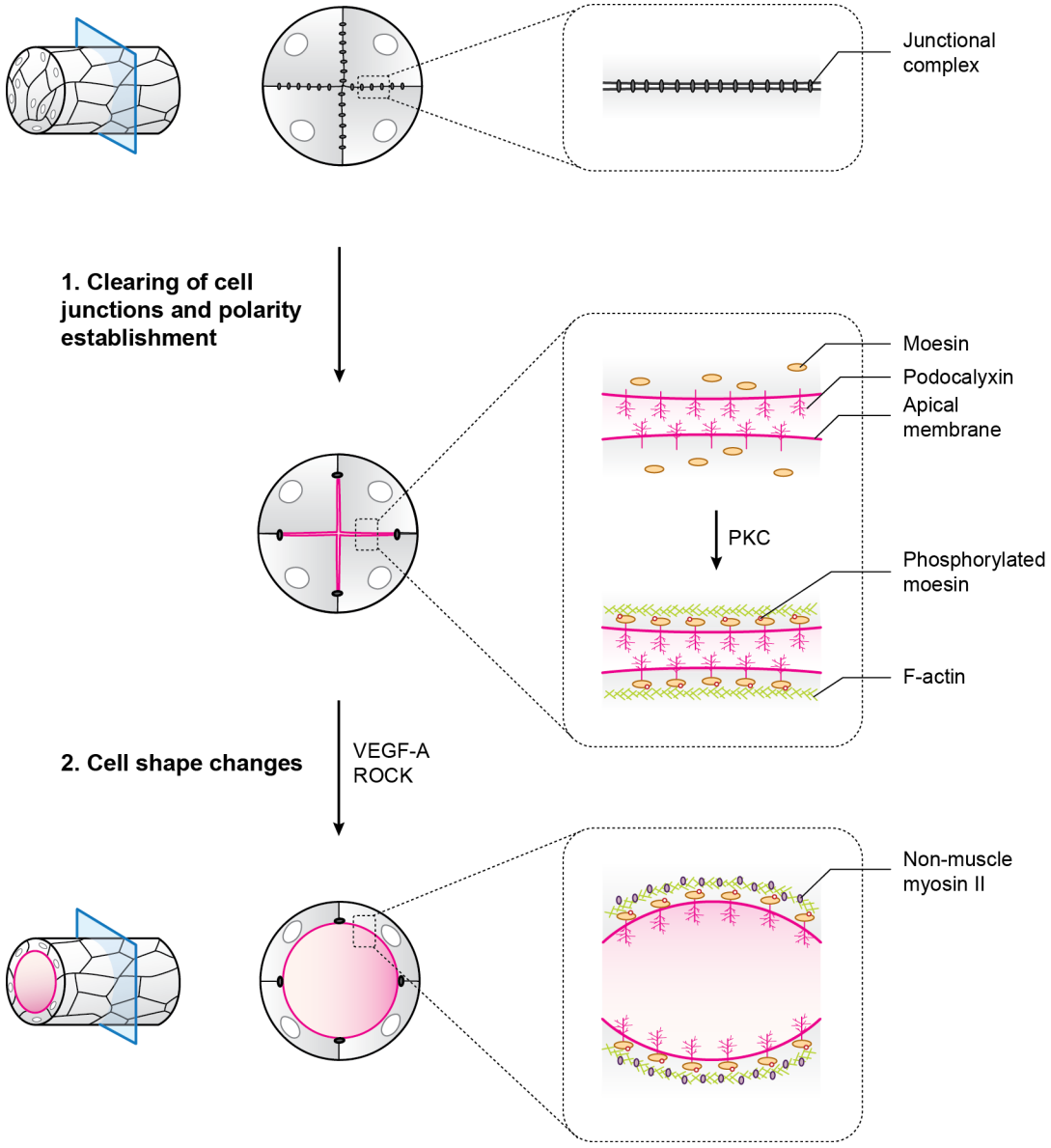


**Figure 1.19. Mechanisms of lumen formation in the mouse dorsal aorta**
Adapted from (Strilic et al., 2009).

Similar morphological events were reported during the formation of the dorsal aorta in mice (Strilic et al., 2009). At the one somite (1S) stage, at embryonic day 8 (E8), endothelial cells are found as clusters sharing extensive junctions. At the 2S stage, junctions are only detected laterally and by the 3S stage, a slit-like extracellular space can be resolved between endothelial cells. From the 3S to 5S stages, lumens larger than 5 μm in diameter open, and enlarge beyond 20 μm at the 6-8S stages as endothelial cells become thinner (Figure 1.19). Together, these observations suggest that the mouse dorsal aorta undergoes cord hollowing following the same morphological events reported in zebrafish embryos. Importantly, no vacuole larger than 0.5 μm is observed during aortic lumen formation in mice, dismissing the hypothesis that lumen could form through a cell hollowing process. Instead, small vesicles are found in the cytoplasm of endothelial cells during the cord-to-tube transition, suggesting that significant vesicular membrane trafficking could participate in lumen formation in this system (Strilic et al., 2009).

Detailed structure and function analysis in mice allowed to identify some of the major molecular events driving lumen formation by cord hollowing in the dorsal aorta. Similarly to what was shown in MDCK cysts, CD34 and podocalyxin sialomucins, found in cytoplasmic vesicles at the 1S stage, accumulate at cell-cell contacts and are then found exclusively at the apical membrane by the 3S stage. Moesin, F-actin and non-muscle myosin II follow the same dynamics: moesin, first cytoplasmic, gets targeted to and phosphorylated at cell-cell contacts; F-actin and myosin II, first present all around the cell membrane, get enriched at junctions; all finally colocalise with podocalyxin at the apical membrane as cells elongate and the lumen opens (Strilic et al., 2009) (Figure 1.19).

Endothelial-specific deletion of VE-Cadherin, podocalyxin and moesin in mouse embryos all lead to failure in aortic lumen formation. In VE-Cadherin knockout embryos, endothelial cells form normal clusters at the 1S stage, but fail to segregate CD34, podocalyxin, moesin, F-actin and non-muscle myosin II at cell-cell contacts. Cells fail to elongate and no patent lumen can be resolved at later stages of development. The knockout of podocalyxin leads to a similar outcome, with diffuse presence of moesin in the cytoplasm and no enrichment of F-actin at junctions. Loss of moesin, or

inhibition of its phosphorylation using panPKC inhibitors, does not affect segregation of podocalyxin but impairs F-actin enrichment at cell junctions. Finally, selective inhibition of myosin II enrichment at junctions through VEGF-A haploinsufficiency or ROCK inhibition does not affect the polarisation of podocalyxin, moesin and F-actin, but lumens fail to form in the affected embryos (Strilic et al., 2009).
Together, these observations suggest a similar model to the one described in MDCK cells, where recruitment of sialomucins at cell junctions allows the separation of apposing membranes through electrostatic repulsion (Strilic et al., 2010), while coupling of podocalyxin to the actomyosin cytoskeleton through phosphorylated moesin, and regulation of actomyosin contraction through VEGF-A and Rho/ROCK signalling, allow the cell shape changes required for the opening of a patent lumen (Strilic et al., 2009) (Figure 1.19).

Similarly to *in vitro*, both cell-ECM and cell-cell contacts have been identified as essential signalling and scaffolding platforms regulating lumen formation in the dorsal aorta. Endothelial-specific deletion of integrin β1 in mice leads to embryonic lethality between E10.5 and E14.5 from severe haemorrhages, with specific occlusion of mid-sized arteries. In these vessels, endothelial cells remain cuboidal in shape, and fail to lumenise. Junctional proteins (Claudin-5, VE-Cadherin, CD99) are found all around the cell membrane and apical polarisation of podocalyxin is lost, suggesting that integrin β1 is required for proper polarity establishment in the dorsal aorta (Zovein et al., 2010). Mislocalisation of Par3 at cell junctions, and accumulation of Rab7-coated vacuoles in the cytoplasm of occluding cells, further suggest conserved roles for the Par complex and membrane trafficking machineries in establishing polarity *in vivo* downstream of integrin signalling (Zovein et al., 2010). Endothelial-specific deletion of Rasip1, a RAP1 effector, additionally supports the idea that attachment to the ECM is required for the transition in cell shape observed during lumen formation in the aorta. *In vitro*, Rasip1 is required for the maturation of focal adhesions, possibly through the recruitment of Arhgap29, a negative regulator of RhoA signalling. *In vivo*, dorsal aortas in Rasip1 knockout embryos fail to lumenise. At the 3S stage, loss of adherence of the endothelial cells to the surrounding mesoderm generates extracellular spaces that grow into large cavities by the 6S stage. Although both podocalyxin and F-actin are found

enriched at the center of the cord, suggesting partial polarisation, junctional complexes and Par3 fail to relocalise laterally, and cells remain cuboidal (Xu et al., 2011). Together, these results suggest that the anchoring of endothelial cells to the ECM is essential for lumen formation in the dorsal aorta.

Remodelling of cell-cell junctions is also critical to the successful opening of lumens during vasculogenesis *in vivo*. As previously mentioned, VE-Cadherin is required for lumen formation and endothelial cell polarisation in the mouse dorsal aorta (Strilic et al., 2009). Additionally, junctions constitute scaffolds for the anchoring of actin fibres, thus orchestrating the cell shape changes driving lumen formation *in vivo*. Angiomotin-like protein 2 (AmotL2), a membrane-associated scaffold protein that couples VE-Cadherin to radial actin fibres in endothelial cells, is required for cell elongation and lumen formation both in zebrafish and mouse embryos. In AmotL2a/b zebrafish morphants, endothelial cells correctly polarise (as seen by the correct segregation of podocalyxin, VE-Cadherin and laminin) but fail to elongate. Interestingly, this correlates with a specific loss of the radial actin fibres connecting the actin cortex at cell junctions, and the overall phenotype is recapitulated by inhibiting actomyosin contraction with blebbistatin. Together with *in vitro* experiments showing that AmotL2 regulates tensile forces at junctions, this suggests a critical role for the contraction of actomyosin fibres anchored at junctions in driving the cell shape changes observed during lumen formation in the dorsal aorta (Hultin et al., 2014). Following its opening, the stability of the aortic lumen also relies on junctional actin dynamics. Additionally to its role as a regulator of endothelial cells attachment to the ECM, Rasip1 was also found to protect lumen integrity by promoting junction maturation: in both zebrafish and mouse embryos, loss of Rasip1 leads to lumen collapse and vascular leakage (Wilson et al., 2013, Wilson and Ye, 2014).

Together, these studies strongly established that lumens form through a cord hollowing process driven by extensive cell shape changes during vasculogenesis *in vivo*. Despite the extensive work carried out *in vitro* showing the ability of endothelial cells to form lumens through vacuole formation and fusion, none of the studies mentioned here were able to report the formation of such structures *in vivo* (Strilic et al., 2009, Xu et al., 2011). Vacuoles were only detected in the context of integrin β1 deficiency, and their

extensive coating with Rab7, a marker for late endosomes and lysosomes, may rather suggest they arise from defective signalling and membrane trafficking downstream of integrins (Zovein et al., 2010).

Interestingly, the molecular events driving lumen formation in the dorsal aorta share striking similarities with the mechanisms identified in the MDCK cyst model and in the Drosophila trachea (see 1.4.2.2.2), highlighting exceptional conservation between organs and species in the mechanisms driving the formation of structures of similar geometry.

#### *1.4.3.3 Lumen formation during sprouting angiogenesis in vivo*

The highly dynamic behaviour of endothelial cells during sprouting angiogenesis made the identification of the mechanisms driving lumen formation in this context particularly challenging to study. Several models emerged, and debate started to arise within the field concerning the origin of vascular lumens in angiogenic sprouts.

In 2006, a first study by Weinstein and colleagues proposed the model that sprouting endothelial cells form lumens through vacuole formation and fusion during sprouting angiogenesis *in vivo* (Kamei et al., 2006). In this study, the authors used two-photon time-lapse imaging of transgenic zebrafish embryos expressing either a reporter for Cdc42 (*Tg(fli1:EGFP-cdc42wt)*$^{y48}$) or RFP tagged with a membrane-targeting farnesylation motif (*fli1:mRFP-F*) to follow lumen formation in sprouting ISVs. Acquiring images every 3-5 minutes, they observed the presence of highly dynamic spherical membrane patterns within the cytoplasm of sprouting endothelial cells, and suggested these structures to be intracellular vacuoles (Figure 1.20). Vacuoles formed, disappeared, and eventually fused to open large luminal spaces, similarly to what could be observed *in vitro* in HUVECs cultured in 3D collagen matrices and expressing the same EGFP-Cdc42 reporter as well as a farnesylated EGFP (EGFP-F) reporter. Based on the idea in the field, at the time, that endothelial cells organised in a head-to-tail fashion in ISVs (Childs et al., 2002), the authors suggested vacuole fusion to lead to the formation of unicellular lumens. However, the lack of single cell labelling did not allow to appreciate whether these vacuoles fused intracellularly, giving rise to hollowed cells,

and/or whether fusion at cell junctions participated in expanding intercellular spaces. Injection of quantum dots into the circulation of the embryos confirmed that vacuoles eventually connected to the main circulation to lead to full lumenisation and perfusion of the newly formed vascular loops (Kamei et al., 2006).

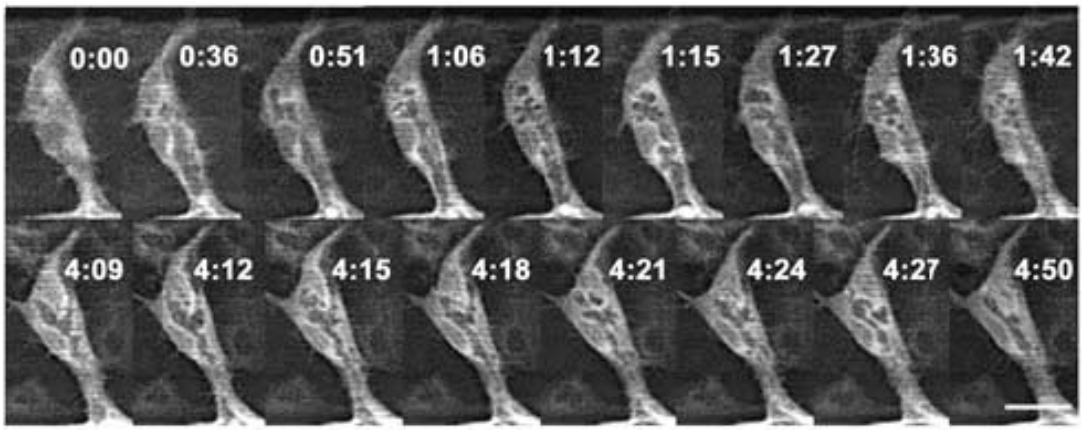


**Figure 1.20. Endothelial tubes assemble from intracellular vacuoles *in vivo***
From (Kamei et al., 2006). "Two-photon time-lapse images of EGFP-positive ventral endothelial cells in growing trunk intersegmental vessels in *Tg(fli1:EGFP-cdc42wt)*$^{y48}$ transgenic animals, showing the emergence of vacuoles and their highly dynamic fusion into a larger intracellular compartment." Time is in hours:minutes. Scale bar is 20 μm.

Vacuoles were only observed in two other studies (Wang et al., 2010, Yu et al., 2015). In 2010, Essner and colleagues observed similar vacuolar structures forming in the cytoplasm of sprouting endothelial cells in ISVs expressing a fluorescent reporter for moesin1 (*Tg(flk1:moesin1-egfp)*). The vacuoles they observed had an average size of 1.08 μm (s.d.: 0.29), rapidly fused with the main luminal compartment, and both unlabelled and labelled vacuoles were found in embryos injected intravenously with dextran, suggesting at least some of these structures arose *de novo* (Wang et al., 2010). Finally, a recent study by Weinstein and colleagues, using single-cell labelling with EGFP-F in zebrafish ISVs and imaging at a rate of one frame per minute, highlighted the coalescence of small membrane vesicles into larger membrane structures that could correspond to vacuoles forming in single sprouting cells. However, the limited duration of the imaging did not allow to follow fusion events and assess whether these structures eventually participated in the expansion of the lumen in the sprouts (Yu et al., 2015).

All other studies investigating lumen formation *in vivo*, using various membrane and cytoskeleton reporters, failed to report the formation of such structures (Blum et al., 2008, Herwig et al., 2011, Lenard et al., 2013, Phng et al., 2015), and the role of vacuole formation and fusion in lumen formation during sprouting angiogenesis *in vivo* is, to date, a debated topic in the field.

In parallel, a consistent body of work revisited the idea that endothelial cells organise themselves in a head-to-tail fashion in angiogenic sprouts (Childs et al., 2002), and suggested major roles for cell junctions in orchestrating lumen formation during sprouting angiogenesis *in vivo* (Blum et al., 2008, Wang et al., 2010, Herwig et al., 2011, Lenard et al., 2013). Using immunostaining for both adherens (VE-Cadherin) and tight (ZO-1) junctions in fixed embryos, Affolter and colleagues carefully analysed endothelial cell organisation within ISVs in the developing trunk of zebrafish embryos (Blum et al., 2008). At 48 hpf, once lumen is formed, ISVs were found to be made of 4 to 6 endothelial cells organised such that several cells surrounded the lumen at any given position along the vessel. During sprouting, while tip cells connected to the stalk of the sprouts through ring-shaped junctions, the rest of the ISVs were found to grow as multicellular structures with longitudinal junctions running along the axis of the entire

sprout (Blum et al., 2008, Wang et al., 2010). Together, these observations started to suggest that the formation of unicellular lumens by vacuole formation and fusion was unlikely to be the sole mechanism driving lumen formation in angiogenic sprouts. Live imaging of transgenic reporter lines for cell junctions (*Tg(fli:GAL4FF;UAS:VE-CadherinΔC-EGFP)*$^{ubs12}$ and *Tg(fli:GAL4FF;UAS:RFP;UAS:EGFP-ZO1)*$^{ubs5}$) allowed to carefully follow the dynamics of cell junctions (Herwig et al., 2011, Lenard et al., 2013), and indeed provided a more complex picture of endothelial cell behaviour during lumen formation in vessels forming through angiogenesis. Focusing on the site of anastomosis between neighbouring ISVs, where the DLAV forms, Affolter and colleagues found that in many instances (37%) junctional rings between connecting tip cells, and between the tip cells and their neighbouring stalk cells, extended longitudinally along the axis of the DLAV prior to lumen formation, to eventually lead to the establishment of new connections between cells from both sides of the vessel, and to the splitting of the former tip cells so that the head-to-tail arrangement was lost (Figure 1.8). Interestingly, podocalyxin was found to accumulate at nascent junctions between tip cells, suggesting their specification as apical domains, and lumen rapidly inflated between cell junctions upon cell rearrangement at the site of anastomosis. On the other hand (in 63% of cases), lumen could be found to expand in single anastomosing cells before cells rearranged, temporarily giving rise to unicellular tubes. Lumen expanded in single cells through the rapid invagination of apical membrane from their junction with their neighbours (Figure 1.8). In all cases observed, cell rearrangements eventually led to the reorganisation of these unicellular lumen portions into multicellular tubes (Herwig et al., 2011, Lenard et al., 2013). Together, these studies strongly established that both uni- and multicellular lumen formation, through membrane invagination and cord hollowing processes respectively, participate to lumen formation during anastomosis.

Interestingly, while the opening of the lumen in the dorsal aorta does not require blood flow and is solely driven by intrinsic cell shape changes (Strilic et al., 2009, Hultin et al., 2014), blood circulation is required both for the invagination of apical membranes into single endothelial cells, and for the separation of membranes between apposing cells during anastomosis. While blood flow is required for the physical opening of the lumen,

cells still rearrange normally and localise podocalyxin at cell junctions in the absence of flow, suggesting that apical-basal polarity is not compromised (Herwig et al., 2011). How blood flow regulates apical membrane expansion and how endothelial cells accommodate blood pressure is not known.

How membrane invagination and cord hollowing processes are regulated during angiogenesis *in vivo*, both at the cellular and molecular levels, still requires considerable investigation. Endothelial-specific deletion in newborn mice of major polarity effectors such as integrin β1, Par3, aPKC, Cdc42, and AmotL2 suggest that these proteins are all dispensable for lumen formation and maintenance during developmental angiogenesis in the mouse retina (Nakayama et al., 2013, Hultin et al., 2014, Barry et al., 2015, Yamamoto et al., 2015), although subtle phenotypes and/or altered endothelial cell dynamics might not be detected in this system. Single-cell labelling and manipulation techniques in zebrafish, combined with high resolution time-lapse imaging, constitute on the other hand powerful tools to build our understanding of these processes. Such studies already identified key roles for VE-Cadherin, moesin1, and junctional F-actin polymerisation through the formin-like protein 3 (FMNL3), in regulating lumen formation and stability during angiogenesis (Wang et al., 2010, Lenard et al., 2013, Sauteur et al., 2014, Phng et al., 2015). In ISVs, F-actin is found as a cortical network supporting the endothelial cell plasma membrane, including the apical membrane, and is particularly enriched at cellular junctions (Wang et al., 2010, Sauteur et al., 2014, Phng et al., 2015). In VE-Cadherin mutant embryos, the F-actin network shows a disorganised architecture, and cells fail to elongate their junctions longitudinally along the vessel axis. Consequently, cells fail to rearrange and mostly stand in a head-to-tail fashion within the sprouts. The same is obtained using a VE-Cadherin reporter lacking the C-terminal binding domain to β-catenin or treating embryos with the actin depolymerisation agent Latrunculin-B (Sauteur et al., 2014), suggesting that VE-Cadherin and its coupling to the actin cytoskeleton are required for the cell shape changes occurring during lumen formation in angiogenic sprouts. Because VE-Cadherin mutant embryos lack blood flow (Lenard et al., 2013), the requirement for VE-Cadherin in lumen formation had to be addressed at the single-cell level. When transplanted into wild-type embryos, VE-Cadherin knockdown cells failed to lumenise (Wang et al.,

2010), suggesting that VE-Cadherin is required for lumen formation during angiogenesis, possibly then through its regulation of cell shape changes in angiogenic sprouts (Sauteur et al., 2014). Additional support to this model comes from a study on FMNL3, an actin nucleator exclusively found at endothelial cell junctions during sprouting. Knockdown of FMNL3 in zebrafish embryos does not alter blood flow, but hinders lumen formation and maintenance while phenocopying the junction elongation and cellular rearrangement defects observed in the VE-Cadherin mutant embryos (Phng et al., 2015). Together, these studies therefore provide strong evidence for a role in cell arrangement in the opening and maintenance of stable lumens during sprouting angiogenesis *in vivo*.

## 1.5 Objectives

An important point of debate in the field is the question of the origin of the apical membrane forming the invagination observed during unicellular lumen formation in angiogenic sprouts *in vivo*. As previously mentioned, vacuoles were suggested to participate in the rapid expansion of the luminal compartment in sprouting endothelial cells *in vivo*. However, work by our own and other groups, focusing on various aspects of endothelial cell biology, and using a variety of reporters for endothelial cell membranes and cytoskeleton components, failed to report the presence of such structures in the cytoplasm of endothelial cells during phases of lumen formation. More importantly, the limited spatial and temporal resolution offered by the studies identifying intracellular vacuoles (hours and minutes) did not seem compatible with the kinetics characterising membrane trafficking events (seconds and milliseconds).

In light of the limits of these studies, my objective was to identify the origin of the apical membrane expanding into single endothelial cells during lumen formation *in vivo*. Because of the need for dynamic information, and the establishment of ISV sprouting in zebrafish as a powerful tool for the study of lumen formation, I decided to follow apical membrane dynamics in this same model where membrane invaginations were previously observed. Following membrane dynamics in sprouting ISVs first required me to establish high spatial (sub-micrometre) and temporal (sub-second) resolution

imaging of endothelial cells. This involved generating appropriate reporters to label the apical membrane of endothelial cells *in vivo*, as well as identifying adapted imaging systems. Although the use of zebrafish as a model organism appeared essential to follow dynamic membrane remodelling events, I also wished to extend my investigations, as far as fixed tissues would allow, to the mouse retina model, to address conservation in mammals, and potentially allow future use of this system to study the genetic basis of the mechanisms identified as driving apical membrane invagination in sprouting cells.

At the same time, I aimed at understanding the role of the actin cytoskeleton in regulating apical membrane expansion during angiogenesis *in vivo*. Because of its established role in forming and shaping apical membranes in all the models of lumen formation presented above, I planned to use high resolution imaging of its dynamics *in vivo*, and chemical and genetic manipulations, to assess its function(s) during apical membrane expansion in angiogenic sprouts.

# Chapter 2. Materials & Methods

## 2.1 Zebrafish experiments

### 2.1.1 Zebrafish care and procedures

Zebrafish (*Danio rerio*) were raised and staged as previously described (Kimmel et al., 1995). Animal procedures were performed in accordance with the United Kingdom's Home Office Animal Act 1986 under the authority of project license PPL 80/2391; animal experiments were approved by LAGeSo (Berlin, Germany) and performed under license number G 0117/15.

### 2.1.2 Transgenic lines

The following transgenic lines were used in this work:

- *Tg(kdr-l:ras-Cherry)*$^{s916}$ (Hogan et al., 2009); drives the expression of the Cherry fluorescent protein tagged with the CAAX motif of human Hras specifically in endothelial cells.
- *Tg(fli1ep:PLCδ-PH-RFP)* (unpublished, generated in our laboratory by Russell Collins); drives the expression of the pleckstrin homology (PH) domain of phospholipase C∂ (PLC∂) fused to RFP specifically in endothelial cells. The PH domain of PLC∂ interacts with phosphatidylinositol (4,5)-biphosphate ($PIP_2$), an early apical determinant in epithelia. The sequence coding for the PH domain of PLC∂ was a gift from Banafshé Larijani (University of the Basque Country, Spain).
- *Tg(fli1ep:EGFP-CAAX)* (unpublished, generated in our laboratory by Ilse Geudens); drives the expression of EGFP tagged with the CAAX motif of human Hras specifically in endothelial cells.
- *Tg(fli1ep:Lifeact-EGFP)* (Phng et al., 2013); drives the expression of Lifeact, a 17-amino acid peptide that binds to F-actin, fused to EGFP specifically in endothelial cells.

### 2.1.3 Transgenesis

Tol2 transgenesis was used to express DNA sequences of interest in zebrafish embryos. The *Tol2* element was first identified in the medaka fish (*Oryzias latipes*) as an autonomous transposon encoding a fully functional transposase. This system was later developed as a transgenesis tool to allow random integration of any DNA sequence of interest flanked by *Tol2* cis sequences into the genome of zebrafish embryos.

Briefly, DNA sequences of interest (including promoter region, coding DNA sequence (CDS) and, if applicable, additional regulatory elements) were cloned using the Multisite Gateway system (Life Technologies) into destination vectors from the Tol2Kit (Kwan et al., 2007) to obtain DNA constructs with the sequence of interest flanked by *Tol2* cis sequences (Figure 2.1). On the other hand, Tol2 transposase mRNA was transcribed from the *pCS-TP* plasmid (Kawakami et al., 2004) using the SP6 mMESSAGE mMACHINE kit (Life Technologies). Zebrafish embryos were then injected at the one-cell stage with 100 pg of Tol2 transposase mRNA and 40 pg of the DNA construct. Translation of the Tol2 transposase mRNA allowed random insertion of the sequence of interest into the genome of the embryos (Figure 2.1). Because of the random nature of the integration events, expression of the transgene was obtained only in single cells throughout the embryo. All experiments mentioning the analysis of embryos with "mosaic expression" of transgenes refer to embryos analysed right after transgenesis, rather than embryos obtained from stable transgenic lines.

### 2.1.4 Cloning and constructs

The following constructs were used for mosaic constitutive expression in zebrafish: *pTol2-fli1ep:EGFP-CAAX* (generated by Ilse Geudens; see map in Appendix), *pTol2-fli1ep:Lifeact-mCherry* (generated by Li-Kun Phng; see map in Appendix).

The LexOP/LexPR system (Emelyanov and Parinov, 2008) was used to generate an inducible reporter for myosin II. Briefly, the LexOP/LexPR system uses a hybrid transcription factor (LexPR transactivator) made of the DNA-binding domain of the

bacterial LexA repressor, a truncated ligand-binding domain of the human progesterone receptor, and the activation domain of the human NF-κB/p65 protein. In presence of mifepristone (RU-486), a synthetic steroid drug, this hybrid transactivator binds to a synthetic operator-promoter harbouring LexA binding sites (*lexOP* promoter), allowing expression of the downstream CDS (Figure 2.2).
This system was implemented in our laboratory by Li-Kun Phng, who designed a *pTol2-fli1ep:LexPR* plasmid (Figure 2.2; see map in Appendix) driving the expression of the LexPR transactivator in endothelial cells, and therefore allowing inducible, endothelial-specific expression of transgenes of interest from a second plasmid using the *lexOP* promoter (unpublished; Figure 2.2; see map in Appendix).

The CDS for the myosin light chain Myl9b was obtained from Source Bioscience (clone I0038156), cloned into a middle entry vector (*pME-myl9b*), and then used along a *p5E-lexOP* 5' entry vector (generated by Li-Kun Phng) and a *p3E-EGFP* 3' entry vector (generated by Russell Collins) to generate a *pTol2-lexOP:myl9b-EGFP* construct (see map in Appendix). *pTol2-fli1ep:LexPR* and *pTol2-lexOP:myl9b-EGFP* plasmids were then co-injected with Tol2 transposase mRNA in one-cell stage embryos. The expression of the *myl9b-EGFP* fusion construct was induced at the onset of lumen formation by treating dechorionated embryos from 26 hpf with 20 µM mifepristone (Sigma, M8046). Green fluorescence could be observed from 3 to 4 hours after the start of the treatment.

In order to generate a dominant-negative form of the Myl9b-EGFP reporter, targeted mutagenesis was performed on the *pME-myl9b* middle entry vector. Based on previous work in cultured mammalian cells (Iwasaki et al., 2001), the following base modifications were introduced using the QuikChange II Site-Directed Mutagenesis Kit (Agilent Technologies): A58G and T61G. These modifications led to the substitution of Alanine for Threonine 18 and Serine 19 in the Myl9b protein, hence its designation as Myl9bAA in this thesis. The *pME-myl9bAA* middle entry vector thus generated was then used to generate a *pTol2-lexOP:myl9bAA-EGFP* dominant-negative reporter construct as previously described.

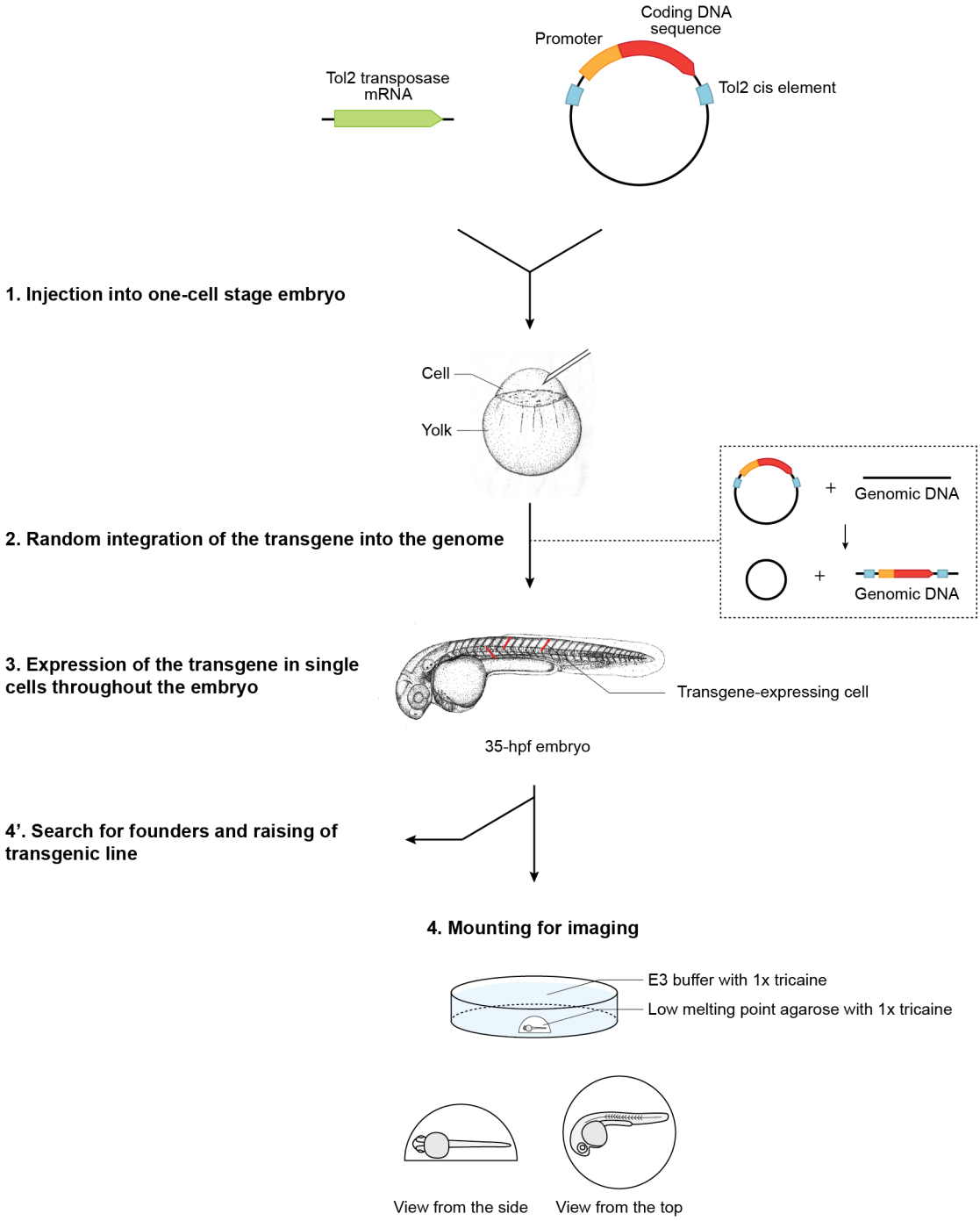


**Figure 2.1. Experimental procedure for live imaging of fluorescent reporters in single cells in zebrafish embryos**
Adapted from (Kimmel et al., 1995) and (Kawakami, 2007).

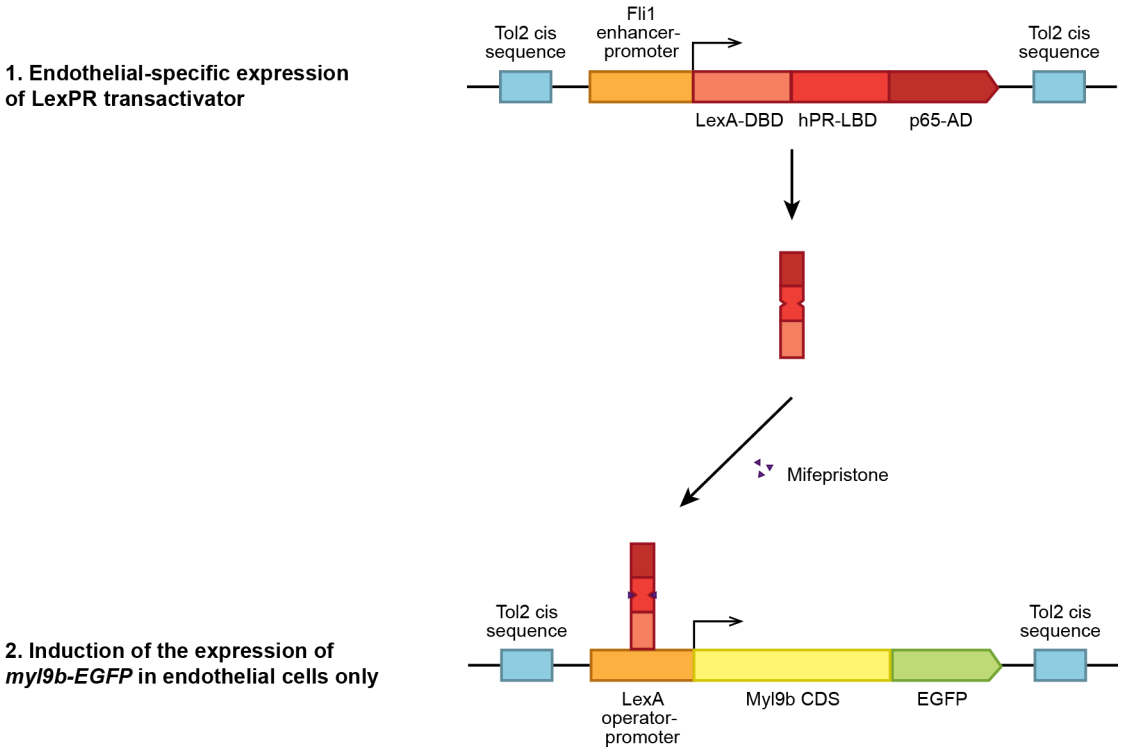


**Figure 2.2. LexOP/LexPR inducible expression system**
Adapted from (Emelyanov and Parinov, 2008).
LexA-DBD, LexA DNA binding domain. hPR-LBD, human progesterone receptor ligand binding domain. p65-AD, p65 activation domain.

### 2.1.5 Embryo preparation for imaging

Embryos were kept in egg water (60 µg/mL Instant Ocean Sea Salts (Cat. #SS15-10) in $dH_2O$) at 28.5°C until processed for imaging.

For imaging, embryos were dechorionated using a pair of fine forceps (Fine Science Tools, Cat. #11254-20), selected for normal morphology, normal heartbeat and presence of circulating red blood cells (indicative of blood flow), and anaesthetised with 0.16 mg/mL (1x) ethyl 3-aminobenzoate methanesulfonate (referred to as tricaine; Sigma, Cat. #E10521). Using a Leica M205 FA fluorescence stereomicroscope, embryos showing expression of the transgene of interest in endothelial cells were selected and transferred to a Petri dish coated with 1% UltraPure™ Agarose (Life Technologies, Cat. #16500-500) and filled with E3 buffer (5 mM NaCl, 0.17 mM KCl, 0.33 mM $CaCl_2$, 0.33 mM $MgSO_4$) supplemented with 1x tricaine.

Embryos were then mounted onto the bottom of 6-cm plastic dishes (Thermo Scientific, Cat. #130181) in single drops of 0.8% UltraPure™ Low Melting Point Agarose (Life Technologies, Cat. #16520-050) in E3 buffer supplemented with 1x tricaine. The amount of agarose used for mounting was kept to a minimum to allow the shortest working distance possible. Embryos were mounted on their side (Figure 2.1), and fine forceps were used until agarose was partially set to keep the embryos from rolling onto their back due to the volume of the yolk. A dozen embryos could be mounted in each dish. Once agarose was fully set, embryos were then covered with 10 mL of E3 buffer with 1x tricaine and brought to the microscope for imaging.

### 2.1.6 Live imaging

Live imaging of zebrafish embryos was performed at 28.5°C on:

- an upright Carl Zeiss LSM 700 confocal microscope using a Zeiss Plan-Apochromat 40x/1.0 NA water dipping objective
- an inverted Andor Revolution 500 spinning disk confocal using a Nikon Plan Apo 60x/1.24 NA water immersion objective, whose access was kindly provided by Pieter Vanden Berghe (Cell Imaging Core Facility, KU Leuven, Belgium)

- an inverted 3i spinning disk confocal using a Zeiss C-Apochromat 63x/1.2 NA water immersion objective, whose access was kindly provided by Thomas Surrey and Nicholas Cade (Francis Crick Institute, Lincoln's Inn Fields Laboratories, London, UK)
- an upright 3i spinning disk confocal using a Zeiss Plan-Apochromat 63x/1.0 NA water dipping objective

Depending on the system capabilities and the needs of the experiment, z-stacks covering the cellular structures of interest were acquired from every 5 seconds to every 15 minutes. Pinhole size (if applicable), gain (if applicable), exposure time (if applicable), and laser power values, were optimised to reach the desired spatial and temporal resolutions while limiting photobleaching and phototoxicity.

### 2.1.7 Laser ablations

Laser ablations of single ISVs or of more defined cellular regions were performed on an upright 3i spinning disk confocal fitted with a Zeiss Plan-Apochromat 63x/1.0 NA water dipping objective using an Ablate™ 532 nm pulse laser, at a theoretical speed of 100 pulses per second and a theoretical energy of 60 μJ. Ablations were performed in single confocal planes along lines spanning the entire thickness of the structures to be ablated (cell body, or membrane and underlying cortex). Laser was applied for 10 ms at 10-20% of the maximum laser power. Ablation of the structures of interest was obtained by performing sequential laser cuts using increasing laser power (starting from 10% with 1% increments, up to 20%) at 5 to 10-second intervals.

### 2.1.8 Image analysis

Images were analysed using the FiJi software (Schindelin et al., 2012). Z-stacks were flattened by maximum intensity projection. XY drifts were corrected using the MultiStackReg plugin (B. Busse, NICHD). Fluorescence bleaching was corrected by Histogram Matching. Kymographs were generated using the MultipleKymograph plugin (J. Rietdorf and A. Seitz, EMBL). Contrast in all images was adjusted in Adobe

Photoshop CS5.1 for visualisation purposes. All images presented in this thesis are representative of the analysed data.

### 2.1.9 Statistical analysis

No statistical method was used to predetermine sample size. The experiments were not randomised. I was not blinded to allocation during experiment and outcome assessment. Statistical analysis was performed with help from Gavin Kelly (Francis Crick Institute, Lincoln's Inn Fields Laboratories, London, UK). A multinomial log-linear model was used to test for association of bleb or cell count in the different defined phenotypic categories with the cell mutation status (WT or AA). The null model was that count variation was only due to experimental batch.

## 2.2 Mouse experiments

### 2.2.1 Mouse care and procedures

Animal procedures were performed in accordance with the United Kingdom's Home Office Animal Act 1986 under the authority of project license PPL 80/2391.
The following mouse strains were used in this study: C57BL/6 and Lifeact-EGFP (Riedl et al., 2010). Lifeact-EGFP mice were genotyped by checking ear biopsies for the presence of bright green fluorescence.

### 2.2.2 Retina dissection

Pups were culled by decapitation at post-natal day 6 (P6). The skin covering the eyes was cut with fine scissors (Fine Science Tools, Cat. #14568-09) and the eyes collected using curved tweezers.

Eyes were then fixed for 1 hour rocking at 4°C in a solution of 4% paraformaldehyde (PFA). 4% PFA solution was prepared by dissolving 40 g of PFA (Sigma, Cat. #441244) in 900 mL of $dH_2O$ heated to 70°C. The solution was then supplemented with

300 µL of NaOH 1M and, once cleared, 100 mL of 10x phosphate buffer saline (PBS; Sigma, Cat. #P5493). pH was adjusted to 7.3-7.4, the final solution filtered, and aliquots frozen and stored at -20°C.

After fixation, eyes were washed once with PBS and kept in PBS on ice until further processing. Retina dissection (Figure 2.3) was performed under a stereomicroscope in a Petri dish filled with PBS. First, the retina was punctured at the limit between the cornea and the sclera using a 26G x 1'' needle (B. Braun, Cat. #16010396E). With the help of fine forceps (Fine Science Tools, Cat. #11254-20) to hold the eye in place, a circular cut was then performed from the puncture hole using spring scissors (Fine Science Tools, Cat. #15000-00). The cornea, lens, iris, hyaloid vessels, and sclera were then removed in this sequence using a pair of fine forceps. Four radial incisions were then made on the extracted retina (Figure 2.3). Retinas were finally transferred to 2 mL Eppendorf tubes with PBS and stored on ice until further processing.

### 2.2.3 Immunofluorescence staining of mouse retinas

Retinas were blocked for 2 hours rocking at 4°C in Claudio's blocking buffer (CBB; 0.5% Triton X-100 (Sigma, Cat. #X-100), 1% bovine serum albumin (BSA; Fisher Scientific, Cat. #BP1600), 2% sheep serum (Sigma, Cat. #S2263), 0.01% sodium deoxycholate (Sigma, Cat. #D6750), 0.02% sodium azide (Sigma, Cat. #S2002)). Retinas were then incubated with primary antibodies diluted to optimised concentrations (Table 2.1) in 1:1 PBS:CBB shaking overnight at 4°C. Retinas were then washed three times for 10 minutes with PBS supplemented with 0.1% Tween-20 (Sigma, Cat. #P2287) (PBST), and incubated for 2 hours at room temperature with secondary antibodies diluted to optimised concentrations (Table 2.1) in 1:1 PBS:CBB. Retinas were then washed three times for 10 minutes with PBST, incubated for 10 minutes in DAPI (Invitrogen, Cat. #D1306) staining solution in PBS, washed once for 10 minutes with PBST, and finally fixed for 10 minutes in 4% PFA solution. Retinas were then kept in PBS at 4°C until processed for mounting.

When isolectin staining of blood vessels was required, retinas were incubated after post-staining fixation for 1 hour at room temperature in PBlec buffer (1% Tween-20, 0.1 mM

$CaCl_2$, 0.1 mM $MgCl_2$, 0.1 mM $MnCl_2$ in PBS, pH 6.8), then overnight at 4°C with isolectin GS-$IB_4$ diluted to optimised concentrations (Table 2.1) in PBlec buffer. Retinas were then washed three times for 10 minutes with PBST, fixed for 10 minutes in 4% PFA solution, then processed for mounting.

Retinas were flat-mounted on glass microscope slides (Thermo Scientific, Cat. #ISO 8037/1) in Vectashield mounting medium (Vector Laboratories, Cat. #H-1000). In order to conserve the 3D architecture of the tissue, slides were covered with one layer of PVC electrical insulation tape (Advance, Cat. #BS EN 60454 Type 2), and a scalpel was used to cut a window where retinas were laid flat, then covered with mounting medium and a glass coverslip (Menzel-Gläser, Cat. #CS2250100).

### 2.2.4 Imaging and image analysis

Samples were imaged with an upright Carl Zeiss LSM 780 microscope using an Alpha Plan-Apochromat 63x/1.46 NA oil objective. Images were analysed using the FiJi software (Schindelin et al., 2012). Z-stacks were flattened by maximum intensity projection. Contrast in all images was adjusted in Adobe Photoshop CS5.1 for visualisation purposes. All images presented in this thesis are representative of the analysed data.

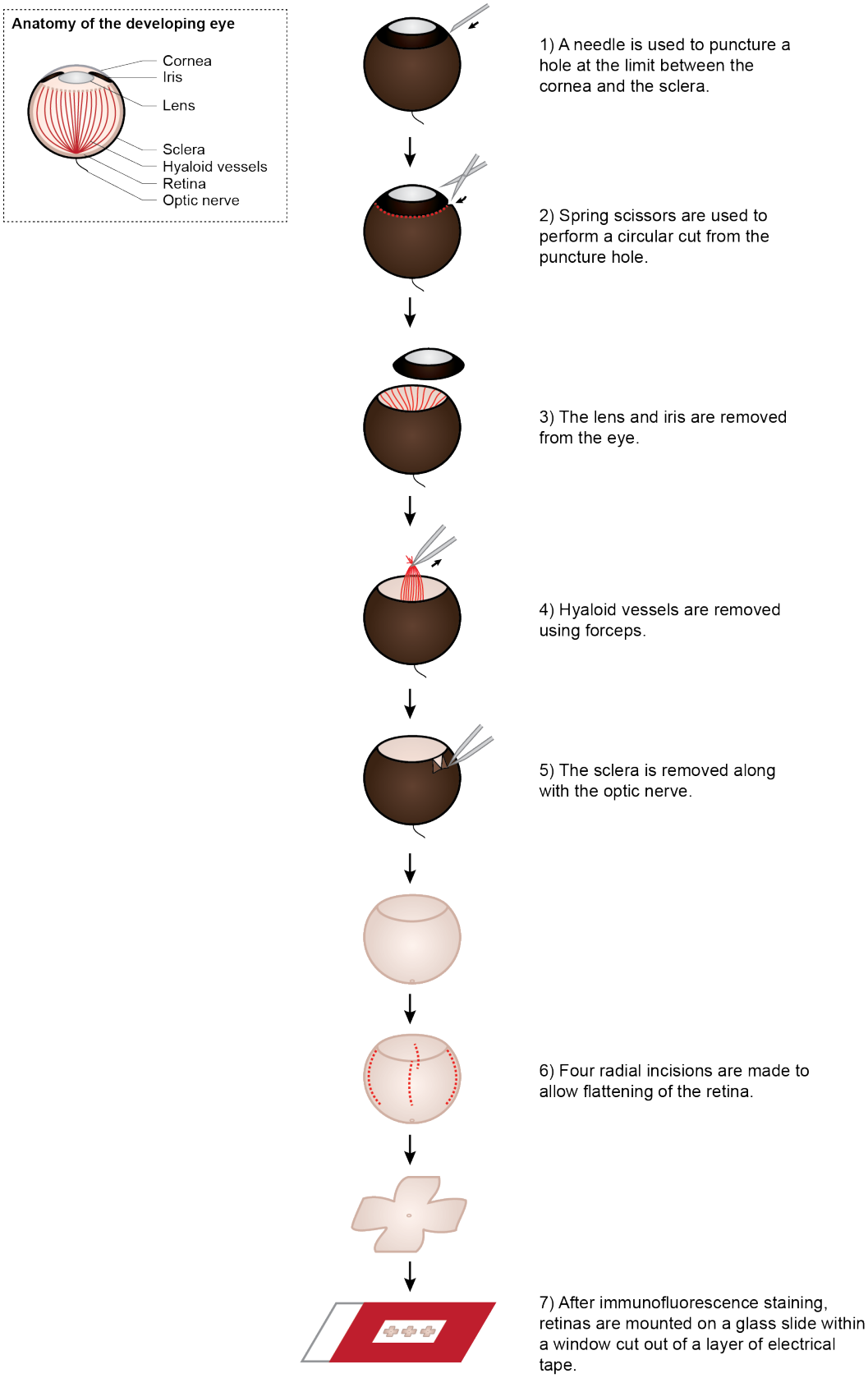


**Figure 2.3. Mouse retina dissection and mounting**

| Antibody | Host | Dilution | Reference |
|---|---|---|---|
| *Primary antibodies* | | | |
| ICAM-2 | Rat | 1:400 | BD Biosciences, Cat. #553326 |
| nmMyosin IIA | Rabbit | 1:100 | Covance, Cat. #PRB-440P |
| pMLC2 | Rabbit | 1:100 | Cell Signalling, Cat. #3671 |
| ZO-1 | Rabbit | 1:400 | Life Technologies, Cat. #61-7300 |
| *Secondary antibodies* | | | |
| Anti-rabbit Alexa Fluor® 488 | Goat | 1:1000 | Life Technologies, Cat. #A-11008 |
| Anti-rat Alexa Fluor® 555 | Goat | 1:1000 | Life Technologies, Cat. #A-21434 |
| *Isolectin* | | | |
| Isolectin GS-$IB_4$ Alexa Fluor® 647 | - | 1:400 | Life Technologies, Cat. #I32450 |

**Table 2.1. List of antibodies used for immunofluorescence staining in mouse retinas**

# Chapter 3. Lumen does not form through vacuole formation and fusion during sprouting angiogenesis *in vivo*

## 3.1 Introduction

Previous studies suggested that lumens form during sprouting angiogenesis *in vivo* through the generation, and later fusion, of intracellular vacuoles in sprouting tip cells (Kamei et al., 2006, Wang et al., 2010, Yu et al., 2015). This process, similar to what has been described and since extensively studied in *in vitro* models of blood vessel formation (Davis et al., 2011, Sacharidou et al., 2012), was suggested to drive lumen formation independently of blood flow (Wang et al., 2010). However, subsequent studies (Herwig et al., 2011, Lenard et al., 2013) failed to observe such structures in a number of zebrafish reporter lines, and started to question the model in which endothelial cells expand lumens through vacuole formation and fusion *in vivo*.

In order to clear this controversy and advance our understanding of the cellular mechanisms driving lumen formation in angiogenic sprouts, and in light of the limits inherent to the aforementioned studies, I decided to establish high resolution imaging of the apical membrane of endothelial cells *in vivo* to follow with high detail apical membrane dynamics during sprouting angiogenesis. This chapter presents the strategy I followed to reach this aim, and the findings I made as a result regarding the mechanisms driving lumen formation during sprouting angiogenesis.

## 3.2 Establishment of high resolution imaging of the apical membrane in *in vivo* models of sprouting angiogenesis

Previous studies suggesting a role for vacuole formation and fusion *in vivo* shared the limit of relying on both low spatial and low temporal resolution in the imaging of these processes. In particular, frame rates of the order of one frame every 3 to 5 minutes did not seem adequate to follow processes as rapid as membrane trafficking and membrane fusion events. Recent studies focused on other aspects of endothelial cell biology such

as junctional dynamics (Lenard et al., 2013, Sauteur et al., 2014, Phng et al., 2015) and vascular remodelling (Lenard et al., 2015) indeed highlighted the importance of performing high resolution imaging in order to draw definite conclusions on the mechanisms at play during such dynamic events.

I decided to establish high resolution imaging of the apical membrane of endothelial cells in two *in vivo* models of sprouting angiogenesis, the post-natal mouse retina vasculature and the zebrafish trunk vasculature. The choice of these two models was based on the points detailed in 1.3. In particular, the mouse retina model offered the highest potential for high spatial resolution imaging, with the vasculature directly accessible at the surface of the tissue, while the use of zebrafish was key to provide temporal information. In addition, I wished to strengthen my study by comparing results in two different models, including a mammalian system.

The establishment of high resolution imaging relied on 1) the selection of markers specific for the apical membrane, and the optimisation of the labelling techniques (as detailed in chapter 2) to obtain high signal-to-noise ratios during imaging, and 2) the choice of appropriate imaging systems.

### 3.2.1 Choice of apical membrane markers

In the mouse retina, my choice turned to the use of antibodies targeting the intercellular adhesion molecule 2 (ICAM-2), a transmembrane glycoprotein expressed at the apical membrane of endothelial cells that binds to lymphocyte function-associated protein 1 (LFA-1), an adhesion molecule expressed at the surface of leukocytes. In mouse retinas collected at post-natal day 6 (P6), all structures staining for podocalyxin, an early apical determinant, were found to also stain for ICAM-2 in endothelial sprouts (Figure 3.1). Since podocalyxin has been identified as one of the earliest determinants recruited at the apical membrane in epithelial tissues (Rodriguez-Boulan and Macara, 2014), including the endothelium (Strilic et al., 2009, Strilic et al., 2010, Herwig et al., 2011), ICAM-2 therefore appeared to be a reliable marker for both early and mature apical structures in endothelial cells. Importantly, in contrast to podocalyxin, immunostaining for ICAM-2 offered very low background signal (Figure 3.1), allowing clear visualisation of the

apical membrane in endothelial sprouts, and therefore making it a marker of choice for the study of lumen formation in mouse retinas.

In zebrafish embryos, expression through Tol2 transgenesis of fluorescent reporters for proteins known to localise at the apical membrane bears the risk of overexpressing functional proteins and thus affecting the biology of the cells. In order to circumvent this event, my choice turned to the use of standard bright fluorophores (EGFP and mCherry) tagged at their C-terminus with a CAAX motif (C standing for cysteine, A for aliphatic amino acid, and X for any amino acid). CAAX motifs are post-translational modification motifs that regulate protein localisation to cell membranes. Briefly, the processing of CAAX sequences through three consecutive enzymatic reactions leads to 1) the addition of a polyisoprene lipid chain to the cysteine, 2) the cleavage of the AAX residues, and 3) the addition of a methyl group at the C-terminus of the protein. This sequence of modifications leads to the formation of a hydrophobic domain that confers affinity for lipid bilayers. CAAX motifs have been shown to regulate protein localisation and associated signalling, one well-studied example being the Ras superfamily of small GTPases (Wright and Philips, 2006).

In the case of endothelial cells, the *Tg(kdr-l:ras-Cherry)*$^{s916}$ zebrafish line (Hogan et al., 2009) has been widely used to study the development of the vasculature, and uses the mCherry fluorophore fused to the C-terminus of the human HRas GTPase to label endothelial cell membranes. By performing high resolution imaging in *Tg(kdr-l:ras-Cherry)*$^{s916}$ embryos, I found that this reporter accumulates at the apical membrane and cell junctions of endothelial cells during lumen formation in intersegmental vessels (ISVs), similarly to a PLC∂-PH-RFP reporter for phosphatidylinositol (4,5)-biphosphate ($PIP_2$), an early apical determinant in epithelia (Figure 3.2 a,b). The mCherry-CAAX reporter additionally only suffered from limited photobleaching (data not shown).

A second zebrafish line expressing EGFP tagged with the CAAX motif from HRas under the control of the endothelial-specific *fli1ep* promoter (*Tg(fli1ep:EGFP-CAAX)*) was generated in our laboratory by Ilse Geudens (KU Leuven), and showed the same localisation at the apical membrane and cell junctions (Figure 3.2 c).

Together, these experiments established ICAM-2, and EGFP-CAAX and mCherry-CAAX, as good reporters for the apical membrane of endothelial cells in mouse retinas and zebrafish ISVs, respectively.

### 3.2.2 Choice of imaging systems

The imaging of mouse retinas was performed using an upright Carl Zeiss LSM 780 confocal laser scanning microscope using an Alpha Plan-Apochromat 63x/1.46 NA oil objective. Although the theoretical resolving power of the lens was 174 nm at a wavelength of 509 nm (emission maximum for EGFP), in practice the XY resolution achieved was estimated at 200-300 nm, due to factors such as light scattering and noise. Images were sampled at 0.132 µm/pixel with fields of view of 135x135 µm. Together, these parameters made possible the visual separation of apical and basal membranes in lumenised vessels (Figure 3.1) and, in theory, the observation of sub-micrometre structures such as membrane vesicles (not shown). Z-stacks were acquired with 1-µm steps.

For live imaging of zebrafish embryos, additional elements needed to be taken into consideration. While previous studies looking at apical membrane dynamics during endothelial cell lumenisation used frame rates of one frame every 3 to 5 minutes (Kamei et al., 2006, Wang et al., 2010), my aim was to reach a temporal resolution in the order of seconds to follow processes as fast as vesicular trafficking. Additionally, photobleaching and phototoxicity had to be reduced to the minimum in order to allow such rapid imaging over a period of several hours.
These considerations led me to choose spinning disk confocal microscopy for imaging in zebrafish. After testing and using several systems (see details in chapter 2) over the course of this work, the best resolution was obtained, and most of the experiments presented in this thesis were performed, using an upright 3i spinning disk confocal microscope using a Zeiss Plan-Apochromat 63x/1.0 NA water dipping objective. This system offered reduced photobleaching and undetectable phototoxicity. The theoretical resolving power of the lens was 255 nm at a wavelength of 509 nm, although in practice the XY resolution achieved was estimated at 300-350 nm. Images were sampled at 0.1

μm/pixel with fields of view of 135x135 μm. This allowed clear visualisation of the apical membrane in sprouting ISVs (Figure 3.2). Z-stacks were acquired with 1-μm steps. Importantly, both the EGFP-CAAX and mCherry-CAAX reporters could be imaged at a rate of up to 5 frames per second.

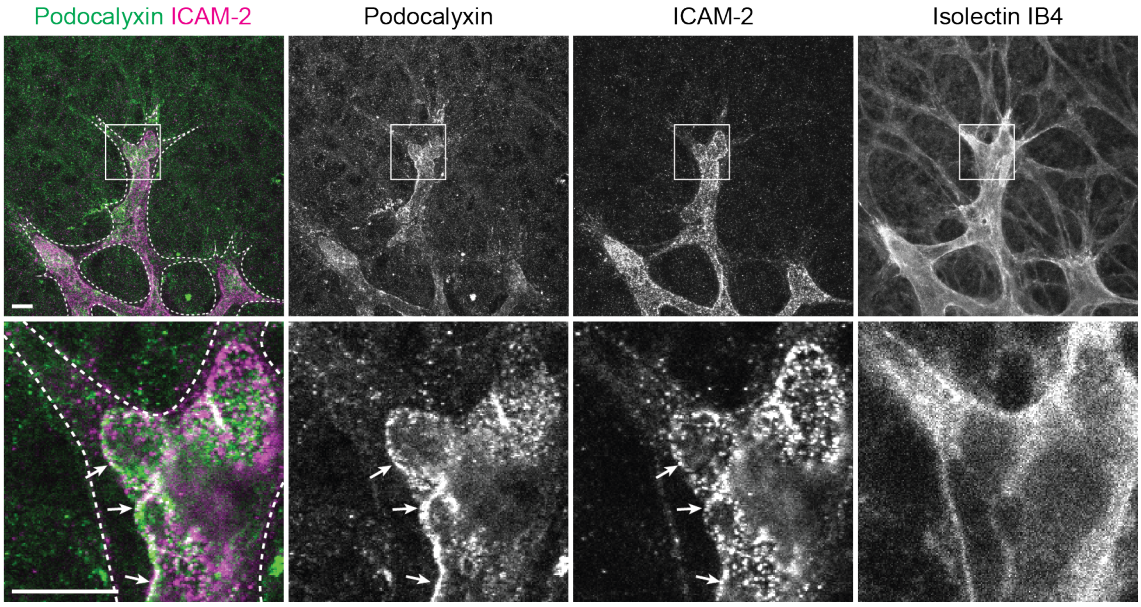


**Figure 3.1. ICAM-2 is a specific marker for the apical membrane in mouse retinas**
Wild-type mouse retinas were collected at P6 and stained for podocalyxin (green), ICAM-2 (magenta), and isolectin $IB_4$. Isolectin $IB_4$ staining was used to delineate the outline of the cell (white dotted line). Top panels are maximum intensity projections. Bottom panels are single z planes. Arrows show co-localisation of podocalyxin and ICAM-2 at the apical membrane. Scale bars are 10 µm.

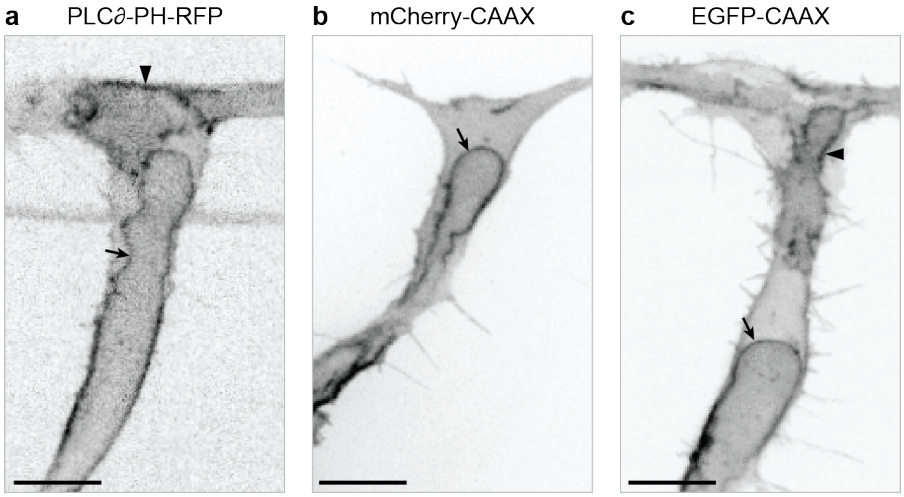


**Figure 3.2. mCherry-CAAX and EGFP-CAAX localise to the apical membrane and cell junctions in sprouting ISVs**
*Tg(fli1ep:PLCδ-PH-RFP)* (a), *Tg(kdr-l:ras-Cherry)*$^{s916}$ (b) and *Tg(fli1ep:EGFP-CAAX)* (c) zebrafish embryos were imaged between 32 and 36 hpf. Arrows show localisation of the reporters at the apical membrane. Arrowheads show localisation at cell junctions. Scale bars are 10 µm.

## 3.3 Lumen does not expand by vacuole formation and fusion in angiogenic sprouts *in vivo*

The apical markers and imaging systems thus identified allowed to image the apical membrane of sprouting endothelial cells in the mouse retina and in zebrafish ISVs with both high spatial and high temporal resolution, and to investigate the cellular morphogenetic events leading to lumen expansion in angiogenic sprouts.

In order to assess whether lumens expand through vacuole formation and fusion *in vivo*, P6 mouse retinas were stained for ICAM-2 and sprouting endothelial cells were screened for the presence of such cellular compartments. From n=487 sprouts analysed in N=9 retinas, only 8 sprouts (1.6 %) showed the presence of large disconnected lumen fragments (Table 3.1 and Figures 3.3 and 3.4 a), suggesting it is very unlikely that the generation of such structures *de novo* is the main mechanism driving lumen formation in the mouse retina vasculature. Importantly, some of these fragments were found to retain what seemed to be white blood cells (Figure 3.4 a, white arrowhead), suggesting these fragments were previously perfused and likely the result of the collapse of pre-existing lumens.

Imaging of *Tg(kdr-l:ras-Cherry)*$^{s916}$ zebrafish embryos from 30 hours post-fertilisation (hpf) supported this hypothesis, and showed that large lumen fragments arise during ISV lumenisation following the collapse of already-formed lumens (Figure 3.4 b). Further imaging showed that these fragments later reconnect to the growing lumen (Figure 3.4 b), or collapse into smaller membrane fragments. More importantly, no vacuole was found to form *de novo* in any of the cells analysed in these experiments (n=10), nor in any of the other experiments presented in this thesis, using a range of reporters for endothelial cell membrane, cytoplasm, and cytoskeleton components.

Together, these results strongly suggest that angiogenic sprouts, both in the mouse retina and in the zebrafish trunk vasculature, do not expand through vacuole formation and fusion.

## 3.4 Lumen expansion is dependent on blood pressure

Whereas it is well established that lumens form independently of blood flow during dorsal aorta formation (Jin et al., 2005), previous studies suggested both flow-independent and flow-dependent lumen formation in ISVs (Wang et al., 2010) and during anastomosis (Herwig et al., 2011, Lenard et al., 2013), respectively. To test whether lumen expansion in angiogenic sprouts requires blood perfusion, *Tg(kdr-l:ras-Cherry)*$^{s916}$ embryos were treated with a four-fold higher dose of tricaine methanesulfonate (4x tricaine) than the dose normally used for anesthesia. Under these conditions, embryos show lower heart rate, loss of blood flow and decreased blood pressure (Lenard et al., 2013). Upon the addition of 4x tricaine mid-way through ISV lumenisation, lumens did not expand further and eventually collapsed (Figure 3.5). However, when placed back in 1x tricaine at 2 days post-fertilisation (dpf), the embryos recovered normal heartbeat, blood flow was re-established (as assessed by the presence of circulating red blood cells) and lumens expanded through the ISVs. Control embryos kept in 1x tricaine for the whole duration of the experiment lumenised normally from 30-35 hpf, while embryos kept in 4x tricaine remained unlumenised (Figure 3.5). Together, these data show that lumen expansion in endothelial sprouts is dependent on cardiac activity and on the presence of blood flow.

## 3.5 Conclusions

As described above, I was able to establish both high spatial (sub-micrometre) and high temporal (sub-second/minute) resolution imaging of lumen formation in two different *in vivo* models of sprouting angiogenesis, the mouse retina vasculature and the zebrafish trunk vasculature. Data obtained from the imaging of lumenising endothelial cells in both models led me to challenge the current model proposed by Weinstein and colleagues (Kamei et al., 2006, Yu et al., 2015) in which they suggest that lumens form during sprouting angiogenesis *in vivo* through the formation and fusion of intracellular vacuoles. Following in detail apical membrane dynamics in single endothelial cells, and using reporters bearing no biological function, I was not able to observe the formation *de novo* of any vacuole in the cytoplasm of lumenising cells, but instead found that

lumen fragments only occasionally arise from the collapse of pre-existing lumens. Additionally, in contradiction to their proposed model, I found that lumens did not expand in the absence of blood flow, suggesting a mechanism of lumen expansion driven by blood pressure in angiogenic sprouts *in vivo*.

| | Uni-cellular | **% of total unicellular** | Multi-cellular | **% of total multicellular** | Total | **% of total lumens** |
|---|---|---|---|---|---|---|
| Expanded | 33 | **57.9** | 302 | **70.2** | 335 | **68.8** |
| Constricted | 17 | **29.8** | 119 | **27.7** | 136 | **27.9** |
| Disconnected | 7 | **12.3** | 1 | **0.2** | 8 | **1.6** |
| Closed | 0 | **0** | 8 | **1.9** | 8 | **1.6** |
| Total | 57 | **100** | 430 | **100** | 487 | **100** |
| **% of total lumens** | **12** | | **88** | | | |

**Table 3.1. Quantitative analysis of lumen conformations in endothelial sprouts in P6 mouse retinas**
Wild-type P6 mouse retinas (N=9) were stained for ICAM-2 and ZO-1. Endothelial sprouts (n=487) were screened by eye and classified into different categories according to the conformation of the lumen in these sprouts (expanded, constricted, disconnected, or closed; for representative examples see Figure 3.3), and on whether these lumens were observed as invaginations into single endothelial cells (unicellular) or were shared between several cells at the tip of the sprout (multicellular).

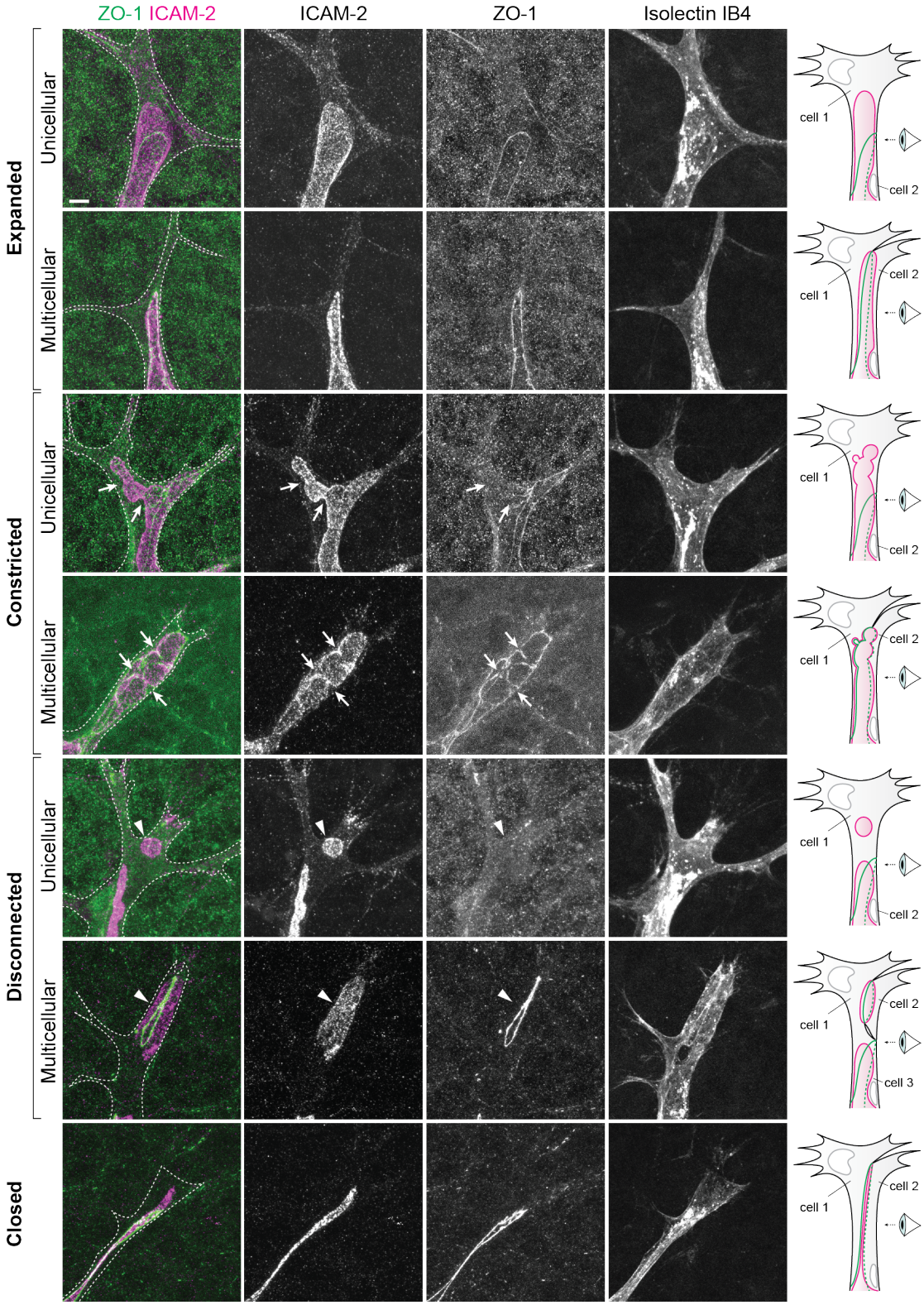


**Figure 3.3. Categorisation of endothelial sprouts according to lumen conformation and cellularity** (continued on next page)
Wild-type P6 mouse retinas were stained for ZO-1 (green), ICAM-2 (magenta) and isolectin $IB_4$. Isolectin $IB_4$ staining was used to delineate the outline of the cells (white

dotted lines). Arrows, points of constriction at the apical membrane. Arrowheads, lumen fragments. Scale bar is 10 µm.

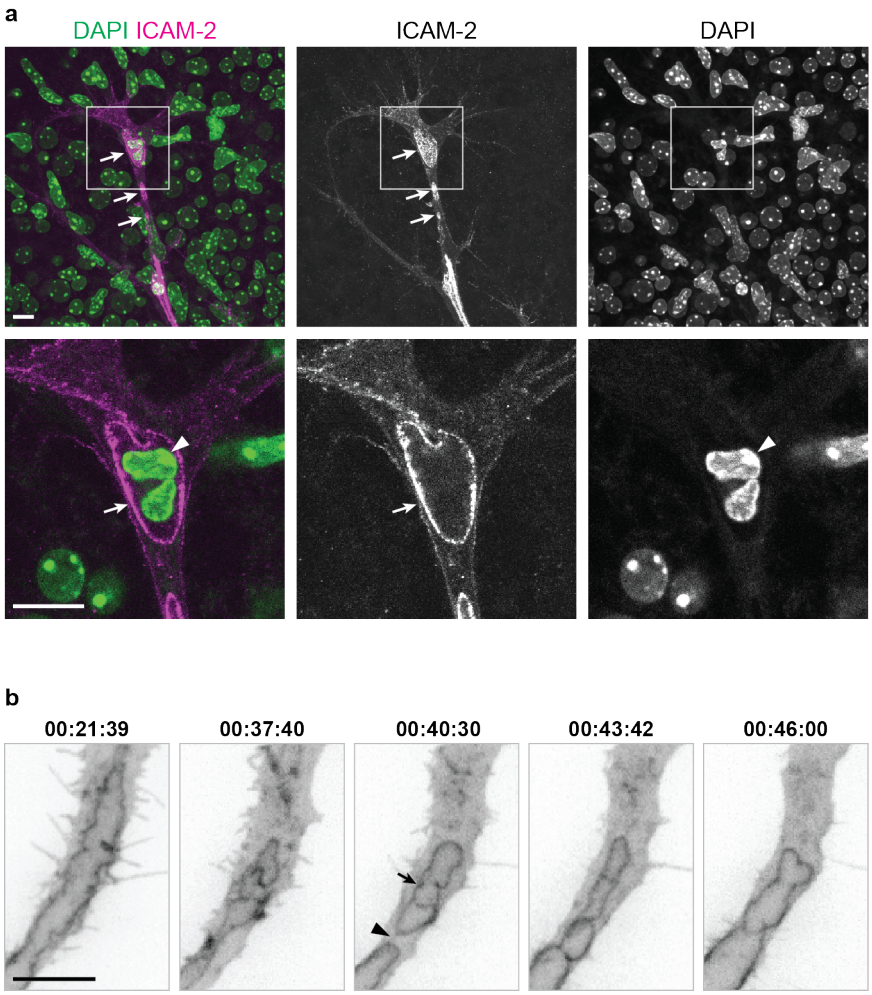


**Figure 3.4. Disconnected lumen fragments arise from the collapse of pre-existing lumens**

a) Wild-type P6 mouse retinas were stained for ICAM-2 (magenta) and DAPI (green). White arrows, disconnected lumen fragments. White arrowhead, trapped white blood cell. Top panels are maximum intensity projections. Bottom panels are single z planes. Scale bars are 10 µm.

b) Embryos with mosaic expression of EGFP-CAAX (n=7) were imaged from 36 hpf. Black arrow, lumen fragment. Black arrowhead, local lumen collapse. Time is in hours:minutes:seconds. Scale bar is 10 µm.

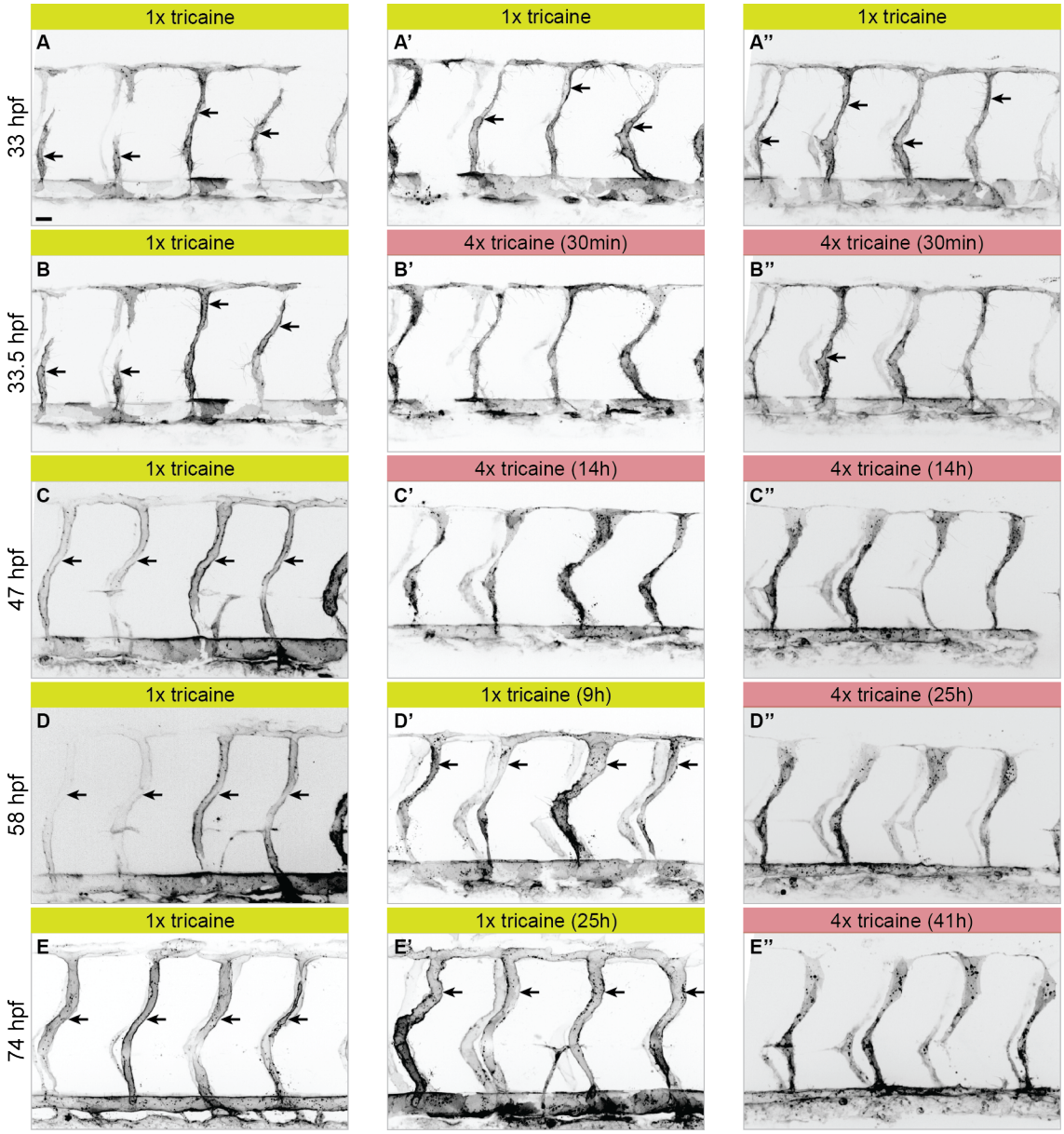


**Figure 3.5. Blood pressure is required for lumen expansion in angiogenic sprouts**
*Tg(kdr-l:ras-Cherry)*$^{s916}$ embryos (n=5 for each condition) were imaged at 33 hpf (A, A', A''). Two (out of three) sets of embryos were then treated with 4x tricaine (A'-E', A''-E''). Blood flow stopped after 20-25 minutes of treatment, as assessed by the absence of circulating red blood cells (not shown). Control embryos (A-E) were left in 1x tricaine. After 14h of treatment with 4x tricaine, a first set of embryos was returned to 1x tricaine (A'-E'). The second set of embryos was kept in 4x tricaine (A''-E''). Arrows, lumens. Scale bar is 10 μm.

# Chapter 4. Blood pressure drives lumen formation by inverse membrane blebbing during sprouting angiogenesis *in vivo*

## 4.1 Introduction

The results presented in the previous chapter suggested that lumens do not expand through *de novo* vacuole formation during sprouting angiogenesis *in vivo*, and that their expansion is dependent on the presence of blood flow as inhibiting heart activity abrogates lumen formation in sprouting ISVs in zebrafish.
In this chapter, I present my finding that apical membrane expands in angiogenic sprouts *in vivo* through a novel mechanism of inverse membrane blebbing.

## 4.2 Angiogenic sprouts expand both unicellular and multicellular lumens *in vivo*

During anastomosis, lumens expand both through apical membrane invagination into single anastomosing cells (unicellular lumen formation), and by *de novo* apical membrane formation at their nascent junction (multicellular lumen formation) (Herwig et al., 2011, Lenard et al., 2013). Since the tip of endothelial sprouts can be occupied by either one or several cells as they compete for the tip position (Jakobsson et al., 2010, Pelton et al., 2014), I asked whether similar mechanisms of lumen formation apply to unicellular and multicellular endothelial sprouts prior to anastomosis.

Using immunostainings for ICAM-2 and zona occludens-1 (ZO-1) in P6 mouse retinas, I was able to image respectively the apical membrane and cell junctions in sprouting tip cells undergoing lumen formation. By doing so, I found that lumens are present either as membrane invaginations into single tip cells, or between cells as they share the tip position (Figure 3.3), suggesting that endothelial cells undergo both unicellular and multicellular lumen formation in the mouse retina. Quantification showed that 88 % of

the sprouts at the vascular front of P6 retinas have multicellular lumens, while the remaining 12 % have unicellular lumens (Table 3.1), suggesting that unicellular lumen formation is a rare and/or short-lived event during sprouting angiogenesis in mice.

Time-lapse imaging of *Tg(kdr-l:ras-Cherry)*$^{s916}$ zebrafish embryos showed that, similar to what was observed in mouse retinas, lumens expand in sprouting ISVs prior to anastomosis, and do so by invagination of the apical membrane either into single tip cells (Figure 4.1 and Movie 4.1), or along cell junctions when the tip of a sprouting ISV is shared between several cells (Figure 4.1 and Movie 4.2).

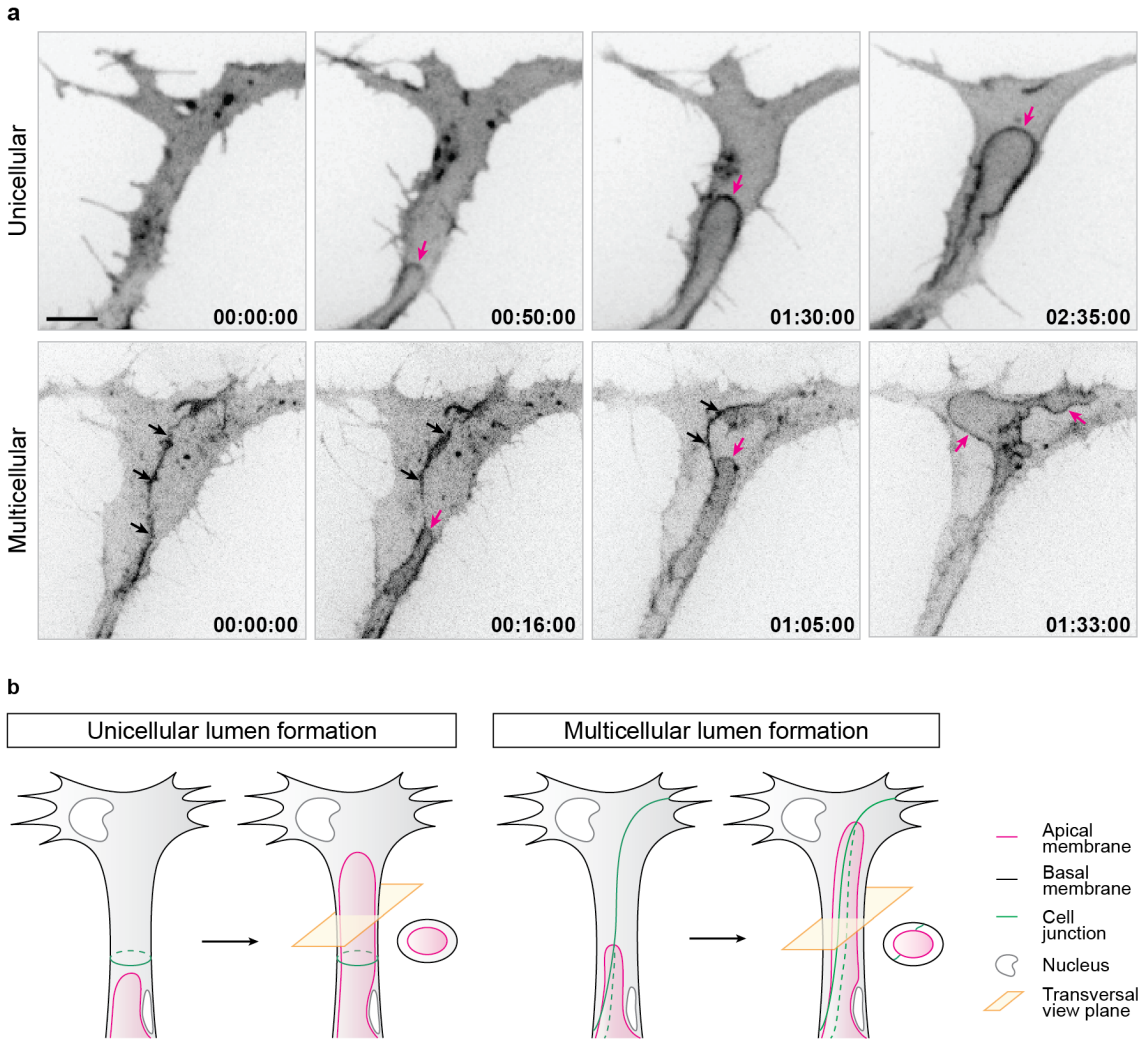


**Figure 4.1. Endothelial sprouts undergo both unicellular and multicellular lumen formation in zebrafish ISVs** (continued on next page)

a) *Tg(kdr-l:ras-Cherry)*$^{s916}$ embryos (n=10) were imaged from 32 hpf. Black arrows, cell junction. Magenta arrows, apical membrane. Time is in hours:minutes:seconds. Scale bar is 10 μm.
b) Schematic illustration of unicellular and multicellular lumen formation in angiogenic sprouts.

## 4.3 Apical membranes expand by inverse membrane blebbing during angiogenesis

### 4.3.1 Apical membranes undergo inverse blebbing during unicellular and multicellular lumen expansion

In order to get a better understanding of the mechanisms responsible for apical membrane expansion in sprouting ISVs, I imaged with high spatial and temporal resolution zebrafish embryos with mosaic expression of EGFP-CAAX. By doing so, I discovered that apical membranes undergo rapid expansion through a process reminiscent of membrane blebbing (Figure 4.2 and Movie 4.3).

In most eukaryotic cells, the plasma membrane is supported by a cortex of actin, myosin, and associated proteins. Because of its contractile properties, this cortex can generate tension and counteract the pressure exerted by the cytoplasm on the plasma membrane; it is thus actively maintaining but also adapting cell shape during processes such as cell division or cell migration. Membrane blebs are small (about 2-10 μm in size) plasma membrane protrusions caused by local rupture of the actomyosin cortex or its detachment from the plasma membrane (bleb initiation, Figure 4.3; and (Cunningham, 1995, Keller and Eggli, 1998, Paluch et al., 2005, Charras et al., 2008)). Under cytoplasmic pressure, the membrane in such actomyosin-free regions inflates from a neck into a spherical protrusion (bleb expansion, Figure 4.3). Bleb expansion is thought to be the result of both tearing of the membrane from the cortex and flow of lipids through the bleb neck, rather than of endocytosis and/or un-wrinkling of the membrane (Charras et al., 2008). Depending on the context, blebs are eventually resolved either by detachment (as seen in apoptosis), forward movement of the cell (during cell migration), or through recruitment and contraction of actomyosin on the inner side of the bleb (bleb retraction, as seen in cell division) (Figure 4.3 and (Charras and Paluch, 2008)).

In endothelial cells, blebbing was observed at the apical membrane during lumen expansion (Figure 4.2 a and Movie 4.3). These blebs however showed inverted polarity in comparison to previously described blebs, with the apical membrane protruding into the cell body. Hence, I propose to name this process “inverse membrane blebbing”. Following expansion, inverse blebs either retracted (Figure 4.2 a, panel B and black arrowheads in Figure 4.2 b) or persisted, in particular as larger structures, leading to an expansion of the luminal compartment (Figure 4.2 a, panel C and white arrowheads in Figure 4.2 b). Interestingly, persisting blebs were only found at the tip of the growing lumen, therefore restricting lumen expansion to this region of the cell. In contrast, blebs arising on the lateral sides of the lumen always retracted. Finally, no bleb was found to detach from the apical membrane (not shown).

Quantitative morphometric analysis of inverse blebs showed that their size, expansion time and speed, as well as retraction time and speed, are of the same order of magnitude as those of classical blebs (Figure 4.4, Table 4.1 and (Cunningham, 1995, Charras et al., 2008)).

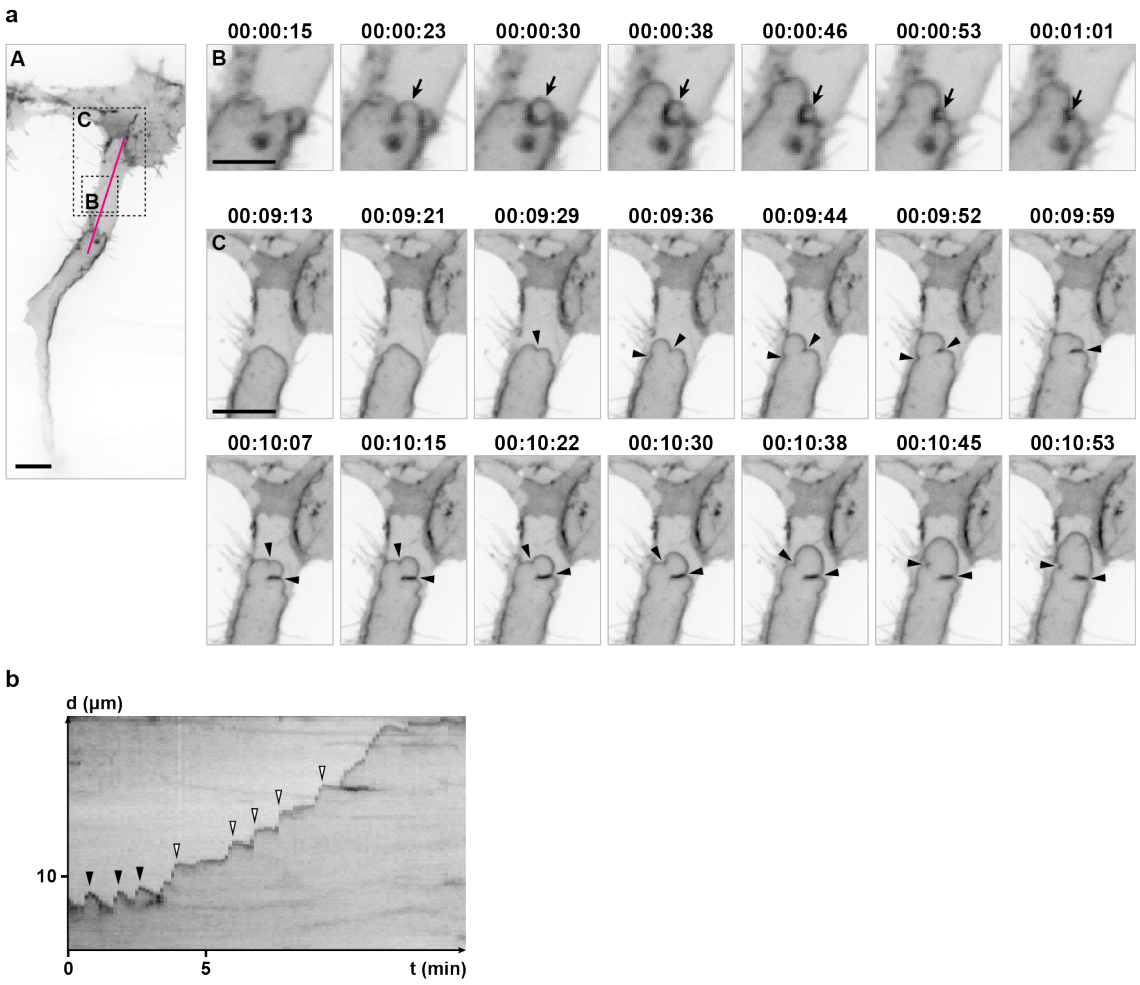


**Figure 4.2. Apical membrane undergoes inverse membrane blebbing during lumen expansion in sprouting ISVs**

Embryos with mosaic expression of EGFP-CAAX (n=7) were imaged from 36 hpf.

a) Arrow in B, retracting bleb. Arrowheads in C, bleb necks. Time is in hours:minutes:seconds. Scale bars are 10 µm (A,C) and 5 µm (B).

b) A kymograph was generated along the magenta line in a, panel A. X axis, time (t) in minutes. Y axis, distance (d) in µm. Black arrowheads, retracting blebs. White arrowheads, non-retracting blebs.

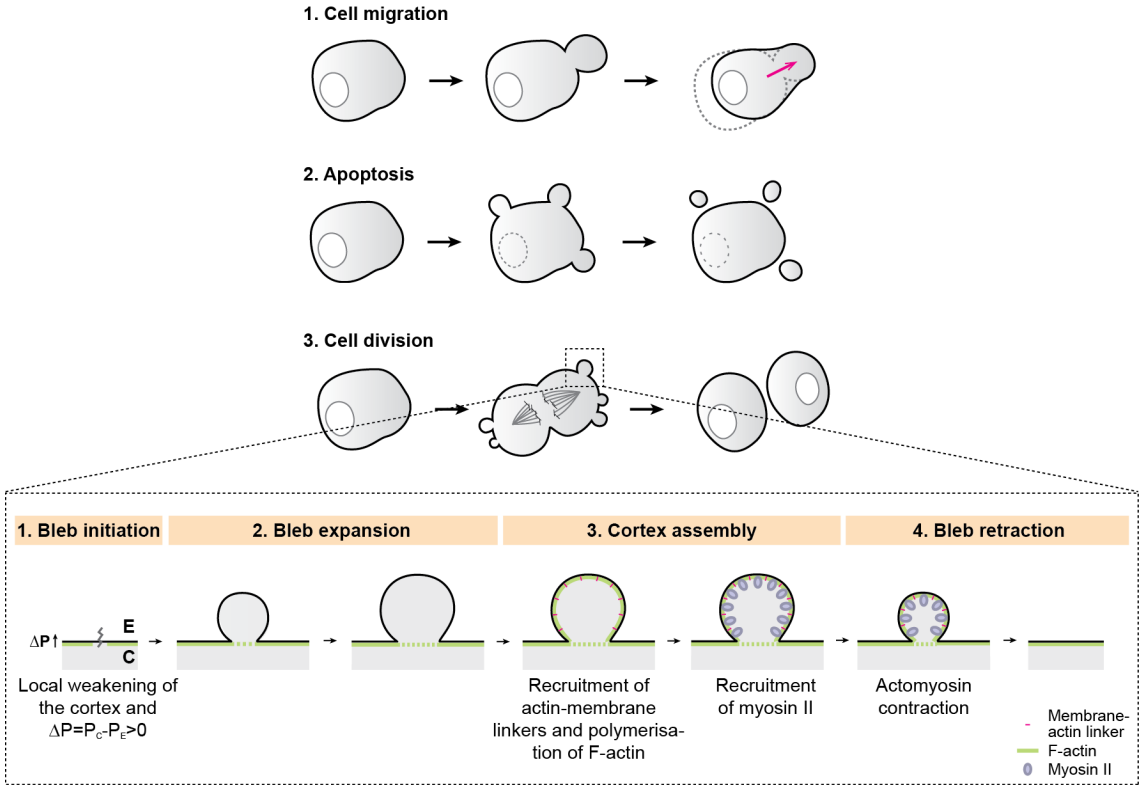


**Figure 4.3. Membrane blebbing: cellular and molecular mechanisms**
Schematic representation of membrane blebbing during cell migration, apoptosis and cell division. Blebs expand following local breakage of the cortex or its detachment from the membrane. When occurring, bleb retraction is driven by actomyosin contraction.

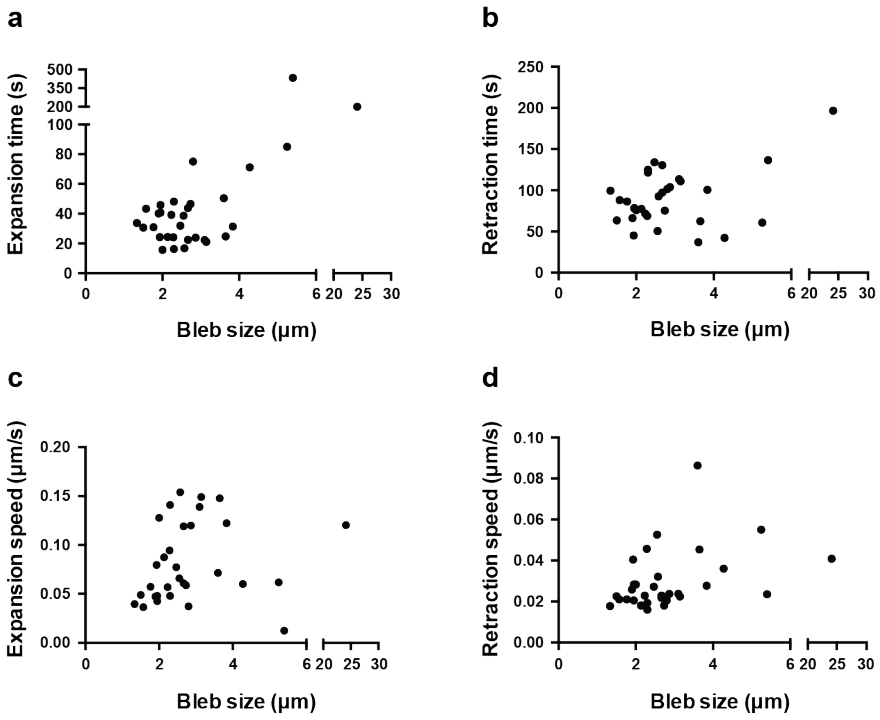


**Figure 4.4. Measurement of expansion time, retraction time, expansion speed, and retraction speed of inverse blebs**
*Tg(kdr-l:ras-Cherry)*$^{s916}$ embryos with mosaic expression of Lifeact-EGFP were used to measure expansion time (a), retraction time (b), expansion speed (c) and retraction speed (d) in relation to bleb size (n=31 blebs, N=3 cells).

| | **Inverse blebs** | **Classical blebs** |
|---|---|---|
| Bleb size (µm) | 3.4 ± 4 | 2 |
| Expansion time (s) | 55 ± 78 | 30 |
| Expansion speed (µm/s) | 0.08 ± 0.04 | 0.25 |
| Retraction time (s) | 90 ± 34 | 120 |
| Retraction speed (µm/s) | 0.03 ± 0.01 | 0.03 |

**Table 4.1. Comparison of properties of classical and inverse blebs**
*Tg(kdr-l:ras-Cherry)*$^{s916}$ embryos with mosaic expression of Lifeact-EGFP were used to measure bleb size, expansion time, retraction time, expansion speed and retraction speed. Values for inverse blebs correspond to mean and standard deviation calculated from n=31 blebs (N=3 cells). Values for classical blebs come from (Charras et al., 2008).

Inverse blebs were observed at the apical membrane of both unicellular (Figure 4.2 and Movie 4.3) and multicellular (Figure 4.5 and Movie 4.4) sprouts during lumen expansion. However, because endothelial cell junctions are highly dynamic (Jakobsson et al., 2010, Sauteur et al., 2014, Phng et al., 2015) and accumulate apical markers during lumenisation (Herwig et al., 2011), I chose for clarity to focus the rest of my analysis on unicellular lumens where non-junctional apical membrane can clearly be distinguished.

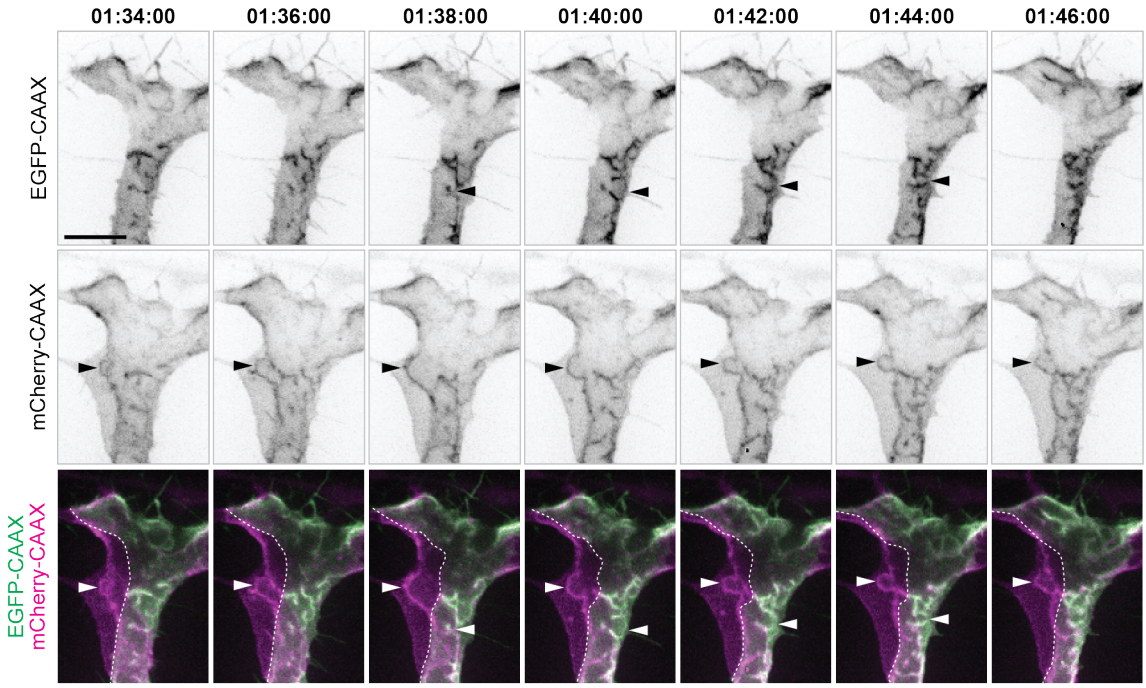


**Figure 4.5. Lumens expanding in multicellular sprouts undergo inverse membrane blebbing**
*Tg(kdr-l:ras-Cherry)*$^{s916}$ embryos with mosaic expression of EGFP-CAAX (n=4) were imaged from 32 hpf. Arrowheads, inverse blebs. Dashed line, cell junction. Time is in hours:minutes:seconds. Scale bar is 10 μm.

### 4.3.2 Inverse blebbing is driven by blood pressure

Because the expansion of classical blebs is driven by cytoplasmic pressure, and because I found that lumen expansion in sprouting ISVs requires blood flow (see chapter 3), I asked whether the growth of inverse blebs at the apical membrane of endothelial cells is driven by blood pressure.

The knockdown or mutation of *troponin 2a* (*tnnt2a*) has been the standard method used to stop heartbeat, and thus inhibit blood flow, in zebrafish embryos. In accordance with my own experiments using tricaine (Figure 3.5), lumens do not expand in ISVs of mutant embryos (own observations and (Herwig et al., 2011)). Additionally, Herwig and colleagues showed that although cell junctions accumulate apical markers in mutant embryos, unicellular regions lack apical domains. Therefore, this method did not seem suitable to address the relationship between blood flow and apical membrane blebbing. Instead, I chose to induce blood pressure drops at the time of lumen expansion, and did so following two different strategies.

I established a first method to stop blood flow in single ISVs by laser ablating the connection of the sprouts to the dorsal aorta in *Tg(fli1ep:EGFP-CAAX)* embryos (Figure 4.6 and Movie 4.5). With this technique, blood flow could be interrupted immediately and irreversibly in single sprouts. Although the cells at the base of the sprouts were lost during ablation, cells at the tip remained viable and did not show any sign of damage; these cells still expanded and retracted multiple filopodia (Figure 4.6 and Movie 4.5). However, following ablation and loss of blood flow, their apical membrane stopped blebbing and the lumen gradually regressed (Figure 4.6 and Movie 4.5), strongly suggesting that inverse blebbing in endothelial cells is indeed driven by blood pressure.

In order to further support this result, I took a second approach where I inhibited then re-started blood flow using high doses of tricaine (Figure 4.7 and Movie 4.6). Following 15-20 minutes of treatment with 4x tricaine, blood flow stopped (as assessed by the absence of circulating red blood cells) and blebs could no longer be observed at the apical membrane of lumenising cells (Figure 4.7, panel B and kymograph). When

returned to 1x tricaine, embryos recovered blood flow and re-expanded lumens by inverse blebbing (Figure 4.7, panel E and kymograph).
Together, these experiments show that the generation of inverse blebs depends on the positive pressure difference existing between the luminal and the cytoplasmic sides of the apical membrane.

Interestingly, treating embryos for a short time with 4x tricaine recapitulated the lumen collapse and re-growth events observed during normal lumen formation (Figure 3.4). In these experiments, stopping blood flow systematically led to the following sequence of events: 1) cessation of apical blebbing (Figure 4.7, panel B), 2) collapse of the lumen (Figure 4.7, panel C), 3) fragmentation of the apical membrane into small vesicles (Figure 4.7, panel D), and, after washout 4) re-growth of the lumen by inverse blebbing (Figure 4.7, panel E). Although no method is currently available to measure in real-time local variations of blood pressure, thus preventing us from establishing a correlation with apical membrane dynamics during normal lumen development, this set of experiments strongly suggests that local lumen collapse and re-growth events occur during normal development following variations in blood pressure.

### 4.3.3 Apical membrane shows constricted patterns in mouse retinas suggestive of lumen expansion by inverse blebbing

In the mouse retina, stainings for ICAM-2 revealed the presence of two major lumen conformations where the apical membrane appeared either expanded or constricted (Figure 3.3 and Table 3.1). This observation suggests that a similar mechanism of apical membrane blebbing might take place during sprouting angiogenesis in mice.

## 4.4 Conclusions

By performing high resolution imaging of apical membrane dynamics in sprouting ISVs, I found that lumens expand during angiogenesis through a previously undescribed mechanism of inverse membrane blebbing. I show that inverse blebs share the same morphology and expansion and retraction rates than classical blebs, and that their

expansion is driven by blood pressure, therefore generating the inverted polarity observed in this system. Finally, imaging in mouse retinas suggests that a similar mechanism might be driving lumen expansion in angiogenic sprouts in mice.

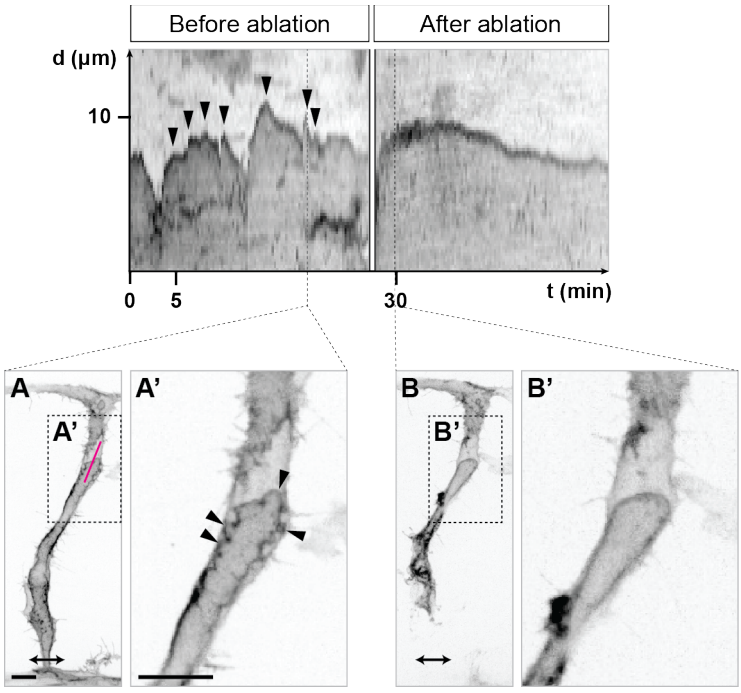


**Figure 4.6. Ablation of the connection of ISVs to the dorsal aorta abrogates inverse blebbing at the apical membrane of lumenising cells**
*Tg(fli1ep:EGFP-CAAX)* embryos (n=6) were imaged from 33 hpf. Ablation was performed at the base of the ISV to stop blood flow in the sprout (double-headed arrow, ablated region). A kymograph was generated along the magenta line in A to follow apical membrane dynamics before and after ablation. X axis, time (t) in minutes. Y axis, distance (d) in µm. Arrowheads, inverse blebs. Scale bars are 10 µm.

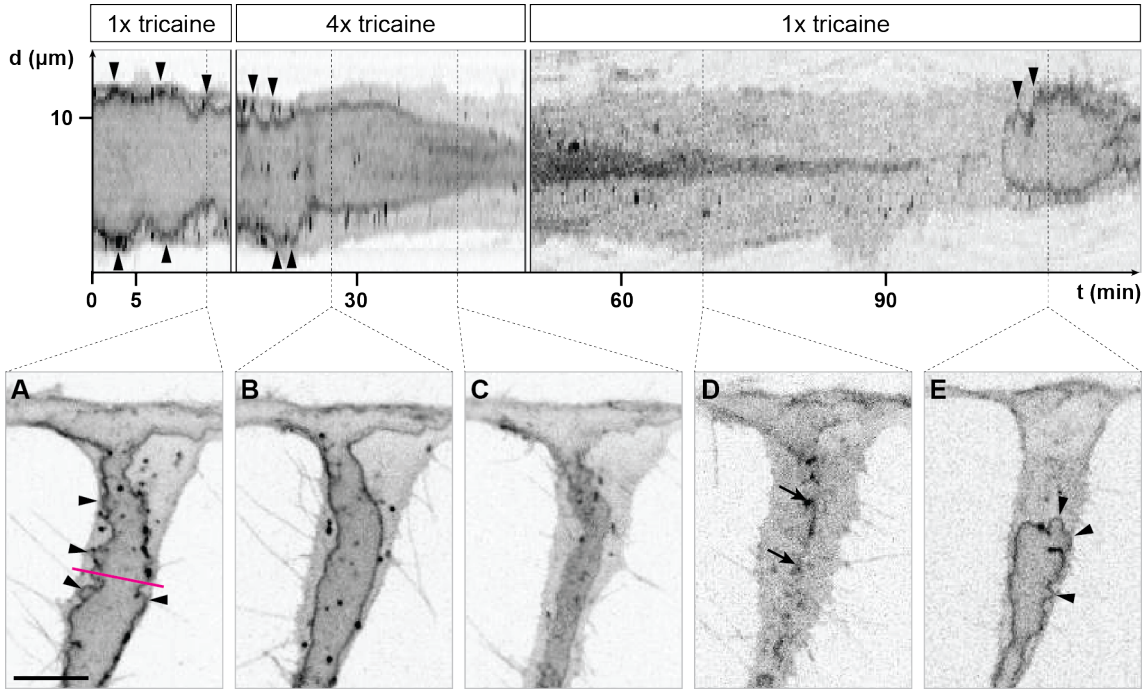


**Figure 4.7. Transient treatment with 4x tricaine leads to transient loss of inverse blebs at the apical membrane of lumenising cells**
*Tg(kdr-l:ras-Cherry)*$^{s916}$ embryos (n=5) were imaged from 32 hpf in 1x tricaine, and then treated with 4x tricaine. Blood flow stopped approximately 15 minutes after the start of the treatment. After 30 minutes of treatment, embryos were washed with E3 buffer and placed back in 1x tricaine. A kymograph was generated along the magenta line in A to follow apical membrane dynamics. X axis, time (t) in minutes. Y axis, distance (d) in µm. Arrowheads, inverse blebs. Arrows, remnants of apical membrane. Scale bar is 10 µm.

# Chapter 5. Endothelial cells regulate inverse blebbing and lumen expansion by local and transient recruitment and contraction of actomyosin

## 5.1 Introduction

In the previous chapter, I showed that the growth and persistence of inverse blebs at the tip of the lumen lead to the expansion of the apical membrane in sprouting endothelial cells. However, all blebs growing on the sides of the lumen, as well as a number of blebs growing at its tip, were found to retract, and did so following similar membrane dynamics as classical blebs. Since retraction of classical blebs, when not by detachment or forward movement of the cell, involves the recruitment and contraction of actomyosin on the inner surface of the bleb (Figure 4.3 and (Charras and Paluch, 2008)), and since initiation of classical blebbing itself is dependent on the properties of the actomyosin cortex (Charras et al., 2008), I decided to investigate if and how actomyosin assembly and contraction regulates inverse membrane blebbing during lumen formation in endothelial cells.

## 5.2 Endothelial cells retract inverse blebs by recruiting and contracting actomyosin at the apical membrane

### 5.2.1 F-actin polymerises around inverse blebs during phases of retraction

In order to follow F-actin dynamics during lumenisation in sprouting ISVs, I imaged zebrafish embryos expressing an endothelial-specific Lifeact-EGFP reporter for F-actin (*Tg(fli1ep:Lifeact-EGFP*) generated in our laboratory by Li-Kun Phng (Phng et al., 2013)). Lifeact is a 17-amino acid peptide that binds to F-actin and offers a reliable system for the labelling of actin structures in eukaryotic cells, both *in vitro* and *in vivo* (Riedl et al., 2008, Riedl et al., 2010, Fraccaroli et al., 2012, Phng et al., 2013). Although it may affect stability of F-actin at high concentrations (Courtemanche et al.,

2016), Lifeact has been shown to bind to F-actin filaments without interfering with their structure and dynamics in multiple cellular systems (Riedl et al., 2008). By imaging embryos expressing both mCherry-CAAX and Lifeact-EGFP reporters (*Tg(kdr-l:ras-Cherry$^{s916}$;fli1ep:Lifeact-EGFP)*), I was able to correlate apical membrane and actin dynamics in endothelial cells during sprouting angiogenesis. Although it was difficult to optically resolve the presence of an actin cortex at the apical membrane of endothelial cells during sprouting, a cortex was clearly visible at the apical membrane at 2 dpf (Figure 5.1), once vessels were fully lumenised and likely experiencing higher levels of blood pressure.

When imaged during phases of lumen expansion, strong polymerisation of F-actin was however observed all around the surface of inverse blebs, from the initiation of retraction until its completion (Figure 5.2 and Movie 5.1). In contrast, blebs that did not retract did not show any polymerisation of F-actin at their surface. These observations therefore suggest that retraction of inverse blebs, similarly to the retraction of classical blebs, involves the recruitment and contraction of actomyosin at the surface of the bleb.

### 5.2.2 Myosin II is recruited around inverse blebs during phases of retraction

In order to assess whether myosin II is also recruited to the apical membrane during bleb retraction, I generated an endothelial-specific reporter for the regulatory light chain of non-muscle myosin II (Myl9b) (Figure 5.3). In order to overcome potential side effects of the overexpression of Myl9b in endothelial cells, the LexPR/LexOP system (see chapter 2) was used to induce the expression of the reporter only from the onset of lumen formation. Additionally, analysis was restricted to cells showing low levels of expression of the reporter. At 2 dpf, cells expressing Myl9b-EGFP showed normal morphology, and Myl9b-EGFP co-localised with a Lifeact-mCherry reporter for F-actin at endothelial cell junctions, at the base of filopodia, and at the apical membrane (Figure 5.1). Together, these observations suggest that this reporter constitutes a reliable tool to image myosin II localisation in endothelial cells, and that myosin II, together with F-actin, forms an actomyosin cortex that supports the apical membrane in lumenised vessels.

In order to follow myosin II dynamics during lumenisation, *Tg(kdr-l:ras-Cherry)*$^{s916}$ embryos with mosaic expression of Myl9b-EGFP were imaged from 35 hpf. Myosin II, similarly to F-actin, was recruited transiently to the surface of inverse blebs during phases of bleb retraction (Figure 5.4). In order to analyse with more detail the timing of assembly of actomyosin at the surface of inverse blebs, Myl9b-EGFP and Lifeact-mCherry reporters were co-expressed in wild-type embryos and imaged at high temporal resolution. Similarly to what has been reported during classical blebbing, F-actin polymerisation preceded the recruitment of myosin II at the surface of inverse blebs (Figures 5.5 and 5.9 and Movie 5.2).

### 5.2.3 Bleb retraction requires actomyosin contraction

In order to address whether the retraction of inverse blebs is driven by the contraction of the actomyosin cortex recruited at their surface, I chose to inhibit actomyosin contraction in endothelial cells and determine the impact of this manipulation on the ability of the cells to retract inverse blebs growing at the apical membrane.

Actomyosin filaments are formed by the association of myosin II molecules in an anti-parallel fashion through their rod domains, and by their attachment to F-actin filaments through the globular heads of their heavy chains (Figure 5.3). The contraction of these actomyosin filaments is dependent on the ATPase activity of the myosin II molecules. Following hydrolysis of ATP, the neck region of myosin II undergoes a conformational change allowing the sliding of the attached F-actin filaments in respect to one another (Figure 5.3).

Non-muscle myosin II is formed by the association of two heavy chains, two regulatory light chains (RLCs), and two essential light chains (ELCs) (Figure 5.3). At the molecular level, actomyosin contractility and assembly are regulated by the phosphorylation of the light and heavy chains of myosin II, respectively. The phosphorylation of the RLCs on Thr18 and Ser19 by a wide range of kinases, including MLCK, ROCK and PKC, has been shown in many cell types to greatly increase the ATPase activity of myosin II in the presence of actin, and to promote filament assembly by allowing the unfolding of the heavy chains otherwise locked in a closed

conformation through a head-to-tail interaction. Phosphorylation of the heavy chains at their C-terminus is also suggested to regulate filament assembly (Vicente-Manzanares et al., 2009).

A common strategy to experimentally inhibit actomyosin contraction is to use blebbistatin, a small molecule inhibitor found to bind the myosin-ADP-Pi complex with high affinity, preventing the release of phosphate and blocking myosin in a state with low affinity for actin (Kovacs et al., 2004). Blebbistatin efficiently inhibits striated muscle myosins, but also, at significantly lower concentrations, non-muscle myosins. On the other hand, smooth muscle myosins were found to be only poorly affected by blebbistatin treatment (Limouze et al., 2004). Blebbistatin therefore appeared as a suitable approach to inhibit actomyosin contraction in endothelial cells *in vivo*, and has since been used successfully to study other aspects of endothelial cell biology in zebrafish (Sauteur et al., 2014).
However, treatment of 30-35 hpf zebrafish embryos with blebbistatin, even at low concentrations of the drug (2.5-10 μM) and for short periods of time (one hour), was found to affect heartbeat and thus perturb blood flow, as assessed by the speed of circulation of red blood cells in the dorsal aorta and posterior cardinal vein (data not shown). Because inverse blebbing is a response of the apical membrane to blood pressure, and because no tool currently allows to measure blood pressure levels in zebrafish embryos, I decided this approach was not suitable to address whether actomyosin contraction in endothelial cells regulates inverse blebbing.

*In vitro*, a form of the myosin II RLC mutated for its two phosphorylation sites (T18A/S19A) has been shown to act as a dominant-negative protein and its expression impaired both stress fibre formation in interphase cells and contractile ring formation in dividing cells (Iwasaki et al., 2001). Therefore, I decided to generate a non-phosphorylatable form of the myosin regulatory light chain Myl9b (Myl9bAA) and to express it mosaically in *Tg(kdr-l:ras-Cherry)*$^{s916}$ embryos, thus affecting actomyosin contraction in single endothelial cells in the embryo. Importantly, in order to circumvent any general and potentially deleterious effects during earlier development, the mutant

reporter (Myl9bAA-EGFP) was put under the control of the LexOP/LexPR expression system, and its expression was induced only from the onset of lumen formation.
This strategy allowed me to successfully inhibit actomyosin contraction in single endothelial cells at the time of lumen formation (Figure 5.6). Upon expression of Myl9bAA-EGFP, I observed a significant difference in the frequency of bleb retraction compared to control cells expressing the wild-type form of Myl9b (Myl9b-EGFP), with larger proportions of blebs showing no or partial retraction (Figure 5.6). These data therefore indicate that bleb retraction is driven by the contraction of the actomyosin recruited at the surface of inverse blebs during lumen expansion.

### 5.2.4 A contractile actomyosin cortex underlines the apical membrane in angiogenic sprouts in mouse retinas

Immunostainings for ICAM-2 in mouse retinas suggested that a similar mechanism of apical membrane blebbing occurs during sprouting angiogenesis in mice (see 4.3.3). In order to address whether actomyosin contraction could also regulate apical membrane expansion in this system, I stained retinas from Lifeact-EGFP$^{+/wt}$ P6 mice for ICAM-2, and retinas from wild-type P6 mice for non-muscle myosin IIA and ICAM-2. By doing so, I found that the apical membrane in sprouting cells undergoing lumen formation is underlined by a cortex of F-actin and non-muscle myosin IIA in mouse retinas (Figure 5.7). The apical membrane of lumenising cells additionally stained for the phosphorylated form of myosin light chain 2 (pMLC2) (Figure 5.7), strongly suggesting that a similar mechanism of regulation of apical membrane expansion through actomyosin contraction could be taking place in sprouting cells in mice.

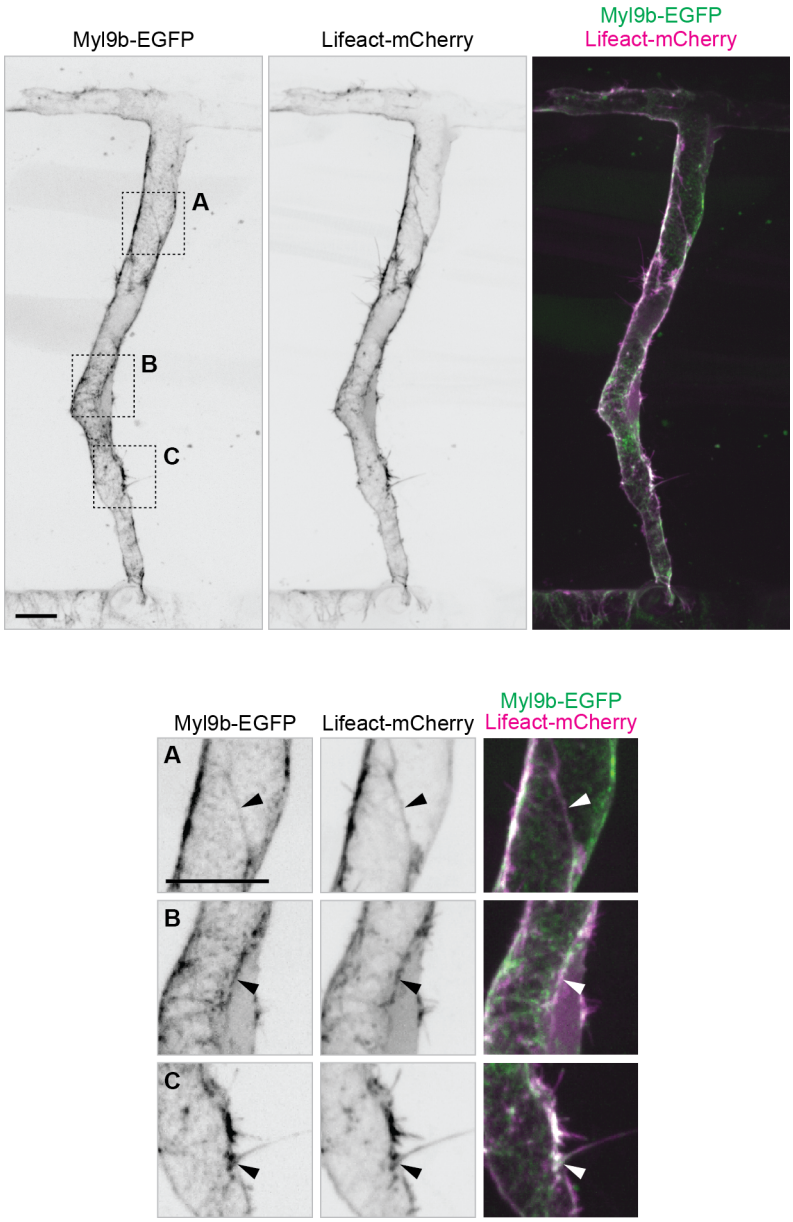


**Figure 5.1. F-actin and myosin II reporters co-localise at cell junctions, at the apical membrane, and at the base of filopodia in zebrafish ISVs**
Embryos with mosaic expression of Myl9b-EGFP and Lifeact-mCherry (n=6) were imaged at 2 dpf. Arrowheads show co-localisation of F-actin and myosin II at cell junctions (A), at the apical membrane (B), and at the base of filopodia (C). Scale bars are 10 μm.

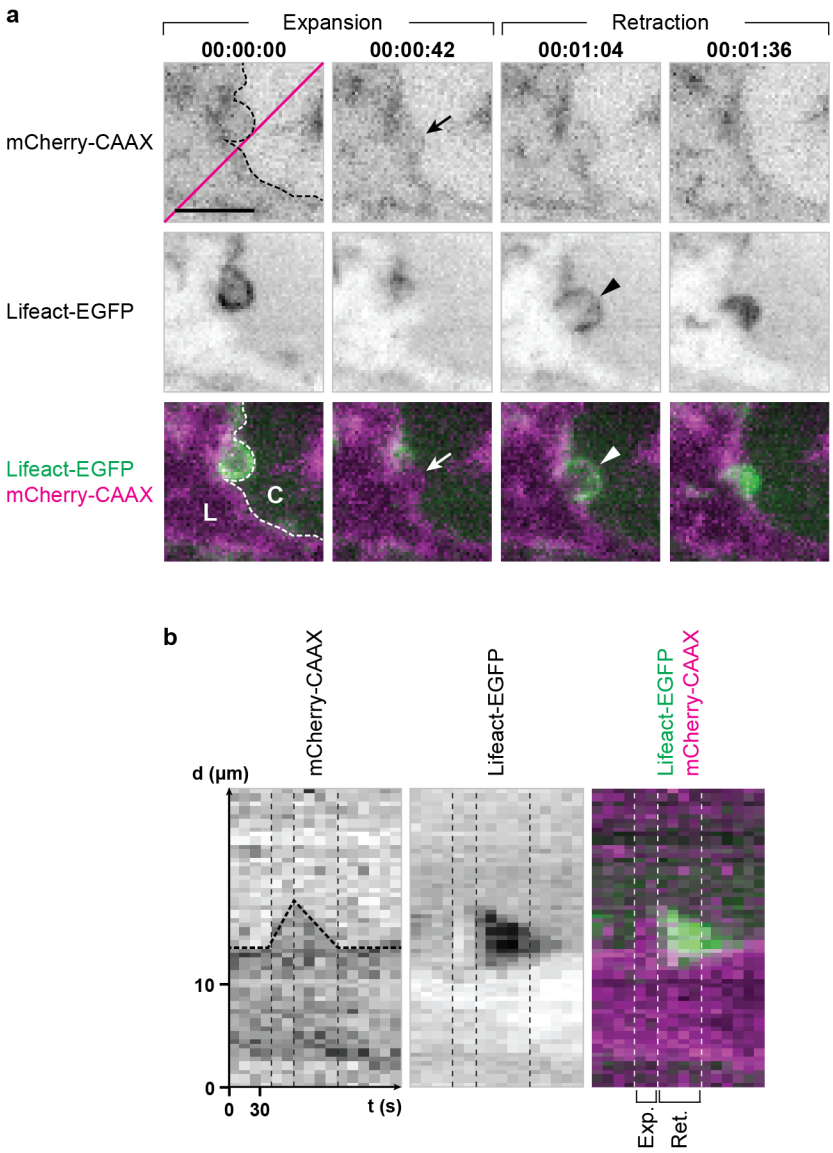


**Figure 5.2. F-actin polymerises at the surface of inverse blebs during phases of retraction**

a) *Tg(kdr-l:ras-Cherry)*$^{s916}$ embryos with mosaic expression of Lifeact-EGFP (n=5) were imaged from 35 hpf. Dotted line, apical membrane. Arrow, expanding apical membrane. Arrowhead, onset of F-actin polymerisation. C, cytoplasm. L, lumen. Time is in hours:minutes:seconds. Scale bar is 5 µm.

b) Kymograph generated along the magenta line in a. X axis, time (t) in seconds. Y axis, distance (d) in µm. Dotted line, apical membrane.

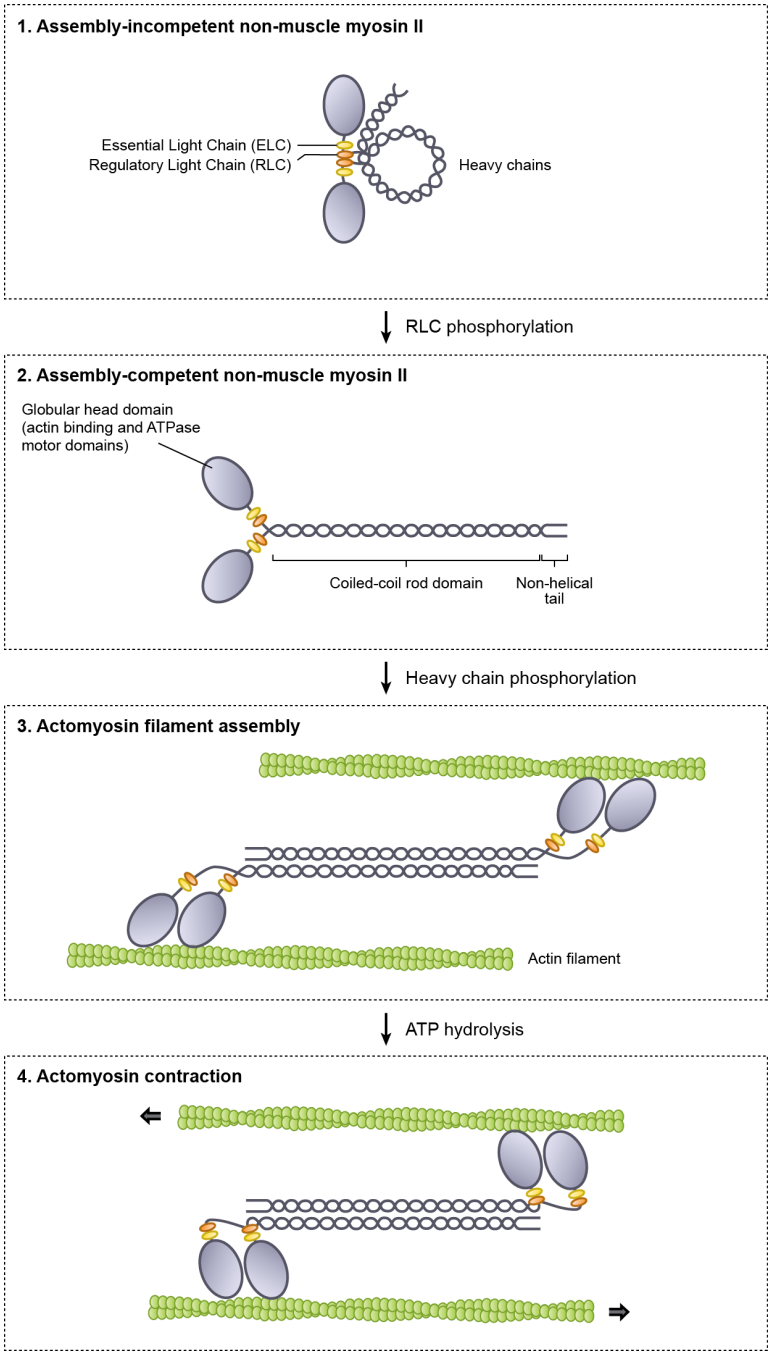


**Figure 5.3. Structure and regulation of actomyosin filament assembly and contraction**

Non-muscle myosin II is formed by the association of two heavy chains, two regulatory light chains (RLCs), and two essential light chains (ELCs). The actin-binding and ATPase activity domains of myosin II are carried by the globular heads of the heavy chains. Non-muscle myosin II becomes assembly-competent following the double phosphorylation of its RLCs on Thr18 and Ser19. Association to actin filaments is allowed through the phosphorylation of the heavy chains at their C-terminus. ATP hydrolysis triggers the bending of the neck region of myosin II, leading to the sliding of the actin filaments in respect to one another. Adapted from (Vicente-Manzanares et al., 2009).

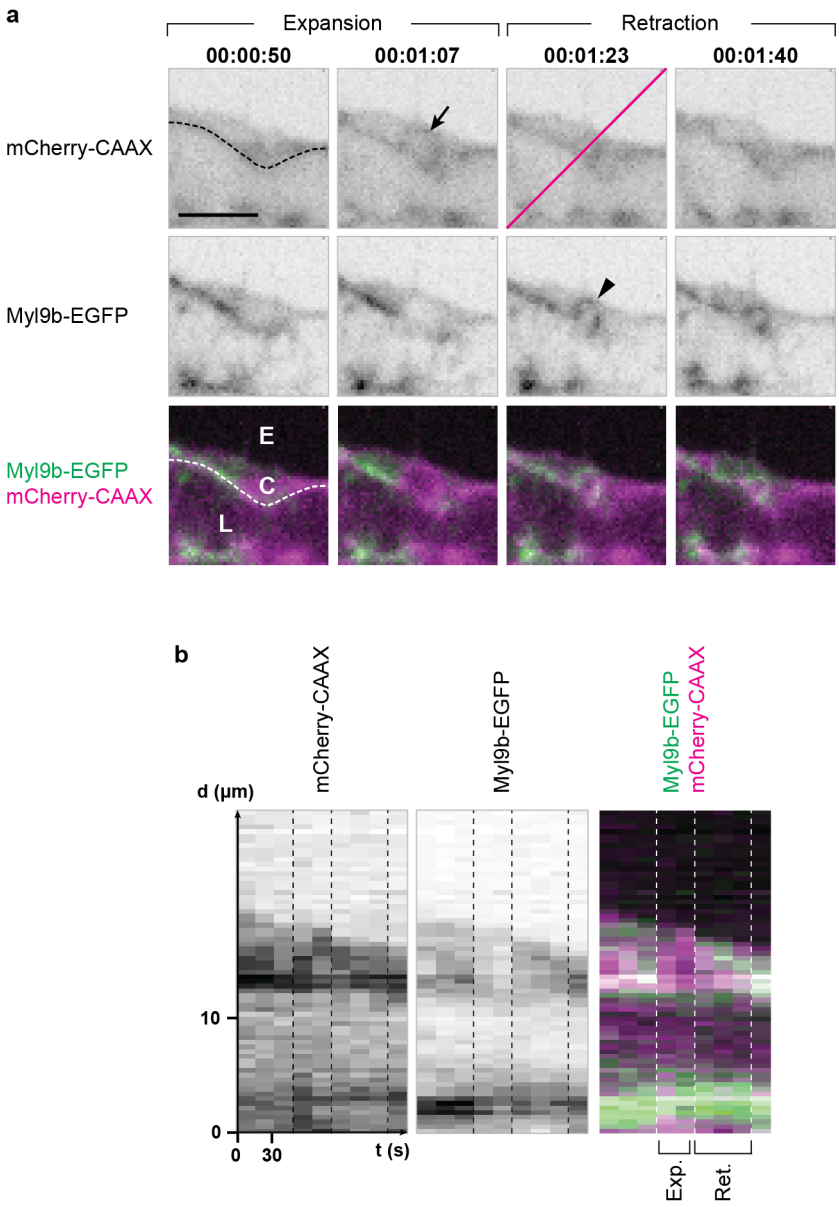


**Figure 5.4. Myosin II is recruited at the surface of inverse blebs during phases of retraction**

a) *Tg(kdr-l:ras-Cherry)*$^{s916}$ embryos with mosaic expression of Myl9b-EGFP (n=3) were imaged from 34 hpf. Dotted line, apical membrane. Arrow, expanding apical membrane. Arrowhead, onset of myosin II recruitment. C, cytoplasm. E, extracellular space. L, lumen. Time is in hours:minutes:seconds. Scale bar is 5 µm.

b) Kymograph generated along the magenta line in a. X axis, time (t) in seconds. Y axis, distance (d) in µm.

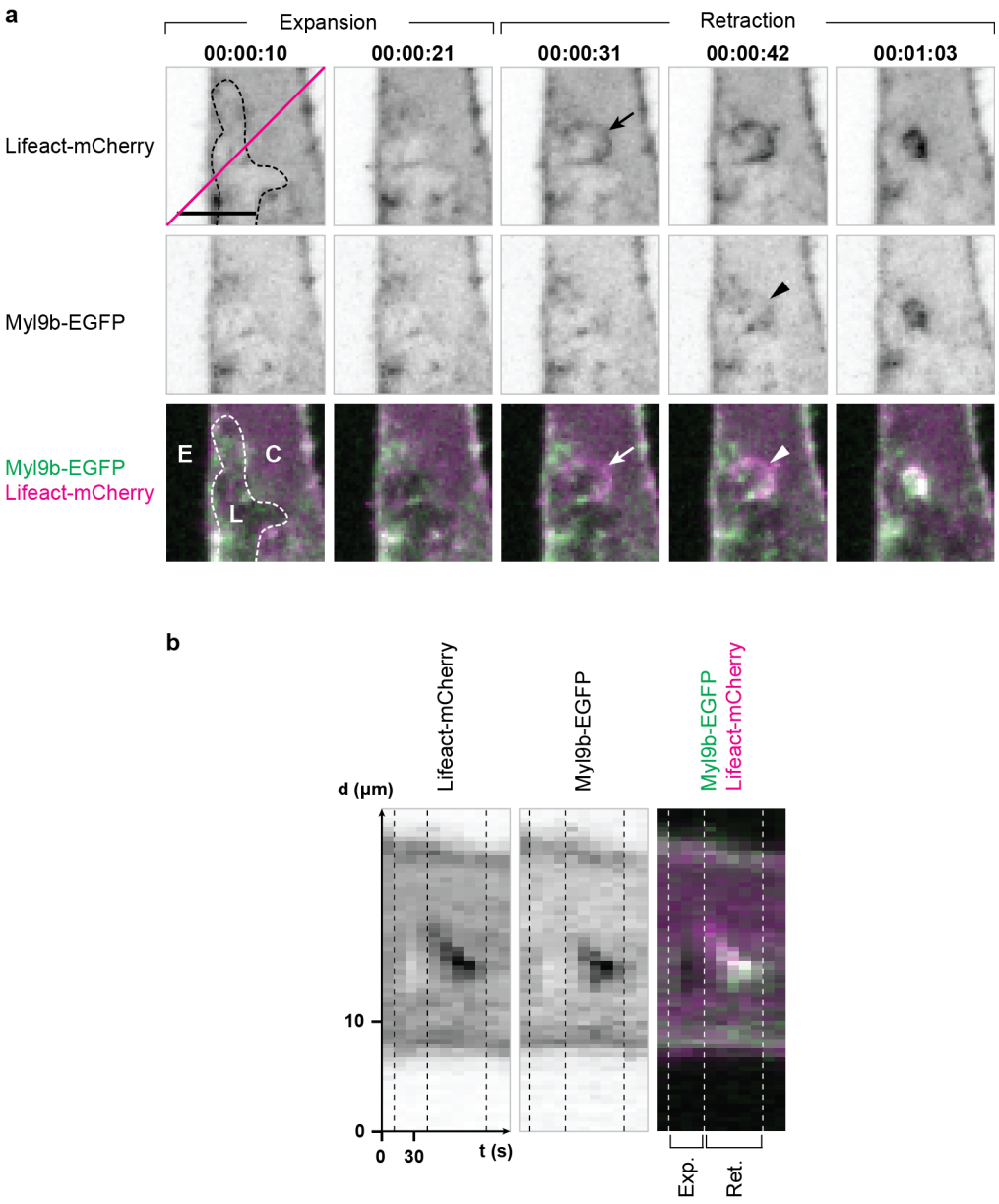


**Figure 5.5. F-actin polymerisation precedes myosin II recruitment at the surface of inverse blebs**

a) Embryos with mosaic expression of Myl9b-EGFP and Lifeact-mCherry (n=5) were imaged from 35 hpf. Arrow, onset of F-actin polymerisation. Arrowhead, onset of myosin II recruitment. C, cytoplasm. E, extracellular space. L, lumen. Time is in hours:minutes:seconds. Scale bar is 5 µm.

b) Kymograph generated along the magenta line in a. X axis, time (t) in seconds. Y axis, distance (d) in µm.

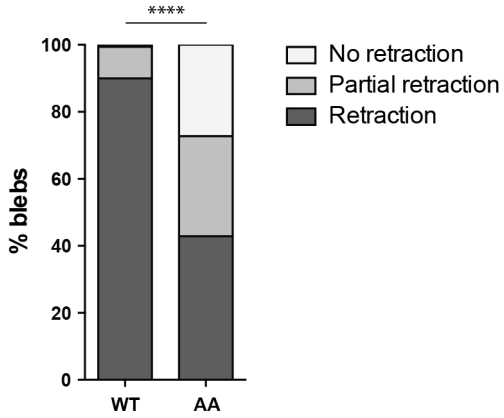


**Figure 5.6. Actomyosin contraction drives bleb retraction**
Embryos with mosaic expression of Myl9b-EGFP or Myl9bAA-EGFP and Lifeact-mCherry were imaged from 34 hpf. Blebs growing on the lateral sides of expanding lumens were assessed for their ability to retract within the maximum time necessary for expansion and retraction (approximately 10 minutes, see Figure 4.4). A multinomial log-linear model was used to test for association of bleb count in the different categories with the mutation status (WT: n=102 blebs, N=5 cells; AA: n=161 blebs, N=5 cells; data pooled from three independent experiments; p=2.1e-13; ****, p<0.0001).

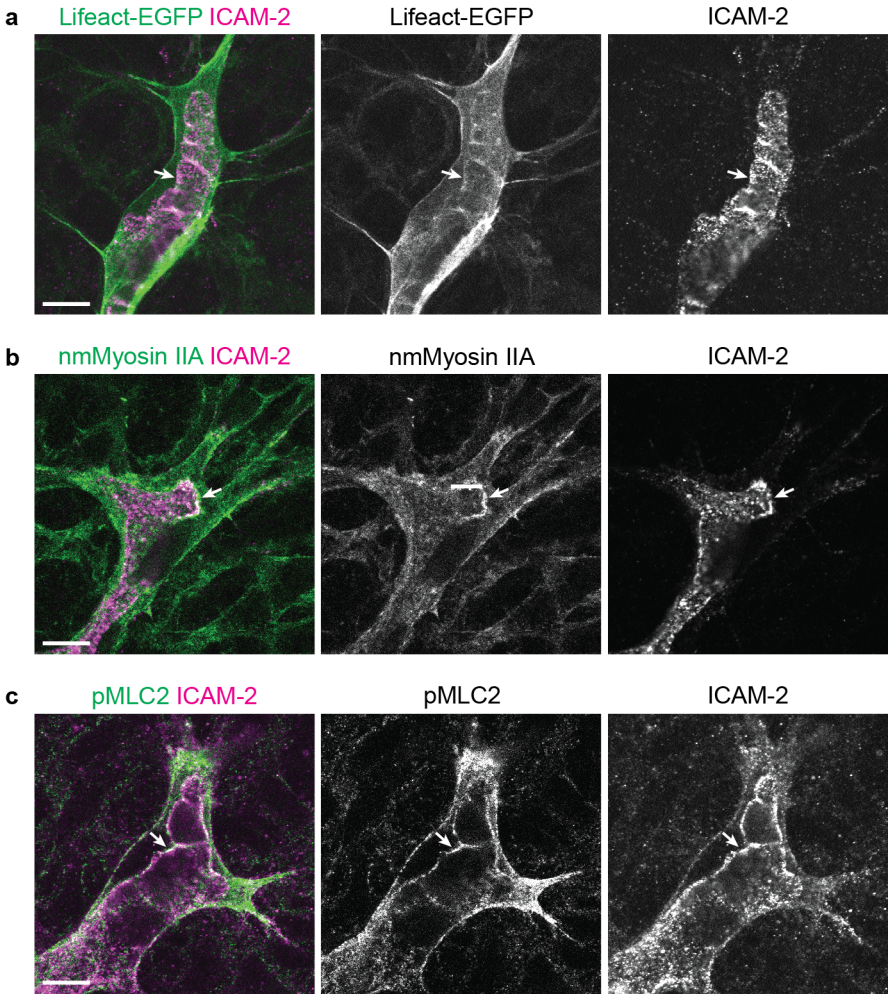


**Figure 5.7. The apical membrane of angiogenic sprouts is lined with a contractile actomyosin cortex in mouse retinas**
Retinas from Lifeact-EGFP$^{+/wt}$ (a) or wild-type (b,c) mice were harvested at P6 and stained for ICAM-2 (a-c), non-muscle myosin IIA (nmMyosin IIA; b), and phosphorylated myosin light chain 2 (pMLC2; c). Arrows show localisation of F-actin, nmMyosin IIA and pMLC2 at the apical membrane. Images correspond to single confocal planes. Scale bar is 10 µm.

## 5.3 Weakening of the actomyosin cortex at the apical membrane triggers inverse blebbing

In most eukaryotic cells, the actomyosin cortex provides the tension necessary to counteract the pressure exerted by the cytoplasm on the plasma membrane, and blebbing has been shown to be the natural response of the membrane to local detachment or rupture of the cortex (Cunningham, 1995, Keller and Eggli, 1998, Paluch et al., 2005, Charras et al., 2008).

In order to understand whether the actomyosin cortex underlying the apical membrane of sprouting endothelial cells also counteracts blood pressure by generating tension at the membrane, and to assess whether its local weakening could be the event behind the initiation of inverse blebs, I decided to perform local ablations of the cortex at the tip of the lumen in sprouting endothelial cells. This technique has been successfully used in previous studies to induce blebbing in mouse fibroblasts (Tinevez et al., 2009).

By performing ablations along lines spanning the entire thickness of the apical membrane and its underlying cortex in *Tg(kdr-l:ras-Cherry$^{s916}$;fli1ep:Lifeact-EGFP)* embryos, I could induce the expansion of inverse blebs at the site of ablation (Figure 5.8 and Movie 5.3). Similarly to inverse blebs growing at the apical membrane during normal lumen formation, the growth of these artificially induced blebs was followed shortly by F-actin polymerisation and bleb retraction (Figure 5.8 and Movie 5.3). These experiments therefore suggest that the actomyosin cortex present at the apical membrane of sprouting cells generates tension to counteract blood pressure in “resting” conditions, and that its local weakening during lumen formation might be the event at the origin of inverse blebbing (Figure 5.9).

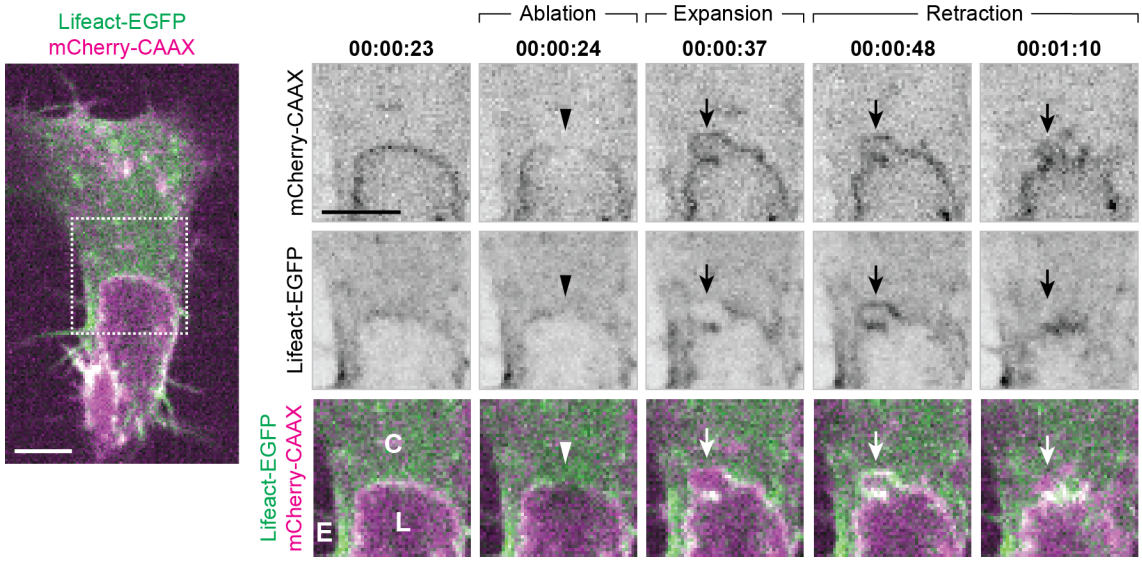


**Figure 5.8. Local ablation of the cortex at the apical membrane of sprouting cells induces inverse blebbing**
*Tg(kdr-l:ras-Cherry$^{s916}$;fli1ep:Lifeact-EGFP)* embryos were imaged from 33 hpf. Laser ablation was performed along a line spanning the entire thickness of the apical membrane and its underlying cortex, at the tip of the growing lumen. In 5 out of 18 cells, ablation resulted in the expansion of an inverse bleb at the apical membrane. Arrowhead, site of ablation. Arrow, inverse bleb. C, cytoplasm. E, extracellular space. L, lumen. Scale bars are 5 μm.

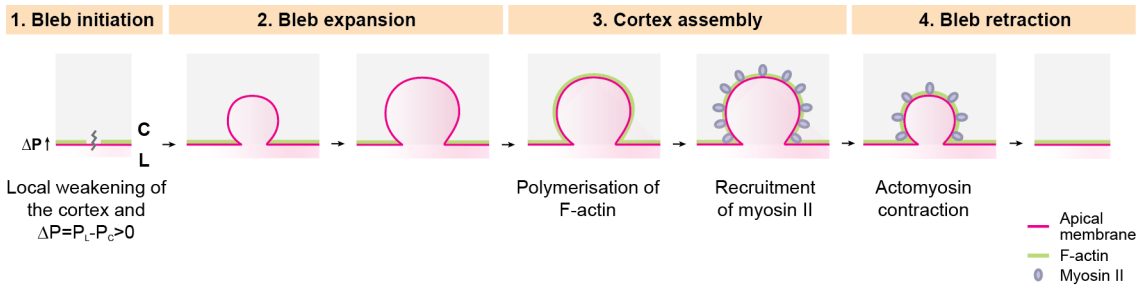


**Figure 5.9. Inverse blebbing: molecular mechanisms**
Schematic representation of inverse blebbing at the apical membrane of endothelial cells. Under blood pressure, and probably following local weakening of the cortex or its detachment from the membrane, blebs expand devoid of any F-actin or myosin II. Retraction occurs following 1) F-actin polymerisation, 2) myosin II recruitment, and 3) contraction of this actomyosin cortex all around the surface of the bleb.

## 5.4 Apical membrane contractility is required for lumen formation and maintenance

In order to assess whether apical membrane contractility is required for proper lumenisation in sprouting ISVs, I induced the expression of the dominant-negative Myl9bAA-EGFP reporter in single endothelial cells in *Tg(kdr-l:ras-Cherry)*$^{s916}$ embryos, from the onset of lumen formation, and checked ISVs made of EGFP-labelled cells for the presence of a lumen at 2 dpf. Quantification of ISVs with Myl9bAA expression revealed a significant difference compared to control ISVs expressing the wild-type form of Myl9b, with a decrease in the proportion of cells showing normal lumens (Figure 5.10). Abnormal ISVs were found to be unlumenised or displayed dilated lumens (Figure 5.10 and 5.11), suggesting that endothelial cell contractility is required for lumen formation and/or maintenance in sprouting ISVs.

In order to determine whether unlumenised ISVs were the result of a failure to expand lumens, or of the collapse of successfully formed lumens, I performed live imaging of Myl9bAA-expressing cells from 30 to 48 hpf. By doing so, I found that cells lacking lumens at 2 dpf were unable to expand their apical membrane during the time window when lumenisation normally occurs in sprouting ISVs (Figure 5.12 and Movie 5.4).

In order to get a deeper mechanistic understanding of the effects of Myl9bAA expression on apical membrane dynamics, I performed fast imaging of both unlumenised and dilated cells at 2 dpf. In both cases, the dynamics of the apical membrane was visibly affected by the expression of Myl9bAA. In unlumenised vessels, lumens initially expanded into Myl9bAA-expressing cells but the apical membrane showed excessive and uncoordinated blebbing. Failure to retract blebs led to new blebs growing on unretracted blebs and occasional disconnection of blebs from the membrane (Figure 5.11 and Movie 5.5), preventing lumen expansion as described above. On the other hand, dilated and partially lumenised cells were also unable to fully retract blebs growing on the lateral sides of the lumen, leading to the expansion in diameter of the lumen and the formation of side lumen branches (Figure 5.11 and Movie 5.6).

The occurrence of the phenotypes presented here depended on the levels of expression of the dominant-negative Myl9bAA reporter (Figure 5.10). The proportion of cells with no or abnormal lumens increased with the level of expression of Myl9bAA. Within this population, dilated lumens were observed in higher proportions in cells with moderate expression of Myl9bAA, while the absence of lumens at 2 dpf was more prominent in cells with strong expression of the reporter (Figure 5.10). These observations could suggest that dilated lumens arise in cells that are still able to contract actomyosin at the apical membrane at sufficient levels to allow partial lumen expansion. Variability in phenotypes may however also be due to some differences within the cell population in the time separating the onset of expression of the transgenes and the onset of lumen expansion.

Together, these data show that sprouting cells require actomyosin contraction at the apical membrane to counteract membrane deformations and thus ensure single, unidirectional lumen expansion in response to blood pressure.

## 5.5 Conclusions

In this chapter, I showed that endothelial cells actively respond to inverse blebbing by transiently and locally polymerising F-actin and recruiting myosin II to the apical membrane. The contraction of actomyosin filaments assembled at the surface of inverse blebs allows their successful retraction, and enables endothelial cells to control the deformations of the apical membrane generated by blood pressure and, ultimately, to control lumen expansion. Impairing the ability of endothelial cells to contract leads to severe lumen defects, and shows that apical contractility is required for lumen formation in sprouting ISVs. Finally, the presence of a contractile actomyosin cortex at the apical membrane of lumenising sprouts in mouse retinas further suggests that this mechanism could be conserved in mammals.

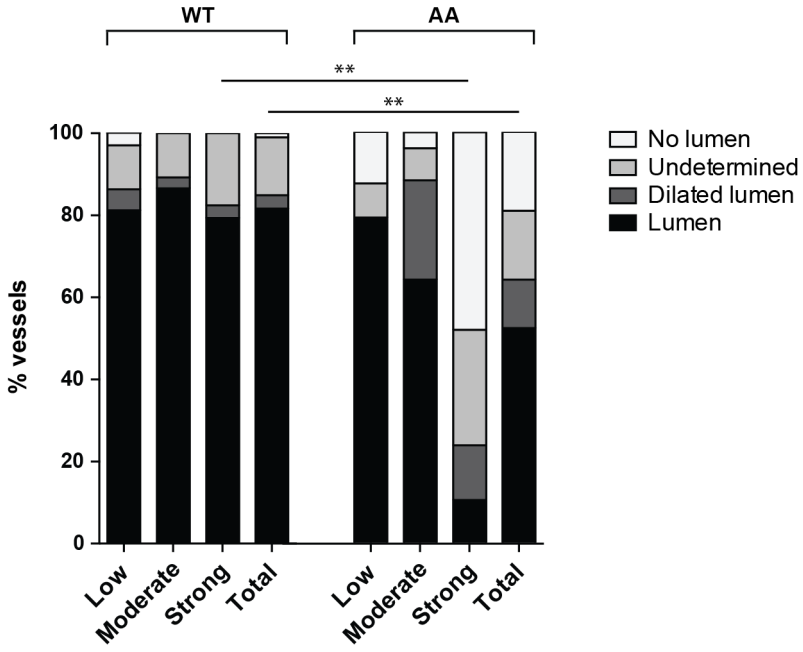


**Figure 5.10. Expression of Myl9bAA from 30 hpf leads to lumen defects in ISVs at 2 dpf**

*Tg(kdr-l:ras-Cherry)*$^{s916}$ embryos with mosaic expression of Myl9b-EGFP or Myl9bAA-EGFP were analysed at 2 dpf. EGFP-positive ISVs were classified by eye into three categories according to their level of EGFP expression (low, moderate, strong) and screened for the presence of a lumen. A multinomial log-linear model was used to test for association of cell count in the different categories with the mutation status (WT: n=55 ISVs, N=24 embryos; AA: n=31 ISVs, N=9 embryos; data pooled from three independent experiments; p=0.30 (low), p=0.11 (moderate), p=0.0002 (high), p=0.00024 (total); **, $p<0.01$). EGFP-positive cells where the presence or absence of a lumen could not be appreciated were referenced as undetermined.

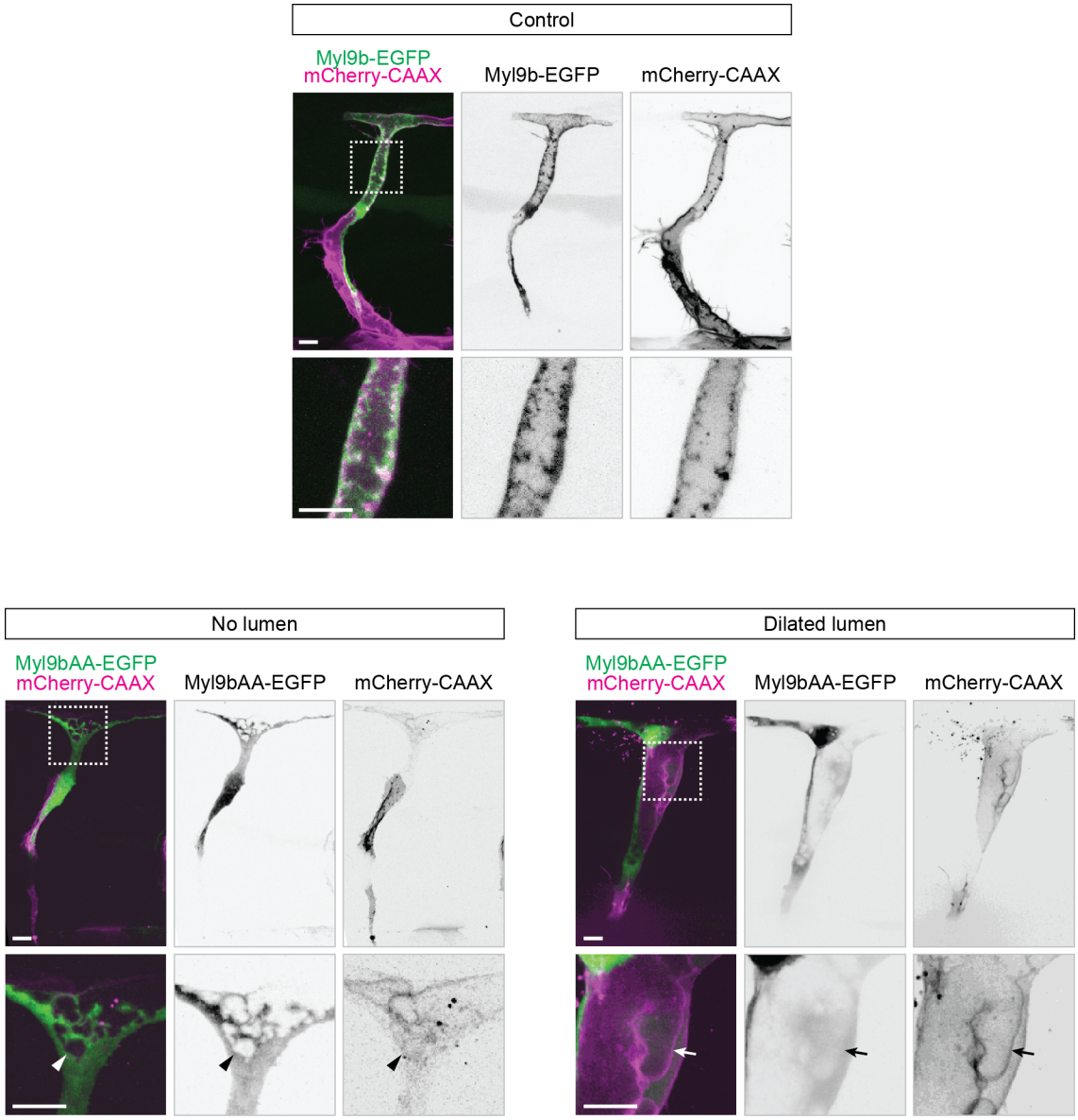


**Figure 5.11. ISVs expressing Myl9bAA show dilated or no lumen at 2 dpf**
*Tg(kdr-l:ras-Cherry)*$^{s916}$ embryos with mosaic expression of Myl9b-EGFP or Myl9bAA-EGFP (n=3) were imaged at 2 dpf. Arrowhead, disconnected lumen fragment. Arrow, side lumen branch. Scale bars are 10 μm.

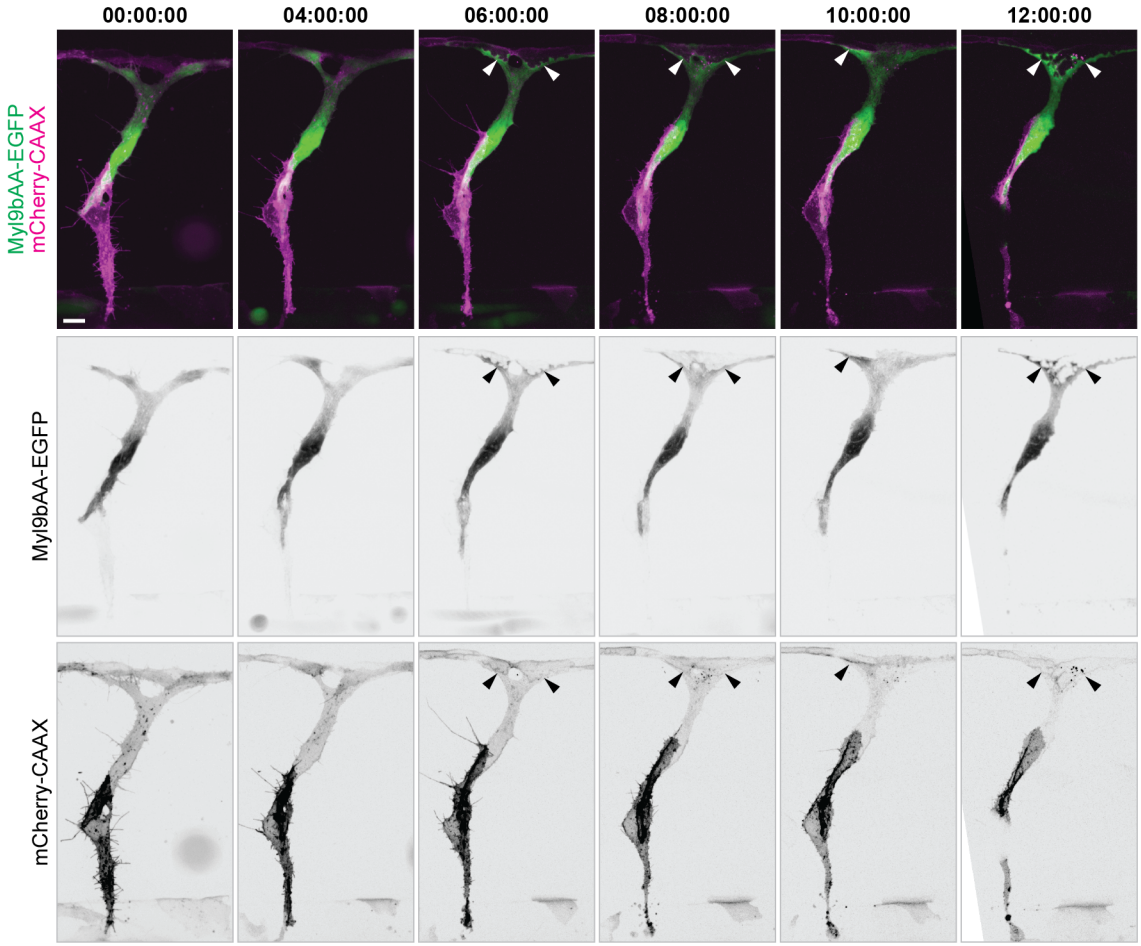


**Figure 5.12. Myl9bAA-expressing endothelial cells lacking lumens at 2 dpf fail to expand lumens**
*Tg(kdr-l:ras-Cherry)*$^{s916}$ embryos with mosaic expression of Myl9bAA-EGFP (n=3) were imaged from 35 hpf. Arrowheads, lumen. Time is in hours:minutes:seconds. Scale bar is 10 μm.

# Chapter 6. Discussion

## 6.1 Summary of the findings

In the present work, I used high spatial and temporal resolution imaging of lumen formation in angiogenic sprouts, both in the zebrafish trunk vasculature and in the mouse retina inner vascular plexus, to dissect the cellular mechanisms of lumen formation during sprouting angiogenesis *in vivo*. Using this approach, I discovered that lumens expand into angiogenic sprouts through a previously undescribed mechanism of inverse membrane blebbing driven by blood pressure. If multiple cells share the tip of a sprout, lumen expands at their junction. In the case of single tip cells, lumen expands as a membrane invagination, thus generating unicellular lumens, as previously reported during anastomosis (Herwig et al., 2011). In both cases, inverse blebs grow at the apical membrane of lumenising cells, leading to the expansion of the luminal compartment between or within single cells. When blood flow is stopped experimentally by laser ablation of the base of the vessel or by tricaine-induced decrease of blood pressure, inverse blebbing ceases and the lumen stops expanding and eventually collapses.

In addition, I found that, similarly to what is observed for classical blebbing in other cell and organism models (Charras and Paluch, 2008), endothelial cells have the ability to retract inverse blebs growing at their apical membrane by recruiting and contracting actomyosin around the bleb membrane. This mechanism allows selective bleb retraction along the apical membrane. When the ability of the cell to contract is altered through the expression of a dominant-negative form of the regulatory light chain of non-muscle myosin II, endothelial cells fail to retract blebs, leading to excessive and uncoordinated deformation of the apical membrane. The affected cells fail to expand lumens and, if partially lumenised, show unresolved blebs and side lumen branches.

Together, this work shows that a tight equilibrium between the forces exerted by the blood on the apical membrane of endothelial cells, and the endogenous contractile responses from the endothelial cells, drives and controls lumen expansion in angiogenic sprouts *in vivo* (Figure 6.1). Immunostainings for the apical membrane and actomyosin in mouse retinas, although only providing static information, suggest that this mechanism might be conserved in mammals, and constitutes a general mechanism of pressure-driven lumen formation in perfused blood vessels.

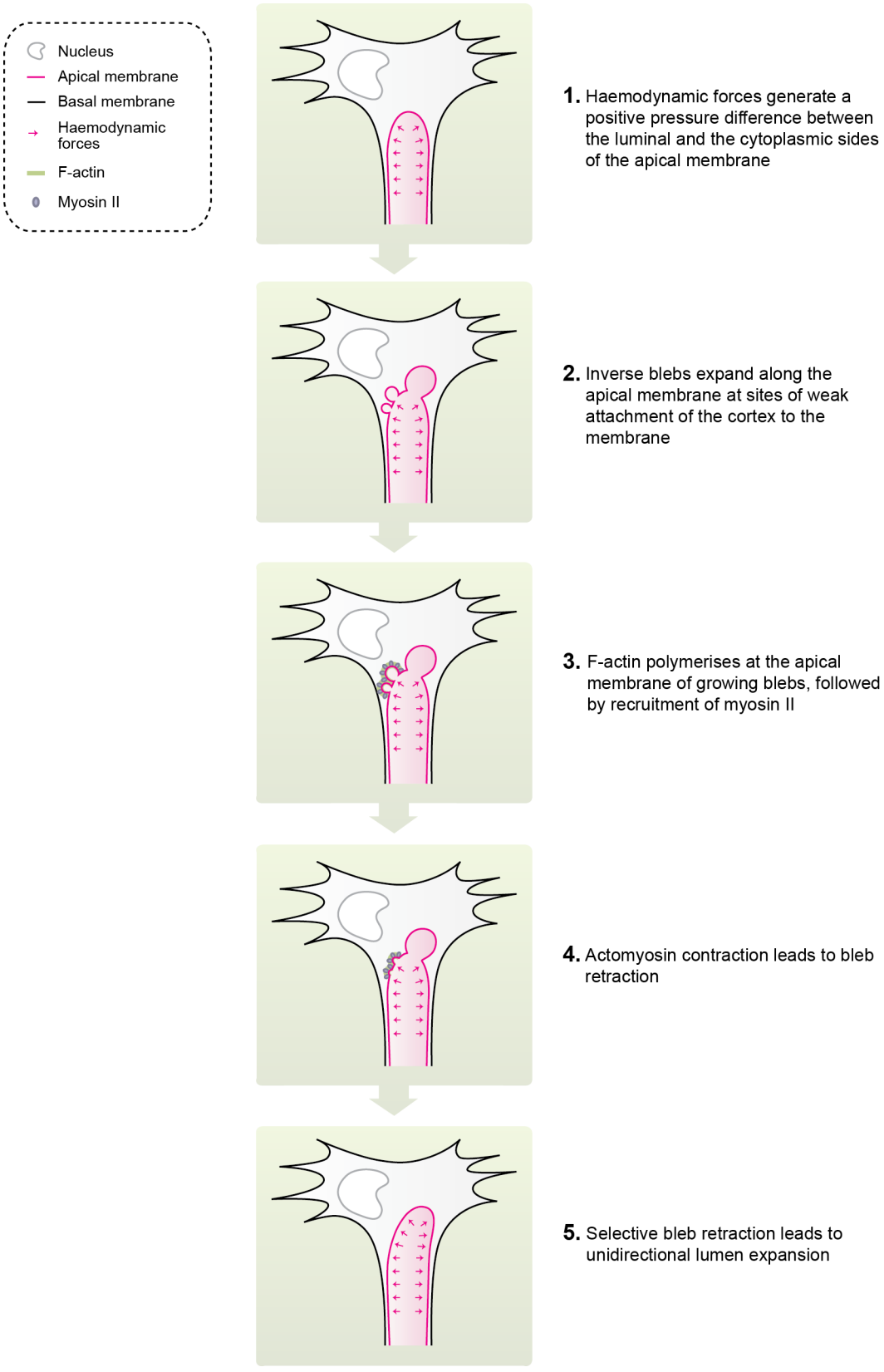


**Figure 6.1. Model of lumen formation by inverse membrane blebbing during sprouting angiogenesis *in vivo***

## 6.2 Cellular mechanisms of vascular lumen formation

### 6.2.1 Revisiting previous models of lumen formation during sprouting angiogenesis *in vivo*

This work challenges the previous model proposed by Weinstein and colleagues (Kamei et al., 2006) that lumens form in angiogenic sprouts *in vivo* through the formation and fusion of intracellular vacuoles in the cytoplasm of sprouting cells. Using reporters for the apical membrane, F-actin and non-muscle myosin II, and fast time-lapse imaging allowing tracking of membrane dynamics within seconds, I could not observe any *de novo* formation of vacuoles in the cytoplasm of lumenising cells. Large isolated lumen fragments were observed, but these structures always derived from the collapse of growing lumens in sprouting ISVs (Figure 3.4). The observation of only a very low number of such fragments in angiogenic sprouts in mouse retinas (1.6% of total sprouts, see Table 3.1) also suggests that vacuole formation and fusion is very unlikely to be the main mechanism of lumen formation in this model.

Several reasons can be advanced to explain the difference between the model of lumen expansion by inverse membrane blebbing that I propose in this work, and the model described by Weinstein and colleagues. First and foremost, their microscopy data suffered from low spatial and temporal resolution and, supported by their finding that endothelial cells form vacuoles *in vitro*, probably led them to mistake inverse blebs for vacuoles in close proximity with the growing lumen. The interval between the acquisition of each frame of their time-lapse series (3 to 5 minutes) is longer than the average time I report for the expansion and retraction of inverse blebs (see Figure 4.4), and therefore did not allow them to follow single blebbing events. Secondly, the main reporter used in their study (EGFP-Cdc42) did not allow clear labelling of the apical membrane, and high fluorescence signal in the cytoplasm of labelled cells contributed to the lack of resolution of the presented time-lapse series. Finally, although viability and normal development of the *Tg(fli1:EGFP-cdc42wt)*$^{y48}$ zebrafish line was confirmed, increased levels of Cdc42 in the cells may have affected membrane dynamics. *In vitro*, it has been reported that expression of exogenous reporters for Cdc42, kRas, and Rap1b significantly enhances tubulogenesis in endothelial cells cultured in 3D collagen matrices (Norden et al., 2016). Overexpression of the wild-type Myl9b-EGFP reporter

was also seen to occasionally affect membrane dynamics and lumen formation in some endothelial cells when expressed at very high levels (not shown). Therefore, expression of exogenous reporters should be kept at the lowest level and carefully controlled to allow the drawing of reliable conclusions. This is the reason why I turned, in the present study, to the use of reporters bearing no biological function (EGFP-CAAX and mCherry-CAAX).

The fact that lumen expansion immediately stops after ablation of the connection of single ISVs to the dorsal aorta strongly suggests a vacuole-independent mechanism of lumen formation. However, the existence of vacuoles and their participation to lumen expansion cannot be completely dismissed. Although the EGFP- and mCherry-CAAX reporters should, in theory, label vacuolar membranes, it is still possible that such structures remained unlabeled, and were therefore missed, in the course of this study. Identification of vacuole-specific markers, or the design of reporters for early apical markers, could further strengthen our current hypothesis of a flow-dependent, vacuole-independent mechanism of lumen formation during sprouting angiogenesis *in vivo*.

### 6.2.2 Relevance of *in vitro* models of vascular lumen formation

This work also more generally raises the question of the relevance of *in vitro* models of tubulogenesis in endothelial cells, as the mechanism at play (vacuole formation and fusion) differs from all mechanisms identified *in vivo* – cord hollowing during vasculogenesis, and cord hollowing and membrane invagination during sprouting angiogenesis. The assay used in most of the *in vitro* studies presented in the introduction to this work (and detailed in 1.3.1) allows lumen formation between endothelial cells coalescing in 3D collagen matrices, in a context resembling the formation of the primary vessels by vasculogenesis. The success of this method is highly dependent on culture conditions (Koh et al., 2008b, Davis et al., 2013), and the first and most extensively used version of this assay relied on the use of phorbol ester, an activator of PKC, to drive vacuole formation *in vitro*. Phorbol ester is a potent inducer of endo- and pinocytosis in many cell types (Swanson et al., 1985, Nilsson et al., 1989, Keller, 1990, Aballay et al., 1999), which raises the question of the relevance of the vacuoles observed using this assay for the more general context of physiological

endothelial lumen formation. The recent switch to a phorbol ester-free cytokine-based assay (Stratman et al., 2011, Davis et al., 2013), where results from previous studies could be confirmed, may provide a better basis for further investigations, although relevance of vacuole-based models of lumen formation for the general understanding of lumen formation during vascular development remains debatable.

*In vitro* models of vascular lumen formation remain an area in need for further development, since such models would allow to easily assess the contribution of individual signalling pathways, as well as of external stimuli such as matrix composition and stiffness, interaction with pericytes, or even perfusion, on tubulogenesis. Considerable efforts currently invest in the development of devices in which endothelial cells are allowed to organise themselves into lumenised networks that are later perfused using pump or reservoir systems (Zheng et al., 2012, Moya et al., 2013, Bichsel et al., 2015, Wang et al., 2016). While such devices will offer important insights into the role of haemodynamics in various aspects of blood vessel formation and remodelling, they could also be considered for the study of lumen formation under flow, if design modifications can be brought to induce sprouting in these systems. Although the field of sprouting angiogenesis benefits from *in vitro* sprouting models from embryonic stem cell aggregates or from beads coated with endothelial cells, none of these systems allows perfusion, therefore lacking what I describe here as a major driver of lumen formation in angiogenic sprouts. These systems could however still provide insights into flow-independent mechanisms of lumen formation, such as, for example, those driving the segregation of apical determinants at cell junctions, since these mechanisms appear to work independently of blood flow (Herwig et al., 2011).

Although the development of such *in vitro* systems would, in principle, allow easy manipulation and fine dissection of the cellular and molecular mechanisms of lumen formation, their setup is challenging. On the other hand, zebrafish established itself as a powerful model for the study of blood vessel formation *in vivo*, and recent technical and technological advances open the door to the fine analysis of endothelial cell behaviour at the single-cell level in specific genetic contexts. TALEN- and CRISPR/Cas9-mediated gene editing techniques, for example, are being developed in many research groups and bear great potential for efficient gene knockout and knockin in zebrafish embryos (Huang et al., 2011, Sander et al., 2011, Hwang et al., 2013b, Hwang et al.,

2013a, Auer et al., 2014, Auer and Del Bene, 2014). Generation of zebrafish lines mutant for potential polarity effectors using these techniques will allow to assess the requirement for these proteins during vascular development. In the event of global effects on the organism and/or to highlight cell-autonomous phenotypes, transplantation of mutant cells into wild-type embryos could allow finer assessment of the role of these proteins at the single-cell level. Additionally, the development of advanced imaging techniques such as spinning disk microscopy (used in this work), single plan illumination microscopy (SPIM), and super resolution microscopy, will offer the opportunity to follow membrane trafficking events and the structure and dynamics of protein complexes during polarity establishment and lumen formation at the subcellular level. Together, these considerations make zebrafish a model of choice for the study of lumen formation during sprouting angiogenesis.

### 6.2.3 Lumen formation during vasculogenesis and angiogenesis *in vivo*: different contexts call for specific mechanisms

Both previous work in the field (Herwig et al., 2011, Lenard et al., 2013) and the present study show that blood flow is required for lumen formation in angiogenic sprouts *in vivo*, by allowing separation of apposing membranes at cell junctions and invagination into single endothelial cells through inverse membrane blebbing. In comparison, the primary vessels that form by vasculogenesis develop and lumenise prior to the establishment of blood circulation, and therefore do so through blood pressure-independent mechanisms involving extensive cell shape changes mediated by the contraction of apically enriched actomyosin (Strilic et al., 2009). It is interesting to note how vessels developing in different physiological contexts have adopted different mechanisms of lumen formation, although both require extensive cell shape changes under the control of the actin cytoskeleton and involve, to some extent for angiogenesis, cord hollowing mechanisms.

It will be important to extend the present study to different vascular beds, organisms, and to adult angiogenesis. In particular, it will be interesting to address the differences that may exist between physiological and pathological contexts, especially those presenting altered blood perfusion and/or pressure, such as cancer and diabetes (Potente

et al., 2011). Other vascular beds in zebrafish embryos, such as the brain vasculature or the subintestinal vascular plexus, could provide further insights into the variability existing in the mechanisms of lumen formation. Some of these vessels might additionally prove useful to dissect in more detail the molecular mechanisms at play during membrane invagination. In fact, while the arrangement of endothelial cells in ISVs is relatively heterogeneous, vessels in the brain vasculature have been identified as highly stereotypic. The palatocerebral artery, for example, always lumenises first through apical membrane invagination into the anastomosing tip cells, before cells rearrange to lead to the establishment of a multicellular tube (Lenard et al., 2013). The fin regeneration model in adult zebrafish could also be considered for the study of lumen formation in the adult and in the context of wound healing (Xu et al., 2014). Finally, many mouse models of pathological angiogenesis are available. While the study of fixed tissues would provide only limited information on apical membrane dynamics, dynamic data could be obtained using intravital imaging of angiogenesis in live animals, for example in the brain using cranial windows (Kienast et al., 2010).

## 6.3 Molecular mechanisms of vascular lumen formation

### 6.3.1 Establishment of apical-basal polarity

Studies in MDCK cysts built a detailed model for the segregation of apical and basal determinants during lumen formation between contacting cells. Work carried in *in vitro* models of vascular lumen formation suggests that many of the identified regulators of apical-basal polarity establishment in MDCK cysts are also required in endothelial cells, although these findings mostly rely on siRNA and biochemical interaction studies, and would benefit from more extensive analysis by time-lapse imaging of protein localisation and dynamics.

Some of these mechanisms have already been shown to be conserved *in vivo* during the formation of the dorsal aorta. Podocalyxin, moesin, F-actin and non-muscle myosin II were all identified as essential regulators of apical domain specification and cell shape changes during lumen formation in the mouse dorsal aorta (Strilic et al., 2009). Attachment to the ECM through integrin β1 (Zovein et al., 2010) and integrity of cell

junctions (Strilic et al., 2009, Wilson et al., 2013) have also both been reported as polarisation cues required for lumen formation during vasculogenesis. How signalling from cell-ECM and cell-cell interfaces leads to the segregation of the identified apical determinants remains to be addressed.

During sprouting angiogenesis, podocalyxin is found at the apical membrane of lumenising ISVs of zebrafish embryos, and accumulates at the new cell junction forming between anastomosing cells (Herwig et al., 2011). VE-cadherin and moesin1 have also been identified as regulators of lumen formation in sprouting ISVs (Wang et al., 2010). However, post-natal endothelial-specific deletion of integrin β1, Par3, aPKC, and Cdc42 in mice suggests that these proteins are all dispensable for lumen formation in the mouse retina inner plexus (Nakayama et al., 2013, Barry et al., 2015, Yamamoto et al., 2015), and therefore raises the question of whether these mechanisms also regulate lumen formation during sprouting angiogenesis.

It would be interesting to address whether, and if so to what extent, ECM-cell and cell-cell signalling, polarity complexes, Rho GTPases, and Rab-mediated membrane trafficking regulate lumen formation during sprouting angiogenesis *in vivo*. These questions will benefit from high resolution single-cell studies in zebrafish embryos, where the localisation and dynamics of such polarity effectors could be investigated, along with their requirement for lumen formation, taking advantage of the technical advances previously mentioned.

### 6.3.2 The role of the actin cytoskeleton during vascular lumen formation

#### *6.3.2.1 Cell shape changes during lumen formation*

Several studies and the present work have identified and described in detail multiple roles for actin in regulating vascular lumen formation *in vivo*. Drastic cell shape changes are observed both during vasculogenesis and angiogenesis, and are required for lumen formation and maintenance (Strilic et al., 2009, Herwig et al., 2011). Interestingly, cell elongation is observed in both contexts and happens independently of blood flow in both cases, since inhibition of blood flow in zebrafish embryos does not affect cell elongation in angiogenic sprouts (Herwig et al., 2011). However, while cell shape changes drive the opening of lumens during vasculogenesis, the cell elongation

observed during angiogenesis is not sufficient in this context to induce the separation of apposing membranes, a process that requires blood flow.

In the case of vasculogenic lumen formation, although current studies only refer to cell elongation, the topology of lumenised vessels suggests that the apical membrane must also bend and adopt a concave morphology to allow the formation of a tubular structure. Distinction between mechanisms of cell elongation and, if existing, apical membrane bending, has not been addressed yet. Recruitment of F-actin and non-muscle myosin II at the apical membrane, and phosphorylation of myosin II through VEGF-A and ROCK, are required for tubulogenesis in the mouse dorsal aorta, suggesting that the contraction of an apically-enriched actomyosin network drive the cell shape changes observed during lumen formation in this model (Strilic et al., 2009). In zebrafish, AmotL2 is required for the anchoring of radial actin fibres to cell junctions, which are, in turn, required for cell elongation in the dorsal aorta (Hultin et al., 2014). Together, these studies therefore suggest a model where contraction of an apically-enriched actin cortex and, if distinct, of actin fibres connecting cell junctions, drive cell morphology changes during vasculogenesis, through cell elongation and/or apical membrane bending.

During sprouting angiogenesis, cell elongation is also dependent on the coupling of F-actin to VE-Cadherin at cell junctions, and on F-actin polymerisation, partly through FMNL3, but treatment with the myosin II inhibitor blebbistatin suggests that this process does not involve actomyosin contraction (Sauteur et al., 2014, Phng et al., 2015). This difference with the mechanisms described during vasculogenesis might account for the difference observed in the morphogenesis of blood vessels in these two contexts, and could suggest that actomyosin contraction at the apical membrane of aortic endothelial cells is what drives membrane separation and lumen opening, although this remains entirely hypothetical.

Together, the studies carried on the role of actin suggest that different actin structures and/or dynamics might regulate endothelial cell shape changes during vasculogenic and angiogenic lumen formation *in vivo*. In this context, it would be interesting to describe with high detail the subcellular organisation and dynamics of the actin cytoskeleton during lumen formation, and assess the individual contribution that specific networks might have in regulating different cellular processes at different locations in the cell – apical membrane, basal membrane, and cell junctions.

#### *6.3.2.2 Regulation of inverse blebbing at the apical membrane*

Here, I describe a novel role for actin at the apical membrane of sprouting endothelial cells during phases of lumen formation. I show that upon blood pressure-induced membrane deformation, F-actin polymerises locally at the apical membrane, forming transient actin networks whose contraction upon non-muscle myosin II recruitment and activation allows retraction of inverse blebs and control over apical membrane deformation.

What drives actin polymerisation and actomyosin contraction at the apical membrane of endothelial cells remains unknown. During classical blebbing, as shown in constitutively blebbing M2 melanoma cells *in vitro*, an actomyosin cortex assembles at the membrane of expanding blebs through the action of a variety of actin nucleators and linkers. Early recruitment of membrane-actin linkers of the ERM family, such as ezrin and moesin, allows the anchoring of F-actin filaments at the bleb membrane (Charras et al., 2006). F-actin polymerisation itself is regulated by several nucleators. While the formin mDia1 and the Arp2/3 complex have been identified as the major nucleators involved (Bovellan et al., 2014), roles for the formins mDia2, FHOD1, FMNL2, and DIAPH3 have also been reported (Eisenmann et al., 2007, Hannemann et al., 2008, Kitzing et al., 2010, Stastna et al., 2012, Wyse et al., 2012). F-actin polymerisation is then followed by the recruitment of non-muscle myosin II in foci along the newly formed cortex. Phosphorylation of myosin II finally drives contraction of the newly assembled cortex, leading to membrane crumpling and bleb retraction. RhoA is a major regulator of actomyosin contraction, and regulates both actin polymerisation through formins and myosin phosphorylation via ROCK (Sit and Manser, 2011). RhoA was found to regulate blebbing *in vitro*, although the exact mechanism by which it does so remains to be identified (Charras et al., 2006).

It would be of high interest to determine whether the same mechanisms are regulating actomyosin assembly and contraction at the membrane of inverse blebs in endothelial cells. Moesin is required for lumen formation in sprouting ISVs (Wang et al., 2010). Whether the lack of lumen in cells knocked down for moesin results from impaired attachment of the actin cortex to the membrane of expanding blebs is an obvious question. Inducible single-cell loss-of-function approaches such as the one used in this

work to inhibit myosin function could target this question. Preliminary work carried out in our laboratory also suggests a role for RhoA in regulating lumen formation in zebrafish ISVs. Upon inducible expression of dominant-negative or constitutively-active forms of RhoA from 30 hpf, lumen defects are observed at 2 dpf (Li-Kun Phng, unpublished data). Preliminary live imaging experiments however suggest that the whole cortex of endothelial cells is affected by the expression of these constructs, and specific contribution of RhoA in regulating actin assembly and myosin phosphorylation at the apical membrane might be hard to address with the tools that are currently available. The expression of a fluorescence resonance energy transfer (FRET) biosensor for RhoA should hopefully indicate whether activation of RhoA is detected at the apical membrane during phases of lumen expansion (ongoing work). On the other hand, dominant-negative and constitutively-active forms of ROCK and MLCK reporters were generated to address the requirement for both kinases in the regulation of myosin II phosphorylation with hopefully, if involved in this process, narrower effects on the overall cell morphology in comparison to RhoA manipulations.

An important consideration when comparing classical and inverse blebbing is the polarity of these two mechanisms. In classical blebbing, the plasma membrane blebs outwards following the positive pressure difference existing between its cytoplasmic and extracellular sides. In contrast, during inverse blebbing, pressure is higher outside the cell, driving the membrane to bleb inwards. In this case, the membrane has to break through the actin cortex underlying the apical membrane, which might involve more extensive alterations of the actomyosin cortex than in the case of classical blebbing, where the membrane only detaches from it. A second consequence of the difference in bleb polarity is the location of the actomyosin cortex in relation to the bleb membrane. In classical blebbing, an actomyosin cortex assembles on the inner surface of the bleb, and contraction of actomyosin fibres leads to the crumpling of the membrane that is pulled back in its original position. However, during inverse blebbing, the cortex assembles on the outer surface of the bleb, which suggests a pushing, rather than a pulling, of the bleb membrane against the pressure direction during retraction. Whether this means different actin cortex organisation and dynamics are involved in these two processes is an interesting point to consider.

The mechanisms of bleb initiation also deserve further investigation. In classical blebbing, both local breakage of the actin cortex and local detachment of the cortex from the membrane have been reported as mechanisms driving bleb initiation (Cunningham, 1995, Keller and Eggli, 1998, Paluch et al., 2005, Charras et al., 2008). In endothelial cells, local weakening of the cortex by laser ablation induces the formation of inverse blebs at the apical membrane of sprouting cells, and therefore suggests that inverse blebs may arise as well from the local breakage or detachment of the cortex from the apical membrane. An hypothesis could be that inverse blebbing then occurs stochastically within a relatively plastic actin cortex weakened by the pushing forces exerted by the blood on the apical membrane.

In this work, I show that a pressure differential between the luminal and cytoplasmic sides of the apical membrane is required for the initiation of inverse blebbing. When ISVs are severed through ablation of their connection to the dorsal aorta, local breakage of the endothelial barrier leads to the leakage of blood into the microenvironment, and presumably to an instant drop in blood pressure leading to immediate stop of inverse blebbing. However, the values for luminal and cytoplasmic pressures - and therefore the amplitude of the pressure differential - involved in this process are not known. Aortic blood pressure has been successfully measured in zebrafish embryos from 2.5-3 dpf using a servo-null micro-pressure system (Pelster and Burggren, 1996, Hu et al., 2000, Kopp et al., 2005). Kopp and colleagues reported a blood pressure of 0.37 ± 0.04 mmHg (equivalent to 49.33 ± 5.33 Pa) in the ventral aorta of 2.5-3 dpf zebrafish embryos. Blood pressure in single ISVs is likely to show similar values, although local variations, especially as the distance to the heart increases, might be observed. *In vitro*, similar servo-null micro-pressure systems have been used successfully to measure intracellular pressure in primary human fibroblasts (Petrie et al., 2014). *In vitro*, intracellular pressure has been reported to vary between 100 to several 1,000 Pa. Both bodies of literature therefore suggest that blood pressure in zebrafish embryos would be 10 to 100 times lower than intracellular pressure as recorded *in vitro*, which would suggest a pressure differential in the opposite direction to the one reported to drive inverse blebbing in this study. One has to note that intracellular pressure may show highly different values in cells *in vivo*, in comparison to cells cultured *in vitro* on stiff substrates. Additionally, it could be that blood pressure in single ISVs is greater than the

pressure reported in the ventral and dorsal aortae. Addressing these questions will require precise measurement of both luminal and cytoplasmic pressures in ISVs undergoing lumen formation. Although it may prove technically challenging, the use of servo-null micro-pressure systems fitted with glass micropipettes of small diameter (0.5 $\mu$ m in (Petrie et al., 2014)) seems an attractive approach to measure both pressures in live zebrafish embryos.

Why inverse blebbing ceases when the system becomes perfused remains unknown. Theoretically, the connection of ISVs to neighbouring vessels and the establishment of perfusion are likely to lead to a drop in pressure within the single ISVs. This drop in pressure could then lead to a reduction, or even loss or inversion, of the pressure differential required for the initiation of inverse blebbing. Changes in cell arrangement within the vessels and/or in cell architecture - in particular in regards to the structure and dynamics of the cytoskeleton – may also affect the physical properties of the apical membrane of endothelial cells at that stage, and participate in the cessation of inverse blebbing.

One of the most intriguing questions is what drives the selectivity in the occurrence of bleb retraction in endothelial cells, thus allowing expansion of the lumen only in the direction of the growing vessel. Several hypothesis can be advanced. First, the properties of the membrane and/or of its underlying cortex may differ between the tip of the lumen and its sides. An obvious difference is already observable in the topology of the membrane; the high membrane curvature at the tip of the lumen might recruit different molecular machineries through membrane curvature-sensing domains, such as BAR domains and ALPS motifs (Antonny, 2011). A second hypothesis could be that the tip and sides of the lumen experience difference haemodynamic forces related to its topology, although the pressure experienced by the membrane should theoretically be the same along its entire length. In both cases, a resulting heterogeneity in membrane tension could be sensed by tension sensors and relay different signals within the cell. Piezo1, a cation channel activated upon mechanical stress, has, for example, recently been identified as a regulator of endothelial cell elongation in response to shear stress, and is required for blood vessel morphogenesis during embryonic development (Li et al., 2014c, Ranade et al., 2014). Whether Piezo1 or other mechanically-activated ion

channels could regulate signalling at the subcellular level during lumen formation remains to be addressed.

A last consideration relates to the extreme and rapid increase in apical membrane surface area observed during lumen expansion by inverse blebbing. Where does the new apical membrane come from, and which mechanisms regulate its rapid increase? A first step will be to address whether the total surface of the plasma membrane of lumenising endothelial cells increases during lumen formation, or if the apical membrane surface area increases at the expense of other membrane domains, such as the basal membrane. The speed at which the apical membrane is sometimes seen expanding (several micrometres within seconds/minutes) would strongly favour the hypothesis that the apical membrane expands at the expense of the basal domain through a basal shift of junctional complexes. Single-cell labelling with EGFP/mCherry-CAAX and junctional reporters should allow to address this point. Other mechanisms may however contribute to the increase in surface area of the apical membrane. Rapid increase in surface area could be due in part to stretching of the lipid bilayer, although this could only contribute to a 2-3% increase in surface area (Hamill and Martinac, 2001). The membrane of endothelial cells is also known to contain large numbers of caveolae, which are small membrane invaginations 50-100 nm in size (Sowa, 2012). Caveolae have been shown to unfold in reaction to osmotic stress and mechanical stretching in lung endothelial cells *in vitro* and thus buffer membrane tension (Sinha et al., 2011). However, this mechanism would also induce only minor increases in cell surface area (0.1-0.3%). Another, but slower, mechanism could involve the recycling through vesicular trafficking of membrane material from other membrane domains in the cell towards the apical surface. Imaging of the mCherry-CAAX line revealed the presence of cytoplasmic spots moving within the cells during lumen formation. While the exact nature of these spots was not investigated, it is likely they could correspond to vesicles carrying membrane material, and potentially apical determinants, to the expanding apical membrane during lumen formation. Higher time resolution imaging would be necessary to determine the exact origin, destination, and trajectory of these spots, and thus hypothesise on their putative function(s).

Testing these different hypotheses *in vivo* will be challenging, but could be performed following the identification of specific markers for the different membrane domains in the cell, single-cell labelling, and the development of extremely high spatial and temporal resolution imaging.

## 6.4 Conclusion

Together, the present work identifies a novel mechanism of lumen expansion driven by blood pressure during sprouting angiogenesis *in vivo*, and provides an alternative model to the previous debated hypothesis that endothelial cells form lumens through vacuole formation and fusion *in vivo*. It additionally identifies inverse membrane blebbing as a reaction of plasma membranes to high external pressure, and suggests that the process of membrane blebbing, best described in cell division, cell migration and apoptosis, does not require a specific polarity, and more generally occurs in situations where membrane tension and stability of the actin cortex are challenged by internal or external mechanical stresses. In the case of endothelial cells, I find that blebbing bears a morphogenetic role and drives the cell shape changes required for the opening of patent lumens *in vivo*.

# Chapter 7. Appendix

## 7.1 Movie legends

**Movie 4.1. Lumens expand as membrane invaginations into single tip cells** (related to Figure 4.1)
Time-lapse series of an endothelial sprout expressing mCherry-CAAX imaged from 32 hpf. Arrows point at the invagination of the apical membrane into one single tip cell. Time is in hours:minutes:seconds.

**Movie 4.2. Lumens expand along cell junctions when the tip of the sprout is shared between several cells** (related to Figure 4.1)
Time-lapse series of an endothelial sprout expressing mCherry-CAAX imaged from 32 hpf. Arrows point at the expansion of the lumen along the cell junction between the two cells making the tip of the sprout. Time is in hours:minutes:seconds.

**Movie 4.3. Apical membrane undergoes inverse blebbing during lumen expansion** (related to Figure 4.2)
Time-lapse series of an endothelial sprout with mosaic expression of EGFP-CAAX imaged from 36 hpf. The apical membrane shows inverse blebs as the lumen expands into the sprout (black arrow). The red arrow shows a disconnected lumen fragment originating from the collapse of the lumen. Time is in hours:minutes:seconds.

**Movie 4.4. Inverse membrane blebbing drives multicellular lumen expansion** (related to Figure 4.5)
Time-lapse series of an endothelial sprout with mosaic expression of EGFP-CAAX (left panel, green) and expression of mCherry-CAAX (right panel, magenta) imaged from 32 hpf. Inverse blebbing occurs simultaneously in both cells forming the ISV as the lumen expands (white arrows). Time is in hours:minutes:seconds.

**Movie 4.5. Interruption of blood flow by laser ablation inhibits inverse blebbing at the apical membrane of angiogenic sprouts** (related to Figure 4.6)

Time-lapse series of an endothelial sprout expressing EGFP-CAAX imaged from 33 hpf. Laser ablation was performed along a line spanning the entire thickness of the vessel at the place indicated by the red arrow, and at the time indicated. Ablation led to an immediate loss of the inverse blebs at the apical membrane and to gradual regression of the lumen (black arrow). Time is in hours:minutes:seconds.

**Movie 4.6. Interruption of blood flow by tricaine treatment inhibits inverse blebbing at the apical membrane of angiogenic sprouts** (related to Figure 4.7)
Time-lapse series of an endothelial sprout expressing mCherry-CAAX imaged from 34 hpf, before, during and after treatment with 4x tricaine. Blood flow stops about 15-20 minutes after addition of 4x tricaine (data not shown), leading to a loss of the inverse blebs at the apical membrane. Black arrows show expansion of the apical membrane by inverse blebbing before treatment with 4x tricaine and after washout. Time is in hours:minutes:seconds.

**Movie 5.1. F-actin polymerises around inverse blebs as they retract** (related to Figure 5.2)
Time-lapse series of an endothelial sprout with mosaic expression of Lifeact-EGFP (left panel, green) and mCherry-CAAX (right panel, magenta) imaged from 35 hpf. F-actin polymerises around inverse blebs as they retract. Time is in hours:minutes:seconds.

**Movie 5.2. Myosin II is recruited around inverse blebs following F-actin polymerisation** (related to Figure 5.5)
Time-lapse series of an endothelial sprout with mosaic expression of Myl9b-EGFP (left panel, green) and Lifeact-mCherry (right panel, magenta) imaged from 35 hpf. Myosin II is recruited at the apical membrane around inverse blebs shortly after F-actin polymerisation. Time is in hours:minutes:seconds.

**Movie 5.3. Laser ablation of the actomyosin cortex at the apical membrane of growing lumens leads to the expansion of inverse blebs** (related to Figure 5.8)
Time-lapse series of an endothelial sprout expressing Lifeact-EGFP (left panel, green) and mCherry-CAAX (right panel, magenta) imaged from 33 hpf. Laser ablation of the

cell cortex was performed along the indicated black/white line and led to the expansion of a bleb that later retracted (white arrow). Time is in hours:minutes:seconds.

**Movie 5.4. Apical contractility is required for lumen expansion** (related to Figure 5.12)
Time-lapse series of an endothelial sprout with mosaic expression of Myl9bAA-EGFP (left panel, green) and mCherry-CAAX (right panel, magenta) imaged from 35 hpf. The cell expressing Myl9bAA fails to lumenise from the ventral part of the ISV. Lumen pushes into the cell from the dorsal longitudinal anastomotic vessel (DLAV) but fails to expand (white arrows). Time is in hours:minutes:seconds.

**Movie 5.5. Endothelial cells with decreased apical contractility are unable to retract blebs and fail to expand lumens** (related to Figure 5.11)
Time-lapse series of an endothelial sprout with mosaic expression of Myl9bAA-EGFP (left panel, green) and mCherry-CAAX (right panel, magenta) imaged from 48 hpf. The apical membrane undergoes excessive and uncoordinated blebbing and fails to expand. Time is in hours:minutes:seconds.

**Movie 5.6. Partially lumenised endothelial cells with decreased apical contractility are dilated and show side lumen branches** (related to Figure 5.11)
Time-lapse series of an endothelial sprout with mosaic expression of Myl9bAA-EGFP (left panel, green) and mCherry-CAAX (right panel, magenta) imaged from 52 hpf. The ISV is dilated and shows side lumen branches that fail to retract (white arrows). Time is in hours:minutes:seconds.

## 7.2 Plasmid maps

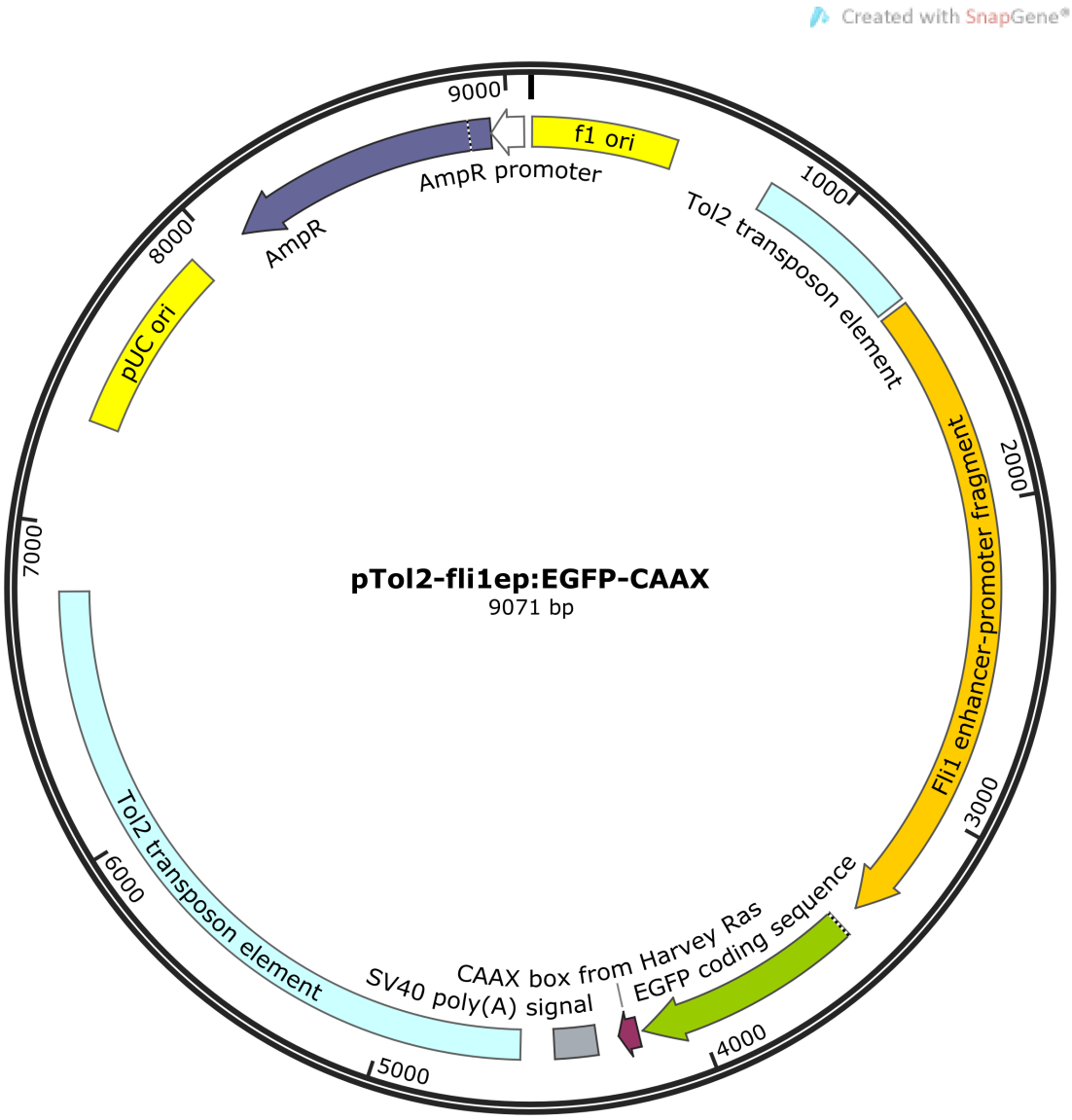


**Figure 7.1. Map of the *pTol2-fli1ep:EGFP-CAAX* plasmid**

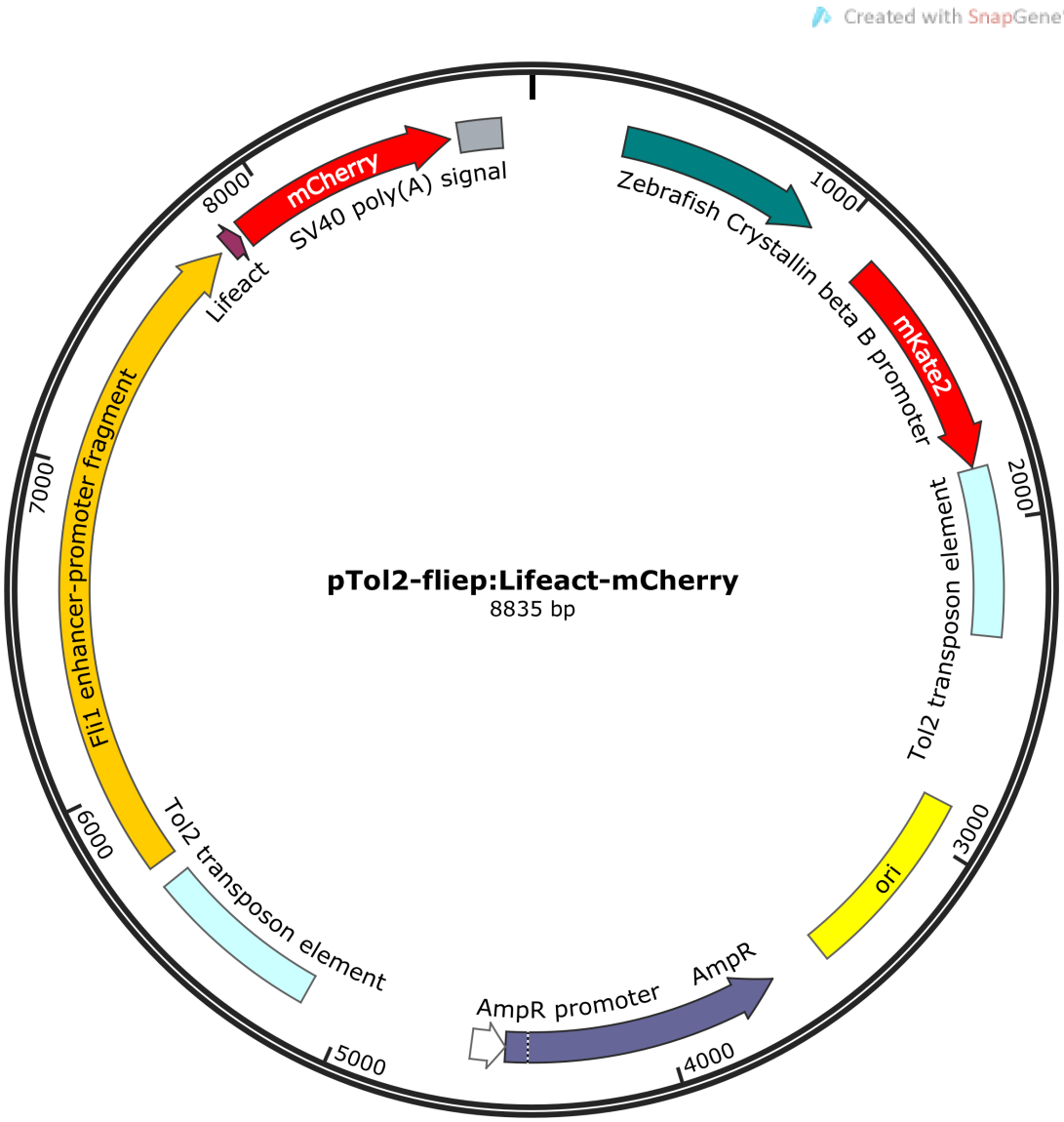


**Figure 7.2. Map of the *pTol2-fli1ep:Lifeact-mCherry* plasmid**

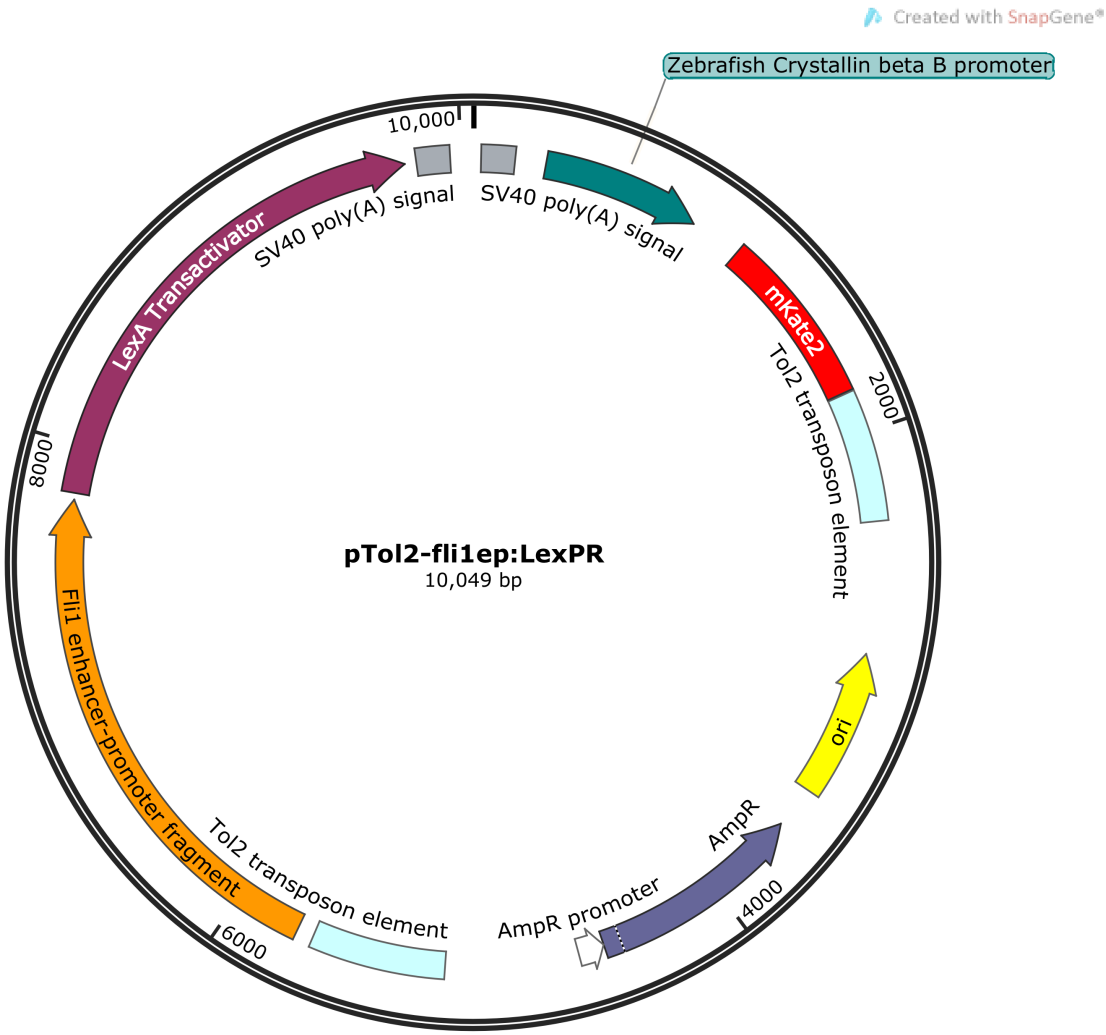


**Figure 7.3. Map of the *pTol2-fli1ep:LexPR* plasmid**

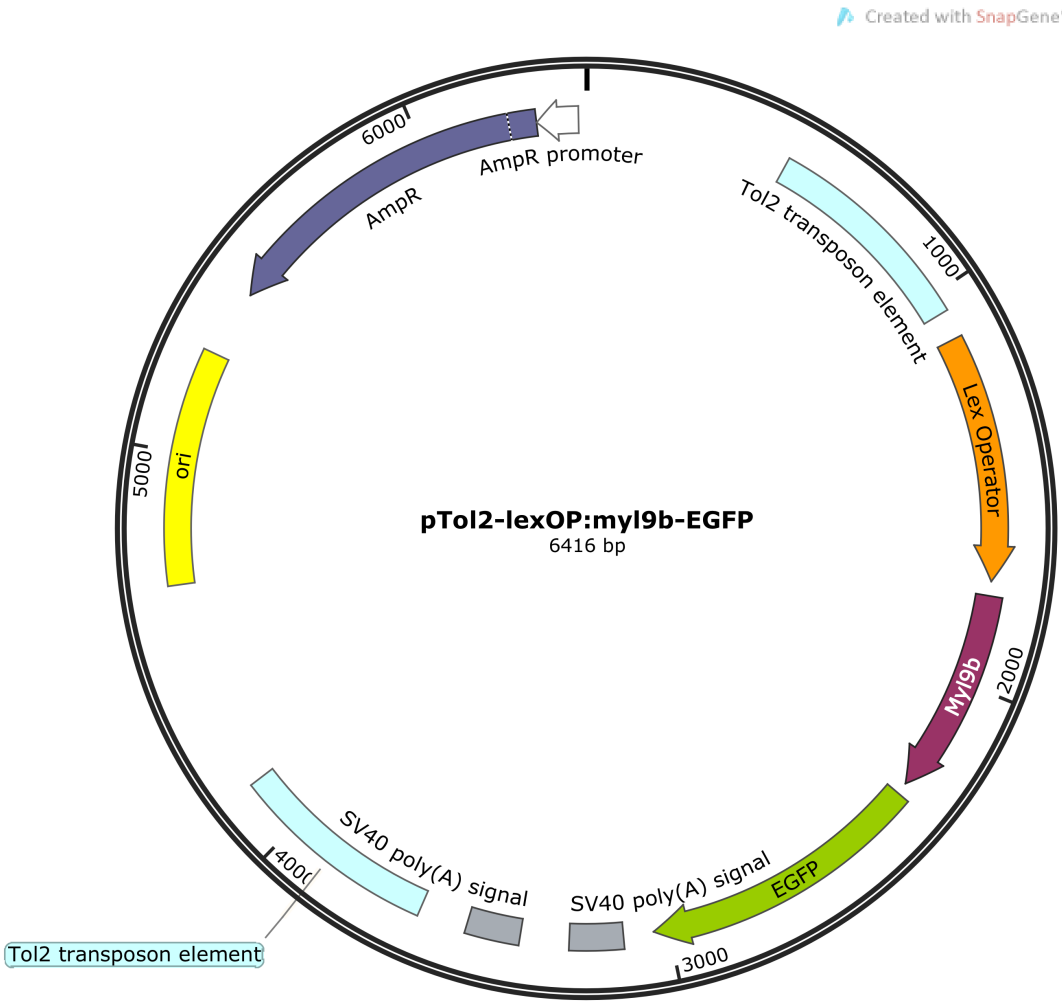


**Figure 7.4. Map of the *pTol2-lexOP:myl9b-EGFP* plasmid**

# Reference List

ABALLAY, A., STAHL, P. D. & MAYORGA, L. S. 1999. Phorbol ester promotes endocytosis by activating a factor involved in endosome fusion. *J Cell Sci,* 112 ( Pt 15)**,** 2549-57.

AFFOLTER, M. & CAUSSINUS, E. 2008. Tracheal branching morphogenesis in Drosophila: new insights into cell behaviour and organ architecture. *Development,* 135**,** 2055-64.

ALBERTS, B., A., J., LEWIS, J., RAFF, M., K., R. & P., W. 2002. *Molecular Biology of the Cell,* New York, Garland Science.

ANDREW, D. J. & EWALD, A. J. 2010. Morphogenesis of epithelial tubes: Insights into tube formation, elongation, and elaboration. *Dev Biol,* 341**,** 34-55.

ANTONNY, B. 2011. Mechanisms of membrane curvature sensing. *Annu Rev Biochem,* 80**,** 101-23.

ARANY, Z., HUANG, L. E., ECKNER, R., BHATTACHARYA, S., JIANG, C., GOLDBERG, M. A., BUNN, H. F. & LIVINGSTON, D. M. 1996. An essential role for p300/CBP in the cellular response to hypoxia. *Proc Natl Acad Sci U S A,* 93**,** 12969-73.

ARROYO, A. G. & IRUELA-ARISPE, M. L. 2010. Extracellular matrix, inflammation, and the angiogenic response. *Cardiovasc Res,* 86**,** 226-35.

AUER, T. O. & DEL BENE, F. 2014. CRISPR/Cas9 and TALEN-mediated knock-in approaches in zebrafish. *Methods,* 69**,** 142-50.

AUER, T. O., DUROURE, K., DE CIAN, A., CONCORDET, J. P. & DEL BENE, F. 2014. Highly efficient CRISPR/Cas9-mediated knock-in in zebrafish by homology-independent DNA repair. *Genome Res,* 24**,** 142-53.

AUGUSTIN, H. G., KOH, G. Y., THURSTON, G. & ALITALO, K. 2009. Control of vascular morphogenesis and homeostasis through the angiopoietin-Tie system. *Nat Rev Mol Cell Biol,* 10**,** 165-77.

AYDOGAN, V., LENARD, A., DENES, A. S., SAUTEUR, L., BELTING, H. G. & AFFOLTER, M. 2015. Endothelial cell division in angiogenic sprouts of differing cellular architecture. *Biol Open,* 4**,** 1259-69.

BAGNAT, M., CHEUNG, I. D., MOSTOV, K. E. & STAINIER, D. Y. 2007. Genetic control of single lumen formation in the zebrafish gut. *Nat Cell Biol,* 9**,** 954-60.

BARRY, D. M., XU, K., MEADOWS, S. M., ZHENG, Y., NORDEN, P. R., DAVIS, G. E. & CLEAVER, O. 2015. Cdc42 is required for cytoskeletal support of endothelial cell adhesion during blood vessel formation in mice. *Development,* 142**,** 3058-70.

BAYLESS, K. J. & DAVIS, G. E. 2002. The Cdc42 and Rac1 GTPases are required for capillary lumen formation in three-dimensional extracellular matrices. *J Cell Sci,* 115**,** 1123-36.

BAYLESS, K. J. & DAVIS, G. E. 2004. Microtubule depolymerization rapidly collapses capillary tube networks in vitro and angiogenic vessels in vivo through the small GTPase Rho. *J Biol Chem,* 279**,** 11686-95.

BAYLESS, K. J., SALAZAR, R. & DAVIS, G. E. 2000. RGD-dependent vacuolation and lumen formation observed during endothelial cell morphogenesis in three-dimensional fibrin matrices involves the alpha(v)beta(3) and alpha(5)beta(1) integrins. *Am J Pathol,* 156**,** 1673-83.

BICHSEL, C. A., HALL, S. R., SCHMID, R. A., GUENAT, O. T. & GEISER, T. 2015. Primary Human Lung Pericytes Support and Stabilize In Vitro Perfusable Microvessels. *Tissue Eng Part A,* 21**,** 2166-76.

BLUM, Y., BELTING, H. G., ELLERTSDOTTIR, E., HERWIG, L., LUDERS, F. & AFFOLTER, M. 2008. Complex cell rearrangements during intersegmental vessel sprouting and vessel fusion in the zebrafish embryo. *Dev Biol,* 316**,** 312-22.

BORGGREFE, T. & OSWALD, F. 2009. The Notch signaling pathway: transcriptional regulation at Notch target genes. *Cell Mol Life Sci,* 66**,** 1631-46.

BOVELLAN, M., ROMEO, Y., BIRO, M., BODEN, A., CHUGH, P., YONIS, A., VAGHELA, M., FRITZSCHE, M., MOULDING, D., THOROGATE, R., JEGOU, A., THRASHER, A. J., ROMET-LEMONNE, G., ROUX, P. P., PALUCH, E. K. & CHARRAS, G. 2014. Cellular control of cortical actin nucleation. *Curr Biol,* 24**,** 1628-35.

BOWERS, S. L., MENG, C. X., DAVIS, M. T. & DAVIS, G. E. 2015. Investigating human vascular tube morphogenesis and maturation using endothelial cell-pericyte co-cultures and a doxycycline-inducible genetic system in 3D extracellular matrices. *Methods Mol Biol,* 1189**,** 171-89.

BRODU, V. & CASANOVA, J. 2006. The RhoGAP crossveinless-c links trachealess and EGFR signaling to cell shape remodeling in Drosophila tracheal invagination. *Genes Dev,* 20**,** 1817-28.

BRYANT, D. M., DATTA, A., RODRIGUEZ-FRATICELLI, A. E., PERANEN, J., MARTIN-BELMONTE, F. & MOSTOV, K. E. 2010. A molecular network for de novo generation of the apical surface and lumen. *Nat Cell Biol,* 12**,** 1035-45.

BRYANT, D. M., ROIGNOT, J., DATTA, A., OVEREEM, A. W., KIM, M., YU, W., PENG, X., EASTBURN, D. J., EWALD, A. J., WERB, Z. & MOSTOV, K. E. 2014. A molecular switch for the orientation of epithelial cell polarization. *Dev Cell,* 31**,** 171-87.

BUECHNER, M. 2002. Tubes and the single C. elegans excretory cell. *Trends Cell Biol,* 12**,** 479-84.

BUECHNER, M., HALL, D. H., BHATT, H. & HEDGECOCK, E. M. 1999. Cystic canal mutants in Caenorhabditis elegans are defective in the apical membrane domain of the renal (excretory) cell. *Dev Biol,* 214**,** 227-41.

BULGAKOVA, N. A. & KNUST, E. 2009. The Crumbs complex: from epithelial-cell polarity to retinal degeneration. *J Cell Sci,* 122**,** 2587-96.

CARMELIET, P. 2005. Angiogenesis in life, disease and medicine. *Nature,* 438**,** 932-6.

CAVIGLIA, S. & LUSCHNIG, S. 2014. Tube fusion: making connections in branched tubular networks. *Semin Cell Dev Biol,* 31**,** 82-90.

CHAKI, S. P., BARHOUMI, R. & RIVERA, G. M. 2015. Actin remodeling by Nck regulates endothelial lumen formation. *Mol Biol Cell,* 26**,** 3047-60.

CHARPENTIER, M. S., TANDON, P., TRINCOT, C. E., KOUTLEVA, E. K. & CONLON, F. L. 2015. A distinct mechanism of vascular lumen formation in Xenopus requires EGFL7. *PLoS One,* 10**,** e0116086.

CHARRAS, G. & PALUCH, E. 2008. Blebs lead the way: how to migrate without lamellipodia. *Nat Rev Mol Cell Biol,* 9**,** 730-6.

CHARRAS, G. T., COUGHLIN, M., MITCHISON, T. J. & MAHADEVAN, L. 2008. Life and times of a cellular bleb. *Biophys J,* 94**,** 1836-53.

CHARRAS, G. T., HU, C. K., COUGHLIN, M. & MITCHISON, T. J. 2006. Reassembly of contractile actin cortex in cell blebs. *J Cell Biol,* 175**,** 477-90.

CHEN, Q., JIANG, L., LI, C., HU, D., BU, J. W., CAI, D. & DU, J. L. 2012. Haemodynamics-driven developmental pruning of brain vasculature in zebrafish. *PLoS Biol,* 10**,** e1001374.

CHILDS, S., CHEN, J. N., GARRITY, D. M. & FISHMAN, M. C. 2002. Patterning of angiogenesis in the zebrafish embryo. *Development,* 129**,** 973-82.

COURTEMANCHE, N., POLLARD, T. D. & CHEN, Q. 2016. Avoiding artefacts when counting polymerized actin in live cells with LifeAct fused to fluorescent proteins. *Nat Cell Biol,* 18**,** 676-83.

CUNNINGHAM, C. C. 1995. Actin polymerization and intracellular solvent flow in cell surface blebbing. *J Cell Biol,* 129**,** 1589-99.

DATTA, A., BRYANT, D. M. & MOSTOV, K. E. 2011. Molecular regulation of lumen morphogenesis. *Curr Biol,* 21**,** R126-36.

DAVIS, G. E. & CAMARILLO, C. W. 1996. An alpha 2 beta 1 integrin-dependent pinocytic mechanism involving intracellular vacuole formation and coalescence regulates capillary lumen and tube formation in three-dimensional collagen matrix. *Exp Cell Res,* 224**,** 39-51.

DAVIS, G. E., KIM, D. J., MENG, C. X., NORDEN, P. R., SPEICHINGER, K. R., DAVIS, M. T., SMITH, A. O., BOWERS, S. L. & STRATMAN, A. N. 2013. Control of vascular tube morphogenesis and maturation in 3D extracellular matrices by endothelial cells and pericytes. *Methods Mol Biol.,* 1066**,** 17-28.

DAVIS, G. E., STRATMAN, A. N., SACHARIDOU, A. & KOH, W. 2011. Molecular basis for endothelial lumen formation and tubulogenesis during vasculogenesis and angiogenic sprouting. *Int Rev Cell Mol Biol,* 288**,** 101-65.

DHANANTWARI, P., LEE, E., KRISHNAN, A., SAMTANI, R., YAMADA, S., ANDERSON, S., LOCKETT, E., DONOFRIO, M., SHIOTA, K., LEATHERBURY, L. & LO, C. W. 2009. Human cardiac development in the first trimester: a high-resolution magnetic resonance imaging and episcopic fluorescence image capture atlas. *Circulation,* 120**,** 343-51.

DRAKE, C. J. & FLEMING, P. A. 2000. Vasculogenesis in the day 6.5 to 9.5 mouse embryo. *Blood,* 95**,** 1671-9.

EBNET, K., AURRAND-LIONS, M., KUHN, A., KIEFER, F., BUTZ, S., ZANDER, K., MEYER ZU BRICKWEDDE, M. K., SUZUKI, A., IMHOF, B. A. & VESTWEBER, D. 2003. The junctional adhesion molecule (JAM) family members JAM-2 and JAM-3 associate with the cell polarity protein PAR-3: a possible role for JAMs in endothelial cell polarity. *J Cell Sci,* 116**,** 3879-91.

EISENMANN, K. M., HARRIS, E. S., KITCHEN, S. M., HOLMAN, H. A., HIGGS, H. N. & ALBERTS, A. S. 2007. Dia-interacting protein modulates formin-mediated actin assembly at the cell cortex. *Curr Biol,* 17**,** 579-91.

ELLERTSDOTTIR, E., LENARD, A., BLUM, Y., KRUDEWIG, A., HERWIG, L., AFFOLTER, M. & BELTING, H. G. 2010. Vascular morphogenesis in the zebrafish embryo. *Dev Biol,* 341**,** 56-65.

EMELYANOV, A. & PARINOV, S. 2008. Mifepristone-inducible LexPR system to drive and control gene expression in transgenic zebrafish. *Dev Biol,* 320**,** 113-21.

EPSTEIN, A. C., GLEADLE, J. M., MCNEILL, L. A., HEWITSON, K. S., O'ROURKE, J., MOLE, D. R., MUKHERJI, M., METZEN, E., WILSON, M. I., DHANDA, A., TIAN, Y. M., MASSON, N., HAMILTON, D. L., JAAKKOLA,

P., BARSTEAD, R., HODGKIN, J., MAXWELL, P. H., PUGH, C. W., SCHOFIELD, C. J. & RATCLIFFE, P. J. 2001. C. elegans EGL-9 and mammalian homologs define a family of dioxygenases that regulate HIF by prolyl hydroxylation. *Cell,* 107**,** 43-54.

FENG, W., WU, H., CHAN, L. N. & ZHANG, M. 2008. Par-3-mediated junctional localization of the lipid phosphatase PTEN is required for cell polarity establishment. *J Biol Chem,* 283**,** 23440-9.

FOLKMAN, J. & HAUDENSCHILD, C. 1980. Angiogenesis in vitro. *Nature,* 288**,** 551-6.

FRACCAROLI, A., FRANCO, C. A., ROGNONI, E., NETO, F., REHBERG, M., ASZODI, A., WEDLICH-SOLDNER, R., POHL, U., GERHARDT, H. & MONTANEZ, E. 2012. Visualization of endothelial actin cytoskeleton in the mouse retina. *PLoS One,* 7**,** e47488.

FRANCO, C. A., JONES, M. L., BERNABEU, M. O., GEUDENS, I., MATHIVET, T., ROSA, A., LOPES, F. M., LIMA, A. P., RAGAB, A., COLLINS, R. T., PHNG, L. K., COVENEY, P. V. & GERHARDT, H. 2015. Dynamic endothelial cell rearrangements drive developmental vessel regression. *PLoS Biol,* 13**,** e1002125.

FRUTTIGER, M. 2007. Development of the retinal vasculature. *Angiogenesis,* 10**,** 77-88.

GAENGEL, K., GENOVE, G., ARMULIK, A. & BETSHOLTZ, C. 2009. Endothelial-mural cell signaling in vascular development and angiogenesis. *Arterioscler Thromb Vasc Biol,* 29**,** 630-8.

GALVEZ-SANTISTEBAN, M., RODRIGUEZ-FRATICELLI, A. E., BRYANT, D. M., VERGARAJAUREGUI, S., YASUDA, T., BANON-RODRIGUEZ, I., BERNASCONE, I., DATTA, A., SPIVAK, N., YOUNG, K., SLIM, C. L., BRAKEMAN, P. R., FUKUDA, M., MOSTOV, K. E. & MARTIN-BELMONTE, F. 2012. Synaptotagmin-like proteins control the formation of a single apical membrane domain in epithelial cells. *Nat Cell Biol,* 14**,** 838-49.

GASSAMA-DIAGNE, A., YU, W., TER BEEST, M., MARTIN-BELMONTE, F., KIERBEL, A., ENGEL, J. & MOSTOV, K. 2006. Phosphatidylinositol-3,4,5-trisphosphate regulates the formation of the basolateral plasma membrane in epithelial cells. *Nat Cell Biol,* 8**,** 963-70.

GERHARDT, H., GOLDING, M., FRUTTIGER, M., RUHRBERG, C., LUNDKVIST, A., ABRAMSSON, A., JELTSCH, M., MITCHELL, C., ALITALO, K., SHIMA, D. & BETSHOLTZ, C. 2003. VEGF guides angiogenic sprouting utilizing endothelial tip cell filopodia. *J Cell Biol,* 161**,** 1163-77.

GERVAIS, L. & CASANOVA, J. 2010. In vivo coupling of cell elongation and lumen formation in a single cell. *Curr Biol,* 20**,** 359-66.

GERVAIS, L., LEBRETON, G. & CASANOVA, J. 2012. The making of a fusion branch in the Drosophila trachea. *Dev Biol,* 362**,** 187-93.

GHAJAR, C. M., GEORGE, S. C. & PUTNAM, A. J. 2008. Matrix metalloproteinase control of capillary morphogenesis. *Crit Rev Eukaryot Gene Expr,* 18**,** 251-78.

GREER, S. N., METCALF, J. L., WANG, Y. & OHH, M. 2012. The updated biology of hypoxia-inducible factor. *EMBO J,* 31**,** 2448-60.

HALL, H. G., FARSON, D. A. & BISSELL, M. J. 1982. Lumen formation by epithelial cell lines in response to collagen overlay: a morphogenetic model in culture. *Proc Natl Acad Sci U S A,* 79**,** 4672-6.

HAMILL, O. P. & MARTINAC, B. 2001. Molecular basis of mechanotransduction in living cells. *Physiol Rev,* 81**,** 685-740.

HANNEMANN, S., MADRID, R., STASTNA, J., KITZING, T., GASTEIER, J., SCHONICHEN, A., BOUCHET, J., JIMENEZ, A., GEYER, M., GROSSE, R., BENICHOU, S. & FACKLER, O. T. 2008. The Diaphanous-related Formin FHOD1 associates with ROCK1 and promotes Src-dependent plasma membrane blebbing. *J Biol Chem,* 283**,** 27891-903.

HELLSTROM, M., PHNG, L. K., HOFMANN, J. J., WALLGARD, E., COULTAS, L., LINDBLOM, P., ALVA, J., NILSSON, A. K., KARLSSON, L., GAIANO, N., YOON, K., ROSSANT, J., IRUELA-ARISPE, M. L., KALEN, M., GERHARDT, H. & BETSHOLTZ, C. 2007. Dll4 signalling through Notch1 regulates formation of tip cells during angiogenesis. *Nature,* 445**,** 776-80.

HERBERT, S. P., HUISKEN, J., KIM, T. N., FELDMAN, M. E., HOUSEMAN, B. T., WANG, R. A., SHOKAT, K. M. & STAINIER, D. Y. 2009. Arterial-venous segregation by selective cell sprouting: an alternative mode of blood vessel formation. *Science,* 326**,** 294-8.

HERWIG, L., BLUM, Y., KRUDEWIG, A., ELLERTSDOTTIR, E., LENARD, A., BELTING, H. G. & AFFOLTER, M. 2011. Distinct cellular mechanisms of blood vessel fusion in the zebrafish embryo. *Curr Biol,* 21**,** 1942-8.

HILDEBRAND, J. D. 2005. Shroom regulates epithelial cell shape via the apical positioning of an actomyosin network. *J Cell Sci,* 118**,** 5191-203.

HILDEBRAND, J. D. & SORIANO, P. 1999. Shroom, a PDZ domain-containing actin-binding protein, is required for neural tube morphogenesis in mice. *Cell,* 99**,** 485-97.

HLUSHCHUK, R., EHRBAR, M., REICHMUTH, P., HEINIMANN, N., STYP-REKOWSKA, B., ESCHER, R., BAUM, O., LIENEMANN, P., MAKANYA, A., KESHET, E. & DJONOV, V. 2011. Decrease in VEGF expression induces intussusceptive vascular pruning. *Arterioscler Thromb Vasc Biol,* 31**,** 2836-44.

HOFMANN, J. J. & IRUELA-ARISPE, M. L. 2007. Notch signaling in blood vessels: who is talking to whom about what? *Circ Res,* 100**,** 1556-68.

HOGAN, B. M., BOS, F. L., BUSSMANN, J., WITTE, M., CHI, N. C., DUCKERS, H. J. & SCHULTE-MERKER, S. 2009. Ccbe1 is required for embryonic lymphangiogenesis and venous sprouting. *Nat Genet,* 41**,** 396-8.

HU, N., SEDMERA, D., YOST, H. J. & CLARK, E. B. 2000. Structure and function of the developing zebrafish heart. *Anat Rec,* 260**,** 148-57.

HUANG, P., XIAO, A., ZHOU, M., ZHU, Z., LIN, S. & ZHANG, B. 2011. Heritable gene targeting in zebrafish using customized TALENs. *Nat Biotechnol,* 29**,** 699-700.

HUGHES, S. & CHANG-LING, T. 2000. Roles of endothelial cell migration and apoptosis in vascular remodeling during development of the central nervous system. *Microcirculation,* 7**,** 317-33.

HULTIN, S., ZHENG, Y., MOJALLAL, M., VERTUANI, S., GENTILI, C., BALLAND, M., MILLOUD, R., BELTING, H. G., AFFOLTER, M., HELKER, C. S., ADAMS, R. H., HERZOG, W., UHLEN, P., MAJUMDAR, A. & HOLMGREN, L. 2014. AmotL2 links VE-cadherin to contractile actin fibres necessary for aortic lumen expansion. *Nat Commun,* 5**,** 3743.

HWANG, W. Y., FU, Y., REYON, D., MAEDER, M. L., KAINI, P., SANDER, J. D., JOUNG, J. K., PETERSON, R. T. & YEH, J. R. 2013a. Heritable and precise zebrafish genome editing using a CRISPR-Cas system. *PLoS One,* 8**,** e68708.

HWANG, W. Y., FU, Y., REYON, D., MAEDER, M. L., TSAI, S. Q., SANDER, J. D., PETERSON, R. T., YEH, J. R. & JOUNG, J. K. 2013b. Efficient genome editing in zebrafish using a CRISPR-Cas system. *Nat Biotechnol,* 31**,** 227-9.

IM, E. & KAZLAUSKAS, A. 2007. Src family kinases promote vessel stability by antagonizing the Rho/ROCK pathway. *J Biol Chem,* 282**,** 29122-9.

ISOGAI, S., HORIGUCHI, M. & WEINSTEIN, B. M. 2001. The vascular anatomy of the developing zebrafish: an atlas of embryonic and early larval development. *Dev Biol,* 230**,** 278-301.

ISOGAI, S., LAWSON, N. D., TORREALDAY, S., HORIGUCHI, M. & WEINSTEIN, B. M. 2003. Angiogenic network formation in the developing vertebrate trunk. *Development,* 130**,** 5281-90.

IVAN, M., KONDO, K., YANG, H., KIM, W., VALIANDO, J., OHH, M., SALIC, A., ASARA, J. M., LANE, W. S. & KAELIN, W. G., JR. 2001. HIFalpha targeted for VHL-mediated destruction by proline hydroxylation: implications for O2 sensing. *Science,* 292**,** 464-8.

IWASAKI, T., MURATA-HORI, M., ISHITOBI, S. & HOSOYA, H. 2001. Diphosphorylated MRLC is required for organization of stress fibers in interphase cells and the contractile ring in dividing cells. *Cell Struct Funct,* 26**,** 677-83.

JAAKKOLA, P., MOLE, D. R., TIAN, Y. M., WILSON, M. I., GIELBERT, J., GASKELL, S. J., VON KRIEGSHEIM, A., HEBESTREIT, H. F., MUKHERJI, M., SCHOFIELD, C. J., MAXWELL, P. H., PUGH, C. W. & RATCLIFFE, P. J. 2001. Targeting of HIF-alpha to the von Hippel-Lindau ubiquitylation complex by O2-regulated prolyl hydroxylation. *Science,* 292**,** 468-72.

JAIN, R. K. 2003. Molecular regulation of vessel maturation. *Nat Med,* 9**,** 685-93.

JAKOBSSON, L., FRANCO, C. A., BENTLEY, K., COLLINS, R. T., PONSIOEN, B., ASPALTER, I. M., ROSEWELL, I., BUSSE, M., THURSTON, G., MEDVINSKY, A., SCHULTE-MERKER, S. & GERHARDT, H. 2010. Endothelial cells dynamically compete for the tip cell position during angiogenic sprouting. *Nat Cell Biol,* 12**,** 943-53.

JIANG, L., ROGERS, S. L. & CREWS, S. T. 2007. The Drosophila Dead end Arf-like3 GTPase controls vesicle trafficking during tracheal fusion cell morphogenesis. *Dev Biol,* 311**,** 487-99.

JIN, S. W., BEIS, D., MITCHELL, T., CHEN, J. N. & STAINIER, D. Y. 2005. Cellular and molecular analyses of vascular tube and lumen formation in zebrafish. *Development,* 132**,** 5199-209.

KAKIHARA, K., SHINMYOZU, K., KATO, K., WADA, H. & HAYASHI, S. 2008. Conversion of plasma membrane topology during epithelial tube connection requires Arf-like 3 small GTPase in Drosophila. *Mech Dev,* 125**,** 325-36.

KALLURI, R. 2003. Basement membranes: structure, assembly and role in tumour angiogenesis. *Nat Rev Cancer,* 3**,** 422-33.

KAMEI, M., SAUNDERS, W. B., BAYLESS, K. J., DYE, L., DAVIS, G. E. & WEINSTEIN, B. M. 2006. Endothelial tubes assemble from intracellular vacuoles in vivo. *Nature,* 442**,** 453-6.

KAWAKAMI, K. 2007. Tol2: a versatile gene transfer vector in vertebrates. *Genome Biol,* 8 Suppl 1**,** S7.

KAWAKAMI, K., TAKEDA, H., KAWAKAMI, N., KOBAYASHI, M., MATSUDA, N. & MISHINA, M. 2004. A transposon-mediated gene trap approach identifies developmentally regulated genes in zebrafish. *Dev Cell,* 7**,** 133-44.

KELLER, H. & EGGLI, P. 1998. Protrusive activity, cytoplasmic compartmentalization, and restriction rings in locomoting blebbing Walker carcinosarcoma cells are related to detachment of cortical actin from the plasma membrane. *Cell Motil Cytoskeleton,* 41**,** 181-93.

KELLER, H. U. 1990. Diacylglycerols and PMA are particularly effective stimulators of fluid pinocytosis in human neutrophils. *J Cell Physiol,* 145**,** 465-71.

KHAN, L. A., ZHANG, H., ABRAHAM, N., SUN, L., FLEMING, J. T., BUECHNER, M., HALL, D. H. & GOBEL, V. 2013. Intracellular lumen extension requires ERM-1-dependent apical membrane expansion and AQP-8-mediated flux. *Nat Cell Biol,* 15**,** 143-56.

KIENAST, Y., VON BAUMGARTEN, L., FUHRMANN, M., KLINKERT, W. E., GOLDBRUNNER, R., HERMS, J. & WINKLER, F. 2010. Real-time imaging reveals the single steps of brain metastasis formation. *Nat Med,* 16**,** 116-22.

KIM, D. J., MARTINEZ-LEMUS, L. A. & DAVIS, G. E. 2013. EB1, p150Glued, and Clasp1 control endothelial tubulogenesis through microtubule assembly, acetylation, and apical polarization. *Blood,* 121**,** 3521-30.

KIM, J., CHUNG, M., KIM, S., JO, D. H., KIM, J. H. & JEON, N. L. 2015. Engineering of a Biomimetic Pericyte-Covered 3D Microvascular Network. *PLoS One,* 10**,** e0133880.

KIMMEL, C. B., BALLARD, W. W., KIMMEL, S. R., ULLMANN, B. & SCHILLING, T. F. 1995. Stages of embryonic development of the zebrafish. *Dev Dyn,* 203**,** 253-310.

KINOSHITA, N., SASAI, N., MISAKI, K. & YONEMURA, S. 2008. Apical accumulation of Rho in the neural plate is important for neural plate cell shape change and neural tube formation. *Mol Biol Cell,* 19**,** 2289-99.

KITZING, T. M., WANG, Y., PERTZ, O., COPELAND, J. W. & GROSSE, R. 2010. Formin-like 2 drives amoeboid invasive cell motility downstream of RhoC. *Oncogene,* 29**,** 2441-8.

KOCHHAN, E., LENARD, A., ELLERTSDOTTIR, E., HERWIG, L., AFFOLTER, M., BELTING, H. G. & SIEKMANN, A. F. 2013. Blood flow changes coincide with cellular rearrangements during blood vessel pruning in zebrafish embryos. *PLoS One,* 8**,** e75060.

KOH, W., MAHAN, R. D. & DAVIS, G. E. 2008a. Cdc42- and Rac1-mediated endothelial lumen formation requires Pak2, Pak4 and Par3, and PKC-dependent signaling. *J Cell Sci,* 121**,** 989-1001.

KOH, W., STRATMAN, A. N., SACHARIDOU, A. & DAVIS, G. E. 2008b. In vitro three dimensional collagen matrix models of endothelial lumen formation during vasculogenesis and angiogenesis. *Methods Enzymol,* 443**,** 83-101.

KOLOTUEV, I., HYENNE, V., SCHWAB, Y., RODRIGUEZ, D. & LABOUESSE, M. 2013. A pathway for unicellular tube extension depending on the lymphatic vessel determinant Prox1 and on osmoregulation. *Nat Cell Biol,* 15**,** 157-68.

KOPP, R., SCHWERTE, T. & PELSTER, B. 2005. Cardiac performance in the zebrafish breakdance mutant. *J Exp Biol,* 208**,** 2123-34.

KOVACS, M., TOTH, J., HETENYI, C., MALNASI-CSIZMADIA, A. & SELLERS, J. R. 2004. Mechanism of blebbistatin inhibition of myosin II. *J Biol Chem,* 279**,** 35557-63.

KRAHN, M. P., KLOPFENSTEIN, D. R., FISCHER, N. & WODARZ, A. 2010. Membrane targeting of Bazooka/PAR-3 is mediated by direct binding to phosphoinositide lipids. *Curr Biol,* 20**,** 636-42.

KROCK, B. L., SKULI, N. & SIMON, M. C. 2011. Hypoxia-induced angiogenesis: good and evil. *Genes Cancer,* 2**,** 1117-33.

KWAN, K. M., FUJIMOTO, E., GRABHER, C., MANGUM, B. D., HARDY, M. E., CAMPBELL, D. S., PARANT, J. M., YOST, H. J., KANKI, J. P. & CHIEN, C. B. 2007. The Tol2kit: a multisite gateway-based construction kit for Tol2 transposon transgenesis constructs. *Dev Dyn,* 236**,** 3088-99.

LAMPUGNANI, M. G., ORSENIGO, F., RUDINI, N., MADDALUNO, L., BOULDAY, G., CHAPON, F. & DEJANA, E. 2010. CCM1 regulates vascular-lumen organization by inducing endothelial polarity. *J Cell Sci,* 123**,** 1073-80.

LAWSON, N. D. & WEINSTEIN, B. M. 2002. In vivo imaging of embryonic vascular development using transgenic zebrafish. *Dev Biol,* 248**,** 307-18.

LE NOBLE, F., MOYON, D., PARDANAUD, L., YUAN, L., DJONOV, V., MATTHIJSEN, R., BREANT, C., FLEURY, V. & EICHMANN, A. 2004. Flow regulates arterial-venous differentiation in the chick embryo yolk sac. *Development,* 131**,** 361-75.

LEE, S. & KOLODZIEJ, P. A. 2002. The plakin Short Stop and the RhoA GTPase are required for E-cadherin-dependent apical surface remodeling during tracheal tube fusion. *Development,* 129**,** 1509-20.

LENARD, A., DAETWYLER, S., BETZ, C., ELLERTSDOTTIR, E., BELTING, H. G., HUISKEN, J. & AFFOLTER, M. 2015. Endothelial cell self-fusion during vascular pruning. *PLoS Biol,* 13**,** e1002126.

LENARD, A., ELLERTSDOTTIR, E., HERWIG, L., KRUDEWIG, A., SAUTEUR, L., BELTING, H. G. & AFFOLTER, M. 2013. In vivo analysis reveals a highly stereotypic morphogenetic pathway of vascular anastomosis. *Dev Cell,* 25**,** 492-506.

LEVAYER, R. & LECUIT, T. 2012. Biomechanical regulation of contractility: spatial control and dynamics. *Trends Cell Biol,* 22**,** 61-81.

LI, D., KUEHN, E. W. & PREKERIS, R. 2014a. Kinesin-2 mediates apical endosome transport during epithelial lumen formation. *Cell Logist,* 4**,** e28928.

LI, D., MANGAN, A., CICCHINI, L., MARGOLIS, B. & PREKERIS, R. 2014b. FIP5 phosphorylation during mitosis regulates apical trafficking and lumenogenesis. *EMBO Rep,* 15**,** 428-37.

LI, J., HOU, B., TUMOVA, S., MURAKI, K., BRUNS, A., LUDLOW, M. J., SEDO, A., HYMAN, A. J., MCKEOWN, L., YOUNG, R. S., YULDASHEVA, N. Y., MAJEED, Y., WILSON, L. A., RODE, B., BAILEY, M. A., KIM, H. R., FU, Z., CARTER, D. A., BILTON, J., IMRIE, H., AJUH, P., DEAR, T. N., CUBBON, R. M., KEARNEY, M. T., PRASAD, K. R., EVANS, P. C., AINSCOUGH, J. F. & BEECH, D. J. 2014c. Piezo1 integration of vascular architecture with physiological force. *Nature,* 515**,** 279-82.

LIMOUZE, J., STRAIGHT, A. F., MITCHISON, T. & SELLERS, J. R. 2004. Specificity of blebbistatin, an inhibitor of myosin II. *J Muscle Res Cell Motil,* 25**,** 337-41.

LOBOV, I. B., CHEUNG, E., WUDALI, R., CAO, J., HALASZ, G., WEI, Y., ECONOMIDES, A., LIN, H. C., PAPADOPOULOS, N., YANCOPOULOS, G. D. & WIEGAND, S. J. 2011. The Dll4/Notch pathway controls postangiogenic blood vessel remodeling and regression by modulating vasoconstriction and blood flow. *Blood,* 117**,** 6728-37.

LOBOV, I. B., RAO, S., CARROLL, T. J., VALLANCE, J. E., ITO, M., ONDR, J. K., KURUP, S., GLASS, D. A., PATEL, M. S., SHU, W., MORRISEY, E. E., MCMAHON, A. P., KARSENTY, G. & LANG, R. A. 2005. WNT7b mediates macrophage-induced programmed cell death in patterning of the vasculature. *Nature,* 437**,** 417-21.

LUBARSKY, B. & KRASNOW, M. A. 2003. Tube morphogenesis: making and shaping biological tubes. *Cell,* 112**,** 19-28.

MADRID, R., ARANDA, J. F., RODRIGUEZ-FRATICELLI, A. E., VENTIMIGLIA, L., ANDRES-DELGADO, L., SHEHATA, M., FANAYAN, S., SHAHHEYDARI, H., GOMEZ, S., JIMENEZ, A., MARTIN-BELMONTE, F., BYRNE, J. A. & ALONSO, M. A. 2010. The formin INF2 regulates basolateral-to-apical transcytosis and lumen formation in association with Cdc42 and MAL2. *Dev Cell,* 18**,** 814-27.

MARTIN, A. C. & GOLDSTEIN, B. 2014. Apical constriction: themes and variations on a cellular mechanism driving morphogenesis. *Development,* 141**,** 1987-98.

MARTIN, A. C., KASCHUBE, M. & WIESCHAUS, E. F. 2009. Pulsed contractions of an actin-myosin network drive apical constriction. *Nature,* 457**,** 495-9.

MARTIN-BELMONTE, F., GASSAMA, A., DATTA, A., YU, W., RESCHER, U., GERKE, V. & MOSTOV, K. 2007. PTEN-mediated apical segregation of phosphoinositides controls epithelial morphogenesis through Cdc42. *Cell,* 128**,** 383-97.

MARTIN-BELMONTE, F. & MOSTOV, K. 2007. Phosphoinositides control epithelial development. *Cell Cycle,* 6**,** 1957-61.

MARTIN-BELMONTE, F. & MOSTOV, K. 2008. Regulation of cell polarity during epithelial morphogenesis. *Curr Opin Cell Biol,* 20**,** 227-34.

MASSON, N., WILLAM, C., MAXWELL, P. H., PUGH, C. W. & RATCLIFFE, P. J. 2001. Independent function of two destruction domains in hypoxia-inducible factor-alpha chains activated by prolyl hydroxylation. *EMBO J,* 20**,** 5197-206.

MASUDA-HIRATA, M., SUZUKI, A., AMANO, Y., YAMASHITA, K., IDE, M., YAMANAKA, T., SAKAI, M., IMAMURA, M. & OHNO, S. 2009. Intracellular polarity protein PAR-1 regulates extracellular laminin assembly by regulating the dystroglycan complex. *Genes Cells,* 14**,** 835-50.

MAVRIA, G., VERCOULEN, Y., YEO, M., PATERSON, H., KARASARIDES, M., MARAIS, R., BIRD, D. & MARSHALL, C. J. 2006. ERK-MAPK signaling opposes Rho-kinase to promote endothelial cell survival and sprouting during angiogenesis. *Cancer Cell,* 9**,** 33-44.

MAXWELL, P. H., WIESENER, M. S., CHANG, G. W., CLIFFORD, S. C., VAUX, E. C., COCKMAN, M. E., WYKOFF, C. C., PUGH, C. W., MAHER, E. R. & RATCLIFFE, P. J. 1999. The tumour suppressor protein VHL targets hypoxia-inducible factors for oxygen-dependent proteolysis. *Nature,* 399**,** 271-5.

MEESON, A. P., ARGILLA, M., KO, K., WITTE, L. & LANG, R. A. 1999. VEGF deprivation-induced apoptosis is a component of programmed capillary regression. *Development,* 126**,** 1407-15.

MELNICK, M., CHEN, H., ZHOU, Y. & JASKOLL, T. 2001. Embryonic mouse submandibular salivary gland morphogenesis and the TNF/TNF-R1 signal transduction pathway. *Anat Rec,* 262**,** 318-30.

MELNICK, M. & JASKOLL, T. 2000. Mouse submandibular gland morphogenesis: a paradigm for embryonic signal processing. *Crit Rev Oral Biol Med,* 11**,** 199-215.

MONAHAN-EARLEY, R., DVORAK, A. M. & AIRD, W. C. 2013. Evolutionary origins of the blood vascular system and endothelium. *J Thromb Haemost,* 11 Suppl 1**,** 46-66.

MONTESANO, R., MATSUMOTO, K., NAKAMURA, T. & ORCI, L. 1991a. Identification of a fibroblast-derived epithelial morphogen as hepatocyte growth factor. *Cell,* 67**,** 901-8.

MONTESANO, R., SCHALLER, G. & ORCI, L. 1991b. Induction of epithelial tubular morphogenesis in vitro by fibroblast-derived soluble factors. *Cell,* 66**,** 697-711.

MORIN, K. T. & TRANQUILLO, R. T. 2013. In vitro models of angiogenesis and vasculogenesis in fibrin gel. *Exp Cell Res,* 319**,** 2409-17.

MOYA, M. L., HSU, Y. H., LEE, A. P., HUGHES, C. C. & GEORGE, S. C. 2013. In vitro perfused human capillary networks. *Tissue Eng Part C Methods,* 19**,** 730-7.

MOYON, D., PARDANAUD, L., YUAN, L., BREANT, C. & EICHMANN, A. 2001. Plasticity of endothelial cells during arterial-venous differentiation in the avian embryo. *Development,* 128**,** 3359-70.

MYLLYMAKI, S. M., TERAVAINEN, T. P. & MANNINEN, A. 2011. Two distinct integrin-mediated mechanisms contribute to apical lumen formation in epithelial cells. *PLoS One,* 6**,** e19453.

NAKAYAMA, M., NAKAYAMA, A., VAN LESSEN, M., YAMAMOTO, H., HOFFMANN, S., DREXLER, H. C., ITOH, N., HIROSE, T., BREIER, G., VESTWEBER, D., COOPER, J. A., OHNO, S., KAIBUCHI, K. & ADAMS, R. H. 2013. Spatial regulation of VEGF receptor endocytosis in angiogenesis. *Nat Cell Biol,* 15**,** 249-60.

NIELSEN, J. S. & MCNAGNY, K. M. 2008. Novel functions of the CD34 family. *J Cell Sci,* 121**,** 3683-92.

NILSSON, M., NILSSON, K. & FORSBECK, K. 1989. Increased endocytosis and formation of multivesicular bodies in phorbol ester-stimulated human monoblastic U-937 cells. *Exp Cell Res,* 181**,** 551-65.

NISHIMURA, T., HONDA, H. & TAKEICHI, M. 2012. Planar cell polarity links axes of spatial dynamics in neural-tube closure. *Cell,* 149**,** 1084-97.

NISHIMURA, T. & TAKEICHI, M. 2008. Shroom3-mediated recruitment of Rho kinases to the apical cell junctions regulates epithelial and neuroepithelial planar remodeling. *Development,* 135**,** 1493-502.

NORDEN, P. R., KIM, D. J., BARRY, D. M., CLEAVER, O. B. & DAVIS, G. E. 2016. Cdc42 and k-Ras Control Endothelial Tubulogenesis through Apical Membrane and Cytoskeletal Polarization: Novel Stimulatory Roles for GTPase Effectors, the Small GTPases, Rac2 and Rap1b, and Inhibitory Influence of Arhgap31 and Rasa1. *PLoS One,* 11**,** e0147758.

O'BRIEN, L. E., JOU, T. S., POLLACK, A. L., ZHANG, Q., HANSEN, S. H., YURCHENCO, P. & MOSTOV, K. E. 2001. Rac1 orientates epithelial apical polarity through effects on basolateral laminin assembly. *Nat Cell Biol,* 3**,** 831-8.

OHH, M., PARK, C. W., IVAN, M., HOFFMAN, M. A., KIM, T. Y., HUANG, L. E., PAVLETICH, N., CHAU, V. & KAELIN, W. G. 2000. Ubiquitination of

hypoxia-inducible factor requires direct binding to the beta-domain of the von Hippel-Lindau protein. *Nat Cell Biol,* 2**,** 423-7.

OLSSON, A. K., DIMBERG, A., KREUGER, J. & CLAESSON-WELSH, L. 2006. VEGF receptor signalling - in control of vascular function. *Nat Rev Mol Cell Biol,* 7**,** 359-71.

OTHMAN-HASSAN, K., PATEL, K., PAPOUTSI, M., RODRIGUEZ-NIEDENFUHR, M., CHRIST, B. & WILTING, J. 2001. Arterial identity of endothelial cells is controlled by local cues. *Dev Biol,* 237**,** 398-409.

OVEREEM, A. W., BRYANT, D. M. & VAN, I. S. C. 2015. Mechanisms of apical-basal axis orientation and epithelial lumen positioning. *Trends Cell Biol,* 25**,** 476-85.

PALUCH, E., PIEL, M., PROST, J., BORNENS, M. & SYKES, C. 2005. Cortical actomyosin breakage triggers shape oscillations in cells and cell fragments. *Biophys J,* 89**,** 724-33.

PARDALI, E., GOUMANS, M. J. & TEN DIJKE, P. 2010. Signaling by members of the TGF-beta family in vascular morphogenesis and disease. *Trends Cell Biol,* 20**,** 556-67.

PELSTER, B. & BURGGREN, W. W. 1996. Disruption of hemoglobin oxygen transport does not impact oxygen-dependent physiological processes in developing embryos of zebra fish (Danio rerio). *Circ Res,* 79**,** 358-62.

PELTON, J. C., WRIGHT, C. E., LEITGES, M. & BAUTCH, V. L. 2014. Multiple endothelial cells constitute the tip of developing blood vessels and polarize to promote lumen formation. *Development,* 141**,** 4121-6.

PETRIE, R. J., KOO, H. & YAMADA, K. M. 2014. Generation of compartmentalized pressure by a nuclear piston governs cell motility in a 3D matrix. *Science,* 345**,** 1062-5.

PHNG, L. K., GEBALA, V., BENTLEY, K., PHILIPPIDES, A., WACKER, A., MATHIVET, T., SAUTEUR, L., STANCHI, F., BELTING, H. G., AFFOLTER, M. & GERHARDT, H. 2015. Formin-mediated actin polymerization at endothelial junctions is required for vessel lumen formation and stabilization. *Dev Cell,* 32**,** 123-32.

PHNG, L. K. & GERHARDT, H. 2009. Angiogenesis: a team effort coordinated by notch. *Dev Cell,* 16**,** 196-208.

PHNG, L. K., STANCHI, F. & GERHARDT, H. 2013. Filopodia are dispensable for endothelial tip cell guidance. *Development,* 140**,** 4031-40.

POLLACK, A. L., RUNYAN, R. B. & MOSTOV, K. E. 1998. Morphogenetic mechanisms of epithelial tubulogenesis: MDCK cell polarity is transiently rearranged without loss of cell-cell contact during scatter factor/hepatocyte growth factor-induced tubulogenesis. *Dev Biol,* 204**,** 64-79.

POTENTE, M., GERHARDT, H. & CARMELIET, P. 2011. Basic and therapeutic aspects of angiogenesis. *Cell,* 146**,** 873-87.

RANADE, S. S., QIU, Z., WOO, S. H., HUR, S. S., MURTHY, S. E., CAHALAN, S. M., XU, J., MATHUR, J., BANDELL, M., COSTE, B., LI, Y. S., CHIEN, S. & PATAPOUTIAN, A. 2014. Piezo1, a mechanically activated ion channel, is required for vascular development in mice. *Proc Natl Acad Sci U S A,* 111**,** 10347-52.

RIEDL, J., CREVENNA, A. H., KESSENBROCK, K., YU, J. H., NEUKIRCHEN, D., BISTA, M., BRADKE, F., JENNE, D., HOLAK, T. A., WERB, Z., SIXT, M. &

WEDLICH-SOLDNER, R. 2008. Lifeact: a versatile marker to visualize F-actin. *Nat Methods,* 5**,** 605-7.

RIEDL, J., FLYNN, K. C., RADUCANU, A., GARTNER, F., BECK, G., BOSL, M., BRADKE, F., MASSBERG, S., ASZODI, A., SIXT, M. & WEDLICH-SOLDNER, R. 2010. Lifeact mice for studying F-actin dynamics. *Nat Methods,* 7**,** 168-9.

RODRIGUEZ-BOULAN, E. & MACARA, I. G. 2014. Organization and execution of the epithelial polarity programme. *Nat Rev Mol Cell Biol,* 15**,** 225-42.

SACHARIDOU, A., KOH, W., STRATMAN, A. N., MAYO, A. M., FISHER, K. E. & DAVIS, G. E. 2010. Endothelial lumen signaling complexes control 3D matrix-specific tubulogenesis through interdependent Cdc42- and MT1-MMP-mediated events. *Blood,* 115**,** 5259-69.

SACHARIDOU, A., STRATMAN, A. N. & DAVIS, G. E. 2012. Molecular mechanisms controlling vascular lumen formation in three-dimensional extracellular matrices. *Cells Tissues Organs,* 195**,** 122-43.

SANDER, J. D., CADE, L., KHAYTER, C., REYON, D., PETERSON, R. T., JOUNG, J. K. & YEH, J. R. 2011. Targeted gene disruption in somatic zebrafish cells using engineered TALENs. *Nat Biotechnol,* 29**,** 697-8.

SAUTEUR, L., KRUDEWIG, A., HERWIG, L., EHRENFEUCHTER, N., LENARD, A., AFFOLTER, M. & BELTING, H. G. 2014. Cdh5/VE-cadherin promotes endothelial cell interface elongation via cortical actin polymerization during angiogenic sprouting. *Cell Rep,* 9**,** 504-13.

SAWYER, J. M., HARRELL, J. R., SHEMER, G., SULLIVAN-BROWN, J., ROH-JOHNSON, M. & GOLDSTEIN, B. 2010. Apical constriction: a cell shape change that can drive morphogenesis. *Dev Biol,* 341**,** 5-19.

SCHINDELIN, J., ARGANDA-CARRERAS, I., FRISE, E., KAYNIG, V., LONGAIR, M., PIETZSCH, T., PREIBISCH, S., RUEDEN, C., SAALFELD, S., SCHMID, B., TINEVEZ, J. Y., WHITE, D. J., HARTENSTEIN, V., ELICEIRI, K., TOMANCAK, P. & CARDONA, A. 2012. Fiji: an open-source platform for biological-image analysis. *Nat Methods,* 9**,** 676-82.

SCHLUTER, M. A., PFARR, C. S., PIECZYNSKI, J., WHITEMAN, E. L., HURD, T. W., FAN, S., LIU, C. J. & MARGOLIS, B. 2009. Trafficking of Crumbs3 during cytokinesis is crucial for lumen formation. *Mol Biol Cell,* 20**,** 4652-63.

SCHOENWOLF, G. C. & POWERS, M. L. 1987. Shaping of the chick neuroepithelium during primary and secondary neurulation: role of cell elongation. *Anat Rec,* 218**,** 182-95.

SCOTT, A. & FRUTTIGER, M. 2010. Oxygen-induced retinopathy: a model for vascular pathology in the retina. *Eye (Lond),* 24**,** 416-21.

SEHNERT, A. J., HUQ, A., WEINSTEIN, B. M., WALKER, C., FISHMAN, M. & STAINIER, D. Y. 2002. Cardiac troponin T is essential in sarcomere assembly and cardiac contractility. *Nat Genet,* 31**,** 106-10.

SIGURBJORNSDOTTIR, S., MATHEW, R. & LEPTIN, M. 2014. Molecular mechanisms of de novo lumen formation. *Nat Rev Mol Cell Biol,* 15**,** 665-76.

SINHA, B., KOSTER, D., RUEZ, R., GONNORD, P., BASTIANI, M., ABANKWA, D., STAN, R. V., BUTLER-BROWNE, G., VEDIE, B., JOHANNES, L., MORONE, N., PARTON, R. G., RAPOSO, G., SENS, P., LAMAZE, C. & NASSOY, P. 2011. Cells respond to mechanical stress by rapid disassembly of caveolae. *Cell,* 144**,** 402-13.

SIT, S. T. & MANSER, E. 2011. Rho GTPases and their role in organizing the actin cytoskeleton. *J Cell Sci,* 124**,** 679-83.

SMITH, J. L. & SCHOENWOLF, G. C. 1988. Role of cell-cycle in regulating neuroepithelial cell shape during bending of the chick neural plate. *Cell Tissue Res,* 252**,** 491-500.

SOWA, G. 2012. Caveolae, caveolins, cavins, and endothelial cell function: new insights. *Front Physiol,* 2**,** 120.

STASTNA, J., PAN, X., WANG, H., KOLLMANNSPERGER, A., KUTSCHEIDT, S., LOHMANN, V., GROSSE, R. & FACKLER, O. T. 2012. Differing and isoform-specific roles for the formin DIAPH3 in plasma membrane blebbing and filopodia formation. *Cell Res,* 22**,** 728-45.

STRATMAN, A. N., DAVIS, M. J. & DAVIS, G. E. 2011. VEGF and FGF prime vascular tube morphogenesis and sprouting directed by hematopoietic stem cell cytokines. *Blood,* 117**,** 3709-19.

STRATMAN, A. N., MALOTTE, K. M., MAHAN, R. D., DAVIS, M. J. & DAVIS, G. E. 2009. Pericyte recruitment during vasculogenic tube assembly stimulates endothelial basement membrane matrix formation. *Blood,* 114**,** 5091-101.

STRILIC, B., EGLINGER, J., KRIEG, M., ZEEB, M., AXNICK, J., BABAL, P., MULLER, D. J. & LAMMERT, E. 2010. Electrostatic cell-surface repulsion initiates lumen formation in developing blood vessels. *Curr Biol,* 20**,** 2003-9.

STRILIC, B., KUCERA, T., EGLINGER, J., HUGHES, M. R., MCNAGNY, K. M., TSUKITA, S., DEJANA, E., FERRARA, N. & LAMMERT, E. 2009. The molecular basis of vascular lumen formation in the developing mouse aorta. *Dev Cell,* 17**,** 505-15.

SWANSON, J. A., YIRINEC, B. D. & SILVERSTEIN, S. C. 1985. Phorbol esters and horseradish peroxidase stimulate pinocytosis and redirect the flow of pinocytosed fluid in macrophages. *J Cell Biol,* 100**,** 851-9.

SWIFT, M. R. & WEINSTEIN, B. M. 2009. Arterial-venous specification during development. *Circ Res,* 104**,** 576-88.

TAKEDA, T., GO, W. Y., ORLANDO, R. A. & FARQUHAR, M. G. 2000. Expression of podocalyxin inhibits cell-cell adhesion and modifies junctional properties in Madin-Darby canine kidney cells. *Mol Biol Cell,* 11**,** 3219-32.

TINEVEZ, J. Y., SCHULZE, U., SALBREUX, G., ROENSCH, J., JOANNY, J. F. & PALUCH, E. 2009. Role of cortical tension in bleb growth. *Proc Natl Acad Sci U S A,* 106**,** 18581-6.

TONNING, A., HEMPHALA, J., TANG, E., NANNMARK, U., SAMAKOVLIS, C. & UV, A. 2005. A transient luminal chitinous matrix is required to model epithelial tube diameter in the Drosophila trachea. *Dev Cell,* 9**,** 423-30.

VICENTE-MANZANARES, M., MA, X., ADELSTEIN, R. S. & HORWITZ, A. R. 2009. Non-muscle myosin II takes centre stage in cell adhesion and migration. *Nat Rev Mol Cell Biol,* 10**,** 778-90.

VON STEIN, W., RAMRATH, A., GRIMM, A., MULLER-BORG, M. & WODARZ, A. 2005. Direct association of Bazooka/PAR-3 with the lipid phosphatase PTEN reveals a link between the PAR/aPKC complex and phosphoinositide signaling. *Development,* 132**,** 1675-86.

WALLS, J. R., COULTAS, L., ROSSANT, J. & HENKELMAN, R. M. 2008. Three-dimensional analysis of vascular development in the mouse embryo. *PLoS One,* 3**,** e2853.

WANG, H. U., CHEN, Z. F. & ANDERSON, D. J. 1998. Molecular distinction and angiogenic interaction between embryonic arteries and veins revealed by ephrin-B2 and its receptor Eph-B4. *Cell,* 93**,** 741-53.

WANG, X., PHAN, D. T., SOBRINO, A., GEORGE, S. C., HUGHES, C. C. & LEE, A. P. 2016. Engineering anastomosis between living capillary networks and endothelial cell-lined microfluidic channels. *Lab Chip,* 16**,** 282-90.

WANG, Y., KAISER, M. S., LARSON, J. D., NASEVICIUS, A., CLARK, K. J., WADMAN, S. A., ROBERG-PEREZ, S. E., EKKER, S. C., HACKETT, P. B., MCGRAIL, M. & ESSNER, J. J. 2010. Moesin1 and Ve-cadherin are required in endothelial cells during in vivo tubulogenesis. *Development,* 137**,** 3119-28.

WATERS, J. P., KLUGER, M. S., GRAHAM, M., CHANG, W. G., BRADLEY, J. R. & POBER, J. S. 2013. In vitro self-assembly of human pericyte-supported endothelial microvessels in three-dimensional coculture: a simple model for interrogating endothelial-pericyte interactions. *J Vasc Res,* 50**,** 324-31.

WELLS, K. L. & PATEL, N. 2010. Lumen Formation in Salivary Gland Development. *In:* S., T. A. & I., M. (eds.) *Salivary Glands. Development, Adaptations and Disease.*: Front Oral Biol. Basal, Karger.

WENGER, R. H., STIEHL, D. P. & CAMENISCH, G. 2005. Integration of oxygen signaling at the consensus HRE. *Sci STKE,* 2005**,** re12.

WILLENBORG, C., JING, J., WU, C., MATERN, H., SCHAACK, J., BURDEN, J. & PREKERIS, R. 2011. Interaction between FIP5 and SNX18 regulates epithelial lumen formation. *J Cell Biol,* 195**,** 71-86.

WILSON, C. W., PARKER, L. H., HALL, C. J., SMYCZEK, T., MAK, J., CROW, A., POSTHUMA, G., DE MAZIERE, A., SAGOLLA, M., CHALOUNI, C., VITORINO, P., ROOSE-GIRMA, M., WARMING, S., KLUMPERMAN, J., CROSIER, P. S. & YE, W. 2013. Rasip1 regulates vertebrate vascular endothelial junction stability through Epac1-Rap1 signaling. *Blood,* 122**,** 3678-90.

WILSON, C. W. & YE, W. 2014. Regulation of vascular endothelial junction stability and remodeling through Rap1-Rasip1 signaling. *Cell Adh Migr,* 8**,** 76-83.

WRIGHT, L. P. & PHILIPS, M. R. 2006. Thematic review series: lipid posttranslational modifications. CAAX modification and membrane targeting of Ras. *J Lipid Res,* 47**,** 883-91.

WU, H., FENG, W., CHEN, J., CHAN, L. N., HUANG, S. & ZHANG, M. 2007. PDZ domains of Par-3 as potential phosphoinositide signaling integrators. *Mol Cell,* 28**,** 886-98.

WYSE, M. M., LEI, J., NESTOR-KALINOSKI, A. L. & EISENMANN, K. M. 2012. Dia-interacting protein (DIP) imposes migratory plasticity in mDia2-dependent tumor cells in three-dimensional matrices. *PLoS One,* 7**,** e45085.

XU, C., HASAN, S. S., SCHMIDT, I., ROCHA, S. F., PITULESCU, M. E., BUSSMANN, J., MEYEN, D., RAZ, E., ADAMS, R. H. & SIEKMANN, A. F. 2014. Arteries are formed by vein-derived endothelial tip cells. *Nat Commun,* 5**,** 5758.

XU, K., SACHARIDOU, A., FU, S., CHONG, D. C., SKAUG, B., CHEN, Z. J., DAVIS, G. E. & CLEAVER, O. 2011. Blood vessel tubulogenesis requires Rasip1 regulation of GTPase signaling. *Dev Cell,* 20**,** 526-39.

YAMAMOTO, H., EHLING, M., KATO, K., KANAI, K., VAN LESSEN, M., FRYE, M., ZEUSCHNER, D., NAKAYAMA, M., VESTWEBER, D. & ADAMS, R. H.

2015. Integrin beta1 controls VE-cadherin localization and blood vessel stability. *Nat Commun,* 6**,** 6429.

YOU, L. R., LIN, F. J., LEE, C. T., DEMAYO, F. J., TSAI, M. J. & TSAI, S. Y. 2005. Suppression of Notch signalling by the COUP-TFII transcription factor regulates vein identity. *Nature,* 435**,** 98-104.

YU, J. A., CASTRANOVA, D., PHAM, V. N. & WEINSTEIN, B. M. 2015. Single-cell analysis of endothelial morphogenesis in vivo. *Development,* 142**,** 2951-61.

YU, W., DATTA, A., LEROY, P., O'BRIEN, L. E., MAK, G., JOU, T. S., MATLIN, K. S., MOSTOV, K. E. & ZEGERS, M. M. 2005. Beta1-integrin orients epithelial polarity via Rac1 and laminin. *Mol Biol Cell,* 16**,** 433-45.

ZHENG, Y., CHEN, J., CRAVEN, M., CHOI, N. W., TOTORICA, S., DIAZ-SANTANA, A., KERMANI, P., HEMPSTEAD, B., FISCHBACH-TESCHL, C., LOPEZ, J. A. & STROOCK, A. D. 2012. In vitro microvessels for the study of angiogenesis and thrombosis. *Proc Natl Acad Sci U S A,* 109**,** 9342-7.

ZOVEIN, A. C., LUQUE, A., TURLO, K. A., HOFMANN, J. J., YEE, K. M., BECKER, M. S., FASSLER, R., MELLMAN, I., LANE, T. F. & IRUELA-ARISPE, M. L. 2010. Beta1 integrin establishes endothelial cell polarity and arteriolar lumen formation via a Par3-dependent mechanism. *Dev Cell,* 18**,** 39-51.